



Université du Québec
à Rimouski

**PALEOMAGNETISME ET HISTOIRE GLACIAIRE DANS
LE GOLFE DE L'ALASKA
RESULTATS DE L'EXPEDITION IODP 341**

Thèse présentée

dans le cadre du programme de doctorat en océanographie

en vue de l'obtention du grade de Ph.D

PAR

© **Julie Heggdal Velle**

Septembre 2019

Composition du jury :

André Rochon, président du jury, Université du Québec à Rimouski

Guillaume St-Onge, directeur de recherche, Université du Québec à Rimouski

Joseph S. Stoner, codirecteur de recherche, Oregon State University

Matthias Forwick, codirecteur de recherche, UiT The Arctic University of Norway

Stefanie Brachfeld, examineuse externe, Montclair State University

Dépôt initial le 07 juillet 2019

Dépôt final le 18 septembre 2019

UNIVERSITÉ DU QUÉBEC À RIMOUSKI
Service de la bibliothèque

Avertissement

La diffusion de ce mémoire ou de cette thèse se fait dans le respect des droits de son auteur, qui a signé le formulaire « *Autorisation de reproduire et de diffuser un rapport, un mémoire ou une thèse* ». En signant ce formulaire, l'auteur concède à l'Université du Québec à Rimouski une licence non exclusive d'utilisation et de publication de la totalité ou d'une partie importante de son travail de recherche pour des fins pédagogiques et non commerciales. Plus précisément, l'auteur autorise l'Université du Québec à Rimouski à reproduire, diffuser, prêter, distribuer ou vendre des copies de son travail de recherche à des fins non commerciales sur quelque support que ce soit, y compris l'Internet. Cette licence et cette autorisation n'entraînent pas une renonciation de la part de l'auteur à ses droits moraux ni à ses droits de propriété intellectuelle. Sauf entente contraire, l'auteur conserve la liberté de diffuser et de commercialiser ou non ce travail dont il possède un exemplaire.

Du mener livet er en kamp

Jeg er enig

Men rett som det er

Er det hjemmekamp

Og vi topper laget

Har sola i ryggen

Medvind

Alle heier på oss

Trygve Skaug

ACKNOWLEDGEMENTS

This PhD has been possible only with the help and support of countless people and I am grateful to all of you.

Dear Guillaume, thank you for your endless optimism and encouragement. Thank you for welcoming me at ISMER six years ago and for your continuous support through the years.

Thank you, Joe. My visits to OSU have always given me tons of new data, motivation, and inspiration; all thanks to your passion and enthusiasm for science.

Matthias, thanks for introducing me to marine geology in 2010, for guiding me through my masters and sticking with me through my PhD.

Special thanks are due to my collaborators within IODP Exp. 341. Thank you, Mo Walczak, Alan Mix, Michelle Penkrot, and John Jaeger, for interesting discussions, complimentary data, thoughts, comments and feedback on this part of the project. Furthermore, I want to thank the captain and crew of the R/V JOIDES Resolution, as well as Leah LeVay, Phil Rumford, and the staff at the IODP Gulf Coast core repository for organizing and assisting with the u-channel sampling.

Many thanks are also owed to the excellent lab team at ISMER; Marie-Pier, Jacques, and Quentin. Thank you for years of great collaboration and fun. I am also grateful to the OSU lab, especially Brendan, Ann, and Rob. Thanks for welcoming me at OSU.

Thanks to GEOTOP and ArcTrain for scholarships and travel grants. The meetings and events organized by these two organizations have allowed me to meet new friends and colleagues from around the world.

Thanks to my lovely colleagues in the office. All of you have become great friends and are amazing people that I have been so happy and fortunate to share this experience with. Thank you for countless coffee breaks, office discussions, conference road-trips, and baro nights; Myriam, Quentin, Pierre-Arnaud, Charles, Elissa, Matthieu, Arthur, Edouard, Sarah, Naïs, Yan, Omi, Fatma, Simon F., and Simon N.

My parents and my family -thank you for always being there for me, even from across the Atlantic. Thanks for encouraging me and believing in me; I owe this PhD to you. I am also grateful to my second family, Kris and the Leytems. Thanks for making me feel at home in Oregon.

RÉSUMÉ

Les études paléomagnétiques sont fondamentales à la compréhension des variations temporelles et spatiales du champ magnétique terrestre et des mécanismes de la géodynamo qui le génère. Les signaux des directions et intensité paléomagnétiques sont également souvent utilisés pour améliorer la chronostratigraphie et faciliter les corrélations stratigraphiques entre les enregistrements. En plus des analyses paléomagnétiques standards, des données de magnétisme environnemental du sédiment ont été obtenues. Ces propriétés reflètent les processus environnementaux ayant affecté le sédiment de la source au puits, et sont donc des proxys particulièrement utiles pour la reconstruction des environnements passés.

Le golfe de l'Alaska est un lieu clé pour les études paléomagnétiques et de magnétisme environnemental. Les séquences sédimentaires obtenues-ici ont une haute résolution temporelle, apportant des informations sur la dynamique méconnue du lobe nord-ouest de l'inlandsis de la Cordillère (NCIS), ainsi que la possibilité d'obtenir des enregistrements paléomagnétiques provenant d'une région sous-échantillonnée. L'objectif général de cette étude est de construire un enregistrement paléomagnétique qui va permettre une étude détaillée de la dynamique du champ magnétique terrestre, ainsi que de l'évolution de la NCIS à travers le Pléistocène supérieur et l'Holocène. Pour répondre à cet objectif, deux des sites de forage de l'expédition IODP 341 dans le golfe de l'Alaska en 2013 ont été étudiés : le site U1418 du cône sous-marin Surveyor à une profondeur de 3667 m, et le site U1419 situé sur le haut du talus continental à une profondeur de 687 m. Les 64,6 premiers mètres de l'enregistrement du site U1418 ont été étudiés, tandis que l'entière section de 112 m CCSF-A du site U1419 a été étudiée.

Dans le premier chapitre, les paramètres magnétiques environnementaux du site U1419 sont analysés. Combinées aux images digitales obtenues par *CT-scan* et aux estimations de densité, les propriétés magnétiques du sédiment sont utilisées comme un moyen de reconstruire la dynamique du lobe nord-ouest de l'inlandsis de la Cordillère au cours des derniers ~54 000 ans (cal BP). Les résultats indiquent que le golfe de l'Alaska aurait expérimenté une alternance entre des conditions de haute productivité et des conditions glaciaires au cours du début et du milieu du stage isotopique marin 3 (52 700 - 42 700 cal yr BP). Ce chapitre suggère aussi que la progression vers des conditions de maximum glaciaire aurait débuté aussi tôt que 41 800 cal yr BP et aurait duré jusqu'à 14 700 cal yr BP, donnant une période glaciaire étendue éventuellement nommée le « dernier maximum glaciaire de

l'Alaska ». Les fluctuations de la marge glaciaire auraient été plus complexes à partir de 25 000 cal yr BP avant la déglaciation à 18 000 cal yr BP.

Le chapitre 2 met l'accent sur l'enregistrement paléomagnétique du site 1419 et introduit le modèle d'âge du site 1418. Les résultats démontrent que l'enregistrement n'est pas optimal pour l'étude de la paléointensité, en particulier à cause d'une minéralogie magnétique complexe et de processus post-dépôt. Cependant, les paramètres de direction semblent avoir été affectés seulement à un faible degré, et nous soutenons que l'inclinaison mesurée à 20 mT correspond à la meilleure estimation d'inclinaison possible. L'inclinaison du site U1419 mesurée en laboratoire a été comparée aux données obtenues à bord du navire sur les carottes U1419 et U1418 et à celles obtenues lors du sondage préliminaire du site U1419, le tout indiquant une bonne corrélation globale entre ces différents enregistrements du golfe de l'Alaska. La comparaison avec d'autres enregistrements régionaux indique que l'inclinaison du site U1419 a capté un signal géomagnétique régional, l'intervalle entre 15 000 et 30 000 cal yr BP étant la partie la plus robuste de l'enregistrement.

Finalement, le chapitre trois fait état de l'enregistrement paléomagnétique du site U1418. À ce site, le vecteur paléomagnétique complet (inclinaison, déclinaison et paléointensité) a été reconstruit pour les derniers 27 000 ans (cal BP), apportant de nouvelles informations aux données paléomagnétiques du golfe de l'Alaska. La comparaison de l'inclinaison et de la déclinaison avec d'autres enregistrements régionaux indique que ce site a capté les variations paléomagnétiques séculaires à l'échelle régionale. La correspondance de l'inclinaison entre les sites U1418 et U1419 a permis d'ajuster le modèle d'âge du site U1418 et d'augmenter la précision des limites d'âges sur ce site... La comparaison de l'intensité normalisée avec les enregistrements régionaux et globaux suggère qu'un signal global a pu être enregistré, mais que les variations à l'échelle du millénaire nécessitent plus de précisions.

Les trois chapitres de cette thèse se complètent et apportent de nouvelles informations concernant l'histoire glaciaire du golfe de l'Alaska, ainsi que des enregistrements paléomagnétiques robustes et précis qui pourront favoriser les corrélations stratigraphiques régionales.

Mots clés : Paléomagnétisme, magnétisme environnemental, inlandsis de la Cordillère, golfe de l'Alaska, Pacifique nord-est, Pléistocène supérieur, Holocène

ABSTRACT

Paleomagnetic studies are key in order to understand the temporal and spatial complexities of Earth's magnetic field and its driving mechanism the geodynamo. Records of paleomagnetic directions and/or intensity are also frequently used to improve chronostratigraphy and to facilitate stratigraphic correlation between records. Obtained along with most standard paleomagnetic analyses, is information on the sediment's rock magnetic properties. These properties reflect the environmental processes that the sediment has gone through from source to sink and are, therefore, useful proxies for reconstructing past environments.

The Gulf of Alaska is a key location for paleomagnetic and environmental magnetic studies. The sedimentary sequences found here are of high temporal resolution, offering insights to the poorly constrained dynamics of the northwestern lobe of the Cordilleran Ice Sheet (NCIS), as well as the possibility to obtain paleomagnetic records from an under-sampled region of the world. The general objective of this study is to construct a paleomagnetic record that will permit a detailed study of the Earth's magnetic field dynamics, as well as the evolution of the NCIS through the late Pleistocene and Holocene. To achieve this objective, two of the drill Sites from the 2013 IODP Expedition 341 in the Gulf of Alaska were studied. Site U1418 from the upper Surveyor Fan at a water depth of 3667 m, and Site U1419 from the upper continental slope at a water depth of 687 m. The uppermost 64.6 meters of the spliced record were studied at Site U1418, whereas the entire splice of 112 m CCSF-A was studied at Site U1419.

In the first chapter, the environmental magnetic record of Site U1419 is explored. Along with CT scans and density estimates, the sediment's magnetic properties are used as a means of reconstructing the dynamics of the northwestern lobe of the Cordilleran Ice Sheet for the past ~54,000 cal yr BP. Results indicate that the Gulf of Alaska may have experienced conditions alternating between high productivity and glacial conditions during early and mid-Marine Isotope Stage 3 (52,700-42,700 cal yr BP). This chapter also suggests that the build-up to glacial maximum conditions may have started as early as 41,800 cal yr BP and lasted until 14,700 cal yr BP; an extended glacial period tentatively named the Alaskan LGM. More complex ice front dynamics are suggested from 25,000 cal yr BP before deglaciation from 18,000 cal yr BP.

Chapter two focuses on the paleomagnetic record of Site U1419 and introduces the U1418 age model. Results show that the record is not suitable for paleointensity studies, most likely due to a complex magnetic mineralogy and post-depositional processes. However, the directional record seems to have been affected only to a minor degree and we argue that the inclination as measured at 20 mT is the most reliable inclination estimate. Site U1419

inclination was compared to the U1419 and U1418 shipboard inclinations as well as the U1419 site survey core, showing a general agreement between these Gulf of Alaska records. Comparison with other regional records indicate that the U1419 inclination record has captured a regional geomagnetic signal, with the interval between 15,000 and 30,000 cal yr BP being the most robust part of the record.

In chapter three, the paleomagnetic record of Site U1418 is studied. At this Site, the full paleomagnetic vector (inclination, declination, and paleointensity) was recreated for the past 27,000 cal yr BP, adding new perspectives on the paleomagnetic records of the Gulf of Alaska. Comparisons of U1418 inclination and declination to other regional records indicate that this site has captured regional scale paleomagnetic secular variations. The similarity between Site U1418 and U1419 inclination allowed an adjustment of the U1418 age model, increasing the resolution of this Site's age constraints. Comparing the U1418 normalized intensity to regional and global records suggest that a long-term global signal may have been recorded, whereas millennial-scale variability needs further constraints.

The three chapters of this thesis compliment and build upon each other, and provide new information regarding the glacial history of the Gulf of Alaska, as well as a robust and well-constrained paleomagnetic record that will aid in regional stratigraphic correlation.

Keywords: Paleomagnetism, environmental magnetism, Cordilleran Ice Sheet, Gulf of Alaska, northeast Pacific, late Pleistocene, Holocene

TABLE OF CONTENTS

ACKNOWLEDGEMENTS.....	ix
RÉSUMÉ.....	xi
ABSTRACT.....	xiii
TABLE OF CONTENTS.....	xv
LIST OF TABLES.....	xx
LIST OF FIGURES.....	xxi
LIST OF ABBREVIATIONS, ACRONYMS AND SYMBOLS.....	xxvii
GENERAL INTRODUCTION.....	1
BACKGROUND.....	1
Paleomagnetism.....	1
Marine sediments and paleomagnetic records.....	1
Pacific paleomagnetic records.....	3
Environmental magnetism.....	4
The Gulf of Alaska.....	7
PROJECT SETTING AND CONTEXT.....	11
International Ocean Drilling Program (IODP) Expedition 341.....	11
RESEARCH OBJECTIVES.....	14
METHODS.....	15
THESIS OVERVIEW.....	18
CONTRIBUTIONS AND COLLABORATIONS.....	19
RESEARCH COMMUNICATION.....	20
Articles in preparation.....	20
Conference contributions.....	20

REFERENCES	22
CHAPTER 1 A LATE PLEISTOCENE ENVIRONMENTAL MAGNETIC RECORD OF NORTHWESTERN CORDILLERAN ICE SHEET DYNAMICS BASED ON IODP EXPEDITION 341 DRILL SITE U1419 IN THE GULF OF ALASKA.....	36
1.1 SUMMARY OF CHAPTER 1	36
1.2 A LATE PLEISTOCENE ENVIRONMENTAL MAGNETIC RECORD OF NORTHWESTERN CORDILLERAN ICE SHEET DYNAMICS BASED ON IODP EXPEDITION 341 DRILL SITE U1419 IN THE GULF OF ALASKA	37
1.3 INTRODUCTION.....	39
1.4 STUDY AREA.....	41
Geological and oceanographic setting.....	41
The northwestern Cordilleran Ice Sheet (NCIS)	42
1.5 METHODS	43
Coring and sampling.....	43
Physical properties.....	44
Continuous magnetic measurements	45
Discrete magnetic measurements	46
Constructed ratios as environmental magnetic proxies	46
Age model	47
1.6 RESULTS	48
Physical properties and lithology	48
Magnetic properties	52
Chronostratigraphy	57
1.7 DISCUSSION	58
Unit III - Period of alternating conditions (54,000 to 41,800 cal yr BP).....	58
Unit II - The Alaskan LGM (41,800 -14,700 cal yr BP).....	60
The Gulf of Alaska record in a regional and global context	63
1.8 CONCLUSIONS.....	66

1.9 ACKNOWLEDGEMENTS.....	66
1.10 REFERENCES	67
CHAPTER 2 A HIGH-RESOLUTION LATE QUATERNARY INCLINATION RECORD FROM IODP EXPEDITION 341 DRILL SITE U1419 IN THE GULF OF ALASKA	77
2.1 SUMMARY OF CHAPTER 2.....	77
2.2 A HIGH-RESOLUTION LATE QUATERNARY INCLINATION RECORD FROM IODP EXPEDITION 341 DRILL SITE U1419 IN THE GULF OF ALASKA	78
2.3 INTRODUCTION	80
2.4 METHODS	81
Coring and u-channel sampling	81
Physical properties	82
Continuous magnetic measurements.....	83
Discrete magnetic measurements.....	85
Age models	85
2.5 RESULTS	88
Chronostratigraphy.....	88
Lithology.....	89
Magnetic remanence and directions.....	90
Magnetic mineralogy, grain size, and concentration	95
2.6 DISCUSSION.....	98
Natural remanent magnetization and directional record	98
Regional comparisons	99
U1419 inclination record.....	106
2.7 CONCLUSIONS	107
2.8 ACKNOWLEDGEMENTS.....	108
2.9 REFERENCES	109

CHAPTER 3 HIGH-RESOLUTION PALEOMAGNETIC SECULAR VARIATION AND RELATIVE PALEOINTENSITY IN THE GULF OF ALASKA: CONSTRAINTS ON THE LATE PLEISTOCENE AND HOLOCENE STRATIGRAPHY OF IODP EXPEDITION 341 SITE U1418.....	119
3.1 SUMMARY OF CHAPTER 3	119
3.2 HIGH-RESOLUTION PALEOMAGNETIC SECULAR VARIATION AND RELATIVE PALEOINTENSITY IN THE GULF OF ALASKA: CONSTRAINTS ON THE LATE PLEISTOCENE AND HOLOCENE STRATIGRAPHY OF IODP EXPEDITION 341 SITE U1418	120
3.3 INTRODUCTION.....	122
3.4 SITE SETTING.....	123
The Gulf of Alaska	123
IODP Expedition 341 drill Site U1418.....	124
3.5 METHODS	125
U-channel sampling.....	125
Continuous magnetic measurements	125
Discrete magnetic measurements	127
CT scanning.....	128
Age model	128
3.6 RESULTS	129
Chronology	129
Physical properties and lithology	130
Magnetic mineralogy, concentration, and grain size.....	131
Paleomagnetic directions.....	134
Remanent magnetization and normalized intensity.....	136
3.7 DISCUSSION	138
Chronostratigraphy	138
Paleomagnetic secular variations (PSV).....	141
Paleointensity	144

3.8 CONCLUSIONS	147
3.9 ACKNOWLEDGEMENTS.....	147
3.10 REFERENCES	148
GENERAL CONCLUSION	158
Introduction.....	158
Chapter 1	158
Chapter 2	163
Chapter 3	165
The Gulf of Alaska records.....	167
Perspectives.....	168
REFERENCES	171

LIST OF TABLES

Table 1: Overview of methods used during this PhD.	17
Table 2: Depth, age, selected magnetic parameters and lithology characteristic for the units and facies described in the text.	50
Table 3: Radiocarbon dates from Site U1418 and EW0408-87JC.....	86
Table 4: Tie-points to the U1419 age model (Walczak et al., in prep).	140

LIST OF FIGURES

Figure 1: Distribution of sedimentary inclination, declination and intensity records (modified from Panovska et al., 2018).	4
Figure 2: Diagram showing the different forcings, sources, processes and environments that influence magnetic grains and can be investigated using the techniques of environmental magnetism (modified from Verosub & Roberts, 1995).	6
Figure 3: Overview map of the Gulf of Alaska and the IODP Exp. 341 drill Sites (note that Site U1417 is located to the south and not included). Estimated LGM maximum extent from Kaufman et al., 2011. AC= Alaska Current; ACC= Alaska Coastal Current.	10
Figure 4: The St. Elias Mountains (left; photo credit J. Jaeger), and the JOIDES Resolution (right; photo credit A. Sakaguchi).	13
Figure 5: Sampling of u-channels at the IODP Gulf Coast Repository at Texas A&M University in College Station in March 2014.	16
Figure 6: Map of the Gulf of Alaska with Site U1419 (yellow star) and other Expedition 341 drill Sites (red circles). The estimated LGM extent (from Kaufman & Manley, 2004) is outlined with an orange dashed line. The location of Site U1419 also marks the location of core EW0408-85JC mentioned in the text.	42
Figure 7: Age model for Site U1419 (Walczak et al., in prep). Blue circles indicate radiocarbon dated intervals from Site U1419. Red circles indicate GRA tie-points to core EW0408-85JC and TC (cf. Fig. 6). Sedimentation rates (cm/kyr) averaged over 500 years below.	48
Figure 8 (next page): Site U1419 magnetic remanence (ARM, IRM and SIRM) and magnetic susceptibility (k_{LF}), k_{ARM}/k_{LF} , hysteresis properties, MDF_{ARM} , and CT density against CCSF-A depth in meters. Magnetic proxies are indicated in top panels, and units referred to in the text are indicated in side panels. Facies described in the text are indicated in different colors.	50

- Figure 9:** U-channel CT scan images from Site U1419 showing examples of different lithologies observed in Site U1419 and described in the text. Brighter/darker intervals reflect higher/lower density, respectively. The arrow indicates the transition between Unit II and Unit Ib at 6.3 m CCSF-A. 53
- Figure 10:** Day plot (Day et al., 1977) with mixing lines from Dunlop (2002a, 2002b) of all Site U1419 discrete samples divided into units as described in the text. Selected hysteresis loops representative for each unit are presented below. 55
- Figure 11 (next page):** An hysteretic susceptibility of the U1419 units plotted against magnetic susceptibility (King et al., 1982) as a proxy for magnetic grain size (given a magnetite mineralogy). Magnetic grain size boundaries are based on synthetic samples from Banerjee et al. (1981) and the plot is adapted from Geiss & Banerjee (2003). Insert shows samples from 6.3-4.0 m CCSF-A in Unit Ib. 56
- Figure 12 (previous page):** Sedimentation rates (Walczak et al., in prep) and selected magnetic properties plotted against age in cal yr BP. Enlarged y axis for k_{ARM}/k_{LF} in Unit II in grey. Events discussed in the text are indicated in different colors. Upper panel shows division of the marine isotope stages (MIS), and the lower panel details the glacial history as interpreted from the U1419 sedimentary record. 62
- Figure 13:** Comparison of Antarctic (EDML in blue; EPICA Community Members, 2010) and Greenland (NGRIP in green; NGRIP Community Members, 2004) oxygen isotope records on the AICC2012 chronology (Veres et al., 2013) and the U1419 magnetic susceptibility record (black). Note the reversed Y-axes on the oxygen isotope records. Interpretation of the U1419 record are marked in colors as in Fig. 12. Heinrich stadials (HS) for reference are marked on the oxygen isotope records in grey. 65
- Figure 14:** Overview of the Gulf of Alaska with IODP Expedition 341 drill Sites indicated. Site U1419 is indicated by a yellow star. This also marks the location of U1419 of site survey core EW0408-85JC mentioned in the text. The Surveyor Fan Site U1418 is indicated by a red triangle. This also marks the location of core EW0408-87JC mentioned in the text. 83
- Figure 15:** Left: U1419 age model (Walczak et al., in prep.) and sedimentation rates. Red circles indicate GRA tie-points to core EW0408-85JC and TC whereas blue circles are calibrated ages from Site U1419. Right: U1418 age model with sedimentation rates for the past 40,000 cal yr BP. Red circles indicate magnetic susceptibility tie-points to

core EW0408-87JC (Praetorius et al., 2015) and blue circles indicate calibrated ages from U1418. Note the difference in Y axes, both for depth and sedimentation rates.89

Figure 16: U1419 natural remanent magnetization (NRM) with all AF demagnetization steps with the 20 mT demagnetization step highlighted in red as it is described in more detail in the text. Note that the NRM is plotted on a log scale. Laboratory remanences (ARM, IRM, and SIRM) as measured before demagnetization, and the maximum angular deviation (MAD) values for the entire range of demagnetization steps.91

Figure 17 (next page): Vector end-point diagrams (Zijderveld, 1967) from four representative intervals of Site U1419 are displayed in top panels. AF demagnetization steps in mT are indicated in grey in panel A. Open circles represent projections on the vertical plane, and closed circles the horizontal plane. Corresponding demagnetization plots are displayed below.92

Figure 18: Selection of PCA ranges for U1419 inclination and MAD values, all with a 40-point smoothing. The inclination as measured at 20 mT highlighted in red as it is described in more detail in the text.94

Figure 19: U1419 inclination measured at 20 mT with the GAD latitude (73.6°) indicated in red; rotated declination as measured at 20 mT, magnetic susceptibility (k_{LF}), ARM susceptibility (k_{ARM}), and MDF of ARM. Details from CT images displaying characteristic lithofacies are shown on the right. Red asterisks mark intervals that are disregarded due to disturbance either during drilling or u-channel sampling.96

Figure 20: Panel A: Day plot (Day et al., 1977) with theoretical mixing lines from Dunlop (2002a, 2002b) of all Site U1419 discrete samples. Panel B: Selected IRM acquisition curves. Panel C: Selected hysteresis loops.97

Figure 21 (next page): Comparison of U1419 shipboard inclination stack (see description in the text) and U1419 u-channel inclination as measured at 20 mT. The expected geocentric axial dipole inclination for the site latitude ($GAD = 73.6^\circ$) is indicated with the grey horizontal line. Red asterisks mark intervals that are disregarded due to disturbance either during drilling or u-channel sampling. Note that the figure includes the lowermost part of the splice (below 96 m CCSF-A) which has been excluded from further comparison.100

Figure 22: Comparison of the U1419 inclination (in black) to U1419 site survey core EW0408-85JC (in blue; Walczak et al., 2017), U1418 shipboard data (in purple), and the NE Pacific sedimentary inclination anomaly stack (NEPSIAS in red; Walczak et al., 2017). Letters are added to facilitate discussion. Note that the upper 1.3 meters of U1419 are removed due to sampling deformation (see text) and that u-channel edges are removed. 102

Figure 23: Comparison of the U1419 inclination record (with 40-point smoothing on intervals with sedimentation rates > 80 cm/kyr) and Expedition 341 Surveyor Fan Site U1418 shipboard inclination stack (with 5-point smoothing on intervals with sedimentation rates > 100 cm/kyr). Both records are plotted on their own individual age models with dates marked in blue and red circles (cf. Fig. 15). Inclination features are indicated with letters in blue to facilitate discussion; note that letters are continued from Figure 22. 104

Figure 24: Comparison of the Site U1419 inclination record (40-point smoothing on intervals with sedimentation rates > 80 cm/kyr) with the Site U1418 shipboard inclination stack (with 5-point smoothing on intervals with sedimentation rates > 100 cm/kyr) and the Western North America inclination stack WNAM17 (relocated to the Gulf of Alaska using a GAD approximation; Reilly, et al., 2018), all on their individual age models. Letters are continued from figures 22 and 23 to facilitate discussion. Note that intervals identified as disturbed and/or deformed in the U1419 record are removed (cf. Fig. 19). 105

Figure 25: Location of IODP Expedition 341 drill Sites in the Gulf of Alaska. Site U1418 is indicated with a yellow star. Site U1418 also marks the location of core EW0408-87JC mentioned in the text. 124

Figure 26: U1418 age model (Velle et al., in prep). Blue circles indicate radiocarbon dated levels of Site U1418. Red circles indicate magnetic susceptibility-based tie-points to the independently dated Gulf of Alaska core EW0408-87JC (Praetorius et al., 2015). 130

Figure 27: Natural remanent magnetization (NRM) with AF demagnetization steps displayed in colors ranging from black (0 mT) to grey (100 mT); anhysteretic remanent magnetization (ARM, isothermal remanent magnetization (IRM), and saturated isothermal remanent magnetization (SIRM) as measured before demagnetization (at 0 mT); magnetic susceptibility (k_{LF}) with a 20-point smoothing (black); and k_{ARM}/k_{LF} with a 20-point smoothing (blue). In a dominantly magnetite magnetic mineralogy,

k_{ARM}/k_{LF} is inversely correlated with magnetic grain size (Thompson & Oldfield, 1986). On the right are three examples of CT-scans showing lithologies typical for Site U1418..... 131

Figure 28: A: Day plot (Day et al., 1977) with theoretical mixing lines from Dunlop (2002a, 2002b) of all Site U1418 discrete samples. B: Anhysteretic susceptibility (k_{ARM}) plotted against magnetic susceptibility (k_{LF} ; King et al., 1982) as a proxy for magnetic grain size (given a magnetite mineralogy). Magnetic grain size boundaries are based on synthetic samples from Banerjee et al. (1981) and the plot is adapted from Geiss & Banerjee (2003). C: Selected hysteresis loops representative of Site U1418. 133

Figure 29: Vector end-point diagrams (Zijderveld, 1967) with corresponding demagnetization plots from four representative intervals of Site U1418. Open (closed) circles represent projections on the vertical (horizontal) plane. 134

Figure 30: Characteristic remanent magnetization (ChRM) inclination and declination as defined between the 25-60 mT AF demagnetization steps, and maximum angular deviation (MAD) values for the complete range of AF demagnetization steps (orange) and for the ChRM range 25-60 mT (black). Declination has been rotated to a mean of zero. All parameters are shown with a 20-point smoothing indicated in bold. 135

Figure 31 (next page): U1418 NRM normalized over the 25-60 mT AF demagnetization steps by ARM (left) and IRM (right) using the ratio method (black) and the slope method (blue). The R value of the slope method is displayed in grey. Scatter plots show the correlation between the normalized intensity and the normalizer used with the corresponding r^2 value. 137

Figure 32: U1418 inclination compared with Exp. 341 drill Site U1419 inclination (Velle et al., in prep), both on their respective age models. Blue circles indicate radiocarbon dated intervals and red circled indicate tie-points to core EW0408-87JC for Site U1418, and tie-points to core EW0408-85JC for Site U1419 (Walczak et al., in prep). Tie-points between the two inclination records are indicated with dashed lines. 139

Figure 33: U1418 age model (in black) with tie-points to the U1419 age model (Walczak et al., in prep) via U1419 inclination (green diamonds). Adjusted age model and sedimentation rates are indicated in red. 141

Figure 34: Comparison of Site U1418 ChRM (25-60 mT) inclination and declination with U1418 shipboard inclination as measured at 20 mT (Velle et al., in prep), U1418

shipboard declination stack, Site U1419 (Velle et al., in prep), EW0408-85JC (Walczak et al., 2017), the Western North America PSV stack rotated to the Gulf of Alaska using a GAD approximation (WNAM; Reilly et al., 2018), and the northeastern Pacific sedimentary inclination anomaly stack (NEPSIAS; Walczak et al., 2017) for the time periods 0-16 cal kyr BP (A) and 16-28 cal kyr BP (B). PSV features are numbered to facilitate discussion. A 40-point smoothing has been applied to parts of the U1418 record where sedimentation rates exceed 100 cm/kyr. 143

Figure 35: Comparison of Site U1418 normalized intensity (NRM/IRM slope) with other regional intensity records; HLY0501-05JPC (Barletta et al., 2008), 02PC (Deschamps et al., 2018), ODP Site 1233 (Lund et al., 2006), MD98-2181 (Stott et al., 2002), and the “overall” RPI record scaled to VADM (including the Iberian margin records and globally distributed marine and lakustrine records; cf. Channell et al., 2018) for the time periods 0-16 cal kyr BP (A) and 16-28 cal kyr BP (B). A 40-point smoothing has been applied to parts of the U1418 record where sedimentation rates exceed 100 cm/kyr. 145

Figure 36: Comparison of the highest resolution interval (16-28 cal kyr BP) of the Site U1418 normalized intensity (NRM/IRM slope) and the Greenland ^{10}Be flux record (Muscheler et al., 2004). A 40-point smoothing has been applied to parts of the U1418 record where sedimentation rates exceed 100 cm/kyr. Note the reversed Y axis for the Greenland ^{10}Be flux record. 146

Figure 37: From the left: Site U1419 magnetic susceptibility and sedimentation rates (averaged over 500 years; Walczak et al., in prep), tentative interpretation of the ice front’s position based on Site U1419, and a summary of the glacial history as interpreted from Site U1419. 161

LIST OF ABBREVIATIONS, ACRONYMS AND SYMBOLS

AF	Alternating field (demagnetization)
AGM	Alternating gradient force (field) magnetometer
ARM	Anhyseretic remanent magnetization
CCSF-A	Core composite depth below seafloor A
CCSF-B	Core composite depth below seafloor B (accounts for expansion in depth)
ChRM	Characteristic remanent magnetization
CSF-A	Core depth below seafloor
CT	Computed tomography
DC	Direct current
Exp.	Expedition
GAD	Geocentric axial dipole
GoA	Gulf of Alaska
H_c	Coercive force
H_{cr}	Remanence of coercivity
INRS-ETE	Institut national de la recherche scientifique - Eau Terre Environnement
IODP	International Ocean Discovery Program
IRD	Ice rafted debris

IRM	Isothermal remanent magnetization
ISMER	Institut des sciences de la mer de Rimouski
k_{ARM}	Susceptibility of anhysteretic remanent magnetization
k_{LF}	Low-field magnetic susceptibility
MAD	Maximum angular deviation
MD	Multi-domain
MDF	Median destructive field
MDF_{ARM}	Median destructive field of anhysteretic remanent magnetization
MIS	Marine isotope stage
M_{rs}	Saturation remanence
M_s	Saturation magnetization
mT	millitesla
NCIS	Northwestern Cordilleran Ice Sheet
NRM	Natural remanent magnetization
OSU	Oregon State University
PSD	Pseudo-single domain
PSV	Paleomagnetic secular variation
RPI	Relative paleointensity
SD	Single domain
SIRM	Saturated isothermal remanent magnetization

T	Tesla
UQAR	Université du Québec à Rimouski
VADM	Virtual axial dipole moment
VGP	Virtual geomagnetic poles

GENERAL INTRODUCTION

BACKGROUND

Paleomagnetism

Direct observations of Earth's magnetic field extend back four centuries but were not systematically organized until the global network of Magnetic Observatories was initiated by Weber and Gauss in the 1840s (e.g., Jackson et al., 2000; Hulot et al., 2010). At present, several observatories and satellites constantly monitor changes in the field both on Earth and from space. Paleomagnetism, the study of field changes in the past, is based on analyses of volcanic rocks, archeological artefacts and sediments, and has become an extensive field of research (e.g., Channell, 1999; Guyodo & Valet, 1999; Gallet et al., 2002, 2009; ; Laj et al., 2004, 2014; Panovska et al., 2018; Korte et al., 2019) and is important in order to improve our understanding of, for example, the geodynamo, links between terrestrial and solar processes, as well as to establish robust chronologies and allow correlation of different proxy records within a region.

Marine sediments and paleomagnetic records

Because of their continuity, sediment records are especially convenient for long-term studies of variations in Earth's magnetic field at a specific location (Tauxe, 1993). In order for sediments to be used as a paleomagnetic archive, it is assumed that they record the intensity and direction of the magnetic field at their time of deposition; the natural remanent magnetization (NRM). However, the exact timing and depth of the acquisition of magnetization in marine sediments is not completely understood, and is also affected by mineral magnetic properties such as the type of mineral, the magnetic grain size and concentration (e.g., Levi & Banerjee, 1976; Tauxe, 1993), and the quality and preservation

of the magnetic signal can be altered by post-depositional (biogenic, chemical and diagenetic) processes (Karlin & Levi, 1983; Clement et al., 1996; Walczak et al., 2017). Due to these effects on magnetic acquisition and preservation in sediments, the quality of the archived magnetic signal and recorded intensity may vary down-core.

The intensity and direction of the surface geomagnetic field varies spatially and temporally over timescales of seconds to thousands of years. Variations in the field occurring during periods of stable polarity are termed paleomagnetic secular variations (PSV), with anomalously large changes in the magnetic field direction, beyond the normal range of PSV, termed geomagnetic excursions. These are defined by a deviation of the virtual geomagnetic pole (VGP) of more than 40-45° from the geographic pole (e.g., Gubbins, 1999; Roberts, 2008; Valet et al., 2008; Laj & Channell, 2015; Lund, 2018).

These changes in direction and relative intensity of the Earth's magnetic field through time make paleomagnetic records useful as a chronological tool. Some excursions are frequently used as stratigraphic markers; for example, the Laschamp excursion at ~41 ka (e.g., Laj et al., 2000; Guillou et al., 2004; Lund et al., 2005; Lascu et al., 2016) and the less constrained Mono Lake excursion at 30-34 ka (e.g., Liddicoat & Coe, 1979; Kent et al., 2002; Laj et al., 2014; Lund et al., 2017a). On a regional scale, directional changes within the normal range of paleomagnetic secular variations can be used as a means of correlations (e.g., Barletta et al., 2008; Walczak et al., 2017; Caron et al., 2018; Deschamps et al., 2018; Reilly et al., 2018). Although correlation of relative paleointensity records may be less straightforward, the use of such records in stratigraphy is already well established and records from several different areas of the globe have been stacked in order to create solid stratigraphic references (e.g., the global Sint-200 by Guyodo & Valet, 1996; Sint-800 by Guyodo & Valet, 1999; GLOPIS-75 by Laj et al., 2004; Sint-2000 by Valet et al., 2005; and PISO-1500 by Channell et al., 2009).

Another application of RPI records and stacks is their inverse relationship to cosmogenic nuclide production rates; at times when the geomagnetic field is stronger, it acts as an efficient shield around the Earth, and fewer cosmic rays enter the upper parts of the atmosphere, and less cosmogenic isotopes (e.g., ^{10}Be , ^{14}C , ^{26}Al , ^{36}Cl) are produced (e.g.,

Masarik & Beer, 1999; Beer et al., 2002; Valet, 2003; Stoner & St-Onge, 2007; Valet et al., 2014). Because this shielding takes place in space, it reflects the global geomagnetic field and an inverse correlation between a given RPI record and cosmogenic nuclide production rates can, therefore, confirm if the RPI record reflects global-scale geomagnetic field variations (e.g., Stoner et al., 2000; St-Onge et al., 2003; Thouveny et al., 2004; Ménabréaz et al., 2011, 2012; Nowaczyk et al., 2013) .

In addition to their role as stratigraphic aids allowing comparisons of different proxy records within a region, paleomagnetic records are important for improving our understanding of the temporal and spatial variations in the Earth's magnetic field. For example, the influence of high-latitude flux lobes on PSV records (e.g., Stoner et al., 2013; Walczak et al., 2017), and the regional expression of secular variations and excursions (e.g., Lund, 2018; Panovska et al., 2018). Constraining the dynamics of such features, as well as their spatial and temporal variability is key to increased understanding of the geodynamo (e.g., Bloxham 2000; Stoner et al., 2013; Lund et al., 2016).

Pacific paleomagnetic records

Although most paleomagnetic studies are focused on the North Atlantic (Fig. 1), some paleomagnetic studies have been carried out in the Pacific Ocean during the past few decades. Records from the south (e.g., Kok & Tauxe, 1999) and the equatorial Pacific (Valet & Meynadier, 1993; Laj et al., 1996; Verosub et al., 1996; Yamazaki & Oda, 2005) span time periods of up to 4 Ma, with a few higher-resolution Pacific studies focusing more on the past 0-70 ka years (e.g., Lund et al., 2006, 2017b). Paleomagnetic studies from the western North Pacific comprise mainly Brunhes and older paleointensity records (Yamazaki, 1999; Yamazaki & Kanamatsu, 2007), as well as the RPI stack NOPAPIS-250 which spans the past 250 kyr (Yamamoto et al., 2007). The 1992 ODP Leg 145 covered most of the North Pacific with a drilling transect from Japan to Canada (Rea et al., 1995; Weeks et al., 1995). Sites 883 and 884 from this ODP Leg were drilled in the southern Gulf of Alaska and formed the basis of a composite paleointensity curve spanning the past 200 kyr (Roberts et al., 1997). More recently, Walczak et al. (2017) studied the high-resolution deglacial and Holocene

paleomagnetic records of cores EW0408-79JC and EW0408-85JC from the Gulf of Alaska and from this constructed the north-east Pacific sedimentary inclination anomaly stack (NEPSIAS). Included in this stack were also other, independently dated, regional records from Alaska, Oregon and Hawaii, indicating that a common, regional inclination signal has been captured in these records.

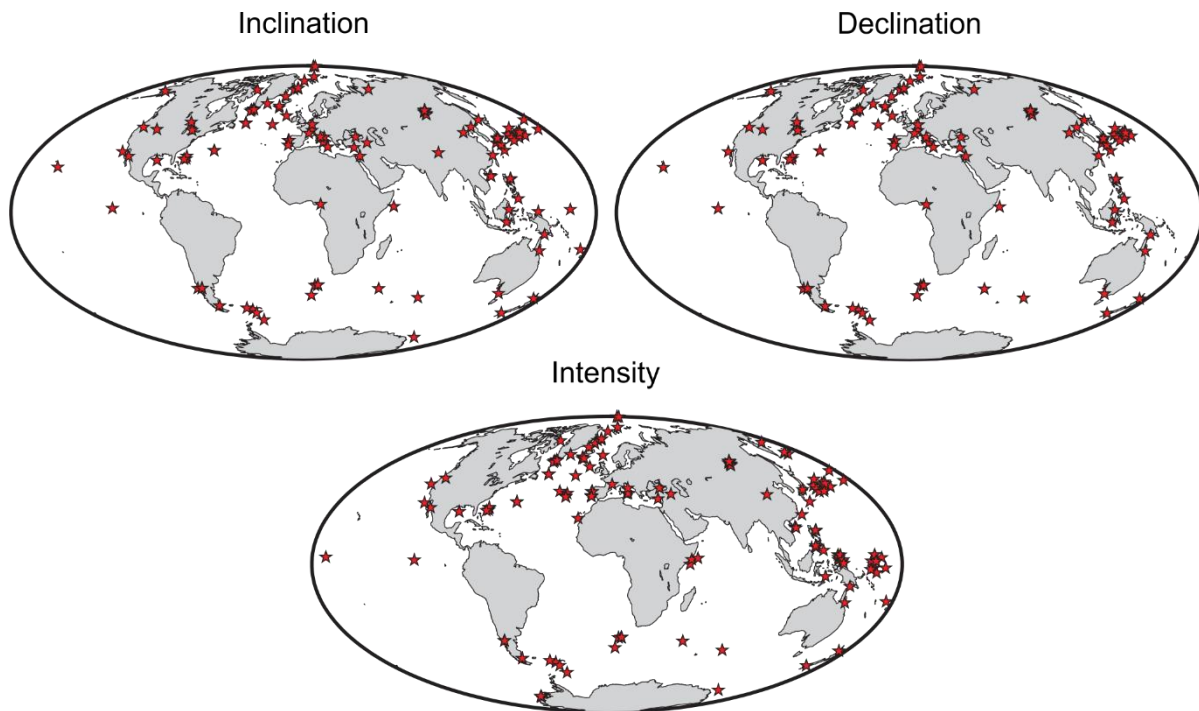


Figure 1: Distribution of sedimentary inclination, declination and intensity records (modified from Panovska et al., 2018).

Environmental magnetism

Iron-bearing minerals have great potential to record the environmental processes they go through both before and after deposition. Such environmental processes include soil formation, weathering, erosion, transport, accumulation and diagenesis of sediments. Furthermore, the mode of erosion and transportation (i.e. wind, ice, and water) will also leave

traces in the sediment which can provide information on past climatic and environmental conditions (Thompson & Oldfield, 1986). Looking into rock magnetic properties can therefore be very useful in paleoclimate studies. Even very small quantities of magnetic minerals can be detected with magnetic measurement systems, and such analyses are usually non-destructive, efficient and sensitive to minute amounts of magnetic grains (e.g., Verosub & Roberts, 1995; Dekkers, 1997; Liu et al., 2012). Rock magnetic properties that often are used include low-field magnetic susceptibility (k_{LF}), anhysteretic remanent magnetization (ARM), isothermal remanent magnetization (IRM), and saturation isothermal remanent magnetization (SIRM). These are parameters usually measured during standard paleomagnetic studies and are therefore routinely obtained. Additionally, hysteresis parameters and IRM acquisition curves are useful parameters easily obtained from small sample sizes.

Mineral magnetic properties have successfully been used in sedimentological, paleoceanographic and paleoclimatic studies, and have proven to be a useful correlative and stratigraphic tool for use in sediment cores (e.g., Robinson, 1986; Robinson et al., 1995; Stoner et al., 1996; Kissel et al., 1999; Lisé-Pronovost et al., 2014; Dorfman et al., 2015). For example, magnetic susceptibility can reflect core lithostratigraphy and thereby contribute to identifying glacial vs. interglacial (high vs. low magnetic susceptibility) layers, corresponding to periods of high/low ice-rafted debris (IRD) input and low/high carbonate productivity, respectively (Robinson, 1986). Magnetic susceptibility, ARM and IRM have been used to identify and correlate IRD layers to Heinrich-layers (Thouveny et al., 2000). In the Baffin Bay, studies of mineralogical assemblages and lithofacies have resulted in an improved understanding of the dynamics of the Greenland, Innuitian and Laurentide Ice Sheets through the 115 ka (Simon et al., 2014), while Hatfield et al. (2013) used mineral magnetic properties, with special focus on grain-size specific magnetic variations to distinguish sediment provenance in marine sediment cores from the northern North Atlantic. In the southern Alaskan region, the complex geological setting can be advantageous when determining provenance of marine sediments. Cowan et al. (2006) investigated the mineral magnetic signal of the sediment in three glaciated southern Alaskan fjords and found distinct

differences in the magnetic signal depending on source region. For example, PSD magnetite is characteristic for the Yakutat terrane, whereas fine PSD hysteresis parameters and low magnetic susceptibility is typical for the Chugach terrane. Furthermore, magnetic susceptibility was found to be especially useful in distinguishing the provenance of IRD layers as the different source areas have distinct magnetic expressions (Cowan et al., 2006).

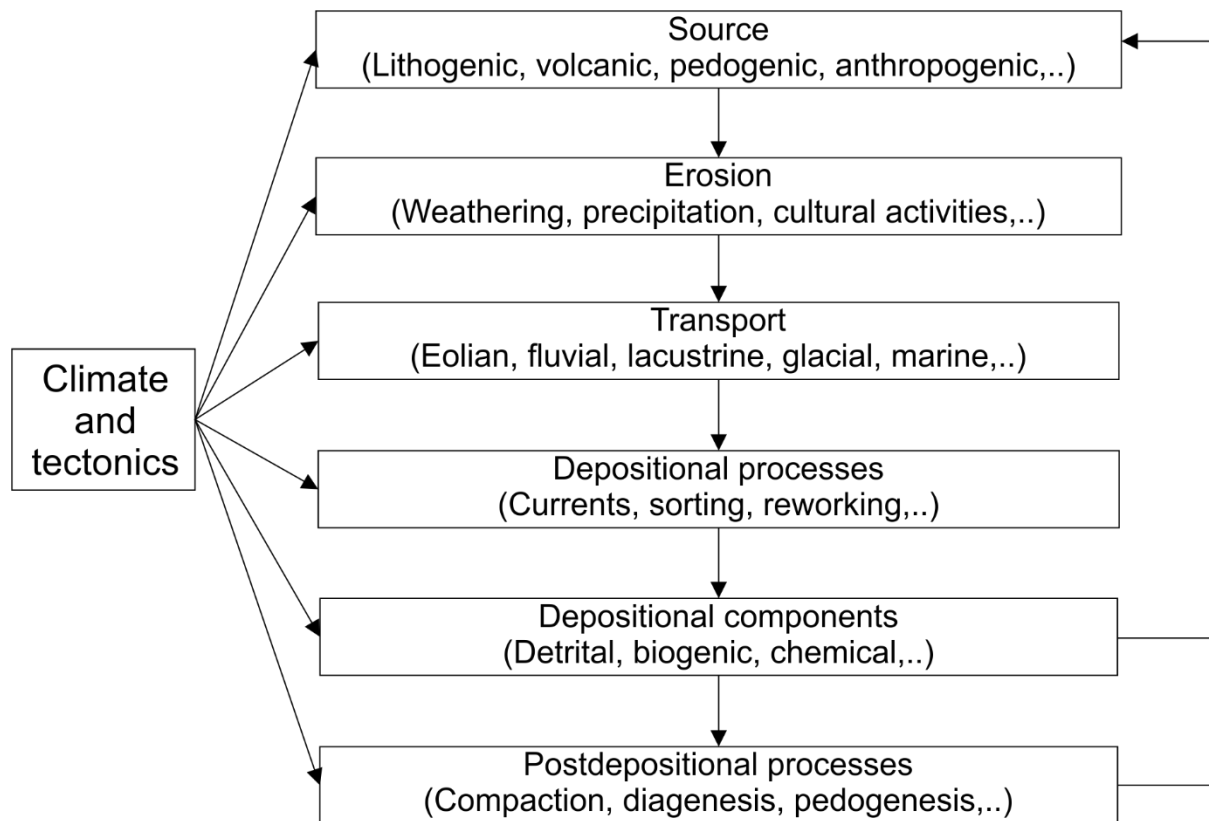


Figure 2: Diagram showing the different forcings, sources, processes and environments that influence magnetic grains and can be investigated using the techniques of environmental magnetism (modified from Verosub & Roberts, 1995).

The Gulf of Alaska

Geologic setting

The Gulf of Alaska (GoA) is located in the subarctic northern Pacific Ocean, off the southern Alaska coast (Fig. 3). The St. Elias Mountains dominate the southeastern coast of Alaska and is the highest coastal mountain range in the world with its >6000 m.a.s.l peaks (e.g., Meigs & Sauber, 2000; Bruhn et al., 2004). In addition to glacial erosion, the St. Elias Mountains are subject to the harsh maritime climate of the North Pacific; including heavy storms and precipitation that are thought to have a great influence on the denudation on the windward side of the orogen (Meigs & Sauber, 2000).

The North Pacific continental margin in the Gulf of Alaska is between approx. 25 and 100 km wide and has an average water depth of 140 m. The bathymetry on the shelf is dominated by several cross-shelf troughs or sea valleys, e.g., the Hinchinbrook and Yakutat Sea Valleys, and the Kayak and Bering Troughs. These troughs formed over time during glacial maxima when glaciers from the northwestern lobe of the Cordilleran Ice Sheet reached the shelf edge (Carlson et al., 1982; Elmore et al., 2013; Montelli et al., 2017). The sedimentary sequence on the shelf is assumed to be 5 km thick consisting of glacial marine sediments deposited through the past 6 Ma (Molnia & Carlson, 1978; Jaeger et al., 1998). At the foot of the continental slope, extending into the Alaskan Abyssal Plain, is the massive Surveyor Fan which occupies an area of $3.42 \times 10^5 \text{ km}^2$ with a sedimentary volume of $6.8 \times 10^5 \text{ km}^3$ (Reece et al., 2011). This fan system started developing in the Miocene and the combination of an active orogen and periods of intense glaciation (Lagoe et al., 1993; Berger et al., 2008; Montelli et al., 2017) has ensured a high flux of sediment to the Surveyor Fan through the past ~20 Ma leaving a sedimentary sequence existing mostly of terrigenous sediment (Reece et al., 2011). The most dominating morphological feature of the Surveyor Fan is the Surveyor Channel; a 700 km long and up to 500 m deep incision cut out by reoccurring turbidity currents (Ness & Kulm, 1973). This channel feeds sediment to the lower part of the Surveyor Fan and was formed around ~1 Ma and has expanded during shelf edge glaciations since (Reece et al., 2011).

Climate and oceanography

The Alaska Current (AC) is a branch of the Pacific subarctic gyre and flows westward in the ocean basin of the GoA (Fig. 3). As the AC reaches the Kenai Peninsula, it turns southwest and continues along the North Pacific margin and the Alaska Peninsula as the Alaskan Stream (Reed & Schumacher, 1986). On the continental shelf is the Alaska Coastal Current (ACC) which is driven westward along the coast by winds and freshwater runoff from the glaciers and rivers of southern Alaska (Royer, 1982; Stabeno et al., 1995, 2004). The GoA is primarily a downwelling system, but as winds relax in summer, short periods of upwelling can occur (Stabeno et al., 2004). Stabeno et al. (2004) found that the El-Niño Southern Oscillation (ENSO) has an effect on the coastal climate of the GoA in that it controls wintertime precipitation which in turn is determining the timing of freshwater runoff. The Pacific Decadal Oscillation (PDO) is thought to have some impact on the weather (temperature and winds) in the GoA, but these signatures are very weak (Stabeno et al., 2004).

Glacial history and paleoceanography

During past glaciations, local glaciers formed in the mountain ranges of southern Alaska and in the eastern Rocky Mountains, and coalesced in the intermediate lowlands to form the regional ice cap known as the Cordilleran Ice Sheet; extending from Washington in the south, to Yukon in the north, and the Bering Sea in the northwest (e.g., Fulton, 1991). The northwestern lobe of the Cordilleran Ice Sheet (NCIS) covered the southern coast of Alaska, bordering on and extending into the Gulf of Alaska (Kaufman & Manley, 2004). Alpine glaciations may have occurred in this region as early as 7 Ma (Lagoe et al., 1993) with the first biofacies indicative of tidewater glaciation in the western Gulf of Alaska encountered between 6.7 and 5 Ma (Lagoe et al., 1993), and the first IRD in the central GoA, observed at 3.5 Ma (Rea & Schrader, 1985). Glaciation around the Gulf of Alaska increased with Northern Hemisphere cooling around 2.5 Ma (Glacial Interval B; Lagoe et al., 1993; Berger et al., 2008) with the most extensive Cordilleran Ice Sheet recently dated to ~2.64 Ma

(Hidy et al., 2013), approximately consistent with the first occurrence of IRD at IODP Exp. 341 distal Surveyor Fan drill Site U1417 at approx. 2.58 Ma (Gulick et al., 2015). Further glacial intensification occurred after the mid-Pleistocene transition (MPT) after ~1 Ma (Glacial Interval C) with glacial advances reaching the GoA shelf edge (Berger et al., 2008; Montelli et al., 2017), forming cross-shelf troughs (e.g., the Hinchinbrook and Yakutat Sea Valleys, and the Kayak and Bering Troughs) that dominate the present day bathymetry of the GoA shelf (Carlson et al., 1982; Elmore et al., 2013).

In contrast to elsewhere in Alaska, little is known regarding the early Wisconsinan extent of the Cordilleran Ice Sheet around the Gulf of Alaska (Kaufman & Manley, 2004; Kaufman et al., 2011). Pre-LGM erosional surfaces have been observed in seismic data from the GoA shelf indicating repeated shelf-wide glacial advances occurring since the mid-Pleistocene (Elmore et al., 2013; Montelli et al., 2017). The Last Glacial Maximum occurred around 23 - 20 kyr ago (Mann & Peteet, 1994; Clapperton, 2000), when several NCIS outlet lobes reached the GoA shelf edge. Ice flow to the shelf edge is thought to have been concentrated in cross-shelf troughs (e.g., Bering Trough, Yakutat Sea Valley) with the shelf areas between troughs possibly remaining ice-free (Elmore et al., 2013). De Vernal & Pedersen (1997) suggested that oceanographic conditions during the LGM were cold with freezing winter conditions and low biogenic fluxes. Based on a foraminiferal oxygen isotope record from the GoA, Praetorius & Mix (2014) suggested that cold and/or salty conditions prevailed in the period between 18 and 16 cal ka BP and that the peak input of IRD occurred between 17.5-16.5 cal ka BP. Glacial stagnation occurred from 16.9 cal ka BP, with glacial retreat starting from 16.6 cal ka BP (Davies et al., 2011) and shortly followed by a warming and/or freshening of surface waters (Praetorius & Mix, 2014). By 14.7 cal ka BP, glaciers had retreated from the shelf into fjords and onto land (Clapperton, 2000; Davies et al., 2011). For the Bølling-Allerød interstadial, de Vernal & Pedersen (1997) and Barron et al. (2009) found indications for a warming in the GoA with laminated sediments and increased surface water productivity. However, according to Addison et al. (2012), the Bølling-Allerød winters may have been cooler than modern winters with seasonal sea ice. During the Younger Dryas (12.9 – 11.7 kyr BP), glaciers re-advanced in southern Alaska (e.g., Briner et al., 2002) and

sea-surface temperatures were once again cool and/or more saline (Davies et al., 2011). From 10-8 cal ka BP, the GoA cooled followed by a gradual warming (Praetorius & Mix, 2014) and increasing surface ocean productivity after 8 kyr BP (de Vernal & Pedersen, 1997). During the Little Ice Age (LIA, AD ~1200 – 1900), glaciers advanced again (e.g., Barclay et al., 2001; Calkin et al., 2001; Elmore et al., 2013) and have been retreating since (Arendt et al., 2002).

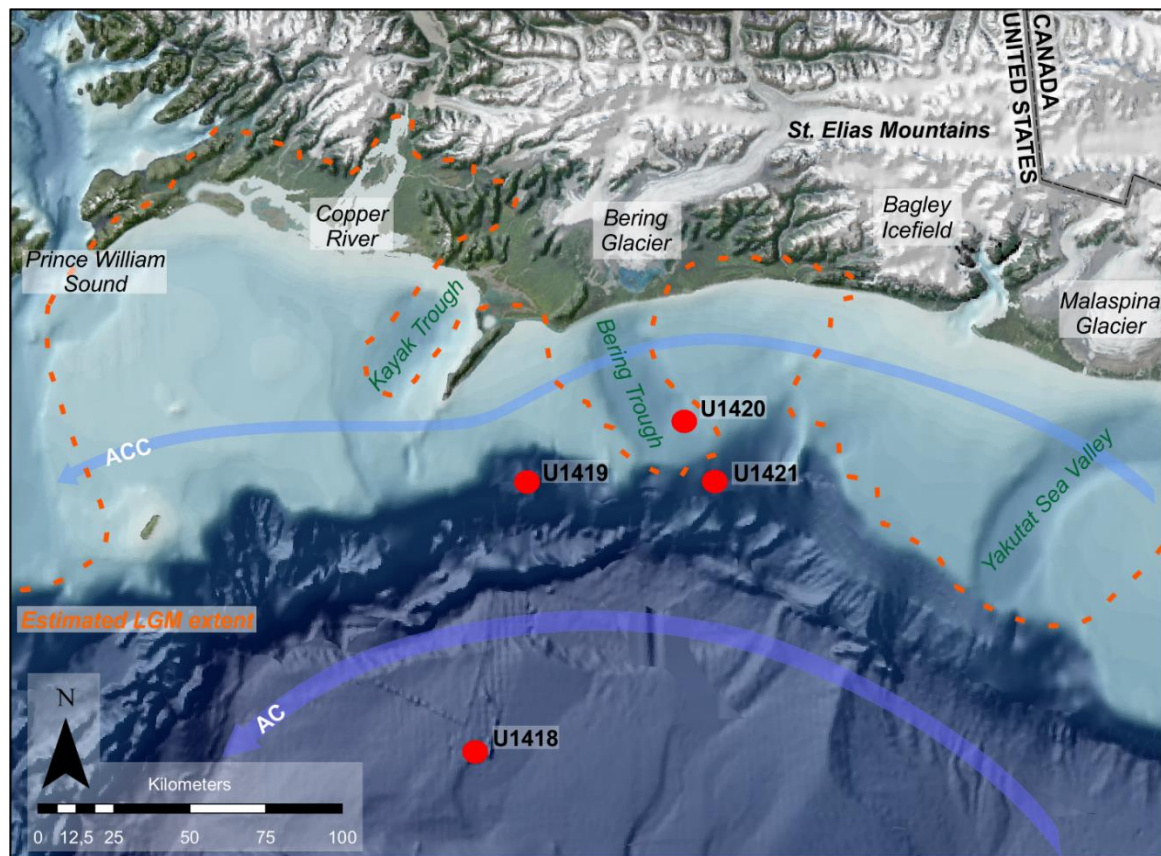


Figure 3: Overview map of the Gulf of Alaska and the IODP Exp. 341 drill Sites (note that Site U1417 is located to the south and not included). Estimated LGM maximum extent from Kaufman et al., 2011. AC= Alaska Current; ACC= Alaska Coastal Current.

PROJECT SETTING AND CONTEXT

As discussed above, paleomagnetic records have several useful and important applications. However, to facilitate a deeper understanding of the temporal and spatial variability of the Earth's magnetic field and its significance for our knowledge about the geodynamo, studies from different parts of the world are needed. Records of high temporal resolution with robust, independent chronologies are especially in demand, not only to allow studies on paleomagnetic variability, but also to improve and calibrate stratigraphic correlations between different proxy records. The North Atlantic region has been the main focus of most paleomagnetic studies (Fig. 1) and improving the global coverage of PSV and RPI records is, therefore, key in order to constrain the spatial and temporal complexity of the geomagnetic field.

The Gulf of Alaska is an excellent location for high-resolution paleoclimate and paleomagnetic studies; the combination of the coastal St. Elias Mountains and the highly erosive glacial systems of southern Alaska has ensured a large flux of terrestrial material to the gulf over millions of years, creating a sedimentary archive with high temporal resolution. This allows detailed studies of the dynamics of the northwestern lobe of the Cordilleran Ice Sheet through time and an opportunity to constrain glacial variations prior to and during the LGM. Furthermore, the terrestrial, fine-grained material rich in magnetic minerals deposited in the GoA should allow studies of changes in the geomagnetic field on millennial timescales and may provide records comparable to the best North Atlantic paleomagnetic records.

International Ocean Drilling Program (IODP) Expedition 341

The International Ocean Drilling Program (IODP) Expedition 341 took place from May 29th to July 29th, 2013 in the Gulf of Alaska, onboard the *JOIDES Resolution*. The Expedition expects to contribute to the understanding of several of the complexities remaining in Neogene climate research and the main objectives of Expedition 341, as stated in the scientific prospectus (Jaeger et al., 2011), are to

- “Document the tectonic response of an active orogenic system to late Miocene to recent climate change;
- Establish the timing of advance and retreat phases of the northwestern Cordilleran Ice Sheet to test its relation to dynamics of other global ice sheets;
- Implement an expanded source-to-sink study of the complex interactions between glacial, tectonic, and oceanographic processes responsible for creation of one of the thickest Neogene high-latitude continental margin sequences;
- Understand the dynamics of productivity, nutrients, freshwater input to the ocean, and surface and subsurface circulation in the northeast Pacific and their role in the global carbon cycle; and
- Document the spatial and temporal behavior during the Neogene of the geomagnetic field at extremely high temporal resolution in an under-sampled region of the globe”

The expedition successfully retrieved more than 3 km of sediment cores from five drilling sites in the GoA continental margin and the adjacent Surveyor Fan (Fig. 3). Multiple holes were drilled at every site to ensure a complete sedimentary record. At each site, the different holes were tied together using shipboard measurements of various sedimentary physical properties (e.g., magnetic susceptibility, color, density, etc.) in order to construct one continuous stratigraphic record (splice). Biostratigraphic, micropaleontological and paleomagnetic analyses during the expedition confirmed that the cores cover the Miocene through Pliocene, Pleistocene and Holocene epochs and that some sites have exceptional sedimentation rates (>380 cm/ka). The Pleistocene sequence is especially thick, indicating that the sediment flux to the GoA was very high during this period. This creates an excellent foundation for further analyses to investigate the climatic, paleomagnetic and tectonic changes of the Pleistocene in high resolution (Jaeger et al., 2014). Sites U1418 and U1419 will be the focus of this thesis and are briefly described below.



Figure 4: The St. Elias Mountains (left; photo credit J. Jaeger), and the JOIDES Resolution (right; photo credit A. Sakaguchi).

Site U1418 ($58^{\circ}46.6095'N$, $144^{\circ}29.5777'W$) is located at a water depth of 3667 m, in the upper part of the Surveyor Fan (Fig. 3). Six holes (A-F) were drilled at this Site, and a core splice of approximately 271 m was created based on the holes A and C-E. Shipboard biostratigraphic and paleomagnetic analyses suggest that this sedimentary sequence covers the past ~ 1 Myr, providing unique insight to this region's paleomagnetic, climatic, and tectonic history (Jaeger et al., 2014). Long-term sedimentation rates (since the mid Pleistocene transition) at Site U1418 have been estimated to 81 cm/kyr (Gulick et al., 2015), but are likely to have been much higher on shorter timescales. The upper 64.6 meters of the U1418 splice were analyzed as part of this PhD project, focusing on the late Pleistocene and Holocene.

Site U1419 ($59^{\circ}31.9297'N$, $144^{\circ}8.0282'W$) is located at a water depth of 687 m, on the upper continental slope between the mouths of the Kayak and Bering cross-shelf troughs; two troughs that are thought to have been formed during the last glacial maximum (e.g., Carlson et al., 1982; Fig. 3). Five holes (A-E) were drilled at this Site and together make up the core splice of 112 m. Preliminary analyses revealed exceptional sedimentation rates of up to 380 cm/kyr covering the late Pleistocene through Holocene (Jaeger et al., 2014). The entire splice from Site U1419 was analyzed in this PhD project.

RESEARCH OBJECTIVES

The overall objective of this thesis is to, based on the Gulf of Alaska sedimentary sequence, construct a paleomagnetic record that will permit a detailed study of the Earth's geomagnetic field dynamics, as well as the evolution of the northwestern Cordilleran Ice Sheet during the late Pleistocene and Holocene in the Gulf of Alaska.

Specific objective 1 – The Gulf of Alaska environmental magnetic record

The first objective of this thesis is to investigate the dynamics of the northwestern Cordilleran Ice Sheet (NCIS) during the late Pleistocene and Holocene using the environmental magnetic record of Site U1419. How do the changes in magnetic properties (e.g., magnetic susceptibility, grain size and mineralogy) reflect changes such as advance and retreat phases of the NCIS? What were the dynamics of the NCIS prior to, and during the LGM? How does the U1419 record complement or add to our current understanding of the glacial history of this region?

Specific objective 2 – The Gulf of Alaska paleomagnetic records

The second objective is to reconstruct late Pleistocene and Holocene geomagnetic variability from the Gulf of Alaska core Sites U1418 and U1419. From these high-resolution records, paleomagnetic directions (inclination and declination) and relative paleointensity will be studied, where permitted, in order to detail millennial-scale geomagnetic variations. How do these records compare with other, independently dated, regional records? What are pronounced similarities or differences? How do these records compare with North Atlantic records and global stacks? What do the Gulf of Alaska paleomagnetic records indicate about the nature of the geomagnetic signal in the northeast Pacific, and what does that reveal about geomagnetic field dynamics?

METHODS

In order to achieve the objectives of this thesis, u-channels were sampled from the presumed pristine center of split cores from the spliced records of Sites U1418 and U1419 (Fig. 5). The sampling took place over a period of two weeks in March 2014 at the IODP Gulf Coast Repository at Texas A&M University in College Station, Texas, USA. A total of 166 u-channels were sampled from Site U1418, of which 53 were analyzed for this PhD project. At Site U1419, 97 u-channels were sampled, all of which were analyzed. In core composite depth below seafloor (CCSF-A), this is equivalent to a 66 m long record at Site U1418, and the entire splice record of 112 m at Site U1419.

Continuous paleomagnetic analyses and magnetic susceptibility measurements were performed at the Paleomagnetism and Marine Geology Laboratory at the *Institut des sciences de la mer de Rimouski* (ISMER) in Rimouski, Canada, and at the Paleo- and Environmental Magnetism Laboratory at Oregon State University (OSU), USA. Discrete magnetic analyses were performed at ISMER. Detailed CT imagery and density information was obtained from each u-channel at *Institut national de la recherche scientifique, Centre Eau Terre Environnement* (INRS-ETE) in Québec City, Canada. Details of these measurements and the treatment of the data obtained is explained in more depth in each chapter. An overview of laboratory analyses performed and parameters obtained is presented in Table 1.



Figure 5: Sampling of u-channels at the IODP Gulf Coast Repository at Texas A&M University in College Station in March 2014.

Table 1: Overview of methods used during this PhD.

Instrument	# of samples		Resolution (cm)	Parameters measured
	U1418	U1419		
2G cryogenic magnetometer	53	97	1	NRM (including paleomagnetic directions) ARM (0.05 mT DC field, 100 mT AF field) ¹ IRM (300 mT) SIRM (950 mT)
	53	97	1	
	53	97	1	
	53	97	1	
Bartington MS2 u-channel loop sensor	53	97	1	Magnetic susceptibility (k_{LF}) ²
Princeton Measurement Corporation MicroMag 2900 alternating gradient force magnetometer (AGM)	54	95	~150	Hysteresis properties (M_s , M_{rs} , H_c , H_{cr}) IRM acquisition curves (on selected samples)
	N/A	9	N/A	
Siemens SOMATOM Definition AS+ 128 CT scanner	53	97	0.04	CT images and density (HU number)

¹Also used to obtain k_{ARM} and MDF_{ARM} .²Analyses performed in three iterations with the means of the three runs presented in the chapters.

THESIS OVERVIEW

This thesis is divided into three chapters where each chapter represents one research paper. Chapter one corresponds to the first objective and is based on Site U1419. Chapters two and three relate to the second objective through studies of Site U1419 and U1418, respectively.

In chapter one, the environmental magnetic record from shelf Site U1419 is interpreted in terms of the glacial dynamics of the north. This high-resolution Site provides insights to the environmental conditions in the Gulf of Alaska during early Marine Isotope Stage 3 (MIS3), as well as the early onset of full glacial conditions.

Velle, J.H., St-Onge, G., Stoner, J.S., Walczak, M.H., Mix, A.C., Jaeger, J.M. and Forwick, M. *A late Pleistocene environmental magnetic record of northwestern Cordilleran Ice Sheet dynamics based on IODP Expedition 341 drill Site U1419 in the Gulf of Alaska.* In prep.

Chapter two explores the high-resolution inclination record from Site U1419. With its high resolution and detailed age model (Walczak et al., in prep), this Site provides a new late Pleistocene inclination record with features that appear to be regionally consistent. This paper also presents the preliminary radiocarbon age model for Site U1418.

Velle, J.H., Walczak, M.H., Reilly, B., St-Onge, G., Stoner, J.S., Fallon, S. and Forwick, M. *A high-resolution late Quaternary inclination record from IODP Expedition 341 drill Site U1419 in the Gulf of Alaska.* In prep.

In the third chapter, the full paleomagnetic vector of Surveyor Fan Site U1418 is reconstructed and compared to other regional records. A comparison between Sites U1418 and U1419 allows for further development of the U1418 age model presented in chapter two and speaks to the advantage of using paleomagnetic records in stratigraphic correlation.

Velle, J.H., St-Onge, G., Stoner, J.S., Walczak, M.H. and Forwick, M. *High-resolution paleomagnetic secular variation and relative paleointensity in the Gulf of Alaska: constraints*

on the late Pleistocene and Holocene stratigraphy of IODP Expedition 341 Site U1418. In prep.

Finally, the conclusions of this thesis are presented. This general discussion will focus on the main results from the three chapters, their implications and limitations, as well as future perspectives.

CONTRIBUTIONS AND COLLABORATIONS

My contribution towards the three chapters of this thesis has been performing the analyses and writing the three chapters. My supervisors G. St-Onge, J. Stoner and M. Forwick have carefully reviewed several iterations of the chapters included in this thesis. The three chapters have also benefitted greatly from the contributions of the co-authors. M. Walczak and A. Mix carried out the radiocarbon analyses and constructed the U1418 and U1419 age models, with support from S. Fallon. B. Reilly organized and stacked the shipboard data used in chapters two and three. J. Jaeger provided useful insights and comments on chapter one.

During the course of my PhD, I have participated in several regional workshops and meetings (GEOTOP, ArcTrain) as well as international conferences (European Geosciences Union, American Geophysical Union, International Sedimentological Congress, *Association francophone pour le savoir*) where I presented results from my three chapters. My contributions at these conferences are outlined below. Furthermore, participation in the second Expedition 341 post-cruise meeting and field trip on the Washington coast provided me with context for this project and allowed me to meet my collaborators. For the course *Nouveaux développements en océanographie* (OCE 92505), I attended the Institute of Rock Magnetism (IRM) summer school at the University of Minnesota, USA. During my PhD, I also participated in the Maria S. Merian Leg 46 in the St. Lawrence Estuary and Gulf, the Labrador Sea and Hudson Strait.

RESEARCH COMMUNICATION

Articles in preparation

Velle, J.H., St-Onge, G., Stoner, J.S., Walczak, M.H., Mix, A.C., Jaeger, J.M. and Forwick, M. A late Pleistocene environmental magnetic record of northwestern Cordilleran Ice Sheet dynamics based on IODP Expedition 341 drill Site U1419 in the Gulf of Alaska. This manuscript will shortly be re-submitted to *Quaternary Science Reviews*.

Velle, J.H., Walczak, M.H., Reilly, B., St-Onge, G., Stoner, J.S., Fallon, S. and Forwick, M. A high-resolution late Quaternary inclination record from IODP Expedition 341 drill Site U1419 in the Gulf of Alaska. This manuscript will shortly be submitted to *Earth and Planetary Science Letters*.

Velle, J.H., St-Onge, G., Stoner, J.S., Walczak, M.H. and Forwick, M. High-resolution paleomagnetic secular variation and relative paleointensity in the Gulf of Alaska: constraints on the late Pleistocene and Holocene stratigraphy of IODP Expedition 341 Site U1418. This manuscript will be submitted to *Earth and Planetary Science Letters*.

Conference contributions

Velle, J.H., St-Onge, G., Stoner, J.S., Mix, A., Walczak, M., Reilly, B. & Forwick, M., 2018. A high-resolution late Quaternary paleomagnetic secular variation record from IODP Expedition 341 drill Site U1418 in the Gulf of Alaska. 20th International sedimentological congress (ISC), August 13 to 17, Québec City, Canada. Talk.

Velle, J.H., St-Onge, G., Stoner, J.S., Mix, A., Walczak, M. & Forwick, M., 2018. Late Pleistocene and Holocene environmental magnetic record of the northwestern Cordilleran Ice Sheet dynamics based on IODP Expedition 341 drill Site U1419 in the Gulf of Alaska. European Geosciences Union (EGU), April 8 to 13, Vienna, Austria. Poster.

- Velle, J.H.**, St-Onge, G., Stoner, J.S., Mix, A., Walczak, M. & Forwick, M., 2017. A 56,000-year environmental magnetic record of the northwestern Cordilleran Ice Sheet dynamics based on IODP Expedition 341 drill Site U1419 in the Gulf of Alaska. GEOTOP annual student meeting, March 24 to 26, Forêt Montmorency, Québec, Canada. Talk.
- Velle, J.H.**, St-Onge, G., Stoner, J.S., Mix, A., Walczak, M., Asahi, H. & Forwick, M., 2016. Ultra-high resolution late Pleistocene paleomagnetic secular variation records from the Gulf of Alaska (IODP Exp. 341 Sites U1418 and U1419). American Geophysical Union (AGU) Fall Meeting, December 12 to 16, San Francisco, California, USA. Poster.
- Velle, J.H.**, St-Onge, G., Stoner, J.S. & Forwick, M., 2015. Paleomagnetism and magnetic properties of IODP Exp. 341 Site U1418. IODP Expedition 341 2nd Post-Cruise Meeting, November 16 to 18, Friday Harbor, Washington, USA. Poster.
- Velle, J.H.**, St-Onge, G., Stoner, J.S., Forwick, M. & IODP Expedition 341 Shipboard Scientists, 2015. Stratigraphie du golfe de l'Alaska au cours de l'Holocène et du Pléistocène supérieur : résultats préliminaires des sites U1418 et U1419 de l'IODP. Association francophone pour le savoir (ACFAS), May 25 to 29, Rimouski, Québec, Canada. Poster.
- Velle, J.H.**, St-Onge, G., Stoner, J.S., Forwick, M., Mix, A., Davies, M. & IODP Exp. 341 shipboard scientists, 2015. Late Pleistocene and Holocene Paleomagnetic Records from the Gulf of Alaska: Preliminary Results of IODP Expedition 341 Sites U1418 and U1419. American Geophysical Union (AGU) Joint Assembly, May 3 to 7, Montréal, Québec, Canada. Poster.
- Velle, J.H.**, St-Onge, G., Stoner, J.S., Forwick, M. & IODP Expedition 341 Shipboard Scientists, 2015. Paleomagnetic record from the Gulf of Alaska: Preliminary results of IODP Expedition 341. GEOTOP annual student meeting, February 13 to 14, Jouvence, Québec, Canada. Poster.

Velle, J.H., St-Onge, G., Stoner, J.S., Forwick, M. & IODP Expedition 341 Shipboard Scientists, 2014. Paleomagnetism and paleoceanography in the Gulf of Alaska. GEOTOP annual student meeting, March 14 to 16, Pohénégamook, Québec, Canada. Poster.

REFERENCES

- Addison, J.A., Finney, B.P., Dean, W.E., Davies, M.H., Mix, A.C., Stoner, J.S. & Jaeger, J.M., 2012.** Productivity and sedimentary ^{15}N variability for the last 17,000 years along the northern Gulf of Alaska continental slope. *Paleoceanography*, **27**, PA1206, doi: 10.1029/2011PA00216
- Arendt, A.A., Echelmeyer, K.A., Harrison W.D., Lingle, C.S: & Valentine, V.B., 2002.** Rapid wastage of Alaska glaciers and their contribution to rising sea level. *Science*, **297**, pp. 382-386, doi: 10.1126/science.1072497
- Barclay, D.J., Calkin, P.E. & Wiles, G., 2001.** Holocene history of Hubbard Glacier in Yakutat Bay and Russell Fiord, southern Alaska. *Geological Society of America Bulletin*, **113(3)**, pp. 388-402, doi: 10.1130/00167606(2001)113<0388:HHOHGI>2.0.CO;2
- Barletta, F., St-Onge, G., Channell, J.E.T., Rochon, A., Polyak, L. & Darby, D., 2008.** High- resolution paleomagnetic secular variation and relative paleointensity records from the western Canadian Arctic: implication for Holocene stratigraphy and geomagnetic field behavior. *Canadian Journal of Earth Sciences*, **45 (11)**, pp. 1265-1281, doi: 10.1139/E08-039
- Barron, J.A., Bukry, D., Dean, W.E., Addison, J.A. & Finney, B., 2009.** Paleoceanography of the Gulf of Alaska during the past 15,000 years: Results from diatoms, silicoflagellates, and geochemistry. *Marine Micropaleontology*, **72**, pp. 176-195, doi: 10.1016/j.marmicro.2009.04.006

- Beer, J., Muscheler, R., Wagner, G., Laj, C., Kissel, C., Kubik, P.W. & Synal, H.-A., 2002.** Cosmogenic nuclides during Isotope Stages 2 and 3. *Quaternary Science Reviews*, **21**, pp. 1129-1139, doi: 10.1016/S0277-3791(01)00135-4
- Berger, A.L., Gulick, S.P., Spotila, J.A., Upton, P., Jaeger, J.M., Chapman, J.B., Worthington, L.A., Pavlis, T.L., Ridgway, K.D., Willems, B.A. & McAleer, R.J., 2008.** Quaternary tectonic response to intensified glacial erosion in an orogenic wedge. *Nature Geoscience*, **1**, pp. 793-799, doi:10.1038/ngeo334
- Bloxham, J., 2000.** The effect of thermal core-mantle interactions on the paleomagnetic secular variation. *Philosophical Transactions of the Royal Society of London. Series A: Mathematical, Physical and Engineering Sciences*, **358**, pp. 1171-1179, doi: 10.1098/rsta.2000.0579
- Briner, J.P., Kaufman, D.S., Werner, A., Caffee, M., Levy, L., Manley, W.F., Kaplan, M.R. & Finkel, R.C., 2002.** Glacier readvance during the late glacial (Younger Dryas?) in the Ahklun Mountains, southwestern Alaska. *Geology*, **30**, pp. 679-682, doi: 10.1130/0091-7613(2002)030<0679:GRDTLG>2.0.CO;2
- Bruhn, R.L., Pavlis, T.L., Plafker, G. & Serpa, L., 2004.** Deformation during terrane accretion in the Saint Elias orogen, Alaska. *Geological Society of America Bulletin*, **116(7-8)**, pp. 771-787, doi: 10.1130/B25182.1
- Calkin, P.E., Wiles, G.C. & Barclay, D.J., 2001.** Holocene coastal glaciation of Alaska. *Quaternary Science Reviews*, **20**, pp. 449-461, doi:10.1016/S0277-3791(00)00105-0
- Carlson, P.R., Bruns, T.R., Molnia, B.F. & Schwab, W.C., 1982.** Submarine valleys in the northeastern Gulf of Alaska: Characteristics and probable origin. *Marine Geology*, **47**, pp. 217-242, doi: 10.1016/0025-3227(82)90070-6
- Caron, M., St-Onge, G., Montero-Serrano, J.C., Rochon, A., Georgiadis, E., Giraudeau, J. & Masse, G., 2018.** Holocene chronostratigraphy of northeastern Baffin Bay based on radiocarbon and palaeomagnetic data. *Boreas*, **48**, pp. 147-165, doi: 10.1111/bor.12346
- Channell, J.E.T., 1999.** Geomagnetic paleointensity and directional secular variation at Ocean Drilling Program (ODP) Site 984 (Bjorn Drift) since 500 ka: Comparisons

- with ODP Site 983 (Gardar Drift). *Journal of Geophysical Research*, **104(B10)**, pp. 22,937-22,951, doi: 10.1029/1999JB900223
- Channell, J.E.T., Xuan, C. & Hodell, D.A., 2009.** Stacking paleointensity and oxygen isotope data for the last 1.5 Myr (PISO-1500). *Earth and Planetary Science Letters*, **283**, pp. 14-23, doi: 10.1016/j.epsl.2009.03.012
- Clapperton, C., 2000.** Interhemispheric synchronicity of Marine Oxygen Isotope Stage 2 glacier fluctuations along the American cordilleras transect. *Journal of Quaternary Science*, **15(4)**, pp. 435-468, doi: 10.1002/1099-1417(200005)15:4<435::AID-JQS552>3.0.CO;2-R
- Clement, B.M., Kent, D.V. & Opdyke, N.D., 1996.** A synthesis of magnetostratigraphic results from Pliocene-Pleistocene sediments cored using the hydraulic piston corer. *Paleoceanography*, **11(3)**, pp. 299-308, doi: 10.1029/95PA03524
- Cowan, E.A., Brachfeld, S.A., Powell, R.D. & Schoolfield, S.C., 2006.** Terrane-specific rock magnetic characteristics preserved in glacial marine sediment from southern coastal Alaska. *Canadian Journal of Earth Sciences*, **43**, pp. 1269-1282, doi: 10.1139/E06-042
- Davies, M.H., Mix, A.C., Stoner, J.S., Addison, J.A., Jaeger, J., Finney, B. & Wiest, J., 2011.** The deglacial transition on the southeastern Alaska Margin: Meltwater input, sea level rise, marine productivity, and sedimentary anoxia. *Paleoceanography*, **26**, PA2223, doi: doi:10.1029/2010PA002051
- de Vernal, A. & Pedersen, T.F., 1997.** Micropaleontology and palynology of core PAR87A-10: A 23,000 year record of paleoenvironmental changes in the Gulf of Alaska, northeast North Pacific. *Paleoceanography*, **12(6)**, pp. 821-830, doi: 10.1029/97PA02167
- Dekkers, M.J., 1997.** Environmental magnetism: an introduction. *Geologie en Mijnbouw*, **76**, pp. 163-182, doi: 10.1023/A:1003122305503
- Deschamps, C.E., St-Onge, G., Montero-Serrano, J.C. & Polyak, L., 2018.** Chronostratigraphy and spatial distribution of magnetic sediments in the Chukchi and

- Beaufort seas since the last deglaciation. *Boreas*, **47** (2), pp. 544-564, doi: 10.1111/bor.12296
- Dorfman, J.M., Stoner, J.S., Finkenbinder, M.S., Abbott, M.B., Xuan, C. & St-Onge, G., 2015.** A 37,000-year environmental magnetic record of aeolian dust deposition from Burial Lake, Arctic Alaska. *Quaternary Science Reviews*, **128**, pp. 81-97, doi: 10.1016/j.quascirev.2015.08.018
- Elmore, C.R., Gulick, S.P.S., Willems, B. & Powell, R., 2013.** Seismic stratigraphic evidence for glacial expanse during glacial maxima in the Yakutat Bay Region, Gulf of Alaska. *Geochemistry Geophysics Geosystems*, **14**(4), pp. 1294-1311, doi: 10.1002/ggge.20097
- Fulton R.J., 1991.** A conceptual model for growth and decay of the Cordilleran Ice Sheet. *Géographie physique et Quaternaire*, 45(3), pp. 281-286, doi: 10.7202/032875ar
- Gallet, Y., Genevey, A. & Le Goff, M., 2002.** Three millennia of directional variation of the Earth's magnetic field in western Europe as revealed by archeological artefacts. *Physics of the Earth and Planetary Interiors*, **131**, pp. 81-89, doi: 10.1016/S0031-9201(02)00030-4
- Gallet, Y., Genevey, A., Le Goff, M., Warmé, N., Gran-Aymerich, J. & Lefèvre, A., 2009.** On the use of archeology in geomagnetism, and vice-versa: Recent developments in archeomagnetism. *Comptes Rendus Physique*, **10**(7), pp. 630-648, doi: 10.1016/j.crhy.2009.08.005.
- Gubbins, D., 1999.** The distinction between geomagnetic excursions and reversals. *Geophysical Journal International*, **137**, pp. F1-F3, doi: 10.1046/j.1365-246x.1999.00810.x
- Guillou, H., Singer, B.S., Laj, C., Kissel, C., Scaillet, S. & Jicha, B.R., 2004.** On the age of the Laschamp geomagnetic excursion. *Earth and Planetary Science Letters*, **227**, pp. 331-343, doi: 10.1016/j.epsl.2004.09.018
- Gulick, S.P.S., Jaeger, J.M., Mix, A.C., Asahi, H., Bahlburg, H., Belanger, C.L., Berbel, G.B.B., Childress, L., Cowan, E., Drab, L., Forwick, M., Fukumura, A., Ge, S., Gupta, S., Kioka, A., Konno, A., LeVay, L.J., März, C., Matsuzaki, K.M.,**

- McClymont, E.L., Moy, C., Müller, J., Nakamura, A., Ojima, T., Ribeiro, F.R., Ridgway, K.D., Romero, O.E., Slagle, A.L., Stoner, J.S., St-Onge, G., Suto, I., Walczak, M.D., Worthington, L.L., Bailey, I., Enkelmann, E., Reece, R. & Swartz, J.M., 2015.** Mid-Pleistocene climate transition drives net mass loss from rapidly uplifting St. Elias Mountains, Alaska. *PNAS*, **112(49)**, pp. 15042-15047, doi: 10.1073/pnas.1512549112
- Guyodo, Y. & Valet, J.-P., 1996.** Relative variations in geomagnetic intensity from sedimentary records: the past 200,000 years. *Earth and Planetary Science Letters*, **143**, pp. 23-36, doi: 10.1016/0012-821X(96)00121-5
- Guyodo, Y. & Valet, J.-P., 1999.** Global changes in intensity of the Earth's magnetic field during the past 800 kyr. *Nature*, 399, pp. 249-252, doi: 10.1038/20420
- Hatfield, R.G., Stoner, J.S., Carlson, A.E., Reyes, A.V. & Housen, B.A., 2013.** Source as a controlling factor on the quality and interpretation of sediment magnetic records from the northern North Atlantic. *Earth and Planetary Science Letters*, **368**, pp. 69-77, doi: 10.1016/j.epsl.2013.03.001
- Hidy, A.J., Gosse, J.C., Froese, D.G., Bond, J.D. & Rood, D.H., 2013.** A latest Pliocene age for the earliest and most extensive Cordilleran Ice Sheet in northwestern Canada. *Quaternary Science Reviews*, **61**, pp. 77-84, doi: 10.1016/j.quascirev.2012.11.009
- Hulot, G., Finlay, C.C., Constable, C.C., Olsen, N. & Manda, M., 2010.** The magnetic field of planet Earth. *Space Science Reviews*, **55(1-4)**, pp. 1-7, doi: 10.1007/s11214-010-9644-0
- Jackson, A., Jonkers, A.R.T. & Walker, M.R., 2000.** Four centuries of geomagnetic secular variation from historical records. *Philosophical Transactions of the Royal Society A*, 358, pp. 957-990, doi: 10.1098/rsta.2000.0569
- Jaeger, J.M., Nittrouer, C.A., Scott, N.D & Milliman, J.D., 1998.** Sediment accumulation along glacially impacted mountainous coastline: north-east Gulf of Alaska. *Basin Research*, **10**, pp. 155-173, doi: 10.1046/j.1365-2117.1998.00059.x

- Jaeger, J., Gulick, S., Mix, A., and Petronotis, K., 2011.** Southern Alaska margin: interactions of tectonics, climate, and sedimentation. *IODP Scientific Prospectus*, **341**, doi:10.2204/iodp.sp.341.2011
- Jaeger, J.M., Gulick, S.P.S., LeVay, L.J., & the Expedition 341 Scientists, 2014.** *Proc. IODP*, 341, College Station, TX (Integrated Ocean Drilling Program).
- Karlin, R. & Levi, S., 1983.** Diagenesis of magnetic minerals of recent haemipelagic sediments. *Nature*, **303**, pp. 327-330, doi: 10.1038/303327a0
- Kaufman, D.S. & Manley, W.F., 2004.** Pleistocene maximum and late Wisconsinan glacier extent across Alaska, U.S.A. *In: Ehlers, J. & Gibbard, P.L. (eds.) 2011. Quaternary Glaciations - Extent and Chronology — Part II, Developments in Quaternary Science*, vol. **2**, pp. 9-27, doi: 10.1016/S1571-0866(04)80182-9.
- Kaufman, D.S., Young, N.E., Briner, J.P. & Manley, W.F., 2011.** Alaska palaeo-glacier atlas (version 2). *In: Ehlers, J., Gibbard, P.L. & Hughes, P.D. (eds.) 2011. Quaternary Glaciations - Extent and Chronology — A Closer Look, Developments in Quaternary Science*, vol. **15**, pp. 427-445, doi: 10.1016/B978-0-444-53447-7.00033-7
- Kent, D.V., Hemming, S.R. & Turrin, B.D., 2002.** Laschamp excursion at Mono Lake? *Earth and Planetary Science Letters*, **3-4**, pp. 151-164, doi: 10.1016/S0012-821X(02)00474-0
- Kissel, C., Laj, C., Labeyrie, L., Dokken, T., Voelker, A. & Blamart, D., 1999.** Rapid climatic variations during marine isotopic stage 3: magnetic analysis of sediments from Nordic Seas and North Atlantic. *Earth and Planetary Science Letters*, **171**, pp. 489-502, 10.1016/S0012-821X(99)00162-4
- Kok, Y.S. & Tauxe, L., 1999.** A relative geomagnetic paleointensity stack from Ontong-Java Plateau sediments for the Matuyama. *Journal of Geophysical Research*, **104(B11)**, pp. 25,401-25,413, doi: 10.1029/1999JB900186
- Korte, M., Brown, M.C., Gunnarson, S.R., Nilsson, A., Panovska, S., Wardinski, I. & Constable, C.G., 2019.** Refining Holocene geochronologies using palaeomagnetic

- records. *Quaternary Geochronology*, **50**, pp. 47-74, doi: 10.1016/j.quageo.2018.11.004
- Lagoë, M.B., Eyles, C.H., Eyles, N. & Hale, C., 1993.** Timing of late Cenozoic tidewater glaciation in the far North Pacific. *Geological Society of America Bulletin*, **105(12)**, pp. 1542-1560, doi: 10.1130/0016-7606(1993)105<1542:TOLCTG>2.3.CO;2
- Laj, C., Kissel, C. & Garnier, F., 1996.** Relative geomagnetic field intensity and reversals for the last 1.8 My from a central equatorial Pacific core. *Geophysical Research Letters*, **23(23)**, pp. 3393-3396, doi: 10.1029/96GL03261
- Laj, C., Kissel, C., Mazaud, A., Channell, J.E.T. & Beer, J., 2000.** North Atlantic palaeointensity stack since 75 ka (NAPIS-75) and the duration of the Laschamp event. *Philosophical Transactions of the Royal Society A*, **358(1768)**, pp. 1009-1025, doi: 10.1098/rsta.2000.0571
- Laj, C., Kissel, C & Beer, J., 2004.** High resolution global paleointensity stack since 75 kyr (GLOPIS-75) calibrated to absolute values. *In: Channell, J.E.T. et al. (eds) Timescales of the Paleomagnetic Field, Geophysical Monograph Series*, vol. **145**, pp. 255-265
- Laj, C., Guillou, H. & Kissel, C., 2014.** Dynamics of the earth magnetic field in the 10-75 kyr period comprising the Laschamp and Mono Lake excursions: New results from the French Chaîne des Puys in a global perspective. *Earth and Planetary Science Letters*, **387**, pp. 184-197, doi: 10.1016/j.epsl.2013.11.031
- Laj, C. & Channell, J.E.T., 2015.** Geomagnetic excursions. *In: Schubert, G. (ed) Treatise on Geophysics volume (Second edition)*, Elsevier, pp. 343-383, doi: 10.1016/B978-0-444-53802-4.00104-4.
- Lascu, I., Feinberg, J.M., Dorale, J.A., Cheng, H. & Edwards, L., 2016.** Age of the Laschamp excursion determined by U-Th dating of a speleothem geomagnetic record from North America. *Geology*, **44(2)**, pp. 139-142, doi: 10.1130/G37490.1
- Levi, S. & Banerjee, S.K., 1976.** On the possibility of obtaining relative paleointensities from lake sediments. *Earth and Planetary Science Letters*, **29**, pp. 219-226, doi: 10.1016/0012-821X(76)90042-X

- Liddicoat, J.C. & Coe, R.S., 1979.** Mono Lake geomagnetic excursion. *Journal of Geophysical Research*, **84(B1)**, pp. 261-271, doi: 10.1029/JB084iB01p00261.
- Lisé-Pronovost, A., St-Onge, G., Gogorza, C., Jouve, G., Francus, P., Zolitschka, B. & the PASADO Science Team, 2014.** Rock-magnetic signature of precipitation and extreme runoff events in south-eastern Patagonia since 51,200 cal BP from the sediments of Laguna Potrok Aike. *Quaternary Science Reviews*, **98**, pp. 110-125, doi:10.1016/j.quascirev.2014.05.029
- Liu, Q., Roberts, A.P., Larrasoaña, J.C., Banerjee, S.K., Guyodo, Y., Tauxe, L. & Oldfield, F., 2012.** Environmental magnetism: Principles and applications. *Reviews of Geophysics*, **50**, RG4002, doi: 10.1029/2012RG000393
- Lund, S.P., Schwartz, M., Keigwin, L. & Johnson, T., 2005.** Deep-sea sediment records of the Laschamp geomagnetic field excursion (~41,000 calendar years before present). *Journal of Geophysical Research*, **110**, B04101, doi: 10.1029/2003JB002943
- Lund, S.P., Stott, L., Schwartz, M., Thunell, R. & Chen, A., 2006.** Holocene paleomagnetic secular variation records from the western Equatorial Pacific Ocean. *Earth and Planetary Science Letters*, **246**, pp. 381-392, doi: 10.1016/j.epsl.2006.03.056
- Lund, S.P., Keigwin, L. & Darby, D., 2016.** Character of Holocene paleomagnetic secular variation in the tangent cylinder: Evidence from the Chukchi Sea. *Physics of the Earth and Planetary Interiors*, **256**, pp. 49-58, doi: 10.1016/j.pepi.2016.03.005
- Lund, S.P., Benson, L., Negrini, R., Liddicoat, J. & Mensing, S., 2017a.** A full-vector paleomagnetic secular variation record (PSV) from Pyramid Lake (Nevada) from 47-17 ka: Evidence for the successive Mono Lake and Laschamp Excursions. *Earth and Planetary Science Letters*, **458**, pp. 120-129, doi: 10.1016/j.epsl.2016.09.036
- Lund, S.P., Schwartz, M. & Stott, L., 2017b.** Long-term palaeomagnetic secular variation and excursions from the western Equatorial Pacific Ocean (MIS2-4). *Geophysical*

- Journal International*, **209**, pp. 587-596, doi: 10.1093/gji/ggx029
- Lund, S.P., 2018.** A new view of long-term geomagnetic field secular variation. *Frontiers in Earth Science*, **6(40)**, doi: 10.3389/feart.2018.00040
- Mann, D.H. & Peteet, D.M., 1994.** Extent and timing of the Last Glacial Maximum in Southwestern Alaska. *Quaternary Research*, **42**, pp. 136-148, doi: 10.1006/qres.1994.1063
- Masarik, J. & Beer, J., 1999.** Simulation of particle fluxes and cosmogenic nuclide production in the Earth's atmosphere. *Journal of Geophysical Research*, **104 D10**, pp. 12,099-12,111, doi: 10.1029/1998JD200091
- Meigs, A. & Sauber, J., 2000.** Southern Alaska as an example of the long-term consequences of mountain building under the influence of glaciers. *Quaternary Science Reviews*, **19**, pp. 1543-1562, doi: 10.1016/S0277-3791(00)00077-9
- Ménabréaz, L., Thouveny, N., Bourlès, D.L., Deschamps, P., Hamelin, B. & Demory, F., 2011.** The Laschamp geomagnetic dipole low expressed as cosmogenic ^{10}Be atmospheric overproduction at ~41 ka. *Earth and Planetary Science Letters*, **312**, pp. 305-317, doi: 10.1016/j.epsl.2011.10.037
- Ménabréaz, L., Bourlès, D.L. & Thouveny, N., 2012.** Amplitude and timing of the Laschamp geomagnetic dipole low from the global atmospheric ^{10}Be overproduction: Contribution of authigenic $^{10}\text{Be}/^9\text{Be}$ ratios in west equatorial Pacific sediments. *Journal of Geophysical Research*, **117 B11101**, doi: 10.1029/2012JB009256
- Molnia, B.F. & Carlson, P.R., 1978.** Surface sedimentary units of northern Gulf of Alaska continental shelf. *The American Association of Petroleum Geologists Bulletin*, **62(4)**, pp. 633-643
- Montelli, A., Gulick, S.P.S., Worthington, L.L., Mix, A., Davies-Walczak, M., Zellers, S.D. & Jaeger, J.M., 2017.** Late Quaternary glacial dynamics and sedimentation variability in the Bering Trough, Gulf of Alaska. *Geology*, **45(3)**, pp. 251-254, doi: 10.1130/G38836.1

- Ness, G.E. & Kulm, L.D., 1973.** Origin and development of Surveyor deep-sea channel. *Geological Society of America Bulletin*, **84(10)**, pp. 3339-3354, doi: 10.1130/0016-7606(1973)84<3339:OADOSD>2.0.CO;2
- Nowaczyk, N.R., Frank, U., Kind, J. & Arz, H.W., 2013.** A high-resolution paleointensity stack of the past 14 to 68 ka from Black Sea sediments. *Earth and Planetary Science Letters*, **384**, pp. 1-16, doi: 10.1016/j.epsl.2013.09.028
- Panovska, S., Constable, C.G. & Brown, M.C., 2018.** Global and regional assessment of paleosecular variation activity over the past 100 ka. *Geochemistry, Geophysics, Geosystems*, **19**, pp. 1559-1580, doi: 10.1029/2017GC007271
- Praetorius, S.K. & Mix, A., 2014.** Synchronization of North Pacific and Greenland climates preceded abrupt deglacial warming. *Science*, **345**, pp. 444-448, doi: 10.1126/science.1252000
- Rea, D.K. & Schrader, H., 1985.** Late Pleistocene onset of glaciation: ice-rafting and diatom stratigraphy of North Pacific DSDP cores. *Palaeogeography, Palaeoclimatology, Palaeoecology*, **49**, pp. 313-325, doi: 10.1016/0031-0182(85)90059-8
- Rea, D.K., Basov, I.A., Krissek, L.A. & the Leg 145 Scientific Party, 1995.** 38 Scientific results of drilling the North Pacific transect. *In: Rea D.K., Basov, I.A., Scholl, D.W. & Allan, J.F. (eds.), Proceedings of the Ocean Drilling Program, Scientific Results, Vol. 145*
- Reece, R.S., Gulick, S.P.S., Horton, B.K., Christeson, G.L. & Worthington, L.L., 2011.** Tectonic and climatic influence on the evolution of the Surveyor Fan and Channel system, Gulf of Alaska. *Geosphere*, **7**, pp. 830-844, doi: 10.1130/GES00654.1
- Reed, R.K. & Schumacher, J.D., 1986.** Physical Oceanography. *In: Hood, D.W., Zimmerman, S.T. (Eds.) The Gulf of Alaska: Physical Environment and Biological Resources.* Ocean Assessment Division, NOAA, USA, pp. 57-75, doi: 10.5962/bhl.title.60759
- Reilly, B.T., Stoner, J.S., Hatfield, R.G., Abbott, M.B., Marchetti, D.W., Larsen, D.J., Finkenbinder, M.S., Hillman, A.L., Kuehn, S.C. & Heil, C.W., 2018.** Regionally

- consistent western North America paleomagnetic directions from 15 to 35 ka: Assessing chronology and uncertainty with paleosecular variation (PSV) stratigraphy, *Quaternary Science Reviews*, **201**, pp. 186-205, doi: 10.1016/j.quascirev.2018.10.016
- Roberts, A.P., Lehman, B., Weeks, R.J., Verosub, K.L. & Laj, C., 1997.** Relative paleointensity of the geomagnetic field over the last 200,000 years from ODP Sites 883 and 884, North Pacific Ocean. *Earth and Planetary Science Letters*, **152**, pp. 11-23, doi: 10.1016/S0012-821X(97)00132-5
- Roberts, A.P., 2008.** Geomagnetic excursions: Knowns and unknowns. *Geophysical Research Letters*, **35**, L17307, doi: 10.1029/2008GL034719
- Robinson, S.G., 1986.** The late Pleistocene palaeoclimatic record of North Atlantic deep-sea sediments revealed by mineral-magnetic measurements. *Physics of the Earth and Planetary Interiors*, **42**, pp. 22-47, doi: 10.1016/S0031-9201(86)80006-1
- Robinson, S.G., Maslin, M.A. & McCave, I.N., 1995.** Magnetic Susceptibility variations in Upper Pleistocene deep-sea sediments of the NE Atlantic: Implications for ice rafting and paleocirculation at the last glacial maximum. *Paleoceanography*, **10(2)**, pp. 221-250, doi: 10.1029/94PA02683
- Royer, T.C., 1982.** Coastal fresh water discharge in the Northeast Pacific. *Journal of Geophysical Research*, **87(C3)**, pp. 2017-2021, doi: 10.1029/JC087iC03p02017
- Simon, Q., Hillaire-Marcel, C., St-Onge, G. & Andrews, J.T., 2014.** North-eastern Laurentide, western Greenland and southern Inuitian ice stream dynamics during the last glacial cycle. *Journal of Quaternary Science*, **29(1)**, pp. 14-26, doi: 10.1002/jqs.2648
- Stabeno, P.J., Reed, R.K. & Schumacher, J.D., 1995.** The Alaska Coastal Current: Continuity of transport and forcing. *Journal of Geophysical Research*, **100(C2)**, pp. 2477-2485, doi:10.1029/94JC02842
- Stabeno, P.J., Bond, N.A., Hermann, A.J., Kachel, N.B., Mordy, C.W. & Overland, J.E., 2004.** Meteorology and oceanography of the northern Gulf of Alaska. *Continental Shelf Research*, **24**, pp. 859-897, doi: 10.1016/j.csr.2004.02.007

- Stoner, J.S., Channell, J.E.T. & Hillaire-Marcel, C., 1996.** The magnetic signature of rapidly deposited detrital layers from the deep Labrador Sea: Relationship to North Atlantic Heinrich layers. *Paleoceanography*, **11(3)**, pp. 309-325, doi: 10.1029/96PA00583
- Stoner, J.S., Channell, J.E.T., Hillaire-Marcel, C. & Kissel, C., 2000.** Geomagnetic paleointensity and environmental record from Labrador Sea core MD95-2024: Global marine sediment and ice core chronostratigraphy for the last 110 kyr. *Earth and Planetary Science Letters*, **183**, pp. 161-177, doi: 10.1016/S0012-821X(00)00272-7
- Stoner, J.S. & St-Onge, G., 2007.** Magnetic stratigraphy in paleoceanography: reversal, excursion, paleointensity and secular variation. *In*: Hillaire-Marcel, C. & De Vernal, A. (eds) Proxies in Late Cenozoic Paleoceanography, Elsevier, pp. 99-138, doi: 10.1016/S1572-5480(07)01008-1
- Stoner, J.S., Channell, J.E.T., Mazaud, A., Strano, S.E. & Xuan, C., 2013.** The influence of high-latitude flux lobes on the Holocene paleomagnetic record of IODP Site U1303 and the northern North Atlantic. *Geochemistry, Geophysics, Geosystems*, **14 (10)**, pp. 4623-4646, doi: 10.1002/ggge.20272
- St-Onge, G., Stoner, J.S. & Hillaire-Marcel, C., 2003.** Holocene paleomagnetic records from the St. Lawrence Estuary, eastern Canada: centennial- to millennial-scale geomagnetic modulation of cosmogenic isotopes. *Earth and Planetary Science Letters*, **209**, pp. 113-130, doi: 10.1016/S0012-821X(03)00079-7
- Tauxe, L., 1993.** Sedimentary records of relative paleointensity of the geomagnetic field: Theory and practice. *Reviews of Geophysics*, **31(3)**, pp. 319-354, doi: 10.1029/93RG01771
- Thompson, R. & Oldfield, F., 1986.** Environmental magnetism. Allen and Unwin, Winchester, Mass.
- Thouveny, N., Moreno, E., Delanghe, D., Candon, L., Lancelot, Y. & Shackleton, N.J., 2000.** Rock magnetic detection of distal ice-rafted debries: clue for the identification of Heinrich layers on the Portuguese margin. *Earth and Planetary Science Letters*, **180**, pp. 61-75, doi: 10.1016/S0012-821X(00)00155-2

- Thouveny, N., Carcaillet, J., Moreno, E., Leduc, G. & Nérini, D., 2004.** Geomagnetic moment variation and paleomagnetic excursions since 400 kyr BP: a stacked record from sedimentary sequences of the Portuguese margin. *Earth and Planetary Science Letters*, **219**, pp. 377-396, doi: 10.1016/S0012-821X(03)00701-5
- Valet, J.-P. & Meynadier, L., 1993.** Geomagnetic field intensity and reversals during the past four million years. *Nature*, **366**, pp. 234-238, doi: 10.1038/366234a0
- Valet, J.-P., 2003.** Time variations in geomagnetic intensity. *Reviews of Geophysics*, **41(1)**, doi: 10.1029/2001RG000104
- Valet, J.-P., Meynadier, L. & Guyodo, Y., 2005.** Geomagnetic dipole strength and reversal rate over the past two million years. *Nature*, **435**, pp. 802-805, doi: 10.1038/nature03674
- Valet, J.-P., Plenier, G. & Herrero-Bervera, E., 2008.** Geomagnetic excursions reflect an aborted polarity state. *Earth and Planetary Science Letters*, **274(3-4)**, pp. 472-478, doi: 10.1016/j.epsl.2008.07.056
- Valet, J.-P., Bassinot, F., Bouilloux, A., Bourlés, D., Nomade, S., Guillou, V., Lopes, F., Thouveny, N. & Dewilde, F., 2014.** Geomagnetic, cosmogenic and climatic changes across the last geomagnetic reversal from Equatorial Indian Ocean sediments. *Earth and Planetary Science Letters*, **397**, pp. 67-79, doi: 10.1016/j.epsl.2014.03.053
- Verosub, K.L. & Roberts, A.P., 1995.** Environmental magnetism: Past, present, and future. *Journal of Geophysical Research*, **100(B2)**, pp. 2175-2192, doi: 10.1029/94JB02713
- Verosub, K.L., Herrero-Bervera, E. & Roberts, A.P., 1996.** Relative geomagnetic paleointensity across the Jaramillo subchron and the Matuyama/Brunhes boundary. *Geophysical Research Letters*, **23(5)**, pp. 467-470, doi: 10.1029/96GL00454
- Walczak, M.H., Stoner, J.S., Mix, A.C., Jaeger, J., Rosen, G.P., Channell, J.E.T., Heslop, D. & Xuan, C., 2017.** A 17,000 yr paleomagnetic secular variation record from the southeast Alaskan margin: Regional and global correlations, *Earth and Planetary Science Letters*, **473**, pp. 177-189, doi: 10.1016/j.epsl.2017.05.022
- Walczak, M.H., Mix, A.C., Fallon, S., Cowan, E., Praetorius, S., Du, J., Hobern, T., Padman, J., Fifield, K., Stoner, J.S., Haley, B., in prep.** Coupled changes in

Northeast Pacific ventilation and Cordilleran Ice Sheet discharge may precede Heinrich Events. *Science*

- Weeks, R.J., Roberts, A.P., Verosub, K.L., Okada, M. & Dubuisson, G.J., 1995.** Magnetostratigraphy of upper Cenozoic sediments from Leg 145, North Pacific Ocean. *In: Rea D.K., Basov, I.A., Scholl, D.W. & Allan, J.F. (eds.), Proceedings of the Ocean Drilling Program, Scientific Results, Vol. 145*
- Yamamoto, Y., Yamazaki, T., Kanamatsu, T., Ioka, N. & Mishima, T., 2007.** Relative paleointensity stack during the last 250 kyr in the northwest Pacific. *Journal of Geophysical Research*, **112**, B01104, doi: 10.1029/2006JB004477
- Yamazaki, T. & Oda, H., 2005.** A geomagnetic paleointensity stack between 0.8 and 3.0 Ma from equatorial Pacific sediment cores. *Geochemistry Geophysics Geosystems*, **6(11)**, doi: 10.1029/2005GC001001
- Yamazaki, T. & Kanamatsu, T., 2007.** A relative paleointensity record of the geomagnetic field since 1.6 Ma from the North Pacific. *Earth Planets Space*, **59**, pp. 785-794, doi: 10.1186/BF03352741
- Yamazaki, T., 1999.** Relative paleointensity of the geomagnetic field during Brunhes Chron recorded in North Pacific deep-sea sediment cores: orbital influence? *Earth and Planetary Science Letters*, **169**, pp. 23-35, doi: 10.1016/S0012-821X(99)00064-3

CHAPTER 1

A LATE PLEISTOCENE ENVIRONMENTAL MAGNETIC RECORD OF NORTHWESTERN CORDILLERAN ICE SHEET DYNAMICS BASED ON IODP EXPEDITION 341 DRILL SITE U1419 IN THE GULF OF ALASKA

1.1 SUMMARY OF CHAPTER 1

In the first chapter, the environmental magnetic record of Site U1419 is explored in order to improve our understanding of the evolution of the northwestern Cordilleran Ice Sheet. The robust age control and high temporal resolution of the U1419 record provides new information about glacial dynamics in this region through the past ~54,000 years.

This chapter, titled “*A late Pleistocene environmental magnetic record of northwestern Cordilleran Ice Sheet dynamics based on IODP Expedition 341 drill Site U1419 in the Gulf of Alaska*” was written by me under the guidance of my supervisor, Guillaume St-Onge, and my co-supervisors Joe Stoner (Oregon State University) and Matthias Forwick (The Arctic University of Norway) who revised several versions of this paper. Maureen Walczak and Alan Mix (Oregon State University), and John Jaeger (University of Florida) contributed with comments and suggestions on a later version of the manuscript. As first author, I performed the analyses, treated and interpreted the data, and wrote the paper. My three supervisors contributed greatly to the realization of this paper through assistance in the lab, help with interpreting data, and comments on the text. Maureen Walczak and Alan Mix constructed the age model that they kindly shared with me. Guillaume St-Onge, Joe Stoner, Matthias Forwick, Maureen Walczak, Alan Mix, and John Jaeger (co-chief scientist) were all part of the shipboard science party during IODP Expedition 341.

Results from this chapter were presented at the annual GEOTOP student meetings in Pohénégamook (2014; poster) and Forêt Montmorency (2017; talk), and at the European Geosciences Union meeting in Vienna (2018; poster).

1.2 A LATE PLEISTOCENE ENVIRONMENTAL MAGNETIC RECORD OF NORTHWESTERN CORDILLERAN ICE SHEET DYNAMICS BASED ON IODP EXPEDITION 341 DRILL SITE U1419 IN THE GULF OF ALASKA

Velle, Julie Heggdal^{a,b,*}; St-Onge, Guillaume^{a,b}; Stoner, Joseph S.^{b,c}; Walczak, Maureen^{c,d}, Mix, Alan C.^c; Jaeger, John M.^e and Forwick, Matthias^f

^a*Canada Research Chair in Marine Geology, Institut des sciences de la mer de Rimouski (ISMER), Université du Québec à Rimouski, Rimouski QC, G5L 3A1, Canada*

^b*GEOTOP Research Center, Montreal QC, Canada*

^c*College of Earth, Ocean, and Atmospheric Sciences, Oregon State University, Corvallis OR97331, United States*

^d*Research School of Earth Sciences, Australian National University, Canberra, ACT, 2601, Australia*

^e*Department of Geological Sciences, University of Florida, Gainesville, FL 32611, United States*

^f*Department of Geosciences, UiT The Arctic University of Norway in Tromsø, Tromsø, 9037, Norway*

**Corresponding author: Julie.Velle@uqar.ca*

ABSTRACT

The 112 m long spliced record from International Ocean Drilling Program (IODP) Expedition 341 continental slope Site U1419 in the Gulf of Alaska was analyzed for physical and magnetic properties in order to better understand the evolution and dynamics of the northwestern Cordilleran Ice Sheet's southern margin during the late Pleistocene. All u-channels were analyzed with a high-resolution CT scanner for the visualization of sedimentary structures and for density estimation. Magnetic measurements include the stepwise AF demagnetization procedure used to study magnetic remanences (natural and laboratory induced), magnetic susceptibility, IRM acquisition curves, and hysteresis loops. These analyses provide information on the sediment's magnetic properties, including magnetic concentration, grain size, and mineralogy. The high-resolution radiocarbon age model for Site U1419 (Walczak et al., in prep) puts the base of the spliced record at ~54,000 cal yr BP. Results indicate that early to mid- Marine Isotope Stage (MIS) 3 was characterized by alternating environmental conditions similar to those previously observed for the deglacial transition (Bølling-Allerød and Younger Dryas), where high productivity intervals characterized by very low magnetic concentration and high coercivity, alternate with periods of stronger glacial influence characterized by high magnetic concentration and low coercivity. The transition into glacial maximum conditions started at ~ 41,800 cal yr BP and lasted until approx. 18,000 cal yr BP. This interval, tentatively named the "Alaskan LGM", was characterized by average sedimentation rates of 250 cm/kyr, that at times exceeded 800 cm/kyr, and persistently high magnetic susceptibility indicating high input of terrigenous material and ice rafted debris (IRD). Larger amplitude variations in magnetic properties from ~25,000 cal yr BP appear to reflect complex sediment transport dynamics at the ice front that could represent several advance and retreat phases of the ice sheet before sustained deglaciation from around 16,800 cal yr BP.

Keywords: Glacial dynamics, environmental magnetism, Alaska, North Pacific, late Pleistocene, Cordilleran Ice Sheet

1.3 INTRODUCTION

Magnetic minerals in sediments reflect the environmental processes they go through both before and after deposition, e.g., soil formation, weathering, and mode of erosion, transport, and accumulation, as well as diagenetic processes (e.g. Thompson & Oldfield, 1986). Modern magnetic measurement methods can detect small quantities of magnetic minerals within a sample and small changes between samples, and such analyses are usually non-destructive and efficient, making insights into past climatic and environmental conditions easily accessible (e.g., Verosub & Roberts, 1995). In the North-Atlantic region, the magnetic susceptibility signature of sediment cores has been used as a method for identifying glacial vs. interglacial (high vs. low magnetic susceptibility) layers, corresponding to periods of high/low Ice-Rafted Debris (IRD) input and low/high carbonate productivity, respectively (Robinson et al., 1995; Stoner et al., 1996). In addition to magnetic susceptibility, rock magnetic properties such as anhysteretic remanent magnetization (ARM) and isothermal remanent magnetization (IRM) have also been used in identification of IRD and Heinrich Layers (Robinson et al., 1995; Stoner et al., 1996; Thouveny et al., 2000). Using a combination of magnetic properties (e.g., hysteresis parameters) the provenance of mineralogical assemblages can be determined, providing information on, for example, past changes in deep-sea circulation (Kissel et al., 1999, 2009) and ice sheet dynamics (e.g., Simon et al., 2014; Hatfield et al., 2016). Compared to the North-Atlantic region, environmental magnetic studies of the North Pacific Ocean are scarce. Cowan et al. (2006) investigated the mineral magnetic signal of the sediment in three glaciated southern Alaskan fjords to develop provenance tracers for the southern Alaskan margin. The study found that no single magnetic parameters can be used to distinguish between different sources, but that

a combination of several parameters can be used as tracers to specific southern Alaskan terranes.

During past glaciations, the Gulf of Alaska was surrounded by an extensive ice cover constituting the northwestern Cordilleran Ice Sheet (NCIS). The proximity to the large moisture source of the North Pacific in combination with the mountainous topography of southern Alaska provided favorable conditions allowing mountain glaciers from the Aleutian Range in the west, the Alaska Range in the north, and the Kenai, Chugach, Wrangell and St. Elias Mountains in the south to coalesce and form the NCIS (e.g., Fulton, 1991; Lagoe et al., 1993; Kaufman & Manley, 2004). With the intensification of Northern Hemisphere glaciations, the NCIS expanded into the Gulf of Alaska initiating repeated shelf edge glaciations from approx. 1 Ma (Berger et al., 2008; Gulick et al., 2015; Montelli et al., 2017). Although the ice cover surrounding the Gulf of Alaska (GoA) was the most extensive in Alaska, very little is known regarding the extent of the NCIS' southern margin prior to the Last Glacial Maximum (LGM). Even during the LGM, advance and retreat cycles into the GoA are poorly constrained and little evidence exists of the timing and dynamics of this portion of the NCIS (e.g., Kaufman & Manley, 2004; Kaufman et al., 2011). Post-LGM and Holocene environmental and oceanographic conditions have been the subject of several studies and are better constrained (e.g. de Vernal & Pedersen, 1997; Barron et al., 2009; Davies et al., 2011; Addison et al., 2012; Praetorius et al., 2015). The 17,400-year high-resolution record of U1419 site survey core EW0408-85JC details the changing environments on the GoA shelf edge during the deglacial transition and Holocene (Davies et al., 2011). This study builds upon the characterization of magnetic properties and sedimentary environments of Davies et al. (2011) and Walczak et al., (2017), and extends the record back to approx. 54,000 cal yr BP. Taking advantage of a detailed radiocarbon age model (Walczak et al., in prep) that defines extremely high rates of sediment accumulation, combined with physical and rock magnetic properties, we provide unique information on glacial dynamics and sedimentary environments of the southern Alaskan margin at an unprecedented temporal resolution.

1.4 STUDY AREA

Geological and oceanographic setting

The Gulf of Alaska is located in the subarctic northern Pacific Ocean, off southern Alaska (Fig. 6). Modern sediment supply to the GoA is dominated by terrigenous material sourced from the southern Alaskan coast, specifically by the Copper River, the Bering and Malaspina glaciers, and rivers and tidewater glaciers draining the Saint Elias Mountains (Fig. 6; e.g., Molnia & Carlson, 1978; Jaeger et al., 1998). These drainage areas cover a complex geological setting, including the Yakutat, Prince William, Chugach, and Wrangelia terranes, as well as the Craig sub-terrane (Silberling et al., 1994). Active mountain building in southern Alaska in combination with periods of intense glaciation have ensured a large flux of sediment to the GoA (e.g., Berger et al., 2008; Gulick et al., 2015; Montelli et al., 2017), with long-term sedimentation rates in the Bering Trough (Site U1421; Fig. 6) estimated to as much as 5-10 m/kyr (Montelli et al., 2017), and 200-300 cm/kyr on the slope (Sites U1419 and U1420; Fig. 6; Gulick et al., 2015).

The oceanographic setting in the GoA is dominated the Alaska Current (AC), a branch of the Pacific subarctic gyre that flows westward in the ocean basin of the GoA. As the AC reaches the Kenai Peninsula, it turns south-west and continues along the North Pacific margin and the Alaska Peninsula as the Alaskan Stream. On the continental shelf is the Alaska Coastal Current (ACC) which is driven westward along the coast by winds and freshwater runoff from the glaciers and rivers of southern Alaska (Fig. 6; Royer, 1982; Stabeno et al., 1995, 2004).

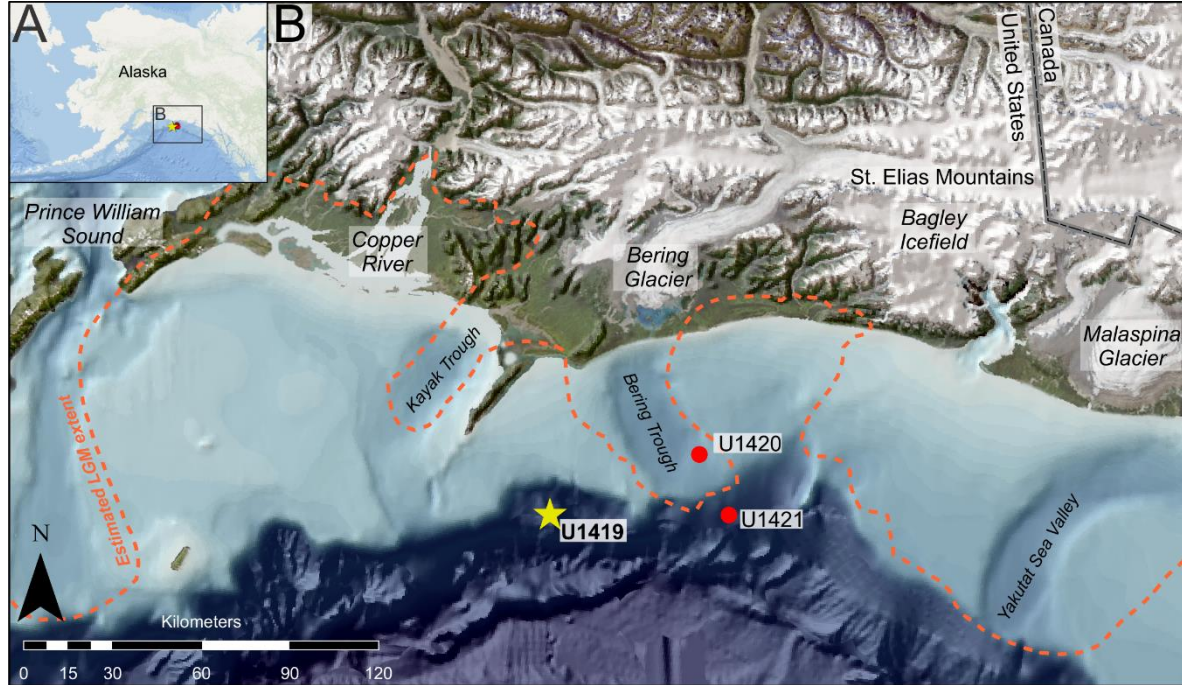


Figure 6: Map of the Gulf of Alaska with Site U1419 (yellow star) and other Expedition 341 drill Sites (red circles). The estimated LGM extent (from Kaufman & Manley, 2004) is outlined with an orange dashed line. The location of Site U1419 also marks the location of core EW0408-85JC mentioned in the text.

The northwestern Cordilleran Ice Sheet (NCIS)

In contrast to elsewhere in Alaska, the early Wisconsinian extent of the Cordilleran Ice Sheet around the GoA is poorly constrained (Kaufman & Manley, 2004; Kaufman et al., 2011). Seismic studies of the Bering Trough show a dynamic history of the Bering Glacier, the largest outlet glacier of the NCIS, with at least three shelf-break advances since the onset of the last glacial cycle (Montelli et al., 2017). The Last Glacial Maximum occurred around 23-20 kyr ago (Mann & Peteet, 1994; Mann & Hamilton, 1995; Clapperton, 2000), when several NCIS outlet lobes reached the GoA shelf edge. Ice flow to the shelf edge is thought to have been concentrated in cross-shelf troughs (e.g., Bering Trough, Yakutat Sea Valley)

with the shelf areas between troughs possibly remaining ice-free (Elmore et al., 2013). De Vernal & Pedersen (1997) suggested that oceanographic conditions during the LGM were cold with freezing winter conditions and low biogenic fluxes. Marine terminating glaciation, as recorded by high rates of IRD delivery to the margin, and cold/salty marine conditions prevailed until ~17 cal ka BP, when glaciers showed early signs of stagnation (Davies et al., 2011; Davies-Walczak et al., 2014). By ~16.5 cal ka BP, glacier retreat had fully commenced, accompanied by warming regional surface waters (Davies et al., 2011; Praetorius et al., 2015). By 14.7 cal ka BP, glaciers had retreated from the shelf into fjords and onto land (Clapperton, 2000; Davies et al., 2011). For the Bølling-Allerød interstadial, de Vernal & Pedersen (1997) and Barron et al. (2009) found indications for a warming in the GoA with laminated sediments and increased surface water productivity. However, according to Addison et al. (2012), the Bølling-Allerød winters may have been cooler than modern winters with formation of seasonal sea ice. During the Younger Dryas (12.9-11.7 kyr BP), glaciers re-advanced in southern Alaska (e.g., Briner et al., 2002) and sea-surface temperatures were once again cool and/or more saline (Davies et al., 2011; Praetorius et al., 2015). A cooling in the GoA from 10-8 cal ka BP was followed by a gradual warming (Praetorius et al., 2015) and increasing surface ocean productivity after 8 kyr BP (de Vernal & Pedersen, 1997). During the Little Ice Age (LIA, AD ~1200-1900), glaciers advanced again (e.g., Calkin et al., 2001; Elmore et al., 2013) and have been retreating since (Arendt et al., 2002).

1.5 METHODS

Coring and sampling

The International Ocean Drilling Program (IODP) Expedition 341 took place in the Gulf of Alaska from May 29th to July 29th, 2013, onboard the *JOIDES Resolution*. The expedition successfully retrieved more than 3 km of sediment cores from five drilling sites on the GoA continental margin and the adjacent Surveyor Fan (Jaeger et al., 2014). Five

holes at Site U1419 (59°31.9297'N; 144°8.0282'W) were drilled at a water depth of 687 meters, on the continental slope between the mouths of the Kayak and Bering cross-shelf troughs (Fig. 6). Based upon shipboard measurements of various sedimentary physical properties (e.g., magnetic susceptibility, color, density, etc.) a continuous stratigraphic record (splice) consisting mostly of sections from holes D and E, but also using holes A, B and C, was established. The depth scale used in this paper is the composite depth below seafloor, or CCSF-A, which assumes that the mudline in the first core section of one hole (U1419B-1H-1A) is the sediment/water interface and allows direct comparison with other measurements made at 1-cm intervals. This depth scale is, however, not corrected for sediment expansion during coring as in CCSF-B (c.f. Jaeger et al., 2014). The splice of Site U1419 comprises the sediment between 0 m CCSF-A (mudline) and 112.1 m CCSF-A.

The u-channel sampling was performed at the IODP Gulf Coast Repository at Texas A&M University in College Station, Texas, USA. U-channels were sampled from the presumably pristine center of split cores using plastic liners with cross-sections of 2x2 cm and lengths up to 1.5 meter. A high density of clasts and compacted sediment prevented the sampling of the intervals between 86.08–89.3 m CCSF-A, 90.2–91.6 m CCSF-A, and the very bottom of the splice from 111.4–112.1 m CCSF-A.

Physical properties

Information on the sediment's physical properties (density), internal structures, and possible coring and/or sampling deformation was obtained using a Siemens SOMATOM Definition AS+ 128 CT scanner at *Institut national de la recherche scientifique, Centre Eau Terre Environnement* (INRS-ETE) in Québec City, Canada. The scanner is capable of detecting density changes as small as 0.1%. Its source/detector rotates in a helicoidal motion around the sample, creating high-resolution (sub-millimeter) images from each rotation. Images were acquired at 0.4 mm intervals with 0.2 mm overlap from one image to another. CT-number profiles were derived for each image and these reflect density changes within the

sediment (e.g., Stoner & St-Onge, 2007; Fortin et al., 2013). The CT-numbers are presented using the Hounsfield scale (HU units; Hounsfield, 1973), spanning from -1024 (density of air) to 3071 HU, where 0 HU is the density of water (e.g., Duchesne et al., 2009; Fortin et al., 2013).

Continuous magnetic measurements

Remanence measurements were performed using 2G Enterprises™ model 755-1.65UC superconducting rock magnetometer at the Paleomagnetism and Marine Geology Laboratory at *Institut des sciences de la mer de Rimouski* (ISMER) in Rimouski, Canada, and at the Paleo-and Environmental Magnetism Laboratory at Oregon State University (OSU), USA. Stepwise alternating field (AF) demagnetization was used to study the natural remanent magnetization (NRM) and laboratory remanent magnetizations. Paleomagnetic results from this study will be presented elsewhere. The u-channel measurements were performed at 1 cm intervals and have a response function with a width at half height of 7-8 cm (Oda & Xuan, 2014). Therefore, the first and last 5 cm of each u-channel were excluded to reduce the edge effect associated with section breaks (Weeks et al., 1993).

Anhyseretic remanent magnetization (ARM) was obtained by implementing a DC biasing field (0.05 mT) on the alternating field (100 mT). Isothermal remanent magnetization (IRM) and saturated isothermal remanent magnetization (SIRM) were induced by using a 2G pulse magnetizer with intensities of 300 and 950 mT, respectively. The u-channels were measured and subsequently demagnetized using peak AF fields of 10, 20, 25, 30, 35, 40, 45, 50 and 60 mT for ARM and IRM, and 0, 10, 30, and 50 mT for SIRM.

Low-field magnetic susceptibility (k_{LF}) analyses were performed in three iterations using a three second measurement period at increments of 1 cm with a Bartington MS2 u-channel loop sensor on a purpose-built automated tracking system at Oregon State

University, USA. Repeated measurements generated the same result for all u-channels, and the values reported in this paper are a mean of three iterations.

Discrete magnetic measurements

Small, discrete samples were collected from the base of each u-channel and analyzed with a Princeton Measurement Corporation MicroMag 2900 alternating gradient force magnetometer (AGM) at ISMER to obtain information on the sediment's hysteresis properties, including coercivity (H_c), coercivity of remanence (H_{cr}), saturation magnetization (M_s), and saturation remanence (M_r). The para/diamagnetic contribution in the samples were corrected for using the MicroMag AGM software. These properties reveal information on the sediment's magnetic mineralogy and grain size (e.g., Day et al., 1977; Dunlop et al., 2002a, 2002b; Peters & Dekkers, 2003).

Constructed ratios as environmental magnetic proxies

The remanent magnetizations ARM and IRM, as well as low-field magnetic susceptibility (k_{LF}) are parameters that reflect the concentration and grain size(s) of the magnetic material within the sample. Similarly, the ARM susceptibility (k_{ARM}) is indicative of magnetic grain size and concentration and is obtained by normalizing the ARM by the biasing field. k_{ARM} is more sensitive to single domain (SD) and smaller pseudo-single domain (PSD) grains and, along with magnetic susceptibility (k_{LF}), which is more sensitive to larger grains (PSD and MD), the k_{ARM}/k_{LF} ratio and a k_{ARM} versus k_{LF} plot can therefore be used as an indicator of relative variations in magnetic grain-size (Banerjee et al., 1981; King et al., 1982, 1983; Verosub & Roberts, 1995; Geiss & Banerjee, 2003). M_r/M_s and H_{cr}/H_c are also useful parameters for magnetic grain size, especially if the sediment is known to consist mainly of magnetite and/or titanomagnetite (Day et al., 1977; Tauxe, 1993; Stoner et al.,

1996; Stoner & St-Onge, 2007). The median destructive field (MDF) was determined using the AF demagnetization data and corresponds to the AF required to reduce the initial remanent magnetization by half. The MDF (MDF_{ARM}) gives insight into the coercivity of the magnetic minerals activated and can, therefore, be used to investigate the sediment's magnetic mineralogy and grain-size. The interpretation of the constructed ratios assumes a magnetic mineralogy dominated by magnetite (e.g., Banerjee et al., 1981).

Age model

The age model for Site U1419 (Fig. 7) is presented by Walczak et al. (in prep) and is based on both radiocarbon dates from Site U1419 as well as on gamma-ray attenuation bulk density (GRA) tie-points to the independently dated site survey core EW0408-85JC (Fig. 6) within the Holocene (Davies-Walczak et al., 2014). BChron (Haslett & Parnell, 2008) was used to generate an age model informed by all planktic foraminiferal dates, although the ΔR value was allowed to vary reflecting the paired benthic radiocarbon data available for this Site. Changes in surface ocean reservoir age were estimated using a simple one-dimensional vertical circulation box model assuming modern mixing (calculated as diffusion) with an input watermass age at 800-1000 m depth informed by the benthic ages. These results were then used to generate a time transient site-specific estimate of the ΔR value, averaging 330 ± 260 years over the past ~45,000 cal yr BP (Walczak et al., in prep). All dates were converted to calendar ages using the MARINE 13 calibration curve (Reimer et al., 2013).

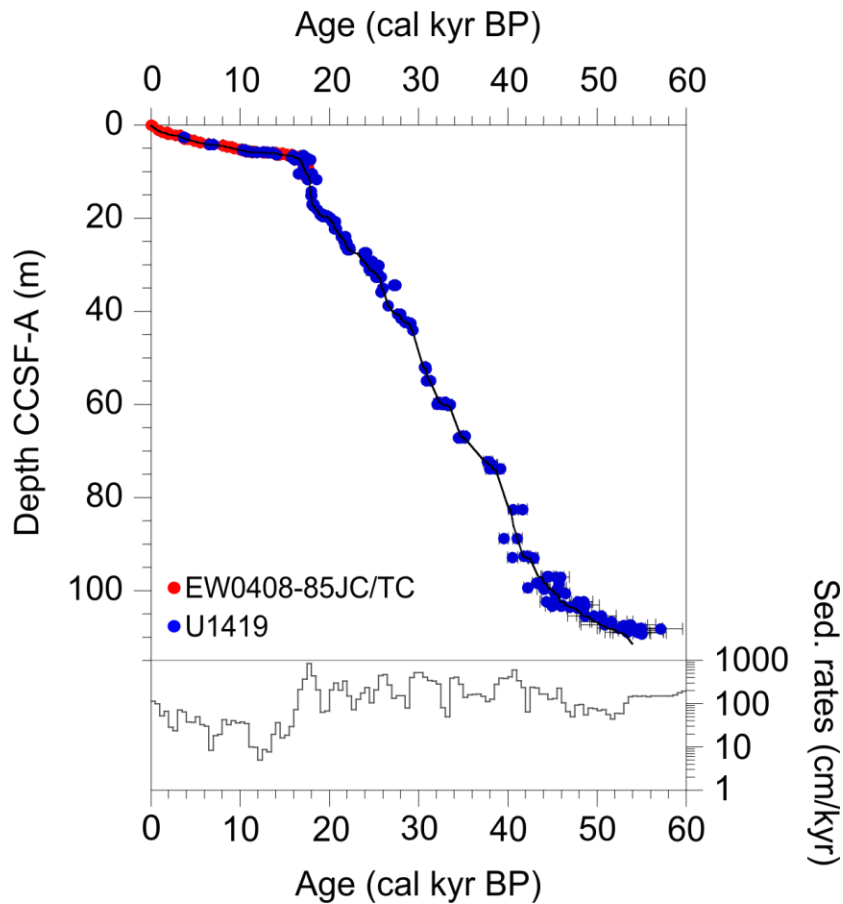


Figure 7: Age model for Site U1419 (Walczak et al., in prep). Blue circles indicate radiocarbon dated intervals from Site U1419. Red circles indicate GRA tie-points to core EW0408-85JC and TC (cf. Fig. 6). Sedimentation rates (cm/kyr) averaged over 500 years below.

1.6 RESULTS

Physical properties and lithology

Based on the magnetic properties observed in this study, the Site U1419 splice is divided into three units. The CT density of the Site is presented in Fig. 8, and selected CT images with representative lithologies are shown in Figure 9. Table 2 summarizes the

lithology and magnetic properties of the units. Lithologies for Units I and II are based on the lithofacies as described by Penkrot et al., 2018. Lithology for Unit III is described here.

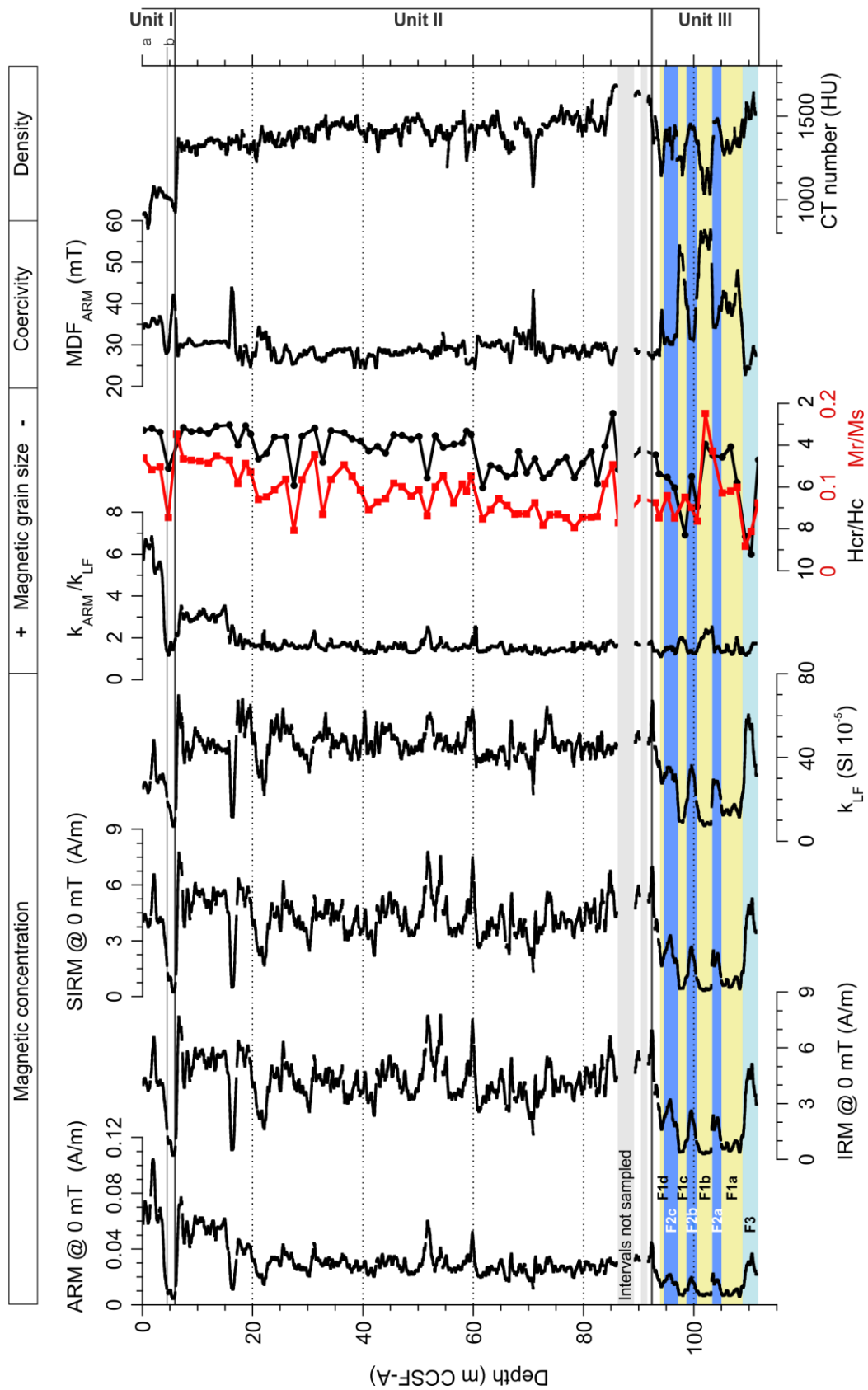
The density of Unit III, in the lowest part of the measured section (111.5-92.5 m CCSF-A), varies between 1050 and 1650 HU. The lithology is characterized as a diamict with varying clast content, and three intervals of lower-density (1050-1200 HU) massive or stratified mud with scattered clasts, as well as a shorter (~60 cm) interval of laminated mud (Jaeger et al., 2014). The boundary to the overlying Unit II (92.5-6.3 m CCSF-A) is defined by an abrupt shift to a higher density (between 1100 and 1700 HU) diamict. With some variations in density and clast content, from clast-poor to clast-rich, this general lithology continues throughout Unit II, although occasionally interrupted by shorter intervals of lower-density (1100-1200 HU) stratified or laminated mud with few clasts (at 76.6-75.7, 71.2-70.7, and 42.9-42.6 m CCSF-A), as well as intervals of stratified sands and/or diamict (cf. Penkrot et al., 2018). Unit I (6.3-0 m CCSF-A) is divided into two subunits; Unit Ib (6.3-4.0 m CCSF-A) and Unit Ia (4.0-0 m CCSF-A). The lowermost ~72 cm of Unit Ib are characterized by low-density, laminated mud without clasts or macrofossils (approx. 45 cm; Fig. 9), overlain by a high-density layer containing very few clasts (approx. 12 cm), followed by another interval of sub-laminated mud (approx. 15 cm). The remaining part of Unit Ib as well as Unit Ia are generally characterized by lower density (800-1100 HU) massive mud (cf. Penkrot et al., 2018). Four 10 - 25 cm thick layers of somewhat higher density (1000-1100 HU) occur within Unit Ia, some of which contain small clasts (Fig. 9).

Table 2: Depth, age, selected magnetic parameters and lithology characteristic for the units and facies described in the text.

Unit	Depth (m CCSF-A)	Age (cal kyr BP) ^a	ARM (10 ⁻³ A/m)	IRM (A/m)	K _{LF} (10 ⁻⁵ SI)	MDF _{ARM} (mT)	Lithology ^b
Ia	0.0-4.0	Present-6.2	69 ± 18	4 ± 0.9	31 ± 8	35 ± 1	Massive mud
Ib	4.0-6.3	6.2-14.7	11 ± 6	1 ± 0.08	16 ± 7	30-50*	Laminated
II	6.3-92.5	14.7-41.8	30 ± 10	4 ± 1	46 ± 10	29 ± 3	Diamict, sandy diamict, stratified diamict
III	92.5-111.5	41.8-54.0	15 ± 8	2 ± 1	25 ± 15	38 ± 10	
F3			~27	~4	~50	~26	Diamict
F2			~16	~2	~27	~35	Diamict
F1			~9	~1	~10	~55	Laminated/ stratified

^aAges from Walczak et al., in prep. ^bLithofacies from Penkrot et al., 2018. *Range presented instead of mean due to large fluctuations within unit (see text).

Figure 8 (next page): Site U1419 magnetic remanence (ARM, IRM and SIRM) and magnetic susceptibility (k_{LF}), k_{ARM}/k_{LF}, hysteresis properties, MDF_{ARM}, and CT density against CCSF-A depth in meters. Magnetic proxies are indicated in top panels, and units referred to in the text are indicated in side panels. Facies described in the text are indicated in different colors.



Magnetic properties

Fig. 8 presents a compilation of the laboratory magnetic remanence data, properties, and constructed ratios of the sediment sequence of Site U1419. Table 2 presents mean magnetic properties for each unit and facies described in the text.

Unit III. Unit III (111.5-92.5 m CCSF-A) is characterized by generally weak magnetic remanence with mean intensities of 0.015 ± 0.008 A/m for ARM, 1.77 ± 1.39 A/m for IRM, and 1.82 ± 1.41 A/m for SIRM. Lower magnetic susceptibilities (mean of $25.3 \times 10^{-5} \pm 14.7 \times 10^{-5}$ SI) are also observed. Generally high values for MDF_{ARM} (mean of 37.9 ± 9.9 mT) indicate higher coercivity than in the overlying units. Changes in magnetic properties generally occur at the same depth intervals within this unit and are grouped into three different facies. The largest peaks in magnetic remanence and susceptibility are observed at the base of the record, between 111-109 m CCSF-A, and are coincident with lower MDF_{ARM} than observed in the rest of Unit III and defines facies 3 (F3). Facies 2 (F2) contains peaks in magnetic susceptibility ($\sim 40 \times 10^{-5}$ SI) between 105-103, 101-99, and 97-94.7 m CCSF-A that coincide with stronger remanence intensities and lower coercivity. Facies 1 (F1) is characterized by magnetic susceptibility lows (between 8 and 10×10^{-5} SI) at 109-105, 103-101, 99-97, and 94.7-93.9 m CCSF-A that are concurrent with similar lows in magnetic remanence, and peaks in MDF_{ARM} (between 50 and 60 mT). The k_{ARM}/k_{LF} ratio (Fig. 8) suggests that there are small variations of magnetic grain size with the alternations, and that F1 intervals are magnetically finer grained. Large amplitude variations are observed in the hysteresis parameters H_{cr}/H_c and M_r/M_s (Fig. 8) that appear to reflect the changes observed from u-channel data. However, the sampling resolution in this interval is too low to determine if these changes are precisely synchronous. The shapes of the hysteresis loops from this unit are consistent with magnetite (Fig. 10; Tauxe et al., 1996). Hysteresis data from Unit III are scattered in the PSD and MD regions of the Day plot (Fig. 10). A Banerjee et al. (1981) plot (Fig. 11) suggests that Unit III samples vary in magnetic grain size from 0.2 to over 5 μm using the King et al. (1983) calibrations (Fig. 11).

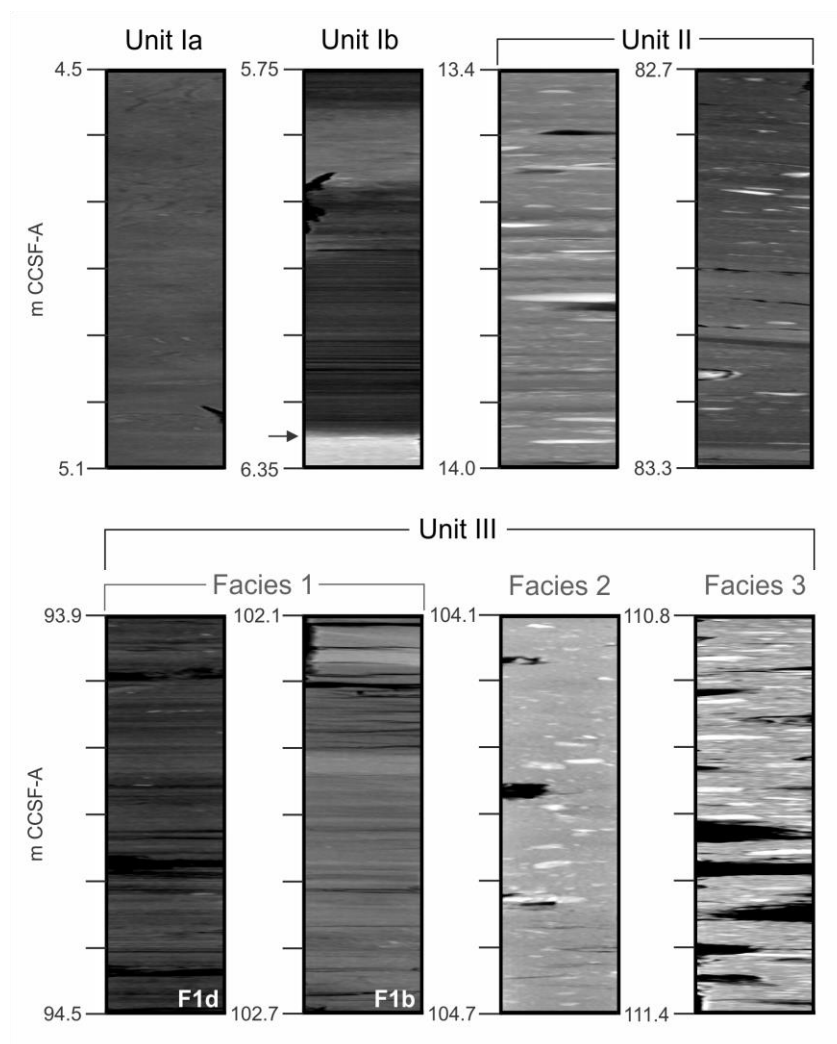


Figure 9: U-channel CT scan images from Site U1419 showing examples of different lithologies observed in Site U1419 and described in the text. Brighter/darker intervals reflect higher/lower density, respectively. The arrow indicates the transition between Unit II and Unit Ib at 6.3 m CCSF-A.

Unit II. The transition to Unit II (from 92.5 m CCSF-A) is marked by a more than two-fold increase in magnetic remanences with means of 0.03 ± 0.01 A/m for ARM, 4.32 ± 1.35 A/m for IRM, and 4.34 ± 1.34 A/m for SIRM. Similarly, magnetic susceptibility is

consistently higher, (mean of $46 \times 10^{-5} \pm 10 \times 10^{-5}$ SI) in Unit II. $k_{\text{ARM}}/k_{\text{LFF}}$ with a mean of 1.75 ± 0.44 is generally lower and with less variability, as is MDF_{ARM} 28.9 ± 2.8 mT. The hysteresis parameters $H_{\text{cr}}/H_{\text{c}}$ and $M_{\text{r}}/M_{\text{s}}$ are similar to those of Unit III, but with less variability (Fig. 8). Hysteresis loops from this unit display a shape typical of magnetite (Fig. 10; Tauxe et al., 1996). Hysteresis data in Unit II plot parallel to, but slightly above, the PSD-MD magnetite mixing line (Dunlop, 2002a, 2002b) in a Day et al. (1977) plot (Fig. 10). In the Banerjee et al. (1981) plot (Fig. 11), using the calibration of King et al. (1983), most samples from Unit II plot between $0.2 \mu\text{m}$ to over $5 \mu\text{m}$, with a few samples plotting below $0.2 \mu\text{m}$.

Smaller-amplitude variations in magnetic properties than in Unit III are observed throughout Unit II, with some covariation observed between the different magnetic properties. Magnetic susceptibility peaks above the Unit II mean (around $50\text{-}60 \times 10^{-5}$ SI) tend to correspond with MDF_{ARM} values slightly below the mean ($25\text{-}27$ mT), as well as with increases in $k_{\text{ARM}}/k_{\text{LFF}}$ (varying between 1.75 and 2.7), at 74.2-73.0, 66.9-66.8, 60.4-58.6, and 52.8-51.6 m CCSF-A with the two latter intervals being especially pronounced in $k_{\text{ARM}}/k_{\text{LFF}}$ (Fig. 8). Other variations within Unit II include a large increase in MDF_{ARM} (up to 40-45 mT), coincident with a decrease in magnetic susceptibility (down to $\sim 30 \times 10^{-5}$ SI) and concentration parameters, between 71.2 and 70.7 m CCSF-A.

Larger fluctuations in magnetic properties are observed above approx. 31 m CCSF-A. Peaks in $k_{\text{ARM}}/k_{\text{LFF}}$ (2-2.5) coincide with intervals of somewhat lowered magnetic remanence and susceptibility ($35\text{-}40 \times 10^{-5}$ SI), as well as somewhat higher MDF_{ARM} (30-35 mT), at 31.0-28.8, and 22.6-20.0 m CCSF-A (Fig. 8). Between 16.8 and 15.9 m CCSF-A, a drop in remanent magnetizations is concurrent with a decrease in magnetic susceptibility (down to $\sim 10 \times 10^{-5}$ SI), an increase in MDF_{ARM} to 40-45 mT, as well as an increase in $k_{\text{ARM}}/k_{\text{LFF}}$ (up to 2.5). At 15.1 m CCSF-A, $k_{\text{ARM}}/k_{\text{LFF}}$ increases further, reaching the highest values observed within Unit II, varying between 2.7 and 3.7. High $k_{\text{ARM}}/k_{\text{LFF}}$ is maintained until 6.8 m CCSF-A. In the same interval, magnetic susceptibility is close to the mean (between 40 and 50×10^{-5} SI), whereas MDF_{ARM} is slightly above the Unit II mean varying around 30 mT.

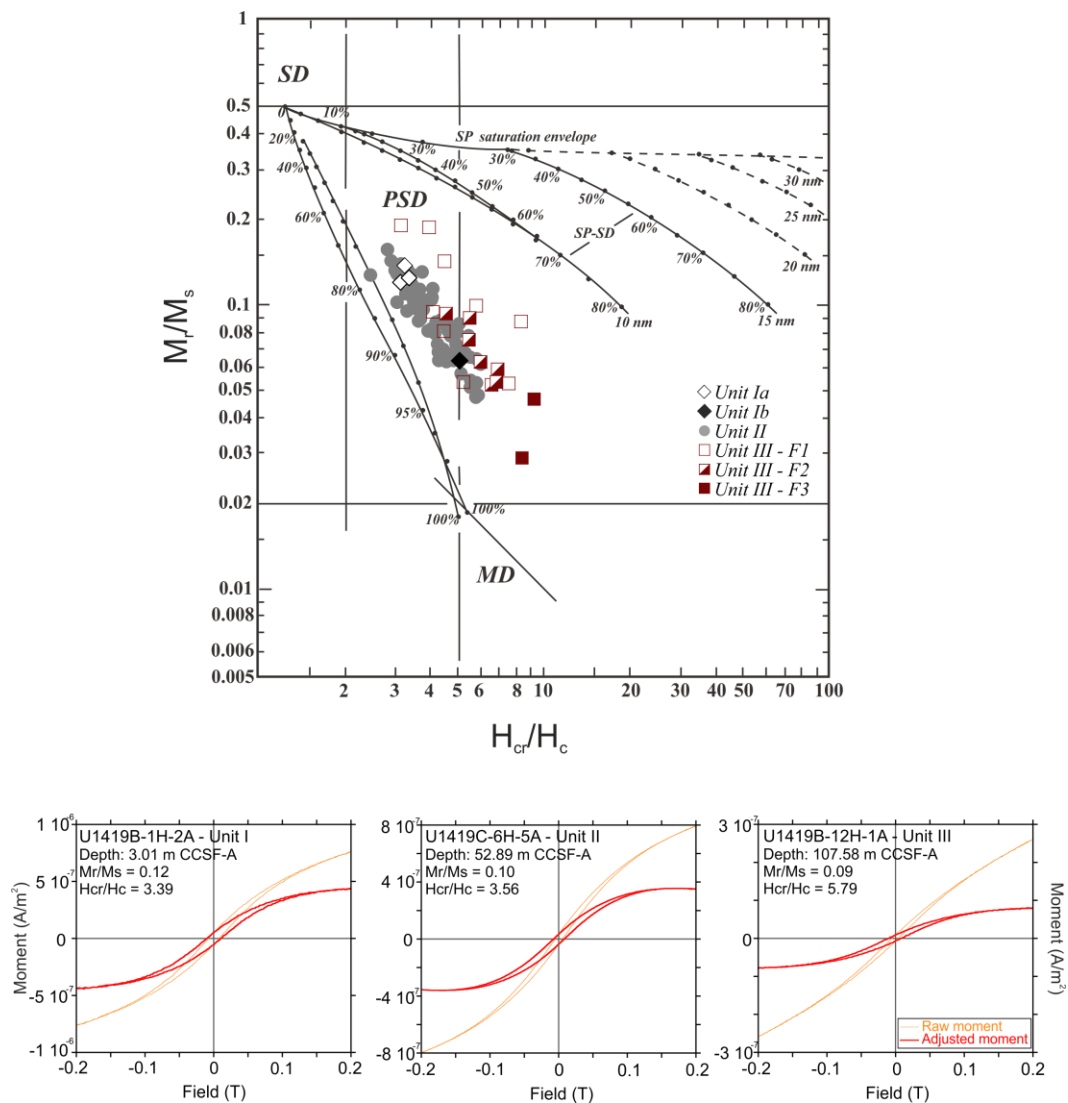
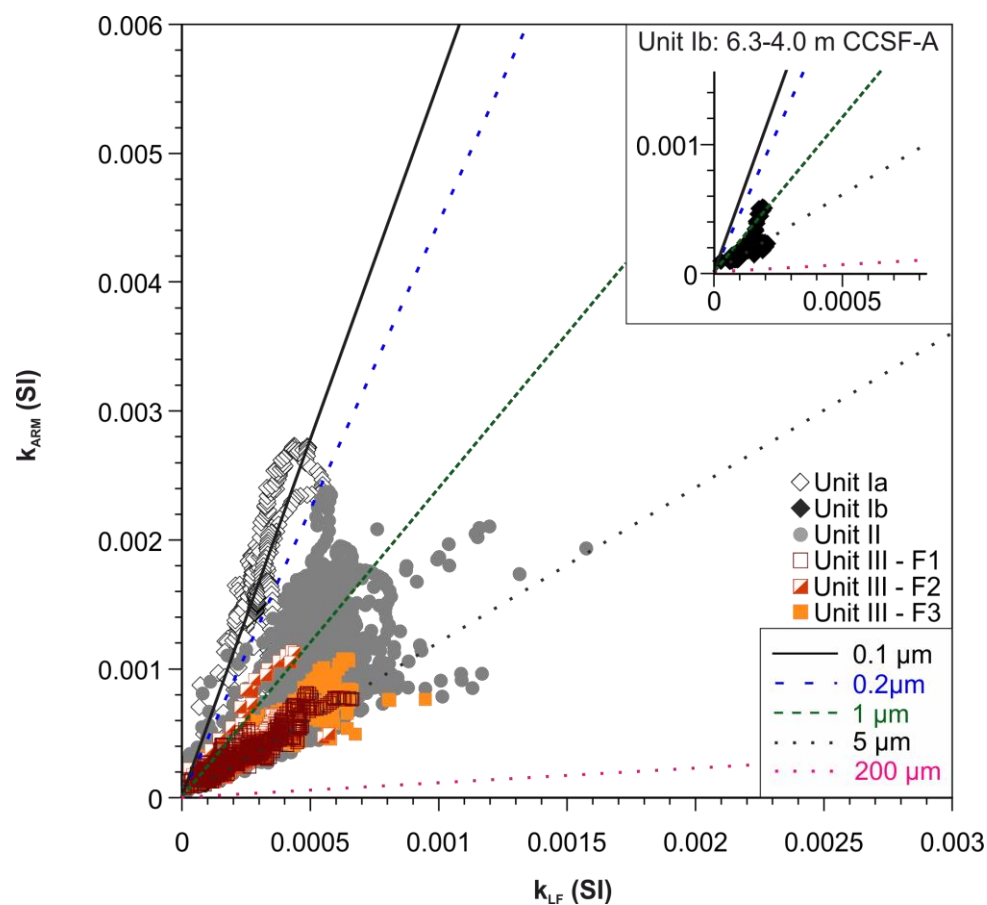


Figure 10: Day plot (Day et al., 1977) with mixing lines from Dunlop (2002a, 2002b) of all Site U1419 discrete samples divided into units as described in the text. Selected hysteresis loops representative for each unit are presented below.

Unit I. Unit Ib (from 6.3-4.0 m CCSF-A) is characterized by weak remanent magnetization intensities; mean of 0.011 ± 0.006 A/m for ARM, 1.15 ± 0.088 A/m for IRM, and 1.18 ± 0.089 A/m for SIRM, as well as lower magnetic susceptibility (mean of $16 \cdot 10^{-5} \pm 7.37 \cdot 10^{-5}$ SI) and mean k_{ARM}/k_{LF} of 1.65 ± 0.44 . From 6 to 5 m CSF-A, the MDF_{ARM} is high

(40-50 mT). From 5 to 4 m CCSF-A, MDF_{ARM} decreases to ~30 mT, indicating a shift from a higher- to lower coercivity magnetic mineralogy. Hysteresis data from Unit Ib plots in the multi-domain (MD) region (Fig. 10). Assuming a magnetite dominated mineralogy, the Banerjee et al. (1981) plot (Fig. 11), using the King et al., (1983) calibration, indicates coarser magnetic grain size ($> 0.2 \mu\text{m}$) of the samples from Unit Ib (Fig. 11) compared to the overlying Unit Ia. Unit Ia (4.0-0 m CCSF-A) is characterized by higher magnetic remanence intensities with mean values of $0.069 \pm 0.018 \text{ A/m}$ for ARM, $4.42 \pm 0.952 \text{ A/m}$ for IRM, and $4.43 \pm 0.949 \text{ A/m}$ for SIRM. Comparatively high k_{ARM}/k_{LIF} mean values of 5.69 ± 1.089 are observed, with moderate MDF_{ARM} of $35.1 \pm 1.4 \text{ mT}$ (Fig. 8). The magnetic susceptibility in this interval is relatively high with a mean of $30.8 \times 10^{-5} \pm 7.61 \times 10^{-5} \text{ SI}$. Hysteresis data from this interval plot within the pseudo-single domain (PSD) region of the Day et al. (1977) plot (Fig. 10; Day et al., 1977; Dunlop, 2002a, 2002b). In the Banerjee et al. (1981) plot (Fig. 11), using the King et al. (1983) calibrations, Unit Ia plots within the magnetic grain size limit of $0.2 \mu\text{m}$. Hysteresis loops from this unit display a shape typical of magnetite (Fig. 10; Tauxe et al., 1996).

Figure 11 (next page): Anhysteretic susceptibility of the U1419 units plotted against magnetic susceptibility (King et al., 1982) as a proxy for magnetic grain size (given a magnetite mineralogy). Magnetic grain size boundaries are based on synthetic samples from Banerjee et al. (1981) and the plot is adapted from Geiss & Banerjee (2003). Insert shows samples from 6.3-4.0 m CCSF-A in Unit Ib.



Chronostratigraphy

According to the age model (Walczak et al., in prep) the base of the splice (and Unit III) at 112 m CCSF-A corresponds to ~54,000 cal yr BP. Sedimentation rates in the lowermost part of the splice vary between 44 and 240 cm/kyr when averaged over 500 years (Fig. 7). The mean sedimentation rates for this interval (54,000-41,800 cal yr BP) are 113 ± 63 cm/kyr, with the highest rates observed between 43,000 and 42,500 cal yr BP, and the lowest rates between 52,000 and 51,500 cal yr BP. Unit II spans the interval from 41,800 to 14,700 cal yr BP (92.5-6.3 m CCSF-A), and sediment accumulation rates within this unit range between 16 and 835 cm/kyr. The highest rates occur in the upper parts of the Unit II between 18,000 and 17,500 cal yr BP, and the lowest from 15,500 cal yr BP to the top of Unit II at 14,700

cal yr BP (Fig. 7). The mean sedimentation rates for the entire Unit II are 250 ± 166 cm/kyr. Unit I spans the time period from ~14,700 cal yr BP to the present (6.3 m CCSF-A to mudline) with sediment accumulation rates varying between 5 and 113 cm/kyr (Walczak et al., in prep.; Fig. 7).

1.7 DISCUSSION

Unit III - Period of alternating conditions (54,000 to 41,800 cal yr BP)

The large changes in magnetic properties within Unit III (Fig. 8) are also associated with variations in lithology as indicated by Figure 9. The magnetic facies within this unit are broken into series of sub-facies (from older to younger; a, b, c, d). Both facies 2 and facies 3 are associated with diamict lithologies (Jaeger et al., 2014), although higher clast content and densities are observed in facies 3. In contrast, facies 1 is accompanied by lower-density massive or stratified mud with scattered clasts, including a laminated interval (F1d; 94.7-93.9 m CCSF-A; Penkrot et al., 2018). The lithology of the lowermost facies 1 interval (F1a; 109-105 m CCSF-A) differs somewhat from others (F1b, F1c, F1d) as sediment density is slightly higher and more clasts are present. Magnetic properties are, however, similar enough for them to be characterized as the same facies (Fig. 8 and 9). All intervals of facies 1 and 2 have higher coercivities ($MDF_{ARM} > 30$ mT) than found for most of the drilled sequence that has MDF_{ARM} typically < 30 mT, whereas facies 3 characteristics are similar to much of the overlying sedimentary package (Unit II; Fig. 8). Superimposed on these larger scale variations are alternations between F1 with much higher coercivities (MDF_{ARM} of 38-55 mT) and F2 with moderately higher coercivities (MDF_{ARM} 30-35 mT).

Facies 3 marks the base of the U1419 splice and predates the local last glacial maximum. The high concentration of magnetic material and low coercivity in combination with a clast-rich diamict suggest that F3 represents a glacial marine environment with frequent ice rafting. In general, this interval is very similar to the overall characteristics of the

overlying Unit II and, along with its high density (1500-1600 HU), is likely to have been rapidly deposited. Facies 3 is interpreted to reflect glacial proximal deposits, perhaps the final stages and/or retreat of an ice sheet as the magnetic signature is similar to that observed in the deglacial transition prior to the Bølling-Allerød (Davies et al., 2011).

The magnetic signature of facies 1 is comparable to those observed in the lowermost part of Unit Ib (6.3-5.6 m CCSF-A), suggesting that they may represent similar environmental conditions. Davies et al. (2011) described the lithology and Walczak et al. (2017) described the magnetic characteristics of this interval in the U1419 site survey core EW0408-85JC (between 831 and ~745 centimeters below seafloor). The lithology contains both laminated and sub-laminated intervals, separated by a ~12 cm (37 cm in EW0408-85JC) interval of massive, slightly higher density mud with clasts consisting mostly of terrigenous silt and clay, with the presence of opal and calcium carbonate (Davies et al., 2011). Based on detailed radiocarbon dating (Davies et al., 2011; Davies-Walczak et al., 2014), this layer was interpreted to represent cool and/or saline surface waters and regional glacier re-advance corresponding to the Younger Dryas, with the laminated interval below and the sub-laminated interval above representing warmer and highly productive conditions of the Bølling-Allerød and early Holocene, respectively. Both the magnetic properties and the lithology of F1 are comparable to these intervals, indicating that facies 1 may have been deposited in environments similar to that of the warm Bølling-Allerød or early Holocene. The occurrence of IRD throughout F1, unlike that of the Bølling-Allerød interval, indicates that tidewater glaciers were present, but that the drill Site was relatively distal to the glacier terminus. The presence of tidewater glaciers may also be indicated by the higher sedimentation rates observed in F1 intervals (65-166 cm/kyr) than that found for the Bølling-Allerød by Davies et al. (2011) of 25 ± 12 cm/kyr. The high coercivity (45-55 mT; Fig. 8) of facies 1 intervals, especially F1b and F1c, and laminations associated with facies 1d, may reflect magnetic diagenesis associated with benthic anoxia, as observed by Davies et al. (2011) and Walczak et al. (2017) in the younger analogue.

The magnetic characteristics of facies 2 intervals and the fact that they are associated with diamict lithologies suggest that they are likely related to an increased input of terrigenous material to the drill Site, representing glacial marine depositional environments with frequent ice rafting. The generally lower amplitude of the F2 intervals suggest that they may have been deposited during more moderate or distal glacial conditions compared to F3 and Unit II, but more proximal than facies 1. Alternating with facies 1, facies 2 might have been deposited in environments comparable to that of the Younger Dryas, as observed by Davies et al. (2011).

Between 42,700 and 41,800 cal yr BP (93.9 and 92.5 m CCSF-A), concentration-dependent parameters, magnetic grain size and density increase approaching values typical to that of Unit II. This short period is interpreted as an intensification, or buildup, of glacial conditions to the prolonged period of glaciation observed in Unit II.

Unit II - The Alaskan LGM (41,800 -14,700 cal yr BP)

The high magnetic concentration within this unit is consistent with an almost continuous flux of terrigenous sediments to the core Site, both in the form of IRD and material deposited from suspension settling. The lithology of Unit II is interpreted as a glacial diamict (Penkrot et al., 2018) with a persistently high input of ice rafted debris, and sediment accumulation rates of up to 835 cm/kyr when averaged over 500 years (Walczak et al., in prep; Fig. 7). These conditions are generally sustained throughout most of Unit II (until 14,700 cal yr BP) leading to the interpretation that this interval represents a prolonged period of glacial conditions, here referred to as the “Alaskan LGM” (Fig. 12). The high sedimentation rates indicate that the glacier front may have been close to the shelf edge throughout this interval. Based on the proximity of Site U1419 to the Bering Trough (Fig. 6) and seismic evidence of past shelf-edge glaciations (Berger et al., 2008; Elmore et al., 2013; Montelli et al., 2017), it is reasonable to assume that the glacier front was proximal to

the core Site for some duration of the Alaskan LGM, perhaps from as early as 41,800 cal yr BP, when the magnetic signal changed drastically.

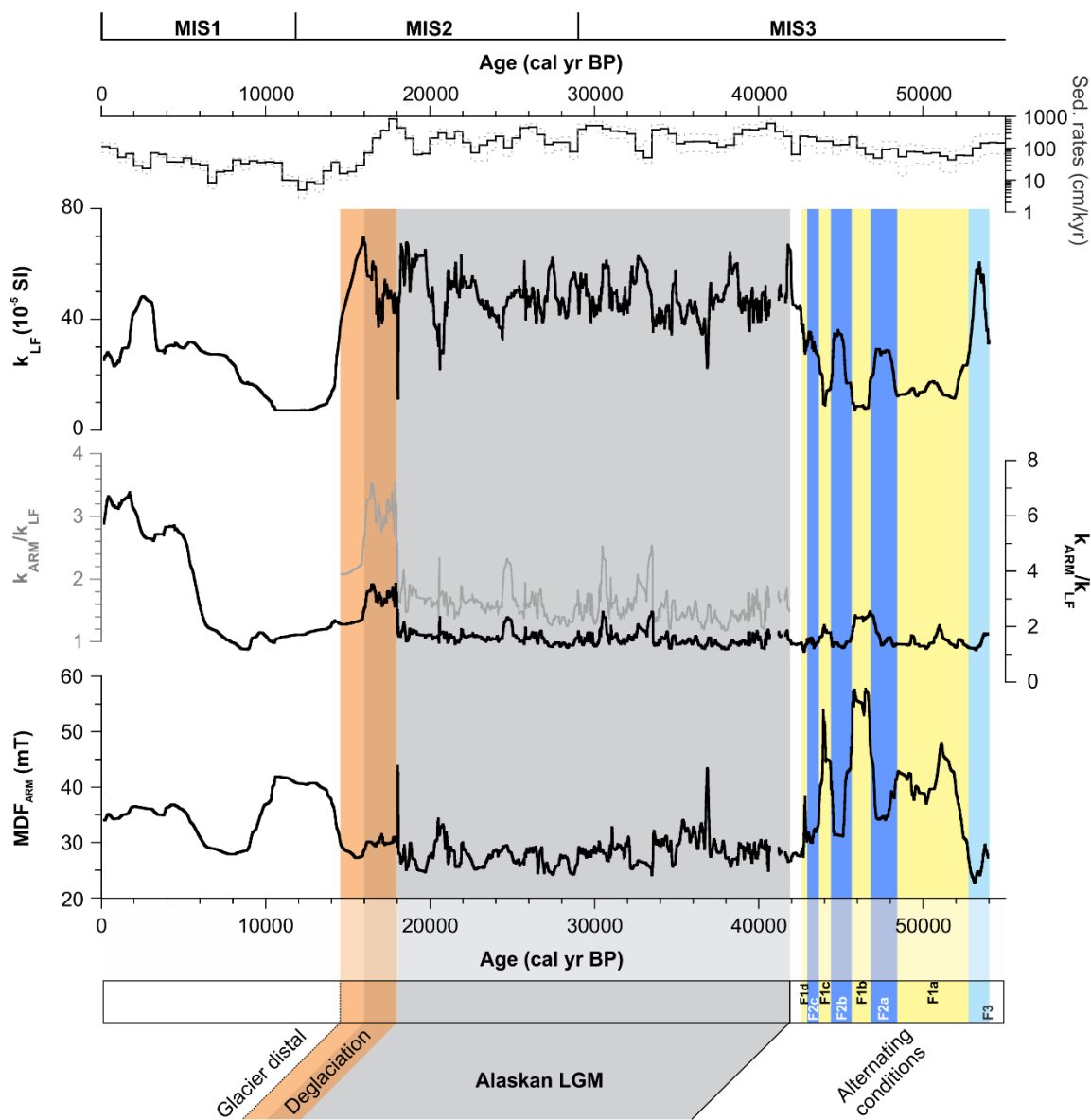


Figure 12 (previous page): Sedimentation rates (Walczak et al., in prep) and selected magnetic properties plotted against age in cal yr BP. Enlarged y axis for $k_{\text{ARM}}/k_{\text{LF}}$ in Unit II in grey. Events discussed in the text are indicated in different colors. Upper panel shows division of the marine isotope stages (MIS), and the lower panel details the glacial history as interpreted from the U1419 sedimentary record.

One interval characterized as laminated mud/ooze with dispersed clasts (Penkrot et al., 2018) and lowered density (1000-1100 HU), coincides with lower magnetic concentrations and higher coercivity at approx. 36,900 cal yr BP (71.2-70.7 m CCSF-A; Fig. 8 and 12). This interval resembles the F1 intervals within Unit III. However, its magnetic concentrations are slightly higher and coercivity is lower than in the F1 intervals. Penkrot et al. (2018) proposed that these particular laminated sediments represent an interval of warming and increased productivity during an otherwise glacially dominated time period.

Intervals with higher magnetic concentration, lower coercivity, and finer magnetic grain size occur in the early parts of the Alaskan LGM, at approx. 38,400 cal yr BP (74.2-73.0 m CCSF-A), 34,900 cal yr BP (66.9-66.8 m CCSF-A), 33,500 cal yr BP (60.4-58.6 m CCSF-A), and 30,900 cal yr BP (52.8-51.6 m CCSF-A; Fig. 12). These intervals coincide with clast-poor diamict lithologies (Penkrot et al., 2018) and may reflect small-scale oscillations in the ice front, giving rise to temporal changes in sediment transport and/or sediment provenance. The two youngest intervals at 33,500 and 30,900 cal yr BP are characterized by notably finer magnetic grain sizes that may be associated with increased input of especially fine-grained material, perhaps from increased meltwater input or a different sediment source (Fig. 12). Previous studies of coastal Alaska sediments have shown distinct variations in magnetic properties depending on provenance (Cowan et al., 2006; Carlson et al., 2017), indicating that the magnetic variations observed throughout U1419 may be linked to changes in sediment source, although defining these different provenances is not possible based solely on the data presented here.

Larger amplitude variations in magnetic parameters are observed between ~25,000 and 16,000 cal yr BP. Intervals of finer magnetic grain sizes, higher coercivity and low magnetic susceptibility occur between 24,700 and 23,600 cal yr BP (31.0-28.8 m CCSF-A), between 20,900 and 20,000 cal yr BP (22.6-20.0 m CCSF-A), and between 18,000 and 16,800 (16.6-7.5 m CCSF-A; Fig. 12). The two older intervals correlate with lithologies of clast-poor diamict with some layers of sandy diamict, whereas the younger is characterized by clast-poor and stratified diamict (Penkrot et al., 2018). The increased variability in magnetic properties and lithology from ~25,000 cal yr BP may reflect a number of advance and retreat phases that could have influenced the provenance of the magnetic material, indicating complex ice-front dynamics and sedimentation during a time previously described as the LGM in southern Alaska (Mann & Peteet, 1994; Mann & Hamilton, 1994). An especially pronounced event of low susceptibility and high coercivity occurs at 18,000 cal yr BP (16.6-15.9 m CCSF-A; Fig. 12). With no significant changes observed in density or lithology (cf. Penkrot et al., 2018) at this particular interval, it could reflect a short-lived pulse of sediment from a different source region characterized by lower-susceptibility material. Directly following this susceptibility low, from 18,000 to 16,800 cal yr BP (15.9-7.5 m CCSF-A), finer magnetic grain size along with the highest sedimentation rates (mean of 500 ± 264 cm/kyr; Walczak et al., in prep) are interpreted to represent initial disintegration of the NCIS' southern margin in the GoA followed by deglaciation and retreat of the ice margin as outlined by Davies et al. (2011) and Walczak et al. (2017).

The Gulf of Alaska record in a regional and global context

Environmental fluctuations in the North Pacific Ocean have been linked to corresponding events both in the North Atlantic as well as in the Southern Ocean suggesting that there may be a combined influence of the two on the North Pacific, with Southern Ocean signals superimposed on North Atlantic atmospheric teleconnections (e.g. Mix et al., 1999; Davies et al., 2011). Using the U1419 magnetic susceptibility record as a proxy for glacial

activity (high k_{LF} , high activity, and low k_{LF} , low activity) allows a tentative comparison of the GoA record to Greenland (NGRIP Community Members, 2004) and Antarctic (EPICA Community Members, 2010) $\delta^{18}O$ ice core records (Fig. 13), and, thus, an assessment of relative timing in glacial and environmental events across the Antarctic, North Atlantic and North Pacific.

Facies 3 may be associated with the glacial termination of the pre-LGM shelf-wide glacial advance as recorded in GoA seismic studies (Elmore et al., 2013; Montelli et al., 2017). These advances are thought to have been at least as extensive as the LGM, reaching the shelf edge and with ice flow not only constrained to the submarine troughs, but possibly extending laterally resulting in a wider ice cover (Elmore et al., 2013), most likely also affecting the western portion of the Bering/Malaspina shelf close to the U1419 drill Site. Elsewhere in Alaska, the penultimate glaciation is defined by the geomorphological evidence existing beyond the well-defined and well-dated LGM limits. Age determination and regional correlation of the penultimate glaciation is difficult, and presumed ages vary from MIS 6 to MIS 4 (Kaufman et al., 2011). In the northern and western Alaska Range, ^{10}Be dates of several moraines indicate moraine stabilization (glacial retreat) around 60-50 ka, at the end of MIS 4 or beginning of MIS3 (Briner et al., 2005; Briner & Kaufman, 2008; Dortch et al., 2010; Matmon et al., 2010).

The alternating environmental conditions subsequent to facies 3 observed in the GoA correspond to early and mid- MIS3 and may be cautiously correlated to similar $\delta^{18}O$ fluctuations observed in the NGRIP Greenland ice core record. The U1419 age model (Walczak et al., in prep) is very well-constrained from 40,000 cal yr BP, allowing a comparison of the GoA record to the Antarctic and Greenland $\delta^{18}O$ ice core records (Fig. 13). Although a one-to-one relationship is not obvious, the shift toward larger-amplitude variations in magnetic properties in the GoA at ~25,000 cal yr BP coincides with the warming observed in the Greenland and Antarctic ice core records, from approx. 24-23 ka.

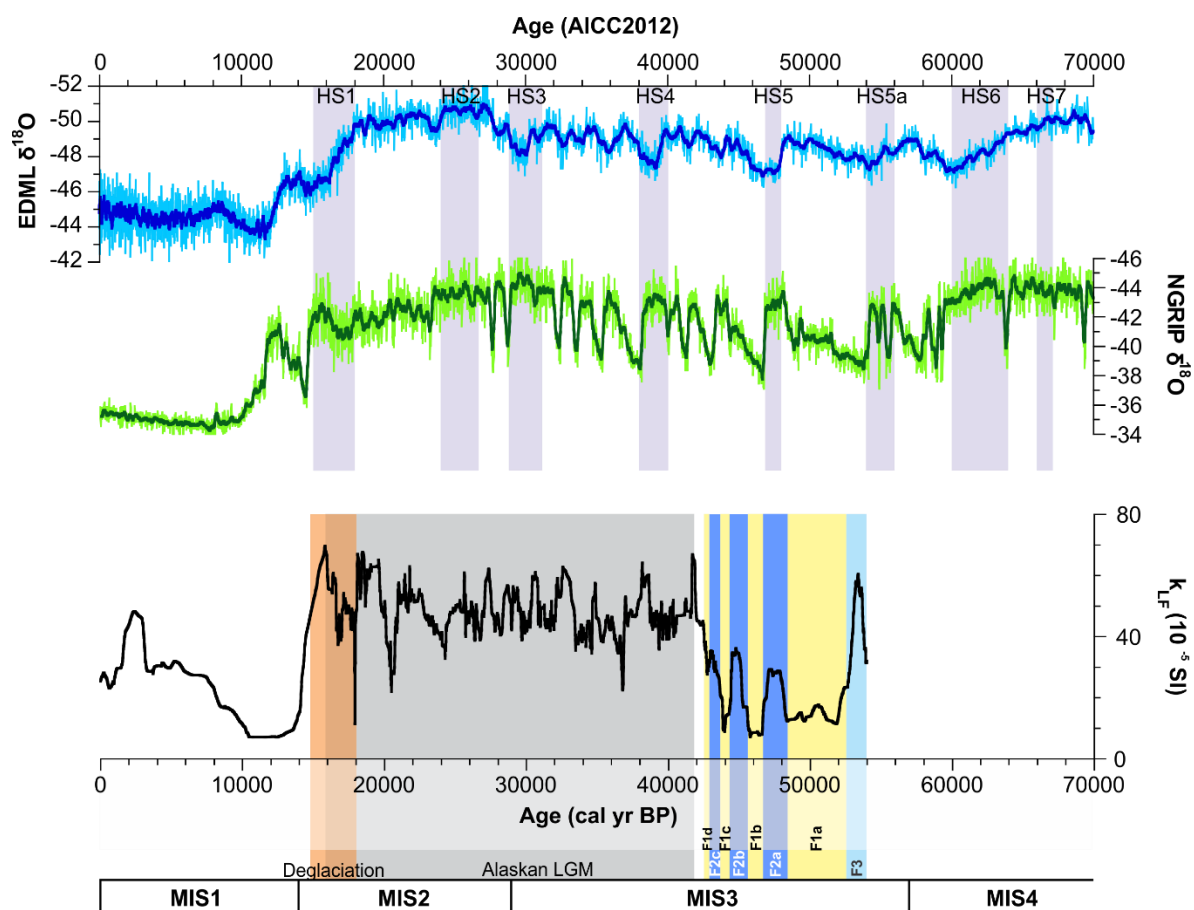


Figure 13: Comparison of Antarctic (EDML in blue; EPICA Community Members, 2010) and Greenland (NGRIP in green; NGRIP Community Members, 2004) oxygen isotope records on the AICC2012 chronology (Veres et al., 2013) and the U1419 magnetic susceptibility record (black). Note the reversed Y-axes on the oxygen isotope records. Interpretation of the U1419 record are marked in colors as in Fig. 12. Heinrich stadials (HS) for reference are marked on the oxygen isotope records in grey.

1.8 CONCLUSIONS

The final stages/retreat of a pre-LGM glaciation may have been recorded at the base of the U1419 spliced record, as facies 3. MIS3 in the GoA was characterized by fluctuating environmental conditions between warmer and more productive environments, similar to that observed in the Bølling-Allerød and the early Holocene (facies 1), and more glacially influenced environments similar to that of the Younger Dryas (facies 2). The build-up to full glacial conditions commenced at approx. 42,700 cal yr BP with glacier-proximal conditions prevailing at the core Site from 41,800 cal yr BP. This Alaskan LGM lasted until 14,700 cal yr BP. It was characterized by high sedimentation rates of up to 835 cm/kyr, and smaller-scale fluctuations in the ice front extent, sedimentary dynamics, and environmental conditions prior to ~25,000 cal yr BP. More complex ice front dynamics of repeated advance- and retreat phases, perhaps with multiple lithogenic sediment sources, dominated the last half of the Alaskan LGM after ~25,000 cal yr BP. Deglaciation may have started around 18,000 cal yr BP and was sustained from approx. 16,800 cal yr BP.

1.9 ACKNOWLEDGEMENTS

Expedition 341 was carried out by the Integrated Ocean Drilling Program (IODP). We thank the IODP-USIO and the captain and crew of the R/V JOIDES Resolution. We are grateful to the staff at the IODP Gulf Coast Repository, especially L. LeVey and P. Rumford, as well as T. Hansen and B. Reilly for their help during u-channel sampling. Special thanks are due to Q. Beauvais and L.-F. Daigle for assistance with the CT scanning; to M.-P. St-Onge and A.M. Ross for help in the lab; and to M. Penkrot for information about lithofacies. This study was possible thanks to a GEOTOP scholarship to the first author, as well a Natural Sciences and Engineering Council of Canada Discovery Grant to G. St-Onge.

1.10 REFERENCES

- Addison, J.A., Finney, B.P., Dean, W.E., Davies, M.H., Mix, A.C., Stoner, J.S. & Jaeger, J.M., 2012.** Productivity and sedimentary ^{15}N variability for the last 17,000 years along the northern Gulf of Alaska continental slope. *Paleoceanography*, **27**, PA1206, doi: 10.1029/2011PA002161
- Arendt, A.A., Echelmeyer, K.A., Harrison, W.D., Lingle, C.S. & Valentine, V.B., 2002.** Rapid wastage of Alaska glaciers and their contribution to rising sea level. *Science*, **297**, pp. 382-386, doi: 10.1126/science.1072497
- Banerjee, S.K., King, J. & Marvin, J., 1981.** A rapid method for magnetic granulometry with applications to environmental studies. *Geophysical Research Letters*, **8(4)**, pp. 333-336, doi: 10.1029/GL008i004p00333
- Barron, J.A., Bukry, D., Dean, W.E., Addison, J.A. & Finney, B., 2009.** Paleooceanography of the Gulf of Alaska during the past 15,000 years: Results from diatoms, silicoflagellates, and geochemistry. *Marine Micropaleontology*, **72**, pp. 176-195, doi: 10.1016/j.marmicro.2009.04.006
- Berger, A.L., Gulick, S.P., Spotila, J.A., Upton, P., Jaeger, J.M., Chapman, J.B., Worthington, L.A., Pavlis, T.L., Ridgway, K.D., Willems, B.A. & McAleer, R.J., 2008.** Quaternary tectonic response to intensified glacial erosion in an orogenic wedge. *Nature Geoscience*, **1**, pp. 793-799, doi: 10.1038/ngeo334
- Briner, J.P., Kaufman, D.S., Werner, A., Caffee, M., Levy, L., Manley, W.F., Kaplan, M.R. & Finkel, R.C., 2002.** Glacier readvance during the late glacial (Younger Dryas?) in the Ahklun Mountains, southwestern Alaska. *Geology*, **30**, pp. 679-682, doi: 10.1130/0091-7613(2002)030<0679:GRDTLG>2.0.CO;2
- Briner, J.P., Kaufman, D.S., Manley, W.F., Finkel, R.C. & Caffee, M.W., 2005.** Cosmogenic exposure dating of late Pleistocene moraine stabilization in Alaska.

- Geological Society of America Bulletin*, **117(7/8)**, pp. 1108-1120, doi: 10.1130/B25649
- Briner, J.P. & Kaufman, D.S., 2008.** Late Pleistocene mountain glaciation in Alaska: key chronologies. *Journal of Quaternary Science*, **23(6-7)**, pp. 659-670, doi: 10.1002/jqs.1196
- Calkin, P.E., Wiles, G.C. & Barclay, D.J., 2001.** Holocene coastal glaciation of Alaska. *Quaternary Science Reviews*, **20**, pp. 449-461, doi: 10.1016/S0277-3791(00)00105-0
- Carlson, A.E., Kilmer, Z., Ziegler, L.B., Stoner, J.S., Wiles, G.C., Starr, K., Walczak, M.H., Colgan, W., Reyes, A.V., Leydet, D.J. & Hatfield, R.G., 2017.** Recent retreat of Columbia Glaciers, Alaska: Millennial context. *Geology*, **45(6)**, pp. 547-550, doi: 10.1130/G38479.1
- Clapperton, C., 2000.** Interhemispheric synchronicity of Marine Oxygen Isotope Stage 2 glacier fluctuations along the American cordilleras transect. *Journal of Quaternary Science*, **15(4)**, pp. 435-468, doi: 10.1002/1099-1417(200005)15:4<435::AID-JQS552>3.0.CO;2-R
- Cowan, E.A., Brachfeld, S.A., Powell, R.D. & Schoolfield, S.C., 2006.** Terrane-specific rock magnetic characteristics preserved in glacial marine sediment from southern coastal Alaska. *Canadian Journal of Earth Sciences*, **43**, pp. 1269-1282, doi: 10.1139/E06-042
- Davies, M.H., Mix, A.C., Stoner, J.S., Addison, J.A., Jaeger, J., Finney, B. & Wiest, J., 2011.** The deglacial transition on the southeastern Alaska Margin: Meltwater input, sea level rise, marine productivity, and sedimentary anoxia. *Paleoceanography*, **26**, PA2223, doi: 10.1029/2010PA002051
- Davies-Walczak, M., Mix, A.C., Stoner, J.S., Southon, J.R., Cheseby, M. & Xuan, C., 2014.** Late Glacial to Holocene radiocarbon constraints on North Pacific Intermediate

- Water ventilation and deglacial atmospheric CO₂ sources. *Earth and Planetary Science Letters*, **397**, pp. 57-66, doi: 10.1016/j.epsl.2014.04.004
- Day, R., Fuller, M. & Schmidt, V.A., 1977.** Hysteresis properties of titanomagnetites: Grain- size and compositional dependence. *Physics of the Earth and Planetary Interiors*, **13**, pp. 260-267, doi: 10.1016/0031-9201(77)90108-X
- de Vernal, A. & Pedersen, T.F., 1997.** Micropaleontology and palynology of core PAR87A-10: A 23,000 year record of paleoenvironmental changes in the Gulf of Alaska, northeast North Pacific. *Paleoceanography*, **12(6)**, pp. 821-830, doi: 10.1029/97PA02167
- Dortch, J.M., Owen, L.A., Caffee, M.W., Li, D. & Lowell, T.V., 2010.** Beryllium-10 surface exposure dating of glacial successions in the Central Alaska Range. *Journal of Quaternary Science*, **25(8)**, pp. 1259-1269, doi: 10.1002/jqs.1406
- Duchesne, M.J., Moore, F., Long, B.F., Labrie, J., 2009.** A rapid method for converting medical Computed Tomography scanner topogram attenuation scale to Hounsfield Unit scale and to obtain relative density values. *Engineering Geology*, **103 (3-4)**, pp. 100-105, doi: 10.1016/j.enggeo.2008.06.009
- Dunlop, D. J., 2002a.** Theory and application of the Day plot (Mrs/Ms versus Hcr/Hc): 1. Theoretical curves and tests using titanomagnetite data, *Journal of Geophysical Research*, **107(B3)**, 2056, doi:10.1029/2001JB000486.
- Dunlop, D. J., 2002b.** Theory and application of the Day plot (Mrs/Ms versus Hcr/Hc): 2. Application to data for rocks, sediments, and soils, *Journal of Geophysical Research*, **107(B3)**, 2057, doi:10.1029/2001JB000487.
- Elmore, C.R., Gulick, S.P.S., Willems, B. & Powell, R., 2013.** Seismic stratigraphic evidence for glacial expanse during glacial maxima in the Yakutat Bay Region, Gulf of Alaska. *Geochemistry Geophysics Geosystems*, **14(4)**, pp. 1294-1311, doi: 10.1002/ggge.20097

- EPICA Community Members, 2006.** Stable oxygen isotopes of ice core EDML. PANGAEA, doi: 10.1594/PANGAEA.552270
- Fortin, D., Francus, P., Gebhardt, A.C., Hahn, A., Kliem, P., Lisé-Pronovost, A., Roychowdhury, R., Labrie, J., St-Onge, G. & the PASADO Science Team, 2013.** Destructive and non-destructive density determination: method comparison and evaluation from the Laguna Potrok Aike sedimentary record. *Quaternary Science Reviews*, **71**, pp. 147-153, doi: 10.1016/j.quascirev.2012.08.024
- Fulton R.J., 1991.** A conceptual model for growth and decay of the Cordilleran Ice Sheet. *Géographie physique et Quaternaire*, **45(3)**, pp. 281-286, doi: 10.7202/032875ar
- Geiss, C.E. & Banerjee, S.K., 2003.** A Holocene-Late Pleistocene geomagnetic inclination record from Grandfather Lake SW Alaska. *Geophysical Journal International*, **153**, pp. 497-507, doi: 10.1046/j.1365-246X.2003.01921.x
- Gulick, S.P.S., Jaeger, J.M., Mix, A.C., Asahi, H., Bahlburg, H., Belanger, C.L., Berbel, G.B.B., Childress, L., Cowan, E., Drab, L., Forwick, M., Fukumura, A., Ge, S., Gupta, S., Kioka, A., Konno, A., LeVay, L.J., März, C., Matsuzaki, K.M., McClymont, E.L., Moy, C., Müller, J., Nakamura, A., Ojima, T., Ribeiro, F.R., Ridgway, K.D., Romero, O.E., Slagle, A.L., Stoner, J.S., St-Onge, G., Suto, I., Walczak, M.D., Worthington, L.L., Bailey, I., Enkelmann, E., Reece, R. & Swartz, J.M., 2015.** Mid-Pleistocene climate transition drives net mass loss from rapidly uplifting St. Elias Mountains, Alaska. *PNAS*, **112(49)**, pp. 15042-15047, doi: 10.1073/pnas.1512549112
- Haslett, J. & Parnell, A., 2008.** A simple monotone process with application to radiocarbon-dated depth chronologies. *Journal of the Royal Statistical Society Series C Applied Statistics*, **57(4)**, pp. 399-418, doi: 10.1111/j.1467-9876.2008.00623.x
- Hatfield, R.G., Reyes, A.V., Stoner, J.S., Carlson, A.E., Beard, B.L., Winsor, K. & Welke, B., 2016.** Interglacial responses of the southern Greenland ice sheet over the

last 430,000 years determined using particle-size specific magnetic and isotopic tracers. *Earth and Planetary Science Letters*, **454**, pp. 225-236, doi: 10.1016/j.epsl.2016.09.014.

Hounsfield, G.N., 1973. Computerized transverse axial scanning (tomography): I. description of system. *British Journal of Radiology*, **46 (552)**, pp. 1016-1022, doi: 10.1259/0007-1285-46-552-1016

Jaeger, J.M., Nittrouer, C.A., Scott, N.D & Milliman, J.D., 1998. Sediment accumulation along glacially impacted mountainous coastline: north-east Gulf of Alaska. *Basin Research*, **10**, pp. 155-173, doi: 10.1046/j.1365-2117.1998.00059.

Jaeger, J.M., Gulick, S.P.S., LeVay, L.J., & the Expedition 341 Scientists, 2014. Proc. IODP, 341, College Station, TX (Integrated Ocean Drilling Program).

Kaufman, D.S. & Manley, W.F., 2004. Pleistocene maximum and Late Wisconsin glacier extents across Alaska, USA. *In: Ehlers, J., Gibbard, P.L. (Eds.), Quaternary Glaciations Extent and Chronology, Part II: North America. Developments in Quaternary Science*, vol. 2 Elsevier, Amsterdam, pp. 9–27.

Kaufman, D.S., Young, N.E., Briner, J.P. & Manley, W.F., 2011. Alaska palaeo-glacier atlas (version 2). *In: Ehlers, J., Gibbard, P.L. & Hughes, P.D. (eds.) 2011. Quaternary Glaciations - Extent and Chronology - A Closer Look, Developments in Quaternary Science*, vol. 15, pp. 427-445, doi: 10.1016/B978-0-444-53447-7.00033-7

King, J., Banerjee, S.K., Marvin, J. & Özdemir, Ö., 1982. A comparison of different magnetic methods for determining the relative grain size of magnetite in natural materials: some results from lake sediments. *Earth and Planetary Science Letters*, **59**, pp. 404-419, doi: 10.1016/0012-821X(82)90142-X

King, J., Banerjee, S.K. & Marvin, J., 1983. A new rock-magnetic approach to selecting sediments for geomagnetic paleointensity studies: application to paleointensity for

- the last 4000 years. *Journal of Geophysical Research*, **88(B7)**, pp. 5911-5921, doi: 10.1029/JB088iB07p05911
- Kissel, C., Laj, C., Labeyrie, L., Dokken, T., Voelker, A. & Blamart, D., 1999.** Rapid climatic variations during marine isotopic stage 3: magnetic analysis of sediments from Nordic Seas and North Atlantic. *Earth and Planetary Science Letters*, **171**, pp. 489-502, doi: 10.1016/S0012-821X(99)00162-4
- Kissel, C., Laj, C., Mulder, T., Wandres, C. & Cremer, M., 2009.** The magnetic fraction: A tracer of deep water circulation in the North Atlantic. *Earth and Planetary Science Letters*, **288**, pp. 444-454, doi: 10.1016/j.epsl.2009.10.005
- Lagoe, M.B., Eyles, C.H., Eyles, N. & Hale, C., 1993.** Timing of late Cenozoic tidewater glaciation in the far North Pacific. *Geological Society of America Bulletin*, **105(12)**, pp. 1542-1560, doi: 10.1130/0016-7606(1993)105<1542:TOLCTG>2.3.CO;2
- Mann, D.H. & Peteet, D.M., 1994.** Extent and timing of the Last Glacial Maximum in Southwestern Alaska. *Quaternary Research*, **42**, pp. 136-148, doi: 10.1006/qres.1994.1063
- Mann, D.H. & Hamilton, T.D., 1995.** Late Pleistocene and Holocene paleoenvironments of the North Pacific coast. *Quaternary Science Reviews*, **14**, pp. 449-471, doi: 10.1016/0277-3791(95)00016-I
- Matmon, A., Briner, J.P., Carver, G., Bierman, P. & Finkel, R.C., 2010.** Moraine chronosequence of the Donnelly Dome region, Alaska. *Quaternary Research*, **74**, pp. 63-72, doi: 10.1016/j.yqres.2010.04.007
- Mix, A.C., Lund, D.C., Pisias, N.G., Boden, P., Bornmalm, L., Lyle, M. & Pike, J., 1999.** Rapid climate oscillations during the last deglaciation reflect Northern and Southern Hemisphere sources. *In*: Clark, P.U., Webb, R.S. & Keigwin, L.D. (eds) *Mechanisms of Global Climate Change at Millennial Time Scales*, American Geophysical Union, Washington, D.C., doi: 10.1029/GM112p0127

- Molnia, B.F. & Carlson, P.R., 1978.** Surface sedimentary units of northern Gulf of Alaska continental shelf. *The American Association of Petroleum Geologists Bulletin*, **62(4)**, pp. 633-643
- Montelli, A., Gulick, S.P.S., Worthington, L.L., Mix, A., Davies-Walczak, M., Zellers, S.D. & Jaeger, J.M., 2017.** Late Quaternary glacial dynamics and sedimentation variability in the Bering Trough, Gulf of Alaska. *Geology*, **45(3)**, pp. 251-254, doi: 10.1130/G38836.1
- North Greenland Ice Core Project members. 2004.** High-resolution record of Northern Hemisphere climate extending into the last interglacial period. *Nature*, **431** (7005), pp. 147-151, doi: 10.1038/nature02805
- Oda, H. & Xuan, C., 2014.** Deconvolution of continuous paleomagnetic data from pass-through magnetometer: A new algorithm to restore geomagnetic and environmental information based on realistic optimization. *Geochemistry, Geophysics, Geosystems*, **15**, pp. 3907-3924, doi: 10.1002/2014GC005513.
- Penkrot, M.L., Jaeger, J.M., Cowan, E.A., St-Onge, G. & LeVay, L., 2018.** Multivariate modelling of glacial marine lithostratigraphy combining scanning XRF, multisensory core properties, and CT imagery: IODP Site U1419. *Geosphere*, **14(4)**, pp. 1935-1960, doi: 10.1130/GES01635.1
- Peters, C. & Dekkers, M.J., 2003.** Selected room temperature magnetic parameters as a function of mineralogy, concentration and grain size. *Physics and Chemistry of the Earth*, **28**, pp. 659-667, doi: 10.1016/S1474-7065(03)00120-7
- Praetorius, S.K., Mix, A.C., Walczak, M.H., Wolhowe, M.D., Addison, J.A. & Prah, F.G., 2015.** North Pacific deglacial hypoxic events linked to abrupt ocean warming. *Nature*, **527**, pp. 362-366, doi: 10.1038/nature15753
- Reimer, P.J., Bard, E., Bayliss, A., Beck, J.W., Blackwell, P.G., Ramsey, C.B., Buck, C.E., Cheng, H., Edwards, R. L., Friedrich, M., Grootes, P.M., Guilderson, T.**

- P., Haflidason, H., Hajdas, I., Hatté, C., Heaton, T. J., Hoffmann, D.L., Hogg, A.G., Hughen, K.A., Kaiser, K.F., Kromer, B., Manning, S.W., Niu, M., Reimer, R.W., Richards, D.A., Scott, E.M., Southon, J.R., Staff, R.A., Turney, C.S. M. and van der Plicht, J., 2013.** IntCal13 and Marine13 Radiocarbon Age Calibration Curves 0–50,000 Years cal BP, *Radiocarbon*, **55(4)**, pp. 1869–1887
- Robinson, S.G., Maslin, M.A. & McCave, I.N., 1995.** Magnetic Susceptibility variations in Upper Pleistocene deep-sea sediments of the NE Atlantic: Implications for ice rafting and paleocirculation at the last glacial maximum. *Paleoceanography*, **10(2)**, pp. 221-250, doi: 10.1029/94PA02683
- Royer, T.C., 1982.** Coastal fresh water discharge in the Northeast Pacific. *Journal of Geophysical Research*, **87(C3)**, pp. 2017-2021, doi: 10.1029/JC087iC03p02017
- Silberling, N.J., Jones, D.L., Monger, J.W.H., Coney, P.J., Berg, H.C., and Plafker, George, 1994.** Lithotectonic terrane map of Alaska and adjacent parts of Canada, *In*: Plafker, George, and Berg, H.C., eds., *The Geology of Alaska*: Geological Society of America, 1 sheet, scale 1:2,500,000
- Simon, Q., Hillaire-Marcel, C., St-Onge, G. & Andrews, J.T., 2014.** North-eastern Laurentide, western Greenland and southern Inuitian ice stream dynamics during the last glacial cycle. *Journal of Quaternary Science*, **29(1)**, pp. 14-26, doi: 10.1002/jqs.2648
- Stabeno, P.J., Reed, R.K. & Schumacher, J.D., 1995.** The Alaska Coastal Current: Continuity of transport and forcing. *Journal of Geophysical Research*, **100(C2)**, pp. 2477-2485, doi: 10.1029/94JC02842
- Stabeno, P.J., Bond, N.A., Hermann, A.J., Kachel, N.B., Mordy, C.W. & Overland, J.E., 2004.** Meteorology and oceanography of the northern Gulf of Alaska. *Continental Shelf Research*, **24**, pp. 859-897, doi: 10.1016/j.csr.2004.02.007

- Stoner, J.S., Channell, J.E.T. & Hillaire-Marcel, C., 1996.** The magnetic signature of rapidly deposited detrital layers from the deep Labrador Sea: Relationship to North Atlantic Heinrich layers. *Paleoceanography*, **11(3)**, pp. 309-325, doi: 10.1029/96PA00583
- Stoner, J.S. & St-Onge, G., 2007.** Magnetic stratigraphy in paleoceanography: reversal, excursion, paleointensity and secular variation. *In: Hillaire-Marcel, C. & de Vernal, A. (eds) Proxies in Late Cenozoic Paleoceanography*, Elsevier, pp. 99-138, doi: 10.1016/S1572-5480(07)01008-1
- Tauxe, L., 1993.** Sedimentary records of relative paleointensity of the geomagnetic field: Theory and practice. *Reviews of Geophysics*, **31(3)**, pp. 319-354, doi: 10.1029/93RG01771
- Tauxe, L., Mullender, T.A.T. & Pick, T., 1996.** Potbellies, wasp-waists, and superparamagnetism in magnetic hysteresis. *Journal of Geophysical Research*, **101(B1)**, pp. 571-583, doi: 10.1029/95JB03041
- Thompson, R. & Oldfield, F., 1986.** Environmental magnetism. Allen and Unwin, Winchester, Mass.
- Thouveny, N., Moreno, E., Delanghe, D., Candon, L., Lancelot, Y. & Shackleton, N.J., 2000.** Rock magnetic detection of distal ice-rafted debries: clue for the identification of Heinrich layers on the Portuguese margin. *Earth and Planetary Science Letters*, **180**, pp. 61-75, doi: 10.1016/S0012-821X(00)00155-2
- Veres, D., Bazin, L., Landais, A., Kele, H.T.M., Lemieux-Dudon, B., Parrenin, F., Martinerie, P., Blayo, E., Blunier, T., Capron, E., Chappellaz, J., Rasmussen, S.O., Severi, M., Svensson, A., Vinther, B. & Wolff, E.W., 2013.** The Antarctic Ice Core Chronology (AICC2012): An optimized multi-parameter and multi-site dating approach for the last 120 thousand years, *Climate of the Past*, **9**, pp. 1733–1748, doi:10.5194/cp-9-1733-2013

- Verosub, K.L. & Roberts, A.P., 1995.** Environmental magnetism: Past, present, and future. *Journal of Geophysical Research*, **100(B2)**, pp. 2175-2192, doi: 10.1029/94JB02713
- Walczak, M.H., Stoner, J.S., Mix, A.C., Jaeger, J., Rosen, G.P., Channell, J.E.T., Heslop, D. & Xuan, C., 2017.** A 17,000 yr paleomagnetic secular variation record from the southeast Alaskan margin: Regional and global correlations, *Earth and Planetary Science Letters*, **473**, pp. 177-189, doi: 10.1016/j.epsl.2017.05.022
- Walczak, M.H., Mix, A.C., Fallon, S., Cowan, E., Praetorius, S., Du, J., Hobern, T., Padman, J., Fifield, K., Stoner, J.S., Haley, B., in prep,** Coupled changes in Northeast Pacific ventilation and Cordilleran Ice Sheet discharge may precede Heinrich Events. *Science*
- Weeks, R.J., Laj, C., Endignoux, L., Fuller, M., Roberts, A., Manganne, R., Blanchard, E. & Goree, W., 1993.** Improvements in long-core measurement techniques: applications in palaeomagnetism and palaeoceanography. *Geophysical Journal International*, **114**, pp. 651-662, doi: 10.1111/j.1365-246X.1993.tb06994.x

CHAPTER 2
A HIGH-RESOLUTION LATE QUATERNARY INCLINATION RECORD
FROM IODP EXPEDITION 341 DRILL SITE U1419 IN THE GULF OF
ALASKA

2.1 SUMMARY OF CHAPTER 2

In the second chapter, the U1419 inclination record is presented. The study suggests that the inclination record between 15,000 and 30,000 cal yr BP is the most robust, reflecting regional scale paleomagnetic secular variations. This chapter also presents a preliminary age model for Exp. 341 Site U1418.

This chapter, titled “*A high-resolution late Quaternary inclination record from IODP Expedition 341 drill Site U1419 in the Gulf of Alaska*” was written by me under the guidance of my supervisor, Guillaume St-Onge, and my co-supervisors Joe Stoner (Oregon State University) and Matthias Forwick (The Arctic University of Norway) who revised several versions of this paper. As first author, I performed the analyses, treated and interpreted the data, and wrote the paper. My three supervisors contributed greatly to the realization of this paper through assistance in the lab, help with interpreting data, and comments on the text. Maureen Walczak (Oregon State University) contributed with the U1419 age model and associated information. With the help of Stewart Fallon (Australian National University), she also performed the radiocarbon analyses and constructed the U1418 age model. Brendan Reilly (Oregon State University) constructed the U1418 and U1419 shipboard stacks used in this study. Guillaume St-Onge, Joe Stoner, Matthias Forwick, and Maureen Walczak were all part of the shipboard science party during IODP Expedition 341.

Results from this chapter were presented at the annual GEOTOP student meeting in Jouvence (2015; poster), at the American Geophysical Union Joint Assembly in Montréal (2015; poster), at the Association francophone pour le savoir (ACFAS) meeting in Rimouski (2015; poster), and at the American Geophysical Union Fall Meeting in San Francisco (2016; poster).

2.2 A HIGH-RESOLUTION LATE QUATERNARY INCLINATION RECORD FROM IODP EXPEDITION 341 DRILL SITE U1419 IN THE GULF OF ALASKA

Velle, Julie Heggdal^{a,b,*} ; Walczak, Maureen^{c,d}; Reilly, Brendan^c; St-Onge, Guillaume^{a,b} ; Stoner, Joseph S.^{b,c}; Fallon, S.^d & Forwick, Matthias^e

^a*Canada Research Chair in Marine Geology, Institut des sciences de la mer de Rimouski (ISMER), Université du Québec à Rimouski, Rimouski QC, G5L 3A1, Canada*

^b*GEOTOP Research Center, Montreal QC, Canada*

^c*College of Earth, Ocean, and Atmospheric Sciences, Oregon State University, Corvallis OR97331, United States*

^d*Research School of Earth Sciences, Australian National University, Canberra, ACT, 2601, Australia*

^e*Department of Geosciences, UiT The Arctic University of Norway in Tromsø, Tromsø, 9037, Norway*

**Corresponding author: Julie.Velle@uqar.ca*

ABSTRACT

International Ocean Drilling Program (IODP) Expedition 341 in the Gulf of Alaska drilled the continental slope at Site U1419, recovering an exceptionally expanded sedimentary record covering the late Pleistocene and Holocene. The natural and laboratory-induced magnetic remanences of u-channels from the 112-meter-long spliced record were studied using the stepwise AF demagnetization procedure. Along with magnetic susceptibility, these parameters provide information about the magnetic properties of the sediment; including magnetic mineralogy, concentration, and grain size. Hysteresis loops were obtained on 95 discrete samples to assess their magnetic domain state and coercivity, and IRM acquisition curves were obtained for nine discrete samples for additional information on the magnetic mineralogy of the sediment. Due to the influence of magnetic mineralogy, lithology, depositional and post-depositional processes, the record is not suitable for paleointensity studies. However, these factors seem to have influenced the inclination record only to a minor extent and, with removal of intervals influenced by the environmental signal and by sampling and/or coring deformation, we are left with a robust geomagnetic signal. We argue that the inclination as measured after the 20 mT demagnetization step alone is the most accurate inclination estimate. The high resolution of the record (sedimentation rates in some intervals < 800 cm/yr) in combination with a detailed age model (Walczak et al., in prep) provides a unique opportunity to resolve centennial to millennial scale paleomagnetic secular variations (PSV). Comparing the U1419 inclination record to other Gulf of Alaska and western North American records shows several inclination features in common. Especially the similarity to IODP Exp. 341 Site U1418 demonstrates that a regional geomagnetic signal has been captured at Site U1419, and that the interval between 15,000 and 30,000 cal yr BP is the most robust part of the record. In addition to the U1419 inclination record, this paper presents the preliminary age model for IODP Exp. 341 Surveyor Fan Site U1418. The age model is based on 23 radiocarbon dates as well as 18 magnetic susceptibility-based tie-points to Gulf of Alaska core EW0408-87JC (Praetorius et al., 2015). The age model indicates that Site U1418 is similar temporal resolution to that of Site U1419, with sedimentation rates exceeding 1000 cm/kyr in some intervals. Together, the U1419

inclination record and U1418 age model offer a new regional correlation tools to this generally under-sampled region of the world.

Keywords: Inclination, paleomagnetic secular variation, North Pacific, Alaska, late Pleistocene

2.3 INTRODUCTION

Paleomagnetic secular variations (PSV) of the Earth's magnetic field recorded in geological archives provide regional expressions of dynamo activity (e.g., Lund, 2018; Korte et al., 2019a), while the variations observed provide a pattern that can be used for regional correlation and stratigraphic dating at millennial (Reilly et al., 2018) and in some cases centennial resolution (e.g., Lund, 1996; Stoner et al., 2007; Ólafsdóttir et al., 2013). Obtaining high-resolution PSV records with robust, independent age control is therefore essential to improve our understanding of geomagnetic change and temporally calibrating stratigraphic correlations.

The continuity of marine records makes them especially useful for paleomagnetic studies. Records from previously and/or presently glaciated margins are of particular interest as sedimentation rates are often high, thereby preserving geomagnetic change at high temporal resolution. Furthermore, the supply of fine-grained terrigenous material to glacial proximal core sites facilitate the generation of high-quality paleomagnetic records with mineral magnetic properties suitable for paleomagnetic studies (e.g., Tauxe, 1993). Being surrounded by present and previous ice sheets, the North Atlantic region is well represented when it comes to paleomagnetic studies with many high-quality records preserved (e.g., Channell, 1999; Stoner et al., 2007; 2013; Lund et al., 2017c). However, to improve our understanding of geomagnetic field dynamics that may be regional in scale, independently dated records from many other parts of the world are needed.

Paleomagnetic directional records from the Pacific sector are mainly obtained from the equatorial and western Pacific Ocean (e.g., Richter et al., 2006; Lund et al., 2017b) in the Pleistocene, and from the Arctic Alaskan margin (e.g., Lisé-Pronovost et al., 2009; Lund et al., 2016; Deschamps et al., 2017) and North American lakes (e.g., Verosub et al., 1986; Peng & King, 1992; Geiss & Banerjee, 2003) in the Holocene, with recent records building on prior data continuing these into the Pleistocene (Lund et al., 2017a; Reilly et al., 2018). In the Gulf of Alaska, one previous paleomagnetic study has been carried out on core EW0408-79JC and U1419 site survey core EW0408-85JC (Walczak et al., 2017). These two sites yielded a 17,400-year record of PSV and, together with other northeast Pacific records, formed the basis for the NEPSIAS inclination anomaly stack. Comparisons of the NEPSIAS stack to northern North Atlantic records demonstrated important connections between these directional records that offers important insights to the North American and Euro/Mediterranean flux lobes, as well as opening up for PSV correlations over longer distances (Walczak et al., 2017). In this study, we build upon the PSV record of Walczak et al. (2017) and extend the inclination record back to ~45,000 cal yr BP. We demonstrate that even in complex environments, the high lithogenic flux and accumulation rates associated with glacial proximal environments, when combined with robust high-resolution chronological control, can provide geomagnetic insights and stratigraphic tuning targets rarely obtained.

2.4 METHODS

Coring and u-channel sampling

The International Ocean Drilling Program (IODP) Expedition 341 took place in 2013 in the Gulf of Alaska, onboard the *JOIDES Resolution*. Site U1419 (59°31.9297'N; 144°8.0282'W) consists of five holes that were drilled on the upper continental slope between the mouths of the Kayak and Bering cross-shelf troughs (Fig. 1), at a water depth of 687

meters. A continuous record (splice) consisting mostly of sections from holes D and E (and to some extent from holes A, B and C), was established based on shipboard measurements of sedimentary physical properties (e.g., magnetic susceptibility, color, density, etc.). The composite depth below seafloor, or CCSF-A, depth scale is used in this paper and assumes that the mudline in the first core section of one hole (U1419B-1H-1A) is the sediment/water interface. This depth scale allows direct comparison with other measurements made at 1-cm intervals but is not corrected for sediment expansion during coring as in CCSF-B (c.f. Jaeger et al., 2014). The splice of Site U1419 comprises the sediment between 0 m CCSF-A (mudline) and 112.1 m CCSF-A.

U-channels were sampled from the presumably pristine center of the archive halves of split cores using 2x2 cm cross-section plastic liners with lengths of up to 1.5 meter at the IODP Gulf Coast Repository at Texas A&M University in College Station, Texas, USA. Highly compacted sediment and an abundance of clasts prevented the sampling of the intervals between 86.08–89.3 m CCSF-A, 90.2–91.6 m CCSF-A, as well as the very bottom of the splice from 111.4–112.1 m CCSF-A.

Physical properties

All u-channels were scanned using a Siemens SOMATOM Definition AS+ 128 CT scanner at *Institut national de la recherche scientifique, Centre Eau Terre Environnement* (INRS-ETE) in Québec City, Canada, for information on the sediment's physical properties (density) and internal structures. High-resolution (sub-millimeter) images were obtained for each 0.4 mm, with 0.2 mm overlap from one image to another. For each image, CT-number profiles reflecting density changes within the sediment were derived (cf. Fortin et al., 2013).

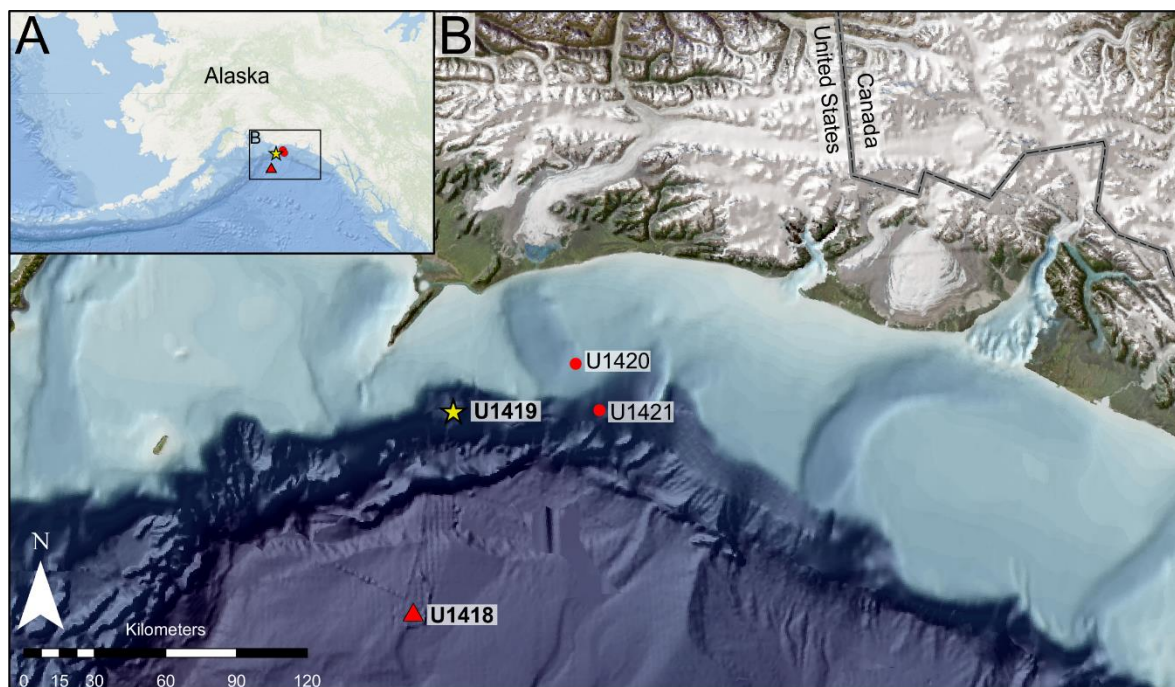


Figure 14: Overview of the Gulf of Alaska with IODP Expedition 341 drill Sites indicated. Site U1419 is indicated by a yellow star. This also marks the location of U1419 of site survey core EW0408-85JC mentioned in the text. The Surveyor Fan Site U1418 is indicated by a red triangle. This also marks the location of core EW0408-87JC mentioned in the text.

Continuous magnetic measurements

Remanence measurements were performed using 2G Enterprises™ model 755-1.65UC superconducting rock magnetometer at the Paleomagnetism and Marine Geology Laboratory at *Institut des sciences de la mer de Rimouski* (ISMER) in Rimouski, Canada, and at the Paleo-and Environmental Magnetism Laboratory at Oregon State University (OSU), USA. Stepwise alternating field (AF) demagnetization was used to study the natural remanent magnetization (NRM) and laboratory remanent magnetizations, all at 1 cm intervals. All archive core halves were measured and demagnetized up to 20 mT onboard the JOIDES Resolution as part of routine shipboard measurements (Jaeger et al., 2014). Any difference between the 0 mT and 20 mT steps seen in the u-channel measurements at ISMER

and OSU therefore correspond to a viscous remanent magnetization acquired by the sediment after its initial shipboard measurement. All u-channels were subsequently demagnetized using peak AF incremented at 5 mT steps from 20 to 70 mT and 10 mT steps from 70 to 100 mT. The anhysteretic remanent magnetization (ARM) was obtained by implementing a DC biasing field (0.05 mT) on the alternating field (100 mT), and the isothermal remanent magnetization (IRM) and saturated isothermal remanent magnetization (SIRM) were induced by using a 2G pulse magnetizer with intensities of 300 and 950 mT, respectively. For ARM and IRM, the u-channels were measured and subsequently demagnetized using peak AF fields of 10, 20, 25, 30, 35, 40, 45, 50 and 60 mT, whereas peak AF fields of 0, 10, 30, and 50 mT were used for SIRM. The magnetometers have response functions of 7-8 cm (Oda & Xuan, 2014), therefore, the first and last 5 cm of each u-channel were excluded to reduce the edge effect associated with section breaks (Weeks et al., 1993). Due to lack of azimuthal orientation during coring, declinations were rotated to a core mean of zero and then additionally rotated to align across the spliced core sections

ARM susceptibility (k_{ARM}) was obtained by normalizing the ARM by the biasing field and is indicative of the concentration of ferrimagnetic material in the sample, while being biased to smaller magnetic grain sizes (Banerjee et al., 1981). The median destructive field (MDF) is based on the AF demagnetization data and is defined as the AF required to reduce the initial remanent magnetization by half. Due to the initial shipboard NRM measurements and demagnetization (up to 20 mT), the calculation of MDF_{NRM} is not straightforward, therefore the MDF of ARM (MDF_{ARM}) is used instead as an indicator of coercivity of the remanence carriers.

Magnetic susceptibility is the magnetic response of a material to an applied magnetic field and is used as an indication of the concentration of magnetic (or magnetizable) material within a sample (Hatfield and Stoner, 2013). Analyses of the low-field magnetic susceptibility (k_{LF}) were performed at the Paleo-and Environmental Magnetism Laboratory at Oregon State University (OSU), USA. Each u-channel was measured three times using a three second measurement period at increments of 1 cm with a Bartington MS2 u-channel

loop sensor on a purpose-built automated tracking system. Similar results were obtained for each measurement of each u-channel, and the mean of the three iterations is reported here.

Discrete magnetic measurements

The Princeton Measurement Corporation MicroMag 2900 alternating gradient force magnetometer (AGM) at ISMER was used to obtain information on the sediment's hysteresis properties; coercivity (H_c), coercivity of remanence (H_{cr}), saturation magnetization (M_s), and saturation remanence (M_r), all of which are indicators of magnetic mineralogy and grain size (e.g. Day et al., 1977). Analyses were performed on small discrete samples collected from the base of each u-channel (approx. every 150 cm). The para- and diamagnetic contribution in the samples were corrected for using the MicroMag AGM software. IRM acquisition curves were obtained from ten selected samples, using a final field of 1 T with measurement increments of 25 mT.

Age models

The U1419 age model (Walczak et al, in prep) is based on radiocarbon dates from Site U1419 and gamma-ray attenuation bulk density (GRA) correlations to the independently dated U1419 site survey core EW0408-85JC (cf. Fig. 14) within the Holocene (Davies-Walczak et al., 2014). BChron (Haslett & Parnell, 2008) was used to generate an age model based on all planktic foraminiferal dates, with ΔR values set to reflect the paired benthic radiocarbon data available for this Site. A simple one-dimensional vertical circulation box model, assuming modern mixing (calculated as diffusion) with an input watermass age at 800-1000 m depth informed by the benthic ages, was used to estimate changes in surface ocean reservoir age. These results were then used to generate a time transient site-specific estimate of the ΔR value, averaging 330 ± 260 years over the past $\sim 45,000$ cal yr BP. All

dates were converted to calendar ages using the MARINE 13 calibration curve (Reimer et al., 2013).

Sediment samples from Site U1418 were sieved at 150 μm and picked for benthic and planktonic foraminifera, with care taken to avoid infaunal benthic species (as per methods reported for U1419 site survey core EW0408-85JC in Davies-Walczak et al., 2014). Radiocarbon analyses were performed at Australian National University (ANU) at the Single Stage Accelerator Mass Spectrometry (SSAMS) Lab in the Research School of Earth Sciences (Fallon et al., 2010). Instrument reproducibility over the course of the project was tracked via the analysis of 32 unleached aliquots of the 18,200 ^{14}C years TIRI/FIRI turbidite standard (Guilderson et al., 2003); individual dates averaged $18,210 \pm 50$ ^{14}C years ($1-\sigma$) and ranged from 18,110 to 18,300 ^{14}C years with individual reported errors of between 45-70 ^{14}C years. The Bayesian age model for U1418 was generated via an evaluation of all available planktic foraminiferal dates (23) and magnetic susceptibility-based tie-points to core EW0408-87JC (cf. Fig. 14; Table 3; Praetorius et al., 2015) in the age modeling program BChron (Haslett & Parnell, 2008). Ages were calibrated using the MARINE 13 calibration curve (Reimer et al., 2013) and a ΔR of 470 ± 80 , encompassing the range of regional modern observations (McNeely et al., 2006).

Table 3: Radiocarbon dates from Site U1418 and EW0408-87JC

Site	Sample name	Mean depth CCSF-A (m)	Age ^{14}C (years)	Age ^{14}C error $\sigma 1$	Calibrated age (cal yr BP)	Calibrated age error $\sigma 1$
EW0408-87JC	EW0408_87JC_38-40P	0.29	1640	15	704	16
EW0408-87JC	EW0408_87JC_207-210P	1.60	8520	20	8505	28
EW0408-87JC	EW0408_87JC_244-246P	1.91	10715	20	11221	14
EW0408-87JC	EW0408_87JC_249-251P	1.94	10740	40	11244	34.5
EW0408-87JC	EW0408_87JC_254-256P	1.96	10975	30	11734	73.5
EW0408-87JC	EW0408_87JC_266-268P	2.11	11090	25	11952	43
EW0408-87JC	EW0408_87JC_280-282P	2.28	11695	30	12695	20.5

EW0408-87JC	EW0408_87JC_300-302P	2.40	12460	40	13427	33.5
EW0408-87JC	EW0408_87JC_328-330P	2.65	13170	40	14195	54.5
EW0408-87JC	EW0408_87JC_340-342P	2.74	13330	45	14595	154.5
EW0408-87JC	EW0408_87JC_380-382P	3.07	13830	30	15475	74
U1418	U1418C_1H3_16-20P	3.18	13923	79	15626	137
EW0408-87JC	EW0408_87JC_419-422P	3.31	14290	40	16145	50
EW0408-87JC	EW0408_87JC_458-462P	3.61	14560	70	16499	110.08
EW0408-87JC	EW0408_87JC_490-494P	3.86	14840	70	16952	105.5
EW0408-87JC	EW0408_87JC_539-542P	4.41	14930	60	17085	82
EW0408-87JC	EW0408_87JC_918-922P	8.09	15060	45	17272	74
U1418	U1418D_2H3_16-20P	8.16	15167	49	17424	63.5
EW0408-87JC	EW0408_87JC_1000-1004P	9.15	15020	50	17212	82
U1418	U1418C_2H3_116-120P	14.17	15180	118	17422	154.5
EW0408-87JC	EW0408_87JC_1447-1450	16.14	15445	40	17753	57.5
U1418	U1418C_2H5_16-20P	16.17	15416	98	17718	114
U1418	U1418D_3H3_6-10P	18.30	15440	79	17745	96
U1418	U1418D_3H5_96-100P	22.20	15454	71	17760	86
U1418	U1418C_3H5_46-50P	26.14	15787	51	18122	70.5
U1418	U1418D_4H2_86-90P	28.15	15826	51	18172	91.5
U1418	U1418D_4H5_36-40P	32.153	16470	53	18841	43.5
U1418	U1418C_4H3_96-100P	34.193	16565	53	18922	47
U1418	U1418D_5H2_26-30P	38.145	17790	59	20411	73.5
U1418	U1418D_5H4_145-148P	42.145	18455	63	21244	97.5
U1418	U1418D_5H6_26-30P	44.145	18804	117	21715	137
U1418	U1418D_6H3_46-50P	50.201	19923	146	22932.5	188.66
U1418	U1418C_6H4_86-90P	56.15	22092	91	25577	87.5
U1418	U1418D_9H3_86-90P	80.192	28323	190	31282	102
U1418	U1418E_2H2_71-75P	90.162	34517	402	37959	573
U1418	U1418E_2H3_120-124P	92.162	37203	536	40914	514.08
U1418	U1418E_2H5_21-25P	94.162	42871	1073	45351	959.08
U1418	U1418A_11H5_76-80P	108.226	53278	4059	55670	4055.9
U1418	U1418C_15H1_62-66P	110.174	51253	3114	53688.5	3096.08
U1418	U1418C_17H1_146-150P	122.223	48036	2062	50422	2058.24
U1418	U1418D_14H5_106-110P	138.224	50268	2740	52606	2691

2.5 RESULTS

Chronostratigraphy

The age model for Site U1419 (Walczak et al., in prep) puts the base of the splice record at ~54,000 cal yr BP. When averaged over 500 years, sedimentation rates at this Site vary between 5 and 835 cm/kyr. The lowest rates are observed in the Holocene and deglacial portion of the record, after 16,500 cal yr BP, with a mean of 36.6 ± 25.6 cm/kyr. Prior to ~16,000 cal yr BP, sedimentation rates vary between 43.5 and 835 cm/kyr with a mean of 210 ± 135 cm/kyr. The highest rates (835 cm/kyr) are observed between 18,000 and 17,500 cal yr BP (Walczak et al., in prep).

In the U1418 age model, six dates older than ~40,000 cal yr BP exist and these are somewhat conjectural. Two dates from 90.2 and 92.2 m CCSF-A give ages of $37,960 \pm 573$ and $40,910 \pm 514$ cal yr BP, respectively. From this, the age model puts 40,000 cal yr BP at 91.5 m CCSF-A. Due to the uncertainties associated with dates > 40,000 cal yr BP, sedimentation rates were calculated for the age model below 40,000 cal yr BP only. The sedimentation rates were estimated assuming constant sedimentation between age constraints. For the interval between 20,000 and 11,000 cal yr BP (37 to 1.9 m CCSF-A), sedimentation rates were calculated between U1418 radiocarbon dates and a few selected EW0408-87JC tie-points only due to several overlapping tie-points and dates (cf. Fig. 15). Sedimentation rates at Site U1418 vary between 15 and 4179 cm/kyr, with a drastic shift in rates occurring at ~17,000 cal yr BP. Prior to 17,000 cal yr BP, sedimentation rates vary between 67 and 4179 cm/kyr with a mean of 1132 ± 1372 cm/kyr. The highest rates are observed between 18,000 and 17,000 cal yr BP. After 17,000 cal yr BP mean sedimentation rates drop to a mean of 31 ± 14 cm/kyr.

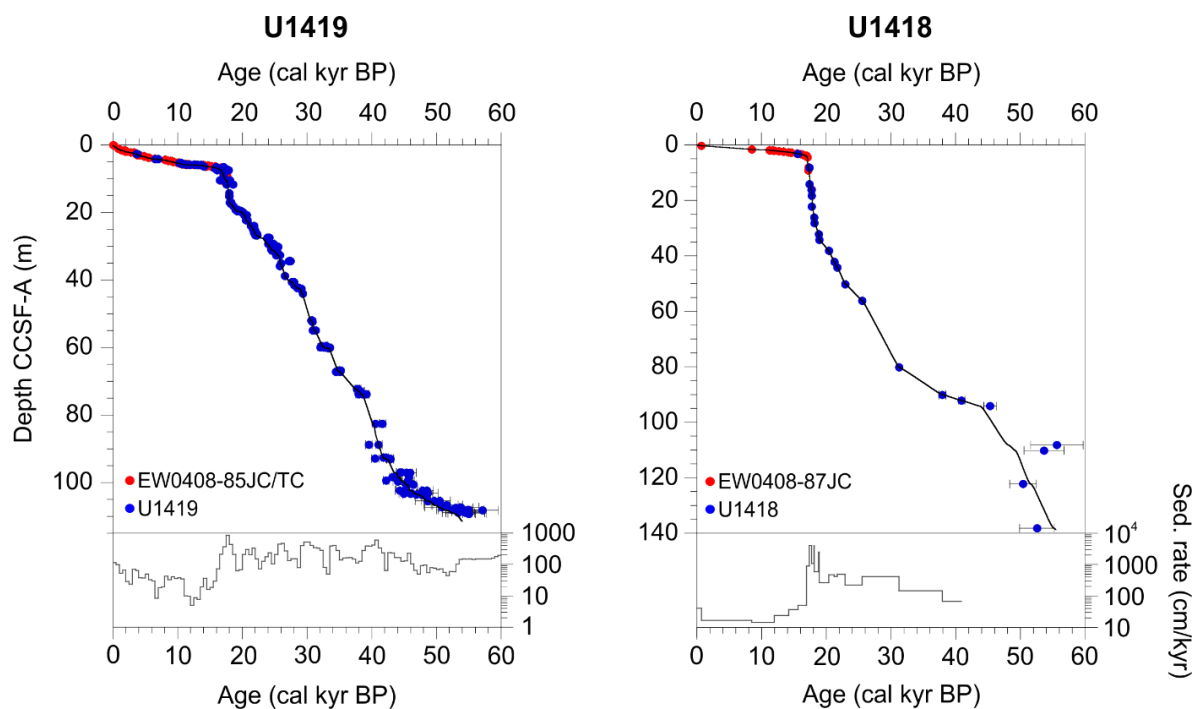


Figure 15: Left: U1419 age model (Walczak et al., in prep.) and sedimentation rates. Red circles indicate GRA tie-points to core EW0408-85JC and TC whereas blue circles are calibrated ages from Site U1419. Right: U1418 age model with sedimentation rates for the past 40,000 cal yr BP. Red circles indicate magnetic susceptibility tie-points to core EW0408-87JC (Praetorius et al., 2015) and blue circles indicate calibrated ages from U1418. Note the difference in Y axes, both for depth and sedimentation rates.

Lithology

Sediments at Site U1419 are dominated by their proximity to a temperate tidewater glacial system, with clast-poor diamict being the most commonly observed lithofacies (Jaeger et al., 2014; Penkrot et al., 2018). In contrast, post glacial sediment in the upper 6.3 m CCSF-A of the splice are characterized by lower density (800-1100 HU) massive muds with two discrete intervals of laminated and sub-laminated mud without clasts (Walczak et al., 2017; Velle et al., in prep). The remainder of the splice is characterized by variations of the diamict lithofacies, including clast-poor to clast-rich diamict, sandy diamict, and stratified

diamict (Penkrot et al., 2018) which are all generally associated with higher densities (1100-1700 HU). A few intervals of lower-density (1100-1200 HU) stratified or laminated muds with few clasts are observed at 76.6-75.7, 71.2-70.7, and 42.9-42.6 m CCSF-A (Velle et al., in prep), likely reflecting more pelagic depositional conditions.

Magnetic remanence and directions

NRM, ARM, and IRM all show decreasing intensities with depth. The highest NRM intensities after 20 mT AF demagnetization are found in the upper 4 m CCSF-A, corresponding to the Holocene (Walczak et al., 2017), with mean values of ~ 0.04 A/m \pm 0.01 A/m. Significant variability in NRM intensities are observed below, with the lowest values of $< 4 \times 10^{-4}$ A/m between 4.0 - 6.3 m, ~ 0.002 A/m between 15.9 - 16.6 m, and $< 4 \times 10^{-5}$ A/m between 97 - 109.2 m CCSF-A (Fig. 16). The overall trend of reduced intensity with depth is illustrated by NRM intensities averaged over 20 m intervals, that decrease from 0.018 ± 0.014 A/m for the 0 to 20 m interval to 0.004 ± 0.003 A/m from 60 to 80 m CCSF-A interval.

As noted above, the laboratory remanent magnetizations show a similar trend with high intensities in the upper 4 m CCSF-A; with values of 0.069 ± 0.018 A/m for ARM, 4.42 ± 0.952 A/m for IRM, and 4.43 ± 0.949 A/m for SIRM (because of the similarities, we discuss them as IRM below). IRM intensities remain generally high through the measured sequence with mean values of 4.34 ± 1.34 A/m between 6.3 and 92.5 m CCSF-A. Much lower values (mean of 1.5 ± 0.02 A/m) are found from 92.5 to 109 m CCSF-A with a return to higher values of ~ 5 A/m at the base (between 109 and 111 m CCSF-A; Fig. 16). In contrast to k_{LF} and IRM, ARM intensities, like NRM intensities, decrease with depth from a mean of 0.04 ± 0.02 A/m from 0 to 20 m to a mean of 0.02 ± 0.007 A/m from 60 to 80 m CCSF-A. Intervals with distinct weak ARM (0.007-0.01 A/m), and IRM and SIRM (0.1-1.0 A/m) are observed between 4.0 and 6.3 m CCSF-A, 15.9 and 16.6 m CCSF-A, and between 97 and 109 m CCSF-A (Fig. 16).

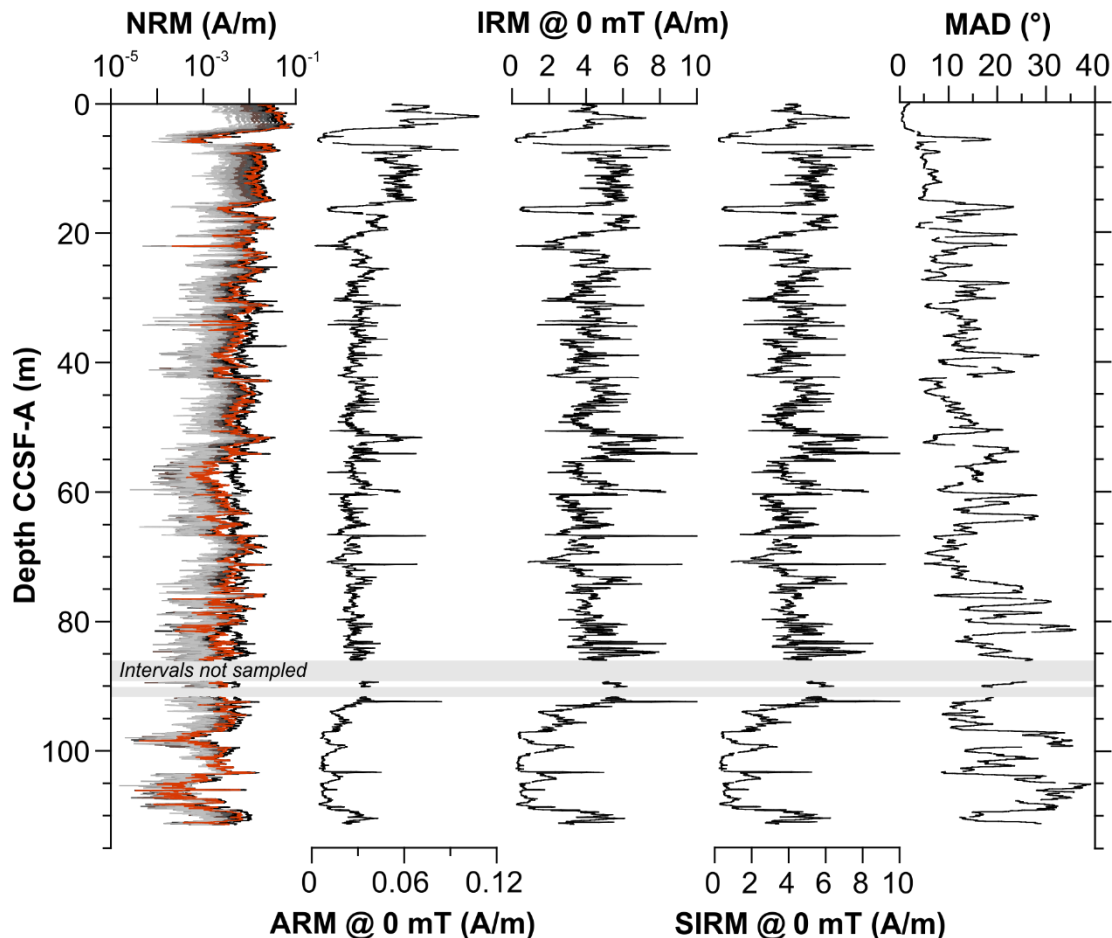
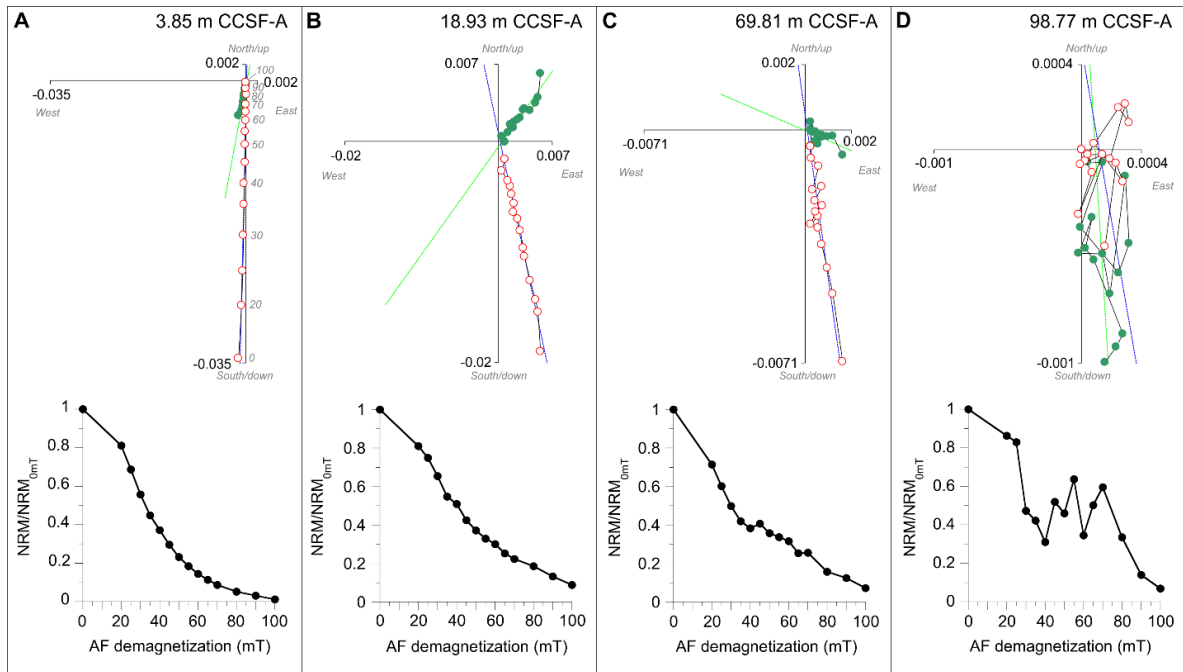


Figure 16: U1419 natural remanent magnetization (NRM) with all AF demagnetization steps with the 20 mT demagnetization step highlighted in red as it is described in more detail in the text. Note that the NRM is plotted on a log scale. Laboratory remanences (ARM, IRM, and SIRM) as measured before demagnetization, and the maximum angular deviation (MAD) values for the entire range of demagnetization steps.

Vector end-point diagrams (Zijderveld plots; Zijderveld, 1967; Fig. 17) document variably well resolved magnetizations that are in general best defined when using the lowest demagnetization steps. Principle component analysis, following the approach outlined by Kirshvink (1980), allow calculation of component magnetizations over various ranges of demagnetization steps while calculating the goodness of fit relative to a straight line using a

statistic known as maximum angular deviation values (MAD; e.g., Khokholov and Hulot, 2016). The upper ~ 5 m, corresponding to the Holocene, are associated with MAD values < 5° whereas higher MAD values of 5-20° are found between 5-6 m CCSF-A, corresponding to the Bølling-Allerød (Davies et al., 2011). Relatively low MAD values of 5-10° are found to a depth of 15 m CCSF-A, with MAD values variable (2.2-45°) and increasing with depth. Lower values are generally associated with higher remanence intensities. Using various subsets of demagnetization steps, Figure 18 shows that MAD values are reduced using ranges restricted to the lower coercivity steps, with little changes in inclination. MAD values based on low coercivity steps (20-40 mT) are mostly < 10° above 30 m CCSF-A, varying around 10° down to 70 m CCSF-A, and > 10° from 70 m CCSF-A to the base of the splice. MAD values are lowest (mean of $15.6^\circ \pm 10^\circ$) when using the lowest coercivity 20-40 mT interval, compared to those derived from a broader range or when using higher coercivity AF demagnetization steps. MAD values increase as intensities decrease, both down core and at the meter level, suggesting that higher AF demagnetization steps are adding noise rather than signal to our directional reconstructions. This is consistent with a mixed magnetic assemblage (see below) where the quality magnetization is dominantly held by the low coercivity ferrimagnetic component that reduces in concentration with depth, a classic signal for progressive reductive diagenesis (Stoner et al., 2003; Rowan et al., 2009; Walczak et al., 2017). This is supported by shipboard sulfate that declines to near zero by 23 m CCSF-A (Jaeger et al., 2014). Therefore, the NRM directions captured from lowest coercivity demagnetization steps are likely to be the most reliable (Fig. 18).

Figure 17 (next page): Vector end-point diagrams (Zijderveld, 1967) from four representative intervals of Site U1419 are displayed in top panels. AF demagnetization steps in mT are indicated in grey in panel A. Open circles represent projections on the vertical plane, and closed circles the horizontal plane. Corresponding demagnetization plots are displayed below.



Component inclinations (Fig. 18) captured from various demagnetization step intervals and inclination measured after the 20 mT AF demagnetization step vary around the expected geocentric axial dipole ($GAD = 73.6^\circ$) inclination for the site latitude. Large-scale inclination patterns are similar (Fig. 18) and the most prominent features can be recognized across the different steps used for PCA analysis. For example, steep inclinations at 20 and 32 m CCSFA, and the interval of shallow variability between 75 and 85 m CCSF-A. Component inclinations calculated from broader and/or higher ranges of AF demagnetization steps display more variability, as well as an increased occurrence and amplitude of shallow inclination intervals compared to that observed when measured after the 20 mT demagnetization step alone. The mean of the 20 mT inclination ($66.4^\circ \pm 18^\circ$) is closer to GAD than the mean values of the component inclinations (means between 59° and 63°). The largest differences between the 20 mT and PCA inclinations occur during shallow inclination intervals that often coincide with highest MAD values and low NRM intensities, suggesting

that higher AF demagnetization steps are introducing increased noise to the directional reconstruction. We, therefore, use the NRM after 20 mT AF demagnetization as our preferred directional record from this Site.

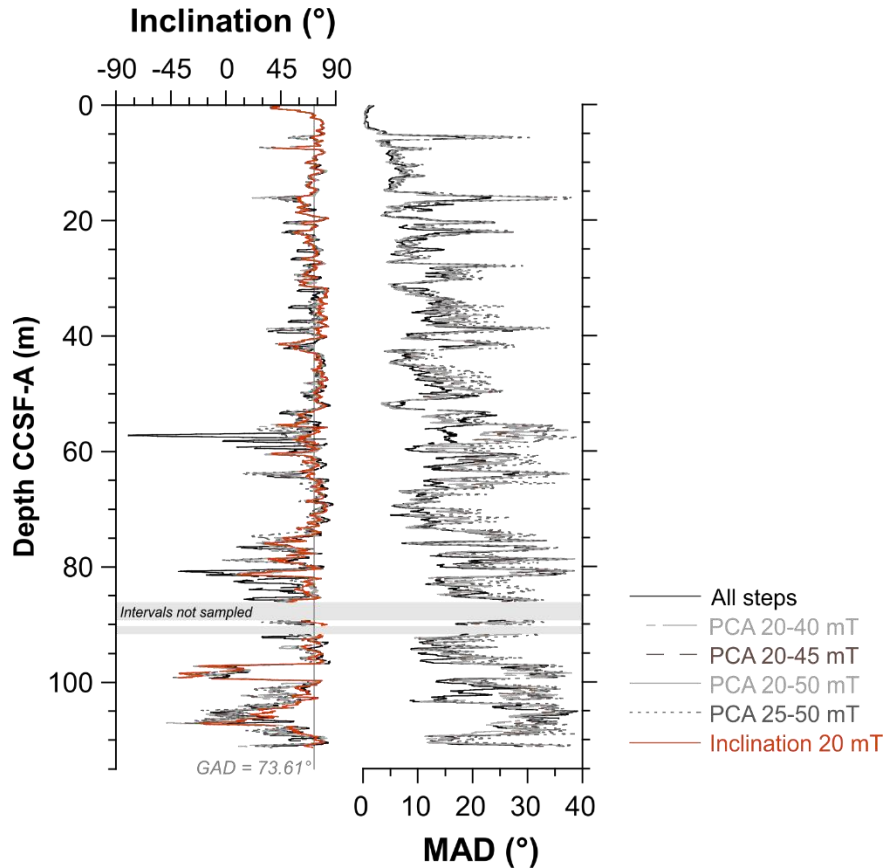


Figure 18: Selection of PCA ranges for U1419 inclination and MAD values, all with a 40-point smoothing. The inclination as measured at 20 mT highlighted in red as it is described in more detail in the text.

As noted above, the 20 mT inclination is generally GAD-like, with larger amplitude variations that include shallow and even negative inclinations more frequently observed below 96 m CCSF-A (Fig. 18). An abrupt shift to shallow (0-30°) and negative (-30°) inclination is observed between 96.9 and 99.5 m CCSF-A and corresponds to a shift in the

splice from one hole to another and general uncertainty in whether a continuous record was recovered (Jaeger et al., 2014). The descriptive information report (DESC; IODP database) confirms drilling disturbance at that depth. This is further corroborated by the CT scans and it is, therefore, reasonable to assume that these shallow and reversed inclinations result from sediment deformation. Similarly, the shallow inclination values ($30\text{-}50^\circ$) at the very top of the splice, between 0 and 1.3 m CCSF-A, are excluded due to soft sediment coring and sampling deformation, as noted in the u-channel sampling notes.

Magnetic mineralogy, grain size, and concentration

The magnetic susceptibility of the sediments at Site U1419 varies between 8×10^{-5} SI and 65×10^{-5} SI, with generally higher values observed between 6.3 and 92.5 m CCSF-A (mean of 46×10^{-5} SI $\pm 10 \times 10^{-5}$ SI). Notably lower magnetic susceptibility values between 8 and 16×10^{-5} SI are observed in the intervals 4-6.3, 93.9-94.7, 97.0-99., 101-103, and 105-109 m CCSF-A (Fig. 19).

Aside from in a few intervals, the MDF_{ARM} generally varies around 30 mT. The low intensity intervals at 109-105, 103-101, 99-97, and 94.7-93.9 m CCSF-A are associated with high > 50 mT MDF_{ARM} values. Whether these high coercivity phases are masked by high ferrimagnetic concentrations in other intervals is not apparent. All but two IRM acquisition curves saturated by 300 mT, further indicating a ferrimagnetic, likely (titano-) magnetite mineralogy (Fig. 20). Two samples from around 103 m CCSF-A did not saturate at 1 T, indicating a higher coercivity magnetic minerals such as e.g., hematite, are present in the low intensity and high MDF_{ARM} intervals (Fig. 19).

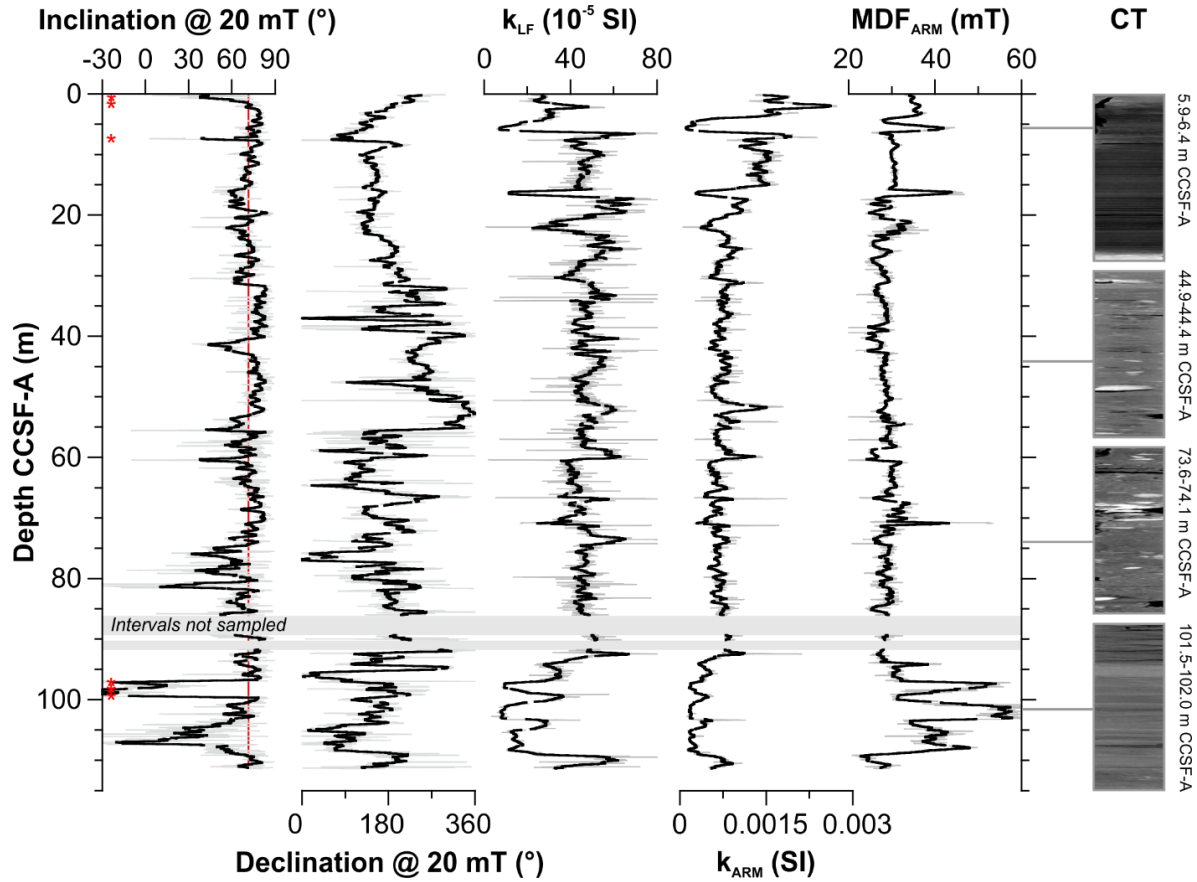


Figure 19: U1419 inclination measured at 20 mT with the GAD latitude (73.6°) indicated in red; rotated declination as measured at 20 mT, magnetic susceptibility (k_{LF}), ARM susceptibility (k_{ARM}), and MDF of ARM. Details from CT images displaying characteristic lithofacies are shown on the right. Red asterisks mark intervals that are disregarded due to disturbance either during drilling or u-channel sampling.

Hysteresis parameters are consistent with a mixture of magnetic grain sizes that fall within the pseudo-single domain (PSD) to multi-domain (MD) regions of a Day et al. (1977) plot, parallel to the Dunlop, (2002a, 2002b) magnetite mixing lines (Fig. 20). Higher coercivity ratios for any given M_r/M_s than expected for magnetite can be driven many factors including distributions of magnetic grain-sizes and mineralogies (Roberts et al., 2018). MDF_{ARM} (Fig. 19) illustrates down-core variations in coercivity, suggesting that there may

be a mixture of magnetic mineralogies. Samples plotting in the MD field are typically found below 60 m CCSF-A, but also occur in the low-intensity interval between 4.5 and 6.3 m CCSF-A, and at higher intensity intervals at ~27.3 and ~51.4 m CCSF-A. The largest scatter in hysteresis data are observed in samples from below 92.5 m CCSF-A.

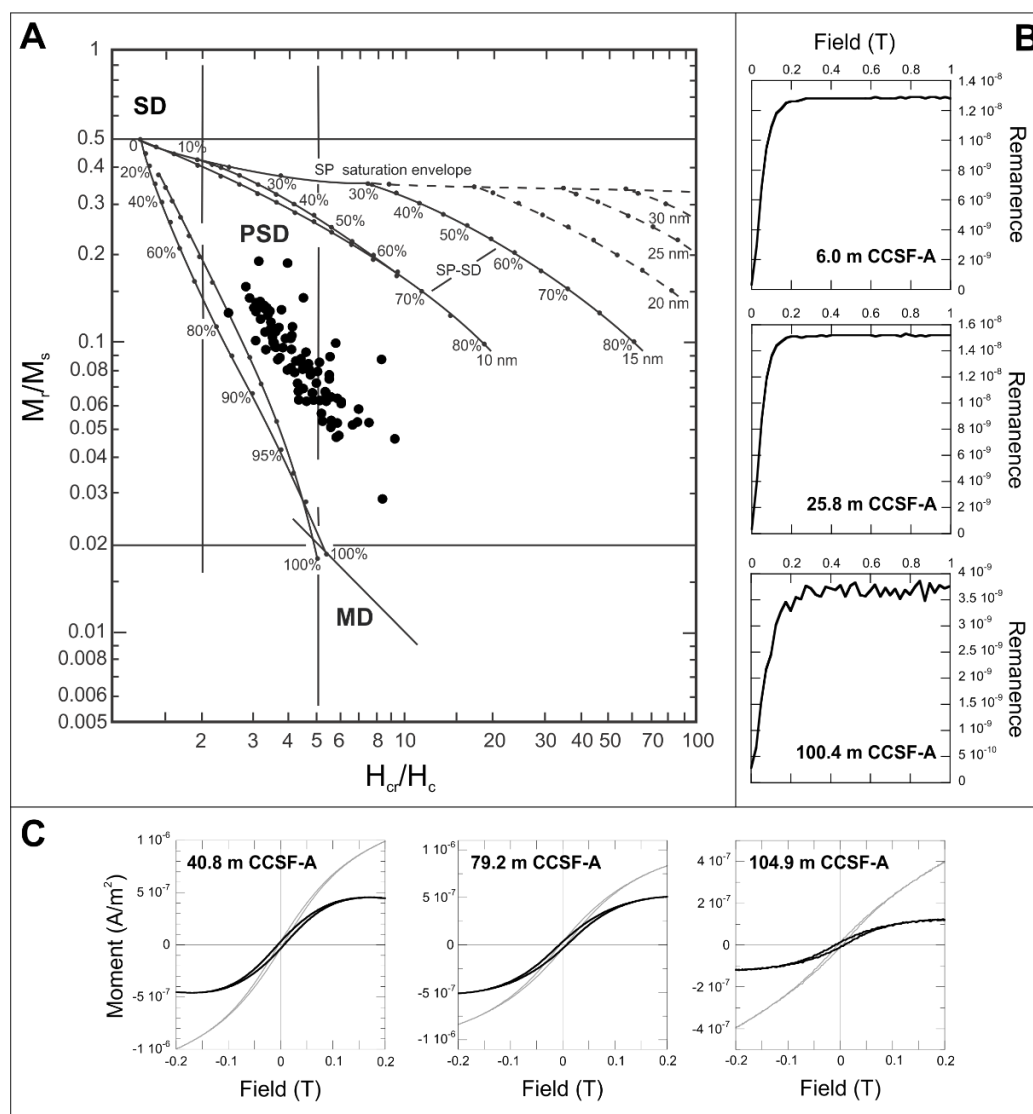


Figure 20: Panel A: Day plot (Day et al., 1977) with theoretical mixing lines from Dunlop (2002a, 2002b) of all Site U1419 discrete samples. Panel B: Selected IRM acquisition curves. Panel C: Selected hysteresis loops.

2.6 DISCUSSION

Natural remanent magnetization and directional record

Variable NRM intensities and the quality of magnetization as measured by the MAD values at Site U1419 are likely a result of an intricate interplay of lithology, magnetic mineralogy, depositional and post-depositional processes (diagenesis). This is illustrated, for example, by the downcore decrease in NRM intensity (Fig. 16) typical of reduction diagenesis (Karlin & Levi, 1983). In addition, difficulties in retrieving and sampling coarse-grained sediments may also have influenced the record. As a result, Site U1419 does not fulfill the criteria generally considered necessary to derive reliable relative paleointensity records (Tauxe, 1993; Stoner & St-Onge 2007). However, as Site U1419 has an exceptional radiocarbon chronology, a rarity for late Pleistocene paleomagnetic records and with sedimentation rates high enough to resolve centennial to millennial scale PSV, records of directional variability could facilitate a deeper geomagnetic understanding. The lack of precise dating often limits our ability for spatial comparison (e.g., Panovska et al., 2018) and as a result our understanding of the dynamics involved in geomagnetic change (Walczak et al., 2017).

Intervals of especially low remanence intensity (<0.001 A/m) coincide with intervals of low susceptibility, high coercivity as indicated by the MDF_{ARM} (Velle et al., in prep), and laminated sediment (Penkrot et al., 2018; Fig. 19) that sometimes also coincide with shallow inclinations. These intervals are characterized by a reduced influx of lithogenic sediment and increased productivity similar to that observed at the site's location during the Bølling-Allerød and earliest Holocene (Davies et al., 2011; Walczak et al., 2017; Velle et al., in prep). Benthic hypoxia led to non-steady state reduction diagenesis that adversely affected the magnetic mineralogy of a few intervals (Walczak et al., 2017), while most of the core preserved a reliable paleomagnetic record. In U1419, the most prominent of these intervals are associated with large-amplitude variations in magnetic concentration and coercivity from 92.5-111.5 m CCSF-A where shallow/negative inclinations occur during laminated and

stratified sediment intervals (Fig. 19). Sediments between 96 m CCSF-A and the base of the splice at 111.5 m CCSF-A, are therefore excluded from further interpretation. According to the age model (Walczak et al., in prep), this puts the base of the interpreted sequence at approx. 43,200 cal yr BP.

The presence of magnetite is indicated by hysteresis loops and IRM acquisition curves (Tauxe et al., 1996; Fig. 20), while the low coercivity implied by the AF demagnetization of the NRM and shown by the MDF_{ARM} suggests that (titano-) magnetite is the main remanence carrier. It is therefore our contention, that despite a weak NRM due to a low and variable concentration of (titano-) magnetite, the preserved remanence provides a reliable inclination estimate on millennial timescales. This is further supported by the inclination varying around the GAD through the entire record (Fig. 19). We contend that the preservation of paleomagnetic information results from ice proximal conditions providing a high concentration of fine-grained terrigenous material that buffers the system against diagenetic transformation, while resulting in great sedimentation rates exceeding 1 m/kyr, and at times 8 m/kyr (Walczak et al., in prep). The latter significantly reduces the interference of sedimentary-driven noise, commonly millimeter to decimeter in scale, on the recording and preservation of paleomagnetic secular variation features that occur on centennial/millennial time scales, and at these sedimentation rates extend over meters. Declination, however, is more difficult to work with, as these heterogenous sediments can give rise to core barrel rotation. While a zero-mean assumption, commonly used to align cores for declination, is also problematic when the 9.5 m length of a core may only be a few thousand years. Declination is therefore excluded from further interpretation.

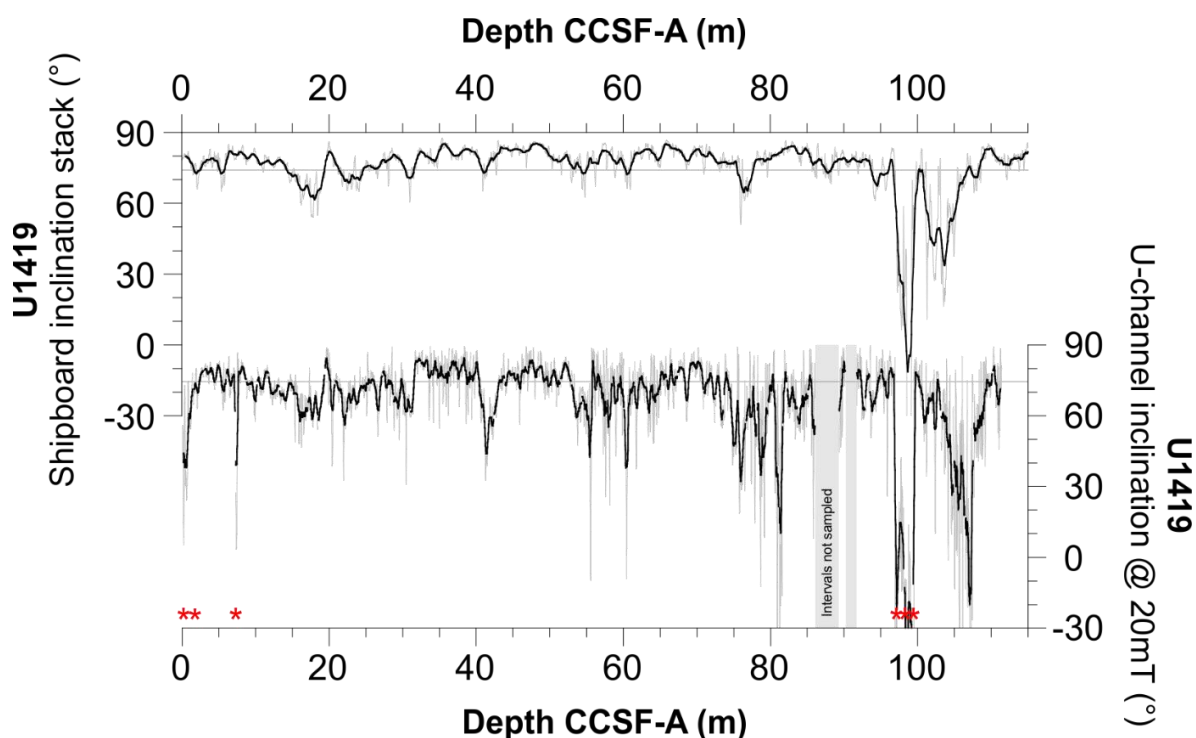
Regional comparisons

The fidelity of the U1419 PSV record can be assessed by comparison, first to the shipboard data as this controls for sampling and coring deformation, the latter as the shipboard data was stacked. Furthermore, the record was compared to other, independently

dated, regional records. Due to the high sedimentation rates and the sedimentary noise in the U1419 inclination record, a 40-point smoothing was used on intervals with sedimentation rates >80 cm/kyr in order to highlight the overall trend in the record.

The U1419 shipboard inclination record is based on all recovered sediments after 20 mT AF demagnetization (Jaeger et al., 2014) that were stacked using a Gaussian weighted running mean with full width at half maximum (FWHM) of 10 cm with edge effects and noted intervals of coring disturbance removed. Although the shipboard data was measured on half core sections that include deformation around the liner (cf. Acton et al., 2002), the stacking procedure reduces random noise, while reinforcing the common signal. The u-channel data collected from the pristine central part of what was deemed to be the best section should preserve the cleanest high-resolution record and agreement between the two represents an important step in reconstructing the geomagnetic signal. The comparison between the U1419 shipboard and u-channel inclinations in Figure 21 illustrates the general agreement between the two records. Shallow inclinations in the upper 1.3 m of the u-channel record are not observed in the shipboard data reflecting deformation during u-channel sampling from the extremely soft and water laden uppermost sediments. Additional intervals of shallow inclination below ~ 70 m CCSF-A may also result from u-channel sampling difficulties in sand and/or clasts rich and/or high density lithofacies (Jaeger et al., 2014; Penkrot et al., 2018; Velle et al., in prep). Some intervals (86.08–89.3, 90.2–91.6, and 111.4–112.1 m CCSF-A; Fig. 21) could not be sampled with u-channels due to these issues.

Figure 21 (next page): Comparison of U1419 shipboard inclination stack (see description in the text) and U1419 u-channel inclination as measured at 20 mT. The expected geocentric axial dipole inclination for the site latitude ($GAD = 73.6^\circ$) is indicated with the grey horizontal line. Red asterisks mark intervals that are disregarded due to disturbance either during drilling or u-channel sampling. Note that the figure includes the lowermost part of the splice (below 96 m CCSF-A) which has been excluded from further comparison.



The Holocene and deglacial portion of the U1419 inclination record was compared to the shipboard inclination stacks from Sites U1418 (Fig. 14) and U1419, U1419 site survey core EW0408-85JC (Walczak et al., 2017), and the Northeast Pacific sedimentary inclination anomaly stack (NEPSIAS; Walczak et al., 2017). NEPSIAS is based on lake sediment records from Alaska, Oregon, and Hawaii, as well as the Gulf of Alaska (EW0408-85JC). The comparison in Figure 22 shows that U1419 inclination features can be correlated to other regional records for the deglacial and Holocene, for example, the transition from shallow to steeper inclinations at 16,000 to 15,000 cal yr BP (*c* to *b* in Fig. 22). Distinctions between the records may be attributed to difference in resolution and chronology, especially for the more distal Site U1418 which only has a few meters of post-glacial deposits (Jaeger et al., 2014). Differences between Site U1419 and the site survey core EW0408-85JC may reflect lithologic (variable sedimentation rates and processes) and sampling noise in this lower accumulation rate part of the record. Lithologic differences between these two sites such as

varying thickness of the laminated and sub-laminated intervals have been noted previously (Velle et al., in prep). The overall similarity noted in Figure 22 and, especially, with the NEPSIAS stack that covers an area of over 30° latitude and longitude (Walczak et al., 2017) indicates that Site U1419 captures regional scale PSV during this time interval.

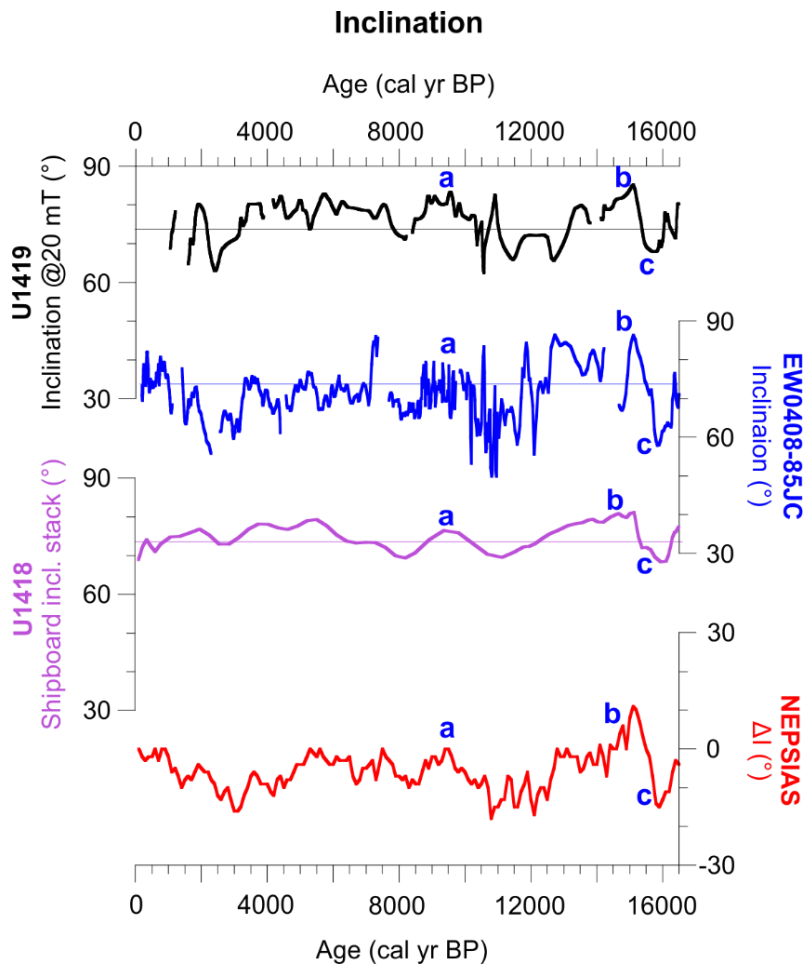


Figure 22: Comparison of the U1419 inclination (in black) to U1419 site survey core EW0408-85JC (in blue; Walczak et al., 2017), U1418 shipboard data (in purple), and the NE Pacific sedimentary inclination anomaly stack (NEPSIAS in red; Walczak et al., 2017). Letters are added to facilitate discussion. Note that the upper 1.3 meters of U1419 are removed due to sampling deformation (see text) and that u-channel edges are removed.

Beyond the past 16,000 years, Site U1419 inclination can be compared to the other high-resolution site drilled during Exp 341. Surveyor Fan Site U1418 (Fig. 14; Jaeger et al., 2014) inclination record is based on stacking of the shipboard derived inclination record of all holes drilled using a Gaussian weighted running mean with full width at half maximum (FWHM) of 10 cm after edge effects and intervals noted as sediment deformation were removed. Long-term sedimentation rates for Site U1418 have been estimated to 81 cm/kyr based on the Matuyama-Brunhes reversal (Gulick et al., 2015). However, radiocarbon dates show that late Pleistocene sedimentation rates were much higher (< 4179 cm/kyr; Fig. 15). A 5-point smoothing filter was applied to the U1418 data in intervals with sedimentation rates > 100 cm/kyr (i.e. after 17,000 cal yr BP). The deeper water depths (3677 m) of this Site on the upper Surveyor Fan and the lower organic carbon content may have spared this record from the same reductive diagenetic influences as sulfate remains above zero to ~83 m CCSF-A, whereas at Site U1419 this transition happens at ~23 m CCSF-A (Jaeger et al., 2014). Figure 23 shows that the two records on their own timescales are strikingly similar with the smoothed records being almost identical back to 25,000 cal yr BP. Apparent similarities are observed after 25,000 cal yr BP as well, with slight chronological offsets. The record is consistent with high-quality Holocene observations suggesting that PSV reflects 1 to 3 kyr long deviations from a GAD (Thompson, 1973). To facilitate discussion, prominent changes in inclination are denoted with blue letters (Fig. 23). It should be noted that transitions from either steep or shallow inclination are often abrupt followed by centennial to millennial variations of lower amplitude. Agreement between the records is less on these timescales. For example, the steep inclination features *f* at ~19,700 cal yr BP and *k* at ~25,000 cal yr BP are separated by intervals of shallow, low amplitude variability that is reasonably consistent across the two records. More discrepancies between U1419 and U1418 are observed after 30,000 cal yr BP, reflecting present chronological uncertainties and sedimentary and/or sampling induced paleomagnetic noise in these complex ice-proximal sedimentary environments, as well as the progressive diagenetic alteration of the (titano-) magnetite recorder at Site U1419. Similar PSV features across these records indicate that

U1419 has captured a largely reliable and well-dated inclination record for the Gulf of Alaska for the last 40 kyr.

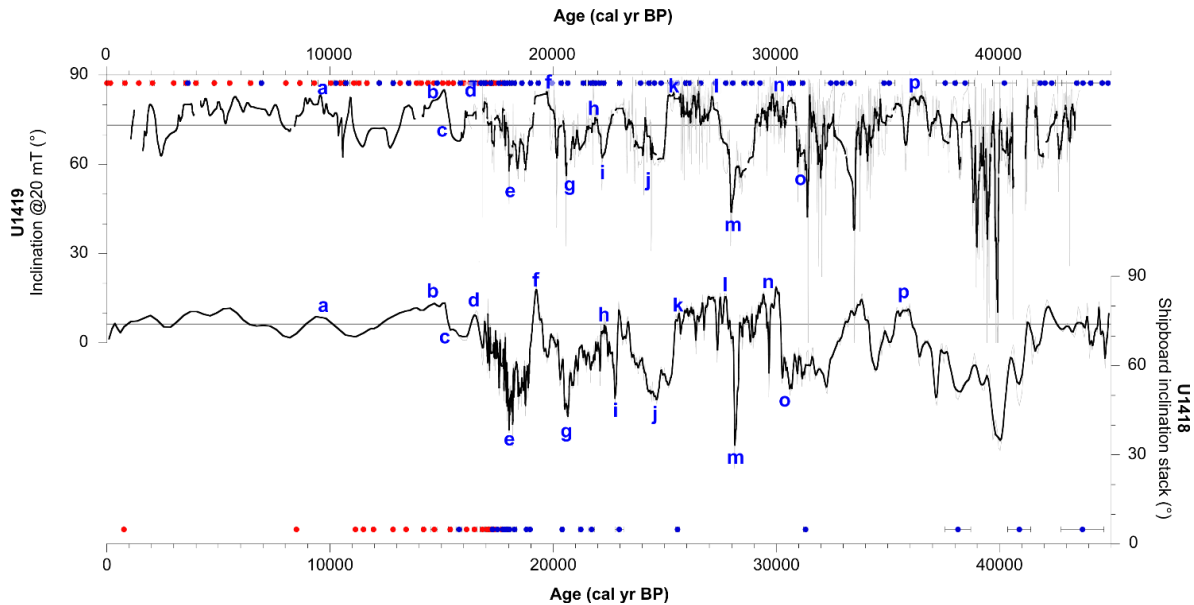


Figure 23: Comparison of the U1419 inclination record (with 40-point smoothing on intervals with sedimentation rates > 80 cm/kyr) and Expedition 341 Surveyor Fan Site U1418 shipboard inclination stack (with 5-point smoothing on intervals with sedimentation rates > 100 cm/kyr). Both records are plotted on their own individual age models with dates marked in blue and red circles (cf. Fig. 15). Inclination features are indicated with letters in blue to facilitate discussion; note that letters are continued from Figure 22.

Comparisons of U1419 inclination between 14,000 and 35,000 cal yr BP with the independently dated Western North America PSV stack (WNAM17; Reilly et al., 2018; Fig. 24) relocated to the Gulf of Alaska using a GAD approximation provide a larger regional perspective. The WNAM17 stack is based on PSV data from Fish Lake (Utah, US), Bear Lake (Utah/Idaho, US), and Bessette Creak (British Columbia, Canada). The overall pattern of the inclination records as well as individual features (e.g., feature *f* at $\sim 19,700$ cal yr BP) can be recognized at Site U1419 and in the WNAM17 stack (Fig. 24). Furthermore, the gradual transition from shallow to steeper inclinations from *g* to *f* and from *e* to *d*, as well as the more abrupt transition from *c* to *b* are recognized in both U1419 and the WNAM17 stack.

The similarity between U1419 u-channel inclination with independently dated Site U1418, and the WNAM17 stack suggests regional geomagnetic consistency, implying that much of the PSV record is driven by large-scale components of the geomagnetic field (Walczak et al., 2017). More records will be needed to determine if the differences observed in Figure 24 are a result of paleomagnetic/chronological noise or smaller scale geomagnetic signals that differ over such a vast region.

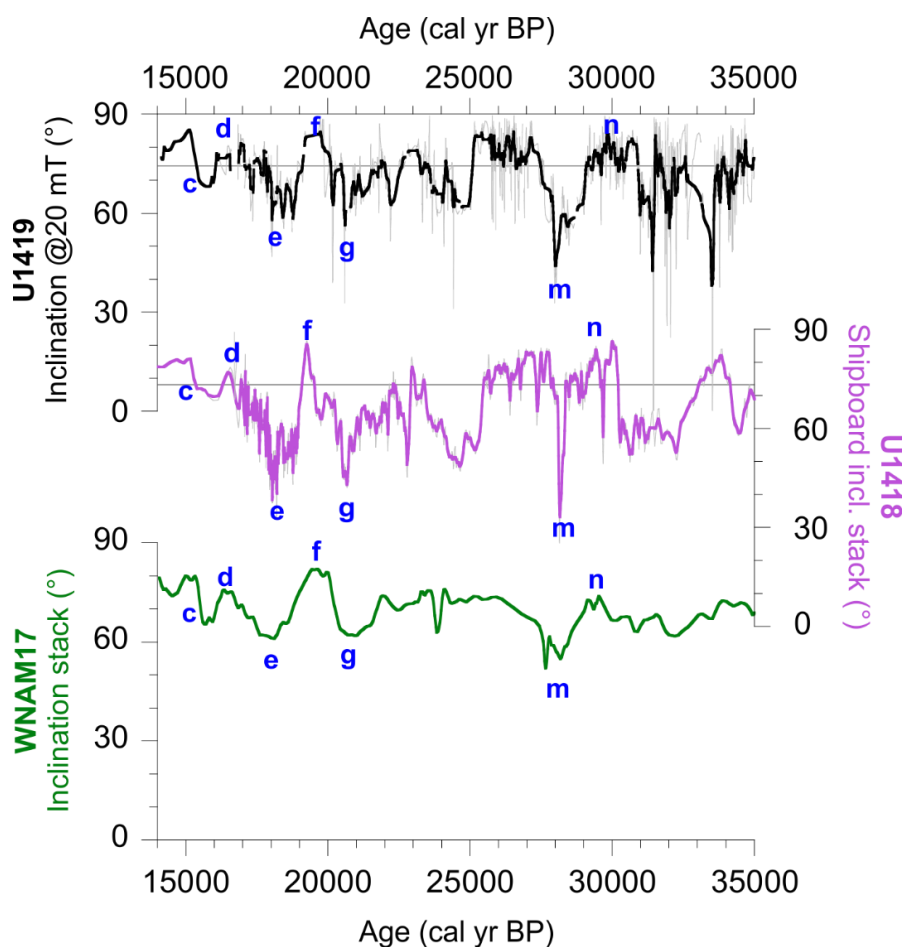


Figure 24: Comparison of the Site U1419 inclination record (40-point smoothing on intervals with sedimentation rates > 80 cm/kyr) with the Site U1418 shipboard inclination stack (with 5-point smoothing on intervals with sedimentation rates > 100 cm/kyr) and the Western North America inclination stack WNAM17 (relocated to the Gulf of Alaska using a GAD approximation; Reilly, et al., 2018), all on their individual age models. Letters are continued from figures 22 and 23 to facilitate discussion. Note that intervals identified as disturbed and/or deformed in the U1419 record are removed (cf. Fig. 19)

U1419 inclination record

After evaluation of the U1419 inclination and comparison with independently dated regional records and stacks, the interval between 15,000 and 30,000 cal yr BP resolves a robust geomagnetic signal of at least regional importance. Among the most prominent features in the U1419 record are abrupt transitions from shallow to steep inclination, *o* to *n*, *m* to *l*, *g* to *f* and from steep to shallow inclinations *k* to *j*, and *f* to *e* (Fig. 23). These are also recognized in the U1418 shipboard record (Fig. 23), and *m* possibly in the WNAM17 stack, although those records are of lower resolution and less well resolved (Fig. 24). The transition of 22.3° from feature *o* at 30,980 cal yr BP (53.6 m CCSF-A) to feature *n* at 52.0 m CCSF-A occurs over ~ 290 years. The lowest point of feature *m* (43.8°) occurs at 41.4 m CCSF-A at an age of $\sim 28,000$ cal yr BP and the recovery to the steeper feature *l* ($82\text{--}83^\circ$) occurs over 1.3 meters, or ~ 900 years. The abrupt transition from *k* to *j* (Fig. 23) occurs at 31.8 m CCSF-A, at 25,200 cal yr BP where the inclination drops from 83° to 62° over 70 cm or ~ 480 years. The steep feature *f* is recognized in the Gulf of Alaska records, as well as in the western North America stack (Fig. 24). In the U1419 record, the steepest inclination values (84.2°) of feature *f* are observed at 19.6 m CCSF-A at 19,700 cal yr BP. The transition to shallow inclinations at *e* occurs over a period of ~ 950 years (or 1.1 meters CCSF-A) to the shallowest inclination (58.2°) observed at 18.5 m CCSF-A at $\sim 18,750$ cal yr BP (Walczak et al., in prep). Features *m*, *k*, and *f* are followed by relatively abrupt transitions in inclination in the U1419 record, with rates of change between 0.03 and 0.07 degrees/year, although we can assume that these rates are a minimum due to sedimentary and u-channel smoothing. These rates are comparable to those found for non-excursion intervals during the late Pleistocene in sediment cores from the western North Atlantic Ocean, of approximately 0.08 degrees/year (Lund et al., 2005), suggesting that the GAD field is no more stable in the North Pacific than in other locations (McElhinny et al., 1996). These rates are, however, much lower than those observed from southwestern US archaeomagnetic data of 0.23 degrees/year associated with the last shallow to steep inclination transition ~ 1000 years ago (Hagstrum & Blinman, 2010) suggesting that we may still be looking at a low pass filtered geomagnetic signal.

Excursions are generally defined by anomalous PSV with deviation of virtual geomagnetic pole (VGP) more than 40-45° from axis of rotation (e.g., Merrill, et al., 1998). Two well-established excursions exist within the time interval explored in this study; the Laschamp excursion at ~41 ka, and the less well constrained Mono Lake excursion (34-30 ka; e.g., Laj & Channell, 2015; Valet et al., 2008; Lund et al., 2017a, 2017b). Despite the increased influence of the environmental signal on some parts of the record in this interval (below ~70 m CCSF-A, or 36,400 cal yr BP), the high resolution of the Sites would be expected to resolve any geomagnetic excursions. Shallow inclinations are observed between 80.4 and 75.6 m CCSF-A (~39,800-39,000 cal yr BP), and at 60.1 m CCSF-A and 55.1 m CCSF-A (~33,100 and ~31,300 cal yr BP, respectively). However, according to the sampling notes, these intervals contain coarser sediments as well as rocks that had to be removed to facilitate u-channel sampling. It is, therefore, more likely that they represent noise, as they are also short in duration, rather than geomagnetic field behavior associated with the Laschamp or Mono Lake geomagnetic excursions.

The lack of clear representations of these events at such high-resolution sites remains somewhat of an enigma. Both paleomagnetic data compilations (Panovska et al., 2018) and field models (Korte et al., 2019b) have found the Laschamp excursion to be less pronounced in the Pacific Hemisphere compared to in the Atlantic Hemisphere, possibly related to generally low sedimentation rates (Panovska et al., 2018). This is, however, not the case for Site U1419 where sedimentation rates between 40,000 and 42,000 cal yr BP are approximated to ~400 cm/kyr (Walczak et al., in prep). Regardless, a first of its kind record of PSV is resolved, that should facilitate a better understanding of the geomagnetic dynamics that give rise to excursions and geomagnetic change in general.

2.7 CONCLUSIONS

In this study, we show that IODP Site U1419 on the Alaskan slope, despite lithologic complexity due to its ice-proximal location and reduction diagenesis due to high productivity,

still preserves a reliable directional PSV record, providing a rare, well-dated and high-resolution record of inclination changes over the last ~43,000 years. This results from great sedimentation rates allowing millennial scale geomagnetic features to be extended over meters and a high flux of fine grained terrigenous material that buffers the paleomagnetic signal and results in its preservation despite the sulfate/methane transition occurring at 15 m CCSF-A. Comparisons with shipboard data, other Gulf of Alaska drill sites and those from the broader northeastern Pacific/western North American region (NEPSIAS, WNAM17) reveal what are apparently common inclination features captured in independently dated records over the past 35,000 years. Based on the local and regional comparisons, the inclination between 15,000 and 30,000 cal yr BP is regarded as the most robust part of the record. The PSV record captures abrupt transitions from shallow to steep (or vice versa) states with lower amplitude variability in between. Comparisons suggest that millennial scale changes are regional in nature and therefore reflect large scale geomagnetic dynamics, but it is too early to determine whether the observed abrupt transitions are a regional feature or only locally apparent. With a well-resolved age model, this Site provides an exceptional target for comparison to facilitate a better understanding of the geomagnetic field. The preliminary U1418 age model suggests that this Site is of similar resolution to that of Site U1419, with some intervals of even higher sedimentation rates (>1000 cm/kyr). This new age model provides further stratigraphic constraints on the Gulf of Alaska records and allows for robust PSV-based regional correlation for records that cannot be as well dated.

2.8 ACKNOWLEDGEMENTS

Expedition 341 was carried out by the Integrated Ocean Drilling Program (IODP). We thank the IODP-USIO and the captain and crew of the R/V JOIDES Resolution. Special thanks are due to the staff at the IODP Gulf Coast Repository, especially L. LeVey and P. Rumford, as well as B. Reilly and T. Hansen for their help during u-channel sampling. We are grateful to Q. Beauvais, M.-P. St-Onge and A.M. Ross for help in the lab. This study was

possible thanks to a GEOTOP scholarship to the first author, as well a Natural Sciences and Engineering Council of Canada Discovery Grant to G. St-Onge.

2.9 REFERENCES

- Acton, G.D., Okada, M., Clement, B.M., Lund, S.P. & Williams, T., 2002.** Paleomagnetic overprints in ocean sediment cores and their relationship to shear deformation caused by piston coring. *Journal of Geophysical Research*, **107 B4**, doi: 10.1029/2001JB000518
- Banerjee, S.K., King, J. & Marvin, J., 1981.** A rapid method for magnetic granulometry with applications to environmental studies. *Geophysical Research Letters*, **8(4)**, pp. 333-336, doi: 10.1029/GL008i004p00333
- Channell, J.E.T., 1999.** Geomagnetic paleointensity and directional secular variation at Ocean Drilling Program (ODP) Site 984 (Bjorn Drift) since 500 ka: Comparisons with ODP Site 983 (Gardar Drift). *Journal of Geophysical Research*, **104 B10**, pp. 22,973-22,951
- Davies, M.H., Mix, A.C., Stoner, J.S., Addison, J.A., Jaeger, J., Finney, B. & Wiest, J., 2011.** The deglacial transition on the southeastern Alaska Margin: Meltwater input, sea level rise, marine productivity, and sedimentary anoxia. *Paleoceanography*, **26**, PA2223, doi: 10.1029/2010PA002051
- Davies-Walczak, M., Mix, A.C., Stoner, J.S., Southon, J.R., Cheseby, M. & Xuan, C., 2014.** Late Glacial to Holocene radiocarbon constraints on North Pacific Intermediate Water ventilation and deglacial atmospheric CO₂ sources. *Earth and Planetary Science Letters*, **397**, pp. 57-66, doi: 10.1016/j.epsl.2014.04.004

- Day, R., Fuller, M. & Schmidt, V.A., 1977.** Hysteresis properties of titanomagnetites: Grain-size and compositional dependence. *Physics of the Earth and Planetary Interiors*, **13**, pp. 260-267, doi: 10.1016/0031-9201(77)90108-X
- Deschamps, C.E., St-Onge, G., Montero-Serrano, J.C. & Polyak, L., 2017.** Chronostratigraphy and spatial distribution of magnetic sediments in the Chukchi and Beaufort seas since the last deglaciation. *Boreas*, **47** (2), pp. 544-564, doi: 10.1111/bor.12296
- Dunlop, D. J., 2002a.** Theory and application of the Day plot (Mrs/Ms versus Hcr/Hc): 1. Theoretical curves and tests using titanomagnetite data, *Journal of Geophysical Research*, **107 B3**, 2056, doi:10.1029/2001JB000486.
- Dunlop, D. J., 2002b.** Theory and application of the Day plot (Mrs/Ms versus Hcr/Hc): 2. Application to data for rocks, sediments, and soils, *Journal of Geophysical Research*, **107 B3**, 2057, doi:10.1029/2001JB000487.
- Geiss, C.E. & Banerjee, S.K., 2003.** A Holocene-Late Pleistocene geomagnetic inclination record from Grandfather Lake SW Alaska. *Geophysical Journal International*, **153**, pp. 497-507, doi: 10.1046/j.1365-246X.2003.01921.x
- Fallon, S.J., Fifield, L.K. & Chappell, J.M., 2010.** The next chapter in radiocarbon dating at the Australian National University: Status report on single stage AMS. *Nuclear Instruments and Methods in Physics Research Section B: Beam Interactions with Materials and Atoms*, **268**, pp. 898-901, doi: 10.1016/j.nimb.2009.10.059
- Fortin, D., Francus, P., Gebhardt, A.C., Hahn, A., Kliem, P., Lisé-Pronovost, A., Roychowdhury, R., Labrie, J., St-Onge, G. & the PASADO Science Team, 2013.** Destructive and non-destructive density determination: method comparison and evaluation from the Laguna Potrok Aike sedimentary record. *Quaternary Science Reviews*, **71**, pp. 147-153, doi: 10.1016/j.quascirev.2012.08.024

- Guilderson, T.P., Southon, J.R. & Brown, T.A., 2003.** High-precision AMS ¹⁴C results on the TIRI/FIRI turbidite. *Radiocarbon*, **45**, pp. 75-80, doi: 10.1017/S0033822200032409
- Gulick, S.P.S., Jaeger, J.M., Mix, A.C., Asahi, H., Bahlburg, H., Belanger, C.L., Berbel, G.B.B., Childress, L., Cowan, E., Drab, L., Forwick, M., Fukumura, A., Ge, S., Gupta, S., Kioka, A., Konno, A., LeVay, L.J., März, C., Matsuzaki, K.M., McClymont, E.L., Moy, C., Müller, J., Nakamura, A., Ojima, T., Ribeiro, F.R., Ridgway, K.D., Romero, O.E., Slagle, A.L., Stoner, J.S., St-Onge, G., Suto, I., Walczak, M.D., Worthington, L.L., Bailey, I., Enkelmann, E., Reece, R. & Swartz, J.M., 2015.** Mid-Pleistocene climate transition drives net mass loss from rapidly uplifting St. Elias Mountains, Alaska. *PNAS*, **112(49)**, pp. 15042-15047, doi: 10.1073/pnas.1512549112
- Hagstrum, J.T. & Blinman, E., 2010.** Archeomagnetic dating in western North America: An updated reference curve based on paleomagnetic and archeomagnetic data sets. *Geochemistry, Geophysics, Geosystems*, **11(6)**, doi: 10.1029/2009GC002979
- Haslett, J. & Parnell, A., 2008.** A simple monotone process with application to radio-carbon-dated depth chronologies. *Journal of the Royal Statistical Society Series C Applied Statistics*, **57(4)**, pp. 399-418, doi: 10.1111/j.1467-9876.2008.00623.x
- Hatfield, R.G. & Stoner, J.S., 2013.** Magnetic proxies and susceptibility. *In*: Elias S.A. (ed) *The Encyclopedia of Quaternary Science* (Second edition), pp. 884-898, doi: 10.1016/B978-0-444-53643-3.00307-1
- Jaeger, J.M., Gulick, S.P.S., LeVay, L.J., & the Expedition 341 Scientists, 2014.** Proc. IODP, 341, College Station, TX (Integrated Ocean Drilling Program).
- Karlin, R. & Levi, S., 1983.** Diagenesis of magnetic minerals of recent haemipelagic sediments. *Nature*, **303**, pp. 327-330, doi: 10.1038/303327a0

- Khokhlov, A. & Hulot, G., 2016.** Principal component analysis of paleomagnetic directions: converting Maximum Angular Deviation (MAD) into an α_{95} angle. *Geophysical Journal International*, **204**, pp. 274-291, doi: 10.1093/gji/ggv451
- Kirschvink, J.L., 1980.** The least-squares line and plane and the analysis of paleomagnetic data. *Geophysical Journal International*, **62(3)**, pp. 699-718, doi: 10.1111/j.1365-246X.1980.tb02601.x
- Korte, M., Brown, M.C., Gunnarson, S.R., Nilsson, A., Panovska, S., Wardinski, I. & Constable, C.G., 2019a.** Refining Holocene geochronologies using palaeomagnetic records. *Quaternary Geochronology*, **50**, pp. 47-74, doi: 10.1016/j.quageo.2018.11.004
- Korte, M., Brown, M.C., Panovska, S. & Wardinski, I., 2019b.** Robust characteristics of the Laschamp and Mono Lake geomagnetic excursions: Results from global field models. *Frontiers in Earth Science*, **7**, pp. 86, doi: 10.3389/feart.2019.00086
- Laj, C. & Channell, J.E.T., 2015.** Geomagnetic excursions. *In: Schubert, G. (ed) Treatise on Geophysics volume (Second edition)*, Elsevier, pp. 343-383, doi: 10.1016/B978-0-444-53802-4.00104-4.
- Lisé-Pronovost, A., St-Onge, G., Brachfeld, S., Barletta, F. & Darby, D., 2009.** Paleomagnetic constraints on the Holocene stratigraphy of the Arctic Alaskan margin. *Global and Planetary Change*, **68**, pp. 85-99, doi: 10.1016/j.gloplacha.2009.03.015
- Lund, S.P., 1996.** A comparison of Holocene paleomagnetic secular variation records from North America. *Journal of Geophysical Research*, **101 B4**, pp. 8007-8024, doi: 10.1029/95JB00039
- Lund, S.P., Schwartz, M., Keigwin, L. & Johnson, T., 2005.** Deep-sea sediment records of the Laschamp geomagnetic field excursion (~41,000 calendar years before

present). *Journal of Geophysical Research*, **110**, B04101, doi: 10.1029/2003JB002943

Lund, S.P., Keigwin, L. & Darby, D., 2016. Character of Holocene paleomagnetic secular variation in the tangent cylinder: Evidence from the Chukchi Sea. *Physics of the Earth and Planetary Interiors*, **256**, pp. 49-58, doi: 10.1016/j.pepi.2016.03.005

Lund, S.P., Benson, L., Negrini, R., Liddicoat, J. & Mensing, S., 2017a. A full-vector paleomagnetic secular variation record (PSV) from Pyramid Lake (Nevada) from 47-17 ka: Evidence for the successive Mono Lake and Laschamp Excursions. *Earth and Planetary Science Letters*, **458**, pp. 120-129, doi: 10.1016/j.epsl.2016.09.036

Lund, S.P., Schwartz, M. & Stott, L., 2017b. Long-term palaeomagnetic secular variation and excursions from the western Equatorial Pacific Ocean (MIS2-4). *Geophysical Journal International*, **209**, pp. 587-596, doi: 10.1093/gji/ggx029

Lund, S.P., Oppo, D. & Curry, W., 2017c. Late Quaternary paleomagnetic secular variation recorded in deep-sea sediments from the Demerara Rise, equatorial west Atlantic Ocean. *Physics of the Earth and Planetary Interiors*, **272**, pp. 17-26, doi: 10.1016/j.pepi.2017.04.010

Lund, S.P., 2018. A new view of long-term geomagnetic field secular variation. *Frontiers in Earth Science*, **6(40)**, doi: 10.3389/feart.2018.00040

McElhinny, M.W., McFadden, P.L. & Merrill, R.T., 1996. The myth of the Pacific dipole window. *Earth and Planetary Science Letters*, **143**, pp. 13-22, doi: 10.1016/0012-821X(96)00141-0

McNeely, R., Dyke, A.S. & Southon, J.R., 2006. Canadian marine reservoir ages, preliminary data assessment, Open File 5049, Geological Survey of Canada, Ottawa.

Merrill, R., McElhinny, M. & McFadden, P., 1998. The Magnetic Field of the Earth, International Geophysics Series, Vol. 63, Academic Press, 531 pp.

- Oda, H. & Xuan, C., 2014.** Deconvolution of continuous paleomagnetic data from pass-through magnetometer: A new algorithm to restore geomagnetic and environmental information based on realistic optimization. *Geochemistry, Geophysics, Geosystems*, **15**, pp. 3907-3924, doi: 10.1002/2014GC005513.
- Ólafsdóttir, S., Geirsdóttir, Á., Miller, G.H., Stoner, J.S. & Channell, J.E.T., 2013.** Synchronizing Holocene lacustrine and marine sediment records using paleomagnetic secular variation. *Geology*, **41** (5), pp. 535–538, doi: 10.1130/G33946.1
- Panovska, S., Constable, C.G. & Brown, M.C., 2018.** Global and regional assessment of paleosecular variation activity over the past 100 ka. *Geochemistry, Geophysics, Geosystems*, **19**, pp. 1559-1580, doi: 10.1029/2017GC007271
- Peng, L. & King, J.W., 1992.** A Late Quaternary geomagnetic secular variation record from Lake Waiau, Hawaii, and the question of the Pacific nondipole low. *Journal of Geophysical Research*, **97 B4**, pp. 4407-4424, doi: 10.1029/91JB03074
- Penkrot, M.L., Jaeger, J.M., Cowan, E.A., St-Onge, G. & LeVay, L., 2018.** Multivariate modelling of glacial marine lithostratigraphy combining scanning XRF, multisensory core properties, and CT imagery: IODP Site U1419. *Geosphere*, **14**(4), pp. 1935-1960, doi: 10.1130/GES01635.1
- Praetorius, S.K., Mix, A.C., Walczak, M.H., Wolhowe, M.D., Addison, J.A. & Prahl, F.G., 2015.** North Pacific deglacial hypoxic events linked to abrupt ocean warming. *Nature*, **527**, pp. 362-366, doi: 10.1038/nature15753
- Reilly, B.T., Stoner, J.S., Hatfield, R.G., Abbott, M.B., Marchetti, D.W., Larsen, D.J., Finkenbinder, M.S., Hillman, A.L., Kuehn, S.C. & Heil, C.W., 2018.** Regionally consistent western North America paleomagnetic directions from 15 to 35 ka: Assessing chronology and uncertainty with paleosecular variation (PSV)

stratigraphy, *Quaternary Science Reviews*, **201**, pp. 186-205, doi: 10.1016/j.quascirev.2018.10.016

Reimer, P.J., Bard, E., Bayliss, A., Beck, J.W., Blackwell, P.G., Ramsey, C.B., Buck, C.E., Cheng, H., Edwards, R. L., Friedrich, M., Grootes, P.M., Guilderson, T. P., Hafliðason, H., Hajdas, I., Hatté, C., Heaton, T. J., Hoffmann, D.L., Hogg, A.G., Hughen, K.A., Kaiser, K.F., Kromer, B., Manning, S.W., Niu, M., Reimer, R.W., Richards, D.A., Scott, E.M., Southon, J.R., Staff, R.A., Turney, C.S. M. and van der Plicht, J., 2013. IntCal13 and Marine13 Radiocarbon Age Calibration Curves 0–50,000 Years cal BP, *Radiocarbon*, **55(4)**, pp. 1869–1887

Richter, C., Venuti, A., Verosub, K.L. & Wei, K.Y., 2006. Variations of the geomagnetic field during the Holocene: Relative paleointensity and inclination record from the West Pacific (ODP Hole 1202B). *Physic of the Earth and Planetary Interiors*, **156**, pp. 179-193, doi: 10.1016/j.pepi.2005.08.006

Roberts, A.P., Tauxe, L., Heslop, D., Zhao, X. & Jiang, Z., 2018. A critical appraisal of the «Day» diagram. *Journal of Geophysical Research: Solid Earth*, **123**, pp. 2618-2644, doi: 10.1002/2017JB015247

Rowan, C.J., Roberts, A.P. & Broadbent, T., 2009. Reductive diagenesis, magnetite dissolution, greigite growth and paleomagnetic smoothing in marine sediments: A new view. *Earth and Planetary Science Letters*, **277**, pp. 223-235, doi: 10.1016/j.epsl.2008.10.016

Stoner, J.S., Channell, J.E.T., Hodell, D.A. & Charles, C.D., 2003. A ~580 kyr paleomagnetic record from the sub-Antarctic South Atlantic (Ocean Drilling Program Site 1089). *Journal of Geophysical Research*, **108 B5**, 2244, doi: 10.1029/2001JB001390

Stoner, J.S, Jennings, A., Kristjansdottir, G.B., Dunhill, G., Andrews, J.T. & Hardardottir, J., 2007. A paleomagnetic approach toward refining Holocene

radiocarbon-based chronologies: Paleooceanographic records from the north Iceland (MD99-2269) and east Greenland (MD99-2322) margins. *Paleoceanography*, **22**, PA1209, doi:10.1029/2006PA001285

Stoner, J.S. & St-Onge, G., 2007. Magnetic stratigraphy in paleoceanography: reversal, excursion, paleointensity and secular variation. *In: Hillaire-Marcel, C. & De Vernal, A. (eds) Proxies in Late Cenozoic Paleooceanography*, Elsevier, pp. 99-138, doi: 10.1016/S1572-5480(07)01008-1

Stoner, J.S., Channell, J.E.T., Mazaud, A., Strano, S. & Xuan, C., 2013. The influence of high-latitude flux lobes in the Holocene paleomagnetic record of IODP Site U1305 and the northern North Atlantic. *Geochemistry Geophysics Geosystems*, **14(10)**, pp. 4623-4646, doi: 10.1002/ggge.20272

Tauxe, L., 1993. Sedimentary records of relative paleointensity of the geomagnetic field: Theory and practice. *Reviews of Geophysics*, **31(3)**, pp. 319-354, doi: 10.1029/93RG01771

Tauxe, L., Mullender, T.A.T. & Pick, T., 1996. Potbellies, wasp-waists, and superparamagnetism in magnetic hysteresis. *Journal of Geophysical Research*, **101 B1**, pp. 571-583, doi: 10.1029/95JB03041

Thompson, R., 1973. Palaeolimnology and palaeomagnetism. *Nature*, **242**, pp. 182-184, doi: 10.1038/242182a0

Valet, J.-P., Plenier, G. & Herrero-Bervera, E., 2008. Geomagnetic excursions reflect an aborted polarity state. *Earth and Planetary Science Letters*, **274(3-4)**, pp. 472-478, doi: 10.1016/j.epsl.2008.07.056

Velle, J.H., St-Onge, G., Stoner, J.S., Mix, A.C., Walczak, M., Jaeger, J.M. & Forwick, M., in prep. A late Pleistocene environmental magnetic record of northwestern Cordilleran Ice Sheet dynamics based on IODP Expedition 341 drill Site U1419 in the Gulf of Alaska.

- Verosub, K.L., Mehringer Jr, P.J. & Waterstraat, P., 1986.** Holocene secular variation in western North America: Paleomagnetic record from Fish Lake, Harney County, Oregon. *Journal of Geophysical Research*, **91 B3**, pp. 3609-3623, doi: 10.1029/JB091iB03p03609
- Walczak, M.H., Stoner, J.S., Mix, A.C., Jaeger, J., Rosen, G.P., Channell, J.E.T., Heslop, D. & Xuan, C., 2017.** A 17,000 yr paleomagnetic secular variation record from the southeast Alaskan margin: Regional and global correlations, *Earth and Planetary Science Letters*, **473**, pp. 177-189, doi: 10.1016/j.epsl.2017.05.022
- Walczak, M.H., Mix, A.C., Fallon, S., Cowan, E., Praetorius, S., Du, J., Hobern, T., Padman, J., Fifield, K., Stoner, J.S., Haley, B., in prep,** Coupled changes in Northeast Pacific ventilation and Cordilleran Ice Sheet discharge may precede Heinrich Events. *Science*
- Weeks, R.J., Laj, C., Endignoux, L., Fuller, M., Roberts, A., Manganne, R., Blanchard, E. & Goree, W., 1993.** Improvements in long-core measurement techniques: applications in palaeomagnetism and palaeoceanography. *Geophysical Journal International*, **114**, pp. 651-662, doi: 10.1111/j.1365-246X.1993.tb06994.x
- Zijderveld, J.D.A., 1967.** Demagnetisation of rocks: Analysis of results, *In*: Collinson, D. et al., (eds) *Methods in Palaeomagnetism*, pp. 254–286, Elsevier, New York.

CHAPTER 3
HIGH-RESOLUTION PALEOMAGNETIC SECULAR VARIATION AND
RELATIVE PALEOINTENSITY IN THE GULF OF ALASKA: CONSTRAINTS
ON THE LATE PLEISTOCENE AND HOLOCENE STRATIGRAPHY OF IODP
EXPEDITION 341 SITE U1418

3.1 SUMMARY OF CHAPTER 3

In the third chapter, the 27,000-year paleomagnetic record of Surveyor Fan Site U1418 is explored. At this high-resolution Site, the full paleomagnetic vector of inclination, declination, and paleointensity is recreated to better understand the geomagnetic signal of the northeastern Pacific region and to establish a robust paleomagnetism-based correlation tool for this region.

This chapter, titled “*High-resolution paleomagnetic secular variation and relative paleointensity in the Gulf of Alaska: Constraints on the late Pleistocene and Holocene stratigraphy of IODP Expedition 341 Site U1418*” was written by me under the guidance of my supervisor, Guillaume St-Onge, and my co-supervisors Joe Stoner (Oregon State University) and Matthias Forwick (The Arctic University of Norway) who revised several versions of this paper. Maureen Walczak (Oregon State University) constructed both the U1418 and U1419 age models that she kindly provided me with, along with any associated information. As first author, I performed the analyses, treated and interpreted the data, and wrote the paper. My three supervisors contributed greatly to the realization of this paper through assistance in the lab, help with interpreting data, and comments on the text. Guillaume St-Onge, Joe Stoner, Matthias Forwick, and Maureen Walczak were all part of the shipboard science party during IODP Expedition 341.

Results from this chapter were presented at the annual GEOTOP student meetings in Pohénégamook (2014; poster) and Jouvence (2015; poster), at the American Geophysical

Union Joint Assembly in Montréal (2015; poster), at the Association francophone pour le savoir (ACFAS) meeting in Rimouski (2015; poster), at the IODP Expedition 341 2nd post-cruise meeting in Friday Harbor (2015; poster), at the American Geophysical Union Fall meeting in San Francisco (2016; poster), and at the International Sedimentological Congress in Québec City (2018; talk).

3.2 HIGH-RESOLUTION PALEOMAGNETIC SECULAR VARIATION AND RELATIVE PALEOINTENSITY IN THE GULF OF ALASKA: CONSTRAINTS ON THE LATE PLEISTOCENE AND HOLOCENE STRATIGRAPHY OF IODP EXPEDITION 341 SITE U1418

Velle, Julie Heggdal^{a,b,*} ; St-Onge, Guillaume^{a,b} ; Stoner, Joseph S.^{b,c} ; Walczak, Maureen^c & Forwick, Matthias^d

^a*Canada Research Chair in Marine Geology, Institut des sciences de la mer de Rimouski (ISMER), Université du Québec à Rimouski, Rimouski QC, G5L 3A1, Canada*

^b*GEOTOP Research Center, Montreal QC, Canada*

^c*College of Earth, Ocean, and Atmospheric Sciences, Oregon State University, Corvallis OR97331, United States*

^d*Department of Geosciences, UiT The Arctic University of Norway in Tromsø, Tromsø, 9037, Norway*

*Corresponding author: Julie.Velle@uqar.ca

ABSTRACT

During the 2013 International Ocean Drilling Program (IODP) Expedition 341 in the Gulf of Alaska, a sedimentary record was retrieved from the upper Surveyor Fan Site U1418.

The upper 64.6 m of the splice were sampled with u-channels, all of which were analyzed with a high-resolution CT scanner for the visualization of sedimentary structures and identification of drilling and/or sampling deformation. All u-channels were subject to magnetic susceptibility measurements, as well as to the AF demagnetization procedure for studies of the natural and laboratory induced magnetic remanences, and information about the magnetic properties of the sediment. Furthermore, hysteresis loops were obtained from 54 discrete samples for additional insights to the magnetic domain state and coercivity of the sediment. The U1418 age model (cf. Velle et al., in prep) puts the base of the studied sedimentary sequence at 27,000 cal yr BP. Analyses show a generally high and stable concentration of pseudo-single domain (PSD) magnetite that carries a well-defined magnetic remanence ($MAD < 5^\circ$). The paleointensity proxy was constructed using the slope method on the 25-60 mT AF demagnetization steps of NRM/IRM. Adjustments to the U1418 age model were made through comparison with the inclination record of the independently dated Exp. 341 Site U1419, increasing the resolution of the age constraints for the paleomagnetic record. Comparisons of the U1418 inclination and declination record to other directional records indicate that Site U1418 has captured regional-scale paleomagnetic secular variations. Comparisons of Site U1418 relative paleointensity to other records on independent age models are, at this point, less conclusive although there are some indications that long-term global geomagnetic intensity trends have been recorded. Along with previously published PSV records from the Gulf of Alaska, Site U1418 aids in defining robust millennial-scale paleomagnetic secular variations (PSV) that permit regional comparison of records. Furthermore, the addition of a high-resolution relative paleointensity (RPI) record from this Site provides a first step in defining paleomagnetic intensity from the northeast Pacific.

Keywords: Paleomagnetic secular variation, relative paleointensity, North Pacific, Alaska, late Pleistocene

3.3 INTRODUCTION

The continuity of marine records makes them attractive targets for paleomagnetic studies, both for regional stratigraphic correlations as well as for improving our understanding of geomagnetic field variations. Reconstructions of either parts of, or the full paleomagnetic vector (inclination, declination, and relative paleointensity; RPI), are proven correlation tools, improving chronology of sedimentary sequences and allowing regional comparisons of proxy records (e.g., Barletta et al., 2008; Ólafsdóttir et al., 2013; Deschamps et al., 2018). Paleomagnetic records also allow exploration of the temporal and spatial patterns of Earth's magnetic field, with new observations suggesting that millennial-scale dynamics may be comparable over large spatial scales (Stoner et al., 2013; Walczak et al., 2017). High-resolution records accompanied by robust chronologies are, therefore, crucial to both empower and assess such observations.

Many high-resolution late Pleistocene paleomagnetic studies have been carried out in the North Atlantic, with the northeast Pacific the focus of only few such studies (cf. Panovaska et al., 2018). Most previous paleomagnetic studies from the North Pacific region are either from lower-resolution records, spanning hundreds of thousands to millions of years (e.g., Weeks et al., 1995; Roberts et al., 1997; Yamamoto et al., 2007), or Holocene records from western North America (Verosub et al., 1986; Hagstrum & Champion, 2002) and Hawaii (Peng & King, 1992). A few recent studies are crossing into the Pleistocene from western North America (e.g., Lund et al., 2017; Reilly et al., 2018) and the northeastern Pacific (Walczak et al., 2017; Velle et al., in prep), and are beginning to define paleomagnetic secular variations (PSV) in this region. However, as sedimentary records are often smoothed, not often continuous, often affected by lithologic and diagenetic variability and rarely well-dated, additional studies are needed to accurately define and assess the regional expressions of the geomagnetic field.

Periods of intense glaciations have resulted in a high flux of fine-grained terrigenous sediment to Gulf of Alaska (Jaeger et al., 2014; Gulick et al., 2015), providing the opportunity

to develop high-quality paleomagnetic records preserving geomagnetic changes at high temporal resolution. Detailed radiocarbon-based age models available from the Gulf of Alaska (Davies et al., 2011; Davies-Walczak et al., 2014; Praetorius et al., 2015; Walczak et al., in prep) allow the age evolution of these geomagnetic records to be examined with high temporal certainty. In this study, we further the exploration of the Gulf of Alaska paleomagnetic record (Walczak et al., 2017; Velle et al., in prep) by adding a high-resolution full vector paleomagnetic reconstruction of late Pleistocene sediments from Integrated Ocean Drilling Program (IODP) Site U1418. This record provides an improved understanding of regional PSV and RPI records and through correlation, enhancements to its chronology.

3.4 SITE SETTING

The Gulf of Alaska

The Gulf of Alaska (GoA) is located in the eastern North Pacific Ocean, off southern Alaska (Fig. 25). The oceanographic setting in the basin of the GoA is dominated by the westward flowing Alaska Current (AC), a branch of the Pacific subarctic gyre. The Alaska Coastal Current (ACC) flows westward on the continental shelf and is driven by a combination of winds and freshwater runoff from southern Alaska glaciers and rivers (Royer, 1982; Stabeno et al., 1995, 2004). Rivers (e.g., the Copper River) and glaciers (e.g., Bering and Malaspina glaciers) are the main transport paths of sediment to the Gulf of Alaska (e.g., Molnia & Carlson, 1978; Jaeger et al., 1998). The geological terranes of southern Alaska include the Yakutat, Prince William, Chugach, and Wrangelia terranes, as well as the Craig sub-terrane (Silberling et al., 1994). Erosion of the active orogen the St. Elias Mountains on the southern Alaskan coast has ensured a high flux of sediment to the GoA, especially during periods of expanded glaciation. This has resulted in the extensive Surveyor Fan with a sedimentary volume of $6.8 \times 10^5 \text{ km}^3$ that extends from the foot of the continental slope into the Alaskan Abyssal Plain (Reece et al., 2011).

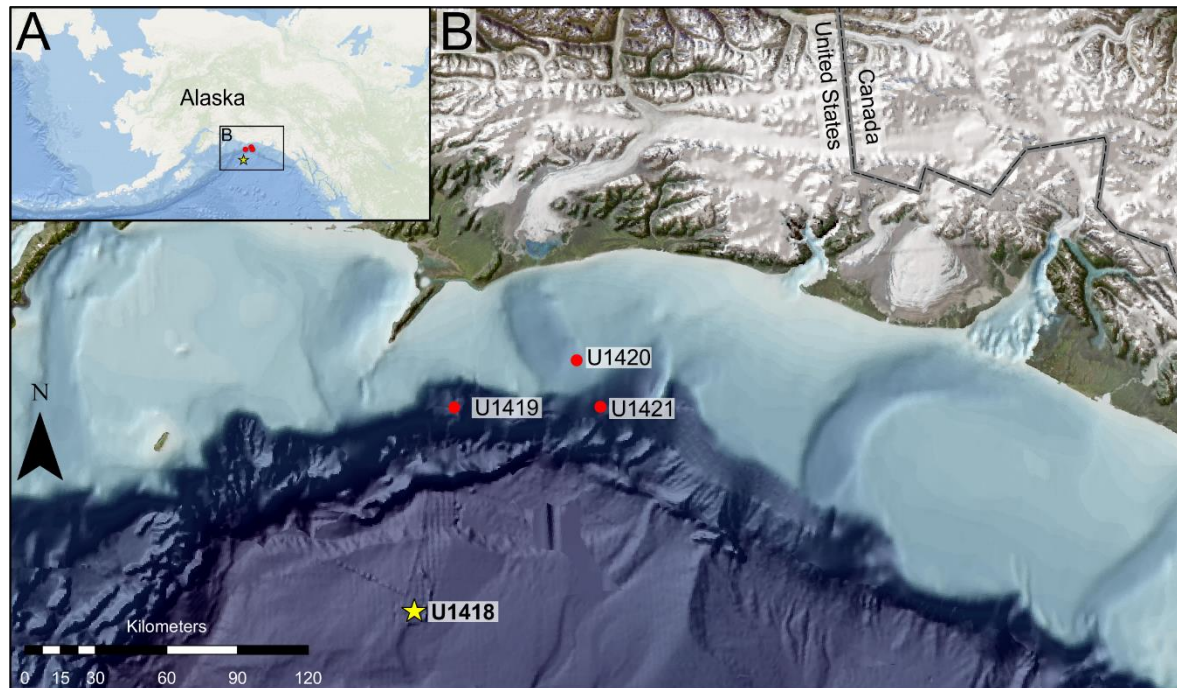


Figure 25: Location of IODP Expedition 341 drill Sites in the Gulf of Alaska. Site U1418 is indicated with a yellow star. Site U1418 also marks the location of core EW0408-87JC mentioned in the text.

IODP Expedition 341 drill Site U1418

International Ocean Drilling Program (IODP) Expedition 341 took place in 2013 in the Gulf of Alaska (GoA) onboard the JOIDES Resolution. More than 3 km of sediment cores from five drill sites on the continental margin and Surveyor Fan were retrieved during the expedition (Jaeger et al., 2014). Site U1418 ($58^{\circ}46.6095'N$, $144^{\circ}29.5777'W$) is located on the upper portion of the Surveyor Fan at a water depth of 3667 m (Fig. 25). Six holes (A to F) were drilled at this Site, recovering a total of 819 m of early Pleistocene to Holocene sediment. Long-term sedimentation rates (since the mid-Pleistocene transition) at the Site were estimated to 81 cm/kyr (Gulick et al., 2015), but are likely to have been much higher during specific shorter time intervals.

The sediment at Site U1418 is generally characterized by interbedded silt and color-banded mud, with lonestones occurring below 3 m CSF-A. Intervals of diatom-bearing to diatom rich mud, volcanic ash, and graded sand beds also occur sporadically throughout. The Pleistocene to Holocene sediment supply to Site U1418 is thought to be mainly settling and overbank deposits from sediment gravity flows from the adjacent channels on the Surveyor Fan, as well as dropstones from iceberg and/or sea-ice rafting (Jaeger et al., 2014).

3.5 METHODS

U-channel sampling

The u-channel sampling was performed at Texas A&M University at the IODP Gulf Coast Repository in College Station, Texas, USA. Plastic liners (u-channels) with cross-sections of 2x2 cm and lengths up to 1.5 meter were sampled in the splice record from the center of the archive halves of split cores. The continuous splice record is based on shipboard measurements of physical properties and magnetic susceptibility using mainly sections of holes C and D, with a few sections from holes A and E. The splice studied here only contains u-channels from cores C and D. The composite depth below seafloor (CCSF-A) depth scale is used in this study and assumes that the mudline in core U1418C-1H is the sediment/water interface (Jaeger et al., 2014). The upper 64.6 m CCSF-A (53 u-channels) of Site U1418 are the focus of this study.

Continuous magnetic measurements

Remanence measurements were performed using the 2G Cryogenic u-channel magnetometers at marine geology and paleomagnetism laboratory at *Institut des sciences de la mer de Rimouski* (ISMER) in Rimouski, Canada, and at the Paleo-and-Environmental

Magnetism Laboratory at Oregon State University, USA. The u-channel magnetometers measure at 1 cm intervals and have response functions with a width at half height of 7-8 cm (Oda & Xuan, 2014). In order to reduce edge effects associated with section breaks, the first and last 5 cm of each u-channel were excluded (Weeks et al., 1993). As part of routine shipboard measurements, archive core halves were measured and demagnetized up to 20 mT onboard the JOIDES Resolution (Jaeger et al., 2014). Therefore, differences between the 0 mT and 20 mT steps observed in the u-channel measurements at OSU and ISMER correspond to a viscous remanent magnetization acquired by the sediment after its initial shipboard measurement.

The stepwise alternating field (AF) demagnetization procedure was used to study the natural remanent magnetization using the following demagnetization steps: 0 and 20 mT, from 20 to 70 mT with 5 mT increments, and from 70 to 100 mT with 10 mT increments. The characteristic remanent magnetization (ChRM) was determined using principal component analysis and the least-square line-fitting method (Kirschvink, 1980) available in the Mazaud spreadsheet (Mazaud, 2005). The anhysteretic remanent magnetization (ARM) was obtained by implementing a DC biasing field (0.05 mT) on the alternating field (100 mT). Normalizing the ARM with the biasing field results in the anhysteretic susceptibility (k_{ARM}) and provides information on magnetic grain size and concentration (e.g., Stoner et al., 1996). Isothermal remanent magnetization (IRM) and saturated isothermal remanent magnetization (SIRM) were induced by using a 2G pulse magnetizer with intensities of 300 and 950 mT, respectively. The u-channels were subsequently demagnetized and measured using the AF demagnetization procedure at peak AF fields of 0, 10, 20, 25, 30, 35, 40, 45, 50, 60, and 80 mT for ARM and IRM, and 0, 10, 30, and 50 mT for SIRM.

The relative paleointensity (RPI) estimate is obtained by normalizing the intensity of the NRM by the intensity of a laboratory induced magnetization (e.g., ARM, IRM). The normalizer should activate the same range of magnetic particles that holds the NRM intensity (Levi & Banerjee, 1976) and should not be coherent with the normalized intensity (Tauxe, 1993). Two methods of normalization were explored in this study; the slope method (Tauxe

et al., 1995) and the ratio method (e.g., Stoner et al., 2000; Barletta et al., 2008; Lisé-Pronovost et al., 2013; Caron et al., 2018). The first determines the slopes of the NRM vs. the normalizer of the selected AF demagnetization interval, while the latter is constructed by averaging the normalized NRM over the selected range of AF demagnetization steps.

Low-field magnetic susceptibility (k_{LF}) was measured using a Bartington MS2 u-channel loop sensor on an automated tracking system at Oregon State University, USA. Each u-channel was measured with three iterations of 1 cm increments. The values reported in this paper are means of the repeated measurements. Magnetic susceptibility is a measure of the concentration of magnetizable material within the sample and can be used in combination with other magnetic properties as a measure of, for example, relative variations in magnetic grain size. k_{ARM}/k_{LF} is one such parameter which varies inversely with magnetic grain size (Thompson & Oldfield, 1986; Stoner et al., 1996).

Discrete magnetic measurements

Fifty-four discrete samples were collected from the base of each u-channel (approx. every 1.5 meters) and measured using a Princeton Measurement Corporation MicroMag 2900 alternating gradient force magnetometer at ISMER. Any para- and diamagnetic contributions in the samples were corrected using the MicroMag AGM software. The AGM analyses provide information on the hysteresis properties of the sediments, including coercivity (H_c), coercivity of remanence (H_{cr}), saturation magnetization (M_s), and saturation remanence (M_r). These properties are useful indicators of magnetic mineralogy, as well as for magnetic grain size if the sediment is mainly magnetite/titanomagnetite (e.g., Day et al., 1977; Tauxe et al., 1996; Dunlop, 2002a, 2002b).

CT scanning

Information on the physical properties of the sediments (density), internal structures, and possible coring and/or sampling deformation was gathered from CT-scans of all u-channels. The scanning was performed at *Institut national de la recherche scientifique, Centre Eau Terre Environnement* (INRS-ETE) in Québec City, Canada, using a Siemens SOMATOM Definition AS+ 128 CT scanner. The scanner is capable of detecting density changes as small as 0.1% and its source/detector rotates 360° around the sample, creating high-resolution (sub-millimeter) images from each rotation. Images were obtained at intervals of 0.4 mm, with 0.2 mm overlap from one image to the next. Furthermore, CT-number profiles reflecting density changes in the sediment were derived for each image (cf. Fortin et al., 2013).

Age model

The U1418 age model (Velle et al., in prep) is based on 23 radiocarbon dates from Site U1418, as well as 18 magnetic susceptibility-based tie-points to core EW0408-87JC (cf. Fig. 25; Praetorius et al., 2015). The Bayesian age model for U1418 was generated in BChron (Haslett & Parnell, 2008) via an evaluation of all available planktic foraminiferal dates. Ages were calibrated using the MARINE 13 calibration curve (Reimer et al., 2013) and a ΔR of 470 ± 80 , encompassing the range of regional modern observations (McNeely et al. 2006).

3.6 RESULTS

Chronology

The date closest to the base of the studied sedimentary sequence (64.6 m CCSF-A) is $25,580 \pm 88$ cal yr BP at 56.15 m CCSF-A (Fig. 26). The next date in the U1418 age model is $31,280 \pm 102$ cal yr BP at 80.19 m CCSF-A. The age model dates the base of the studied sequence at approx. 27,600 cal yr BP. Sedimentation rates were calculated for the age model $< 40,000$ cal yr BP, assuming constant sedimentation between age constraints. Due to several overlapping dates and tie-points in the time interval between 20,000 and 11,000 cal yr BP (37-1.9 m CCSF-A), sedimentation rates were calculated between U1418 radiocarbon dates and a few selected EW0408-87JC tie-points only.

Between 30,000 and 19,000 cal yr BP, sedimentation rates (Fig. 26) vary between 220 and 500 cm/kyr, whereas they vary from 600 and 4200 cm/kyr between 19,000 and 17,000 cal yr BP. After 17,000 cal yr BP, sedimentation rates rapidly drop to < 100 cm/kyr, reaching a low of 15 cm/kyr between 12,000 and 8,500 cal yr BP. Thus, the upper 4 meters CCSF-A of the record span the past 17,000 years, while the lowermost ~60 meters CCSF-A span only an additional 10,000 years.

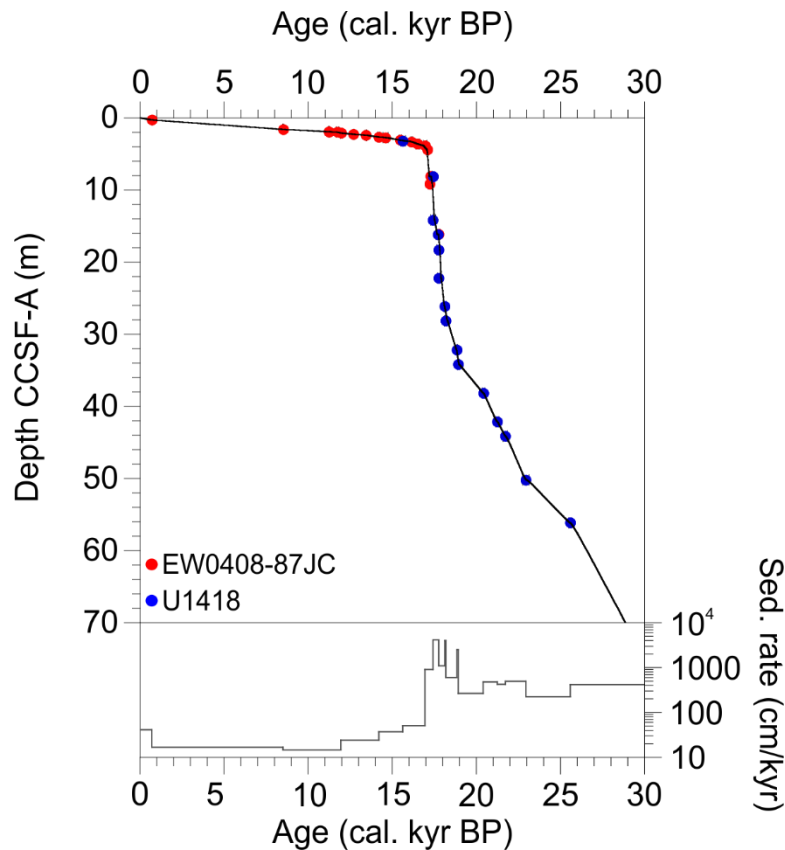


Figure 26: U1418 age model (Velle et al., in prep). Blue circles indicate radiocarbon dated levels of Site U1418. Red circles indicate magnetic susceptibility-based tie-points to the independently dated Gulf of Alaska core EW0408-87JC (Praetorius et al., 2015).

Physical properties and lithology

The upper 3.9 m CCSF-A of Site U1418 is characterized by massive sediment with some bioturbation and macrofossils. Below this depth, the remainder of the studied U1418 sequence consists of laminated and stratified sediments with scattered clasts, as well as some shorter (5-60 cm) intervals of more massive, low-density sediment with clasts (Fig. 27). No change in the general lithology is observed in the studied sequence. Intervals of coring and/or u-channel sampling deformation are identified between 3.77-3.89 m CCSF-A, 4.79-4.88 m

CCSF-A, and 6.10-6.35 m CCSF-A. These intervals have been excluded from further interpretation.

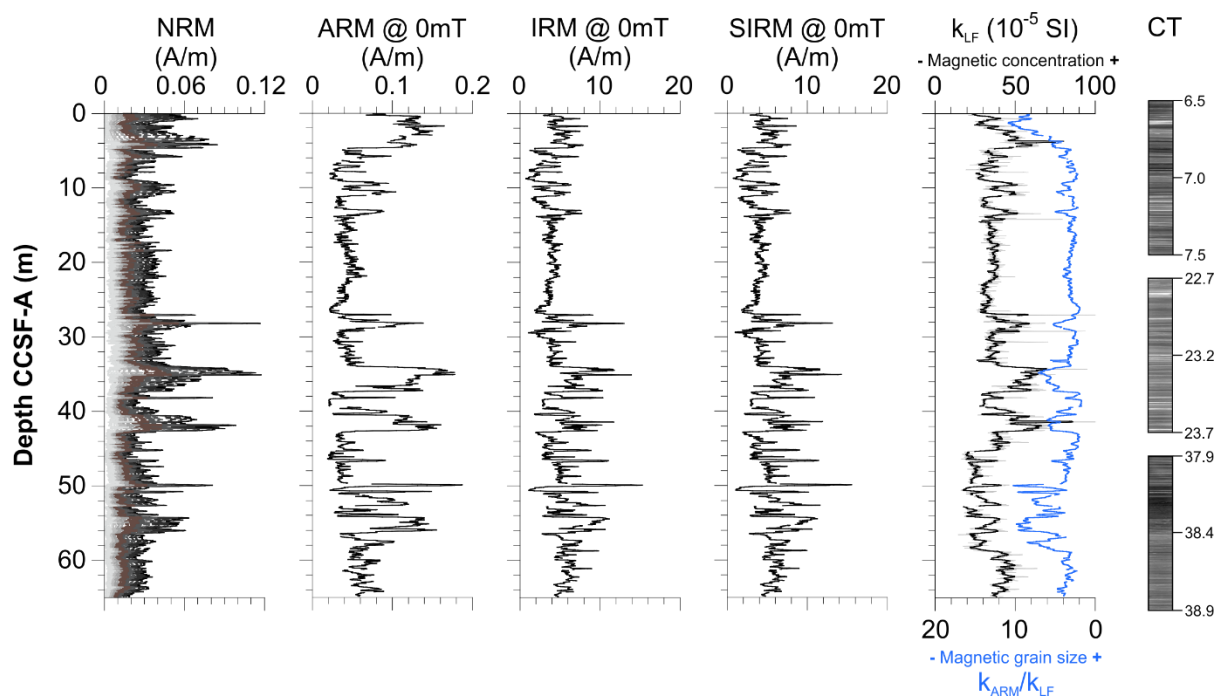


Figure 27: Natural remanent magnetization (NRM) with AF demagnetization steps displayed in colors ranging from black (0 mT) to grey (100 mT); anhysteretic remanent magnetization (ARM, isothermal remanent magnetization (IRM), and saturated isothermal remanent magnetization (SIRM) as measured before demagnetization (at 0 mT); magnetic susceptibility (k_{LF}) with a 20-point smoothing (black); and k_{ARM}/k_{LF} with a 20-point smoothing (blue). In a dominantly magnetite magnetic mineralogy, k_{ARM}/k_{LF} is inversely correlated with magnetic grain size (Thompson & Oldfield, 1986). On the right are three examples of CT-scans showing lithologies typical for Site U1418.

Magnetic mineralogy, concentration, and grain size

Three hysteresis curves from representative intervals are shown in Figure 28 and display the shape typical of magnetite (Tauxe et al., 1996). In the Day plot (Day et al., 1977), all samples lie in the pseudo-single domain (PSD) range. All but three samples plot parallel

to but slightly above the theoretical PSD-MD magnetite mixing line of Dunlop (2002a, 2002b), suggesting the presence of a higher-coercivity magnetic mineral.

The low-field magnetic susceptibility (k_{LF}) of the U1418 sediment varies between 10 and 100×10^{-5} SI with a mean of $40 \pm 10 \times 10^{-5}$ SI (Fig. 27). Somewhat higher values are observed between 26 and 44 m CCSF-A with three distinct peaks (~ 50 - 80×10^{-5} SI) around 28, 35, and 42 m CCSF-A. Similar profiles are observed for the remanent magnetizations, especially NRM and ARM, indicating that there are some down-core variations in the concentration of magnetic grains.

The constructed ratio k_{ARM}/k_{LF} varies inversely with magnetic grain size (in a magnetite mineralogy; Banerjee et al., 1981; King et al., 1982, 1983; Geiss & Banerjee, 2003) and indicates an assemblage of magnetically finer grains at the very top of the record (0-3.5 m CCSF-A), as well as between 49.5-58.5 m CCSF-A. Furthermore, the presence of finer magnetic grain sizes is indicated around 28, 35, and 42 m CCSF-A, concurrent with highs in magnetic concentration. This suggests that sediments in these intervals could be sourced from a different terrane group in this very active sediment dispersal system (Silberling et al., 1994; Cowan et al., 2006). Anhysteretic susceptibility (k_{ARM}) plotted against magnetic susceptibility (k_{LF}) is another grain-size proxy (given a magnetite mineralogy; Fig. 28; Banerjee et al., 1981; King et al., 1982). Using the King et al. (1983) calibrations, magnetic grain-size plots between 0.1 and 1 μm , with some, mostly higher-susceptibility, samples plotting between 1 and 5 μm . In summary, the magnetic parameters collectively indicate that the U1418 sediment consist of a generally high concentration of PSD magnetite.

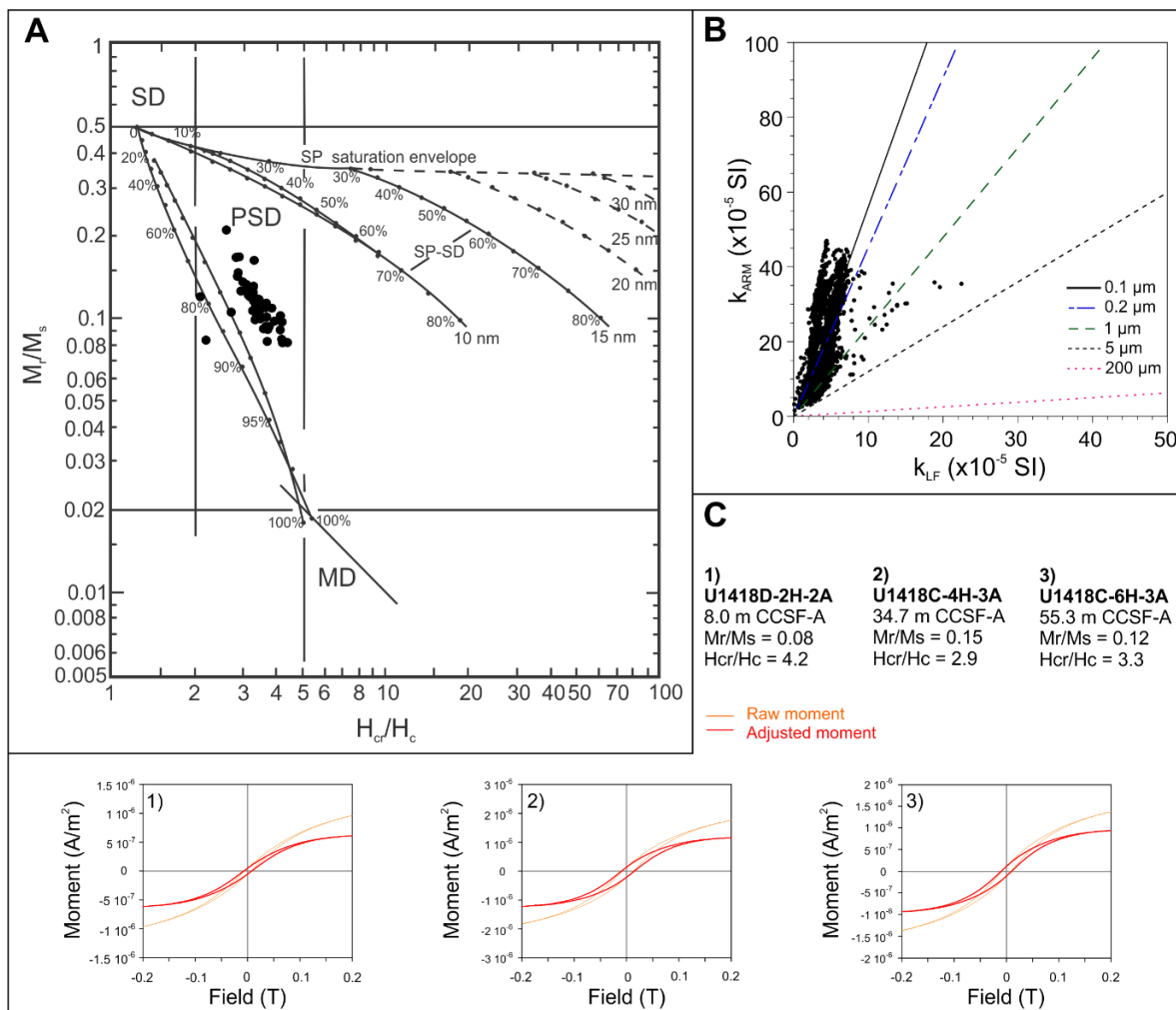


Figure 28: A: Day plot (Day et al., 1977) with theoretical mixing lines from Dunlop (2002a, 2002b) of all Site U1418 discrete samples. B: Anhyseretic susceptibility (k_{ARM}) plotted against magnetic susceptibility (k_{LF} ; King et al., 1982) as a proxy for magnetic grain size (given a magnetite mineralogy). Magnetic grain size boundaries are based on synthetic samples from Banerjee et al. (1981) and the plot is adapted from Geiss & Banerjee (2003). C: Selected hysteresis loops representative of Site U1418.

Paleomagnetic directions

Vector end-point diagrams (Zijderveld, 1967) show that a strong, stable characteristic magnetization (ChRM) can be defined between 25-60 mT after the removal of a weak viscous component at the 20 mT AF demagnetization step (Fig. 29). The component directions were calculated using principal component analysis (Kirschvink, 1980) in a spreadsheet developed by Mazaud (2005), with associated mean maximum angular deviation (MAD) values of $1.6 \pm 0.9^\circ$. The ChRM inclination (Fig. 30) is generally shallower than the expected geocentric axial dipole (GAD; 73°) inclination for the Site latitude, apart from in the upper ~ 3 m CCSF-A, intervals with steeper inclination between 34 and 36 m CCSF-A ($75-89^\circ$), and in the lowermost part of the studied record from 56 m CCSF-A to the base at 64.6 m CCSF-A ($80-89^\circ$; Fig. 30).

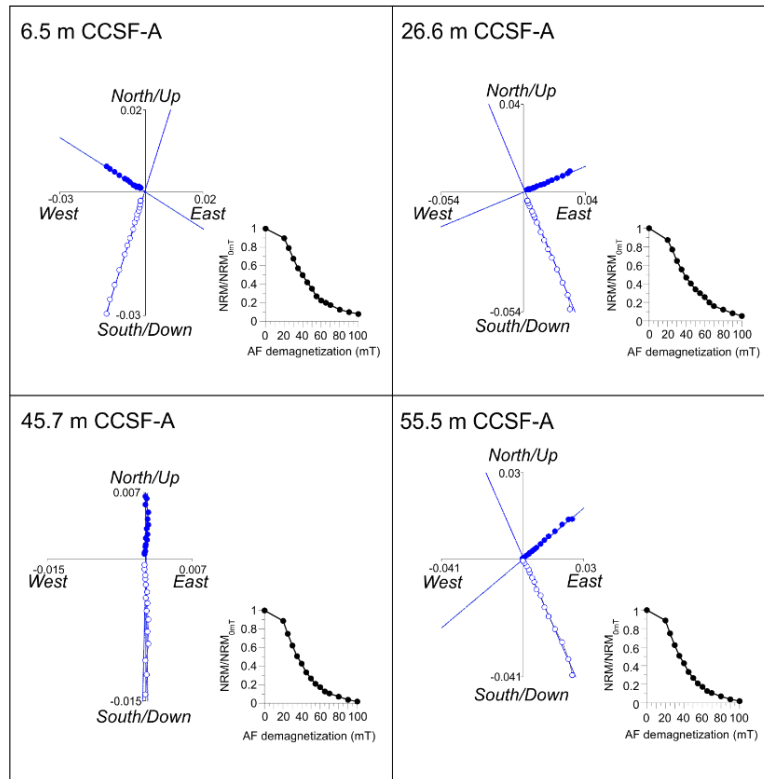


Figure 29: Vector end-point diagrams (Zijderveld, 1967) with corresponding demagnetization plots from four representative intervals of Site U1418. Open (closed) circles represent projections on the vertical (horizontal) plane.

Due to a lack of azimuthal orientation during drilling, the declination was first rotated to a core mean of zero before it was aligned across spliced core sections. At the base of the studied sequence, between 58 and 64.6 m CCSF-A, the initial rotation was insufficient and additional corrections were applied. Some of the shifts in declination are concurrent with more abrupt changes and steeper inclinations, such as at 2.4, 35, and below 56 m CCSF-A.

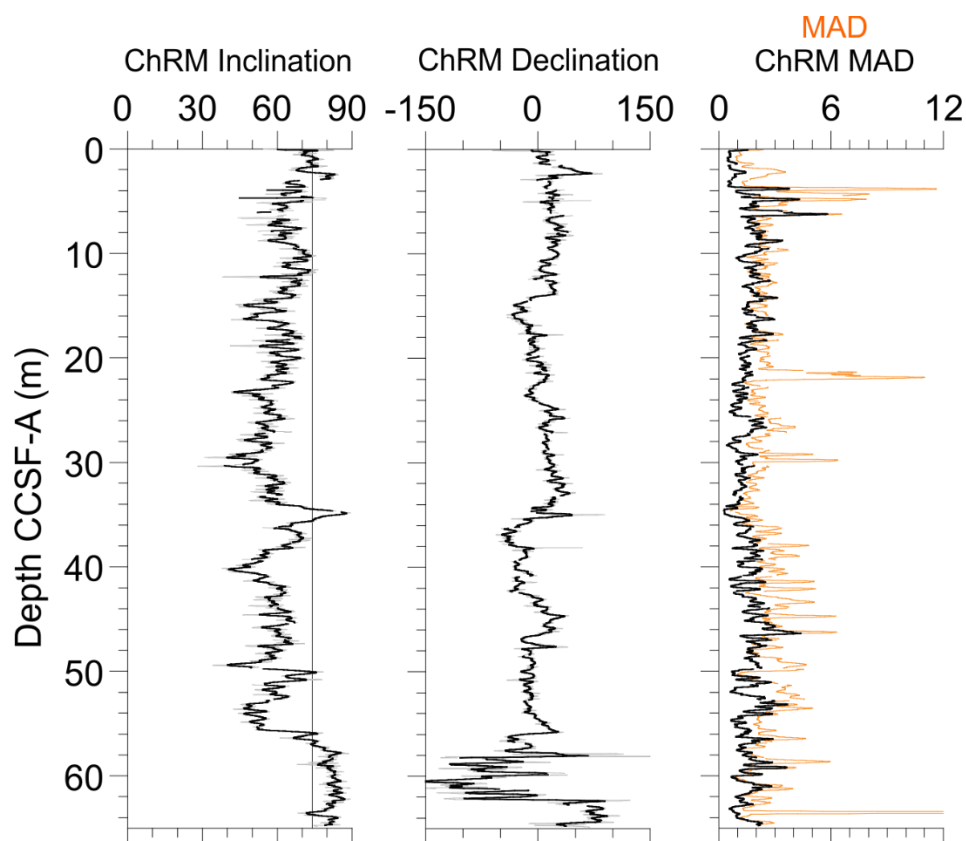


Figure 30: Characteristic remanent magnetization (ChRM) inclination and declination as defined between the 25-60 mT AF demagnetization steps, and maximum angular deviation (MAD) values for the complete range of AF demagnetization steps (orange) and for the ChRM range 25-60 mT (black). Declination has been rotated to a mean of zero. All parameters are shown with a 20-point smoothing indicated in bold.

Remanent magnetization and normalized intensity

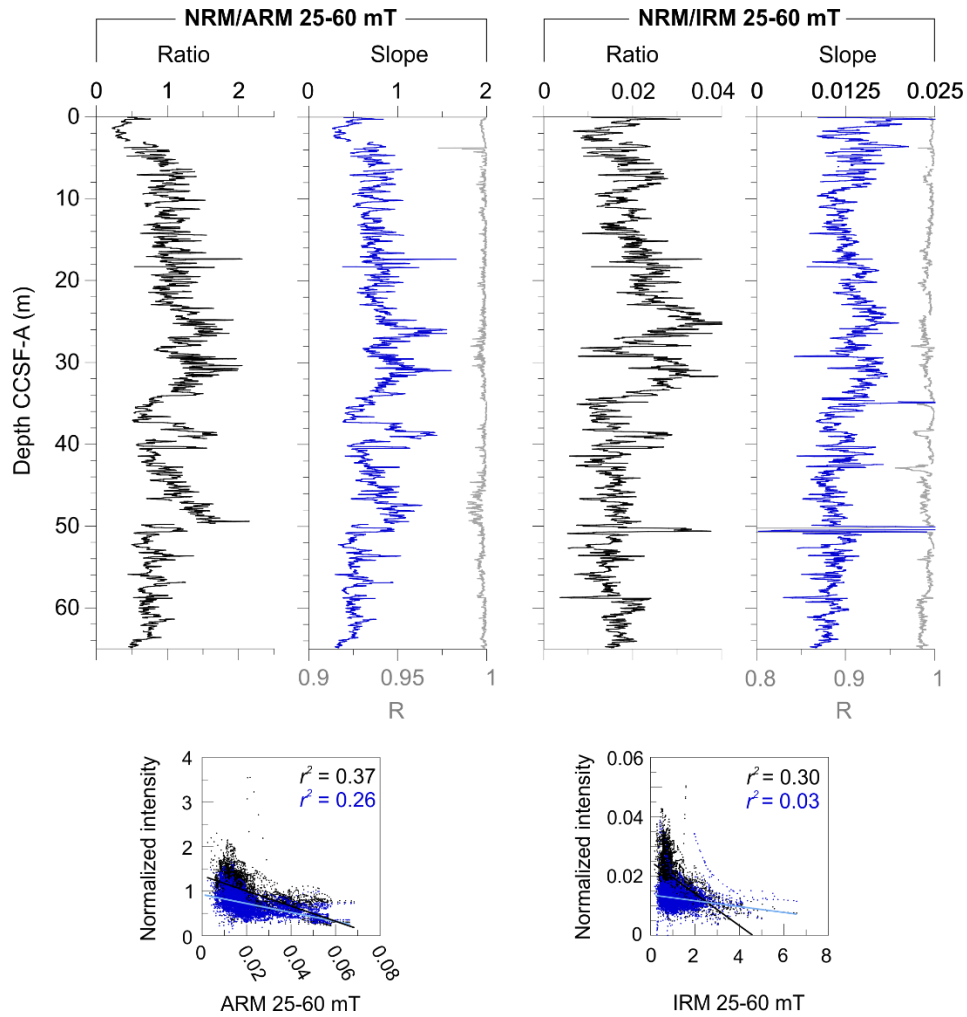
The NRM as measured at 20 mT (demagnetized at AF of 20 mT during expedition) varies between 0.005 and 0.12 A/m with a mean of 0.04 ± 0.02 A/m. Intervals of generally stronger remanence (0.05-0.1 A/m) are observed in the uppermost ~4.8 m CCSF-A of the record, as well as between 27 and 43 m CCSF-A. Three prominent peaks of remanence are also found within this interval; at approx. 28, 35 and 42 m CCSF-A (Fig. 27). The ARM profile is generally similar to that of the NRM. The mean intensity for the ARM as measured at 0 mT is 0.06 ± 0.03 A/m with the highest values (0.16-0.18 A/m) occurring, as also observed in the NRM, in the upper 4.8 m CCSF-A of the record, as well as at 28, 35, and 42 m CCSF-A and, additionally, around 50 and 55 m CCSF-A. Due to the similarities between the IRM imparted at 0.3 T and the SIRM imparted at 0.95 T, the two are reported as IRM in this paper. The IRM varies between 1.2 and 16 A/m with a mean of 4.7 ± 2 A/m. Although not as large in amplitude as in the NRM and ARM, intensity peaks are observed at the same depths of 28, 35, and 42 m CCSF-A.

Several studies have suggested a series of criteria to be fulfilled in order to validate the normalized intensity as a reliable paleointensity proxy (e.g., Levi & Banerjee, 1976; Tauxe, 1993; Stoner & St-Onge, 2007). The magnetic remanence should be carried by stable PSD magnetite in the grain size range of 1-15 μm , and the concentration of magnetic material in the sample should not vary by more than one order of magnitude throughout the record. Furthermore, a strong, single component magnetization should be determined using the stepwise AF demagnetization procedure and resulting MAD values should be below 5° . Moreover, the chosen normalizer should not be coherent with the normalized record. A final step is to compare the normalized record with other regional and global records, and this will be explored in section 3.6 below.

To estimate paleointensity, four normalization approaches were explored using the 25-60 mT demagnetization range; the slopes of NRM/ARM and NRM/IRM, as well as the ratios of NRM/ARM and NRM/IRM (Fig. 31). Linear correlation coefficients (R) were determined

for the slopes and display values close to unity (>0.9) for both NRM/ARM and NRM/IRM, indicating well-defined slopes. ARM slope and ratio yielded similar results, whereas more discrepancies are observed between the IRM-based paleointensity proxies. Correlation between the paleointensity proxy and the normalizer used, NRM/ARM ratio ($r^2 = 0.37$), NRM/ARM slope ($r^2 = 0.26$), and NRM/IRM ratio ($r^2 = 0.30$), suggest that some influence of magnetic mineral concentration and/or grain size remains in the normalized record. However, for the NRM/IRM slope, there is no observed correlation with the normalizer ($r^2 = 0.03$). ARM as a normalizer may be influenced by down-core variations in magnetic grain-size as higher ARM intensities are observed in intervals of finer magnetic grain sizes. Therefore, ARM may overcorrect the NRM in these intervals. The NRM/IRM slope shows the least correlation between the normalized record and the normalizer and is therefore used as our preferred paleointensity proxy. One interval in this proxy (50-51 m CCSF-A) displays highly variable values (between 0 and 0.04) as well as relatively low R values (~ 0.5). This is most likely related to a change in magnetic concentration at this depth and is an artefact of the normalization. This interval is therefore removed from the normalized intensity record. Based on the results presented above, Site U1418 fulfils the criteria for paleointensity reconstruction using the NRM/IRM slope as the paleointensity proxy.

Figure 31 (next page): U1418 NRM normalized over the 25-60 mT AF demagnetization steps by ARM (left) and IRM (right) using the ratio method (black) and the slope method (blue). The R value of the slope method is displayed in grey. Scatter plots show the correlation between the normalized intensity and the normalizer used with the corresponding r^2 value.



3.7 DISCUSSION

Chronostratigraphy

The similarity between Site U1418 shipboard inclination stack and Site U1419 u-channel inclination record was used to support the validity of the PSV record (Velle et al., in prep). Comparing the u-channel ChRM inclination from Site U1418 as presented in this paper

with Site U1419 inclination over the interval between 27,600 and 16,000 cal yr BP (Fig. 32) additionally supports that PSV is recorded and presents an opportunity to assess and potentially even improve the U1418 age model. The U1419 age model (Walczak et al., in prep) is based on GRA tie-points to its site survey core EW0408-85JC/TC that is constrained by 44 radiocarbon dates (Davies-Walczak et al., 2014) in the deglacial and Holocene, as well as radiocarbon dates from U1419 (Walczak et al., in prep).

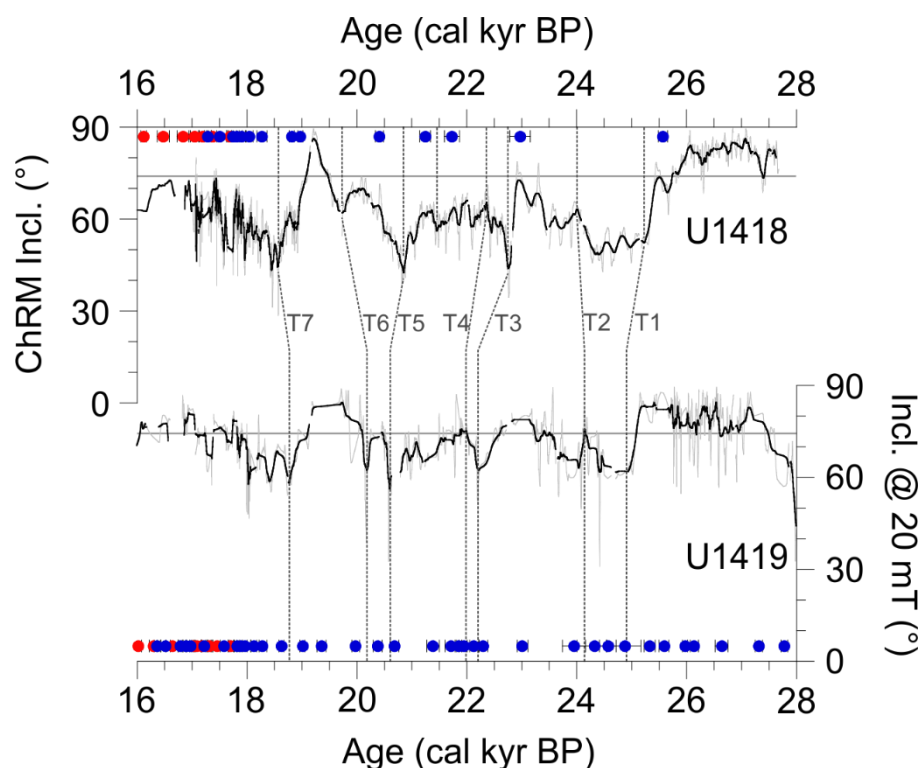


Figure 32: U1418 inclination compared with Exp. 341 drill Site U1419 inclination (Velle et al., in prep), both on their respective age models. Blue circles indicate radiocarbon dated intervals and red circles indicate tie-points to core EW0408-87JC for Site U1418, and tie-points to core EW0408-85JC for Site U1419 (Walczak et al., in prep). Tie-points between the two inclination records are indicated with dashed lines.

If we assume that both sites have the same geomagnetic history and recorded PSV with similar fidelity and temporal offsets relative to radiocarbon dates, then the U1419 extremely well-resolved age model can constrain U1418 age model using PSV correlation. This is especially important in the less well-constrained interval between ~30,000 and 18,000 cal yr BP in U1418, which is also the most robust portion of the U1419 inclination record (cf. Velle et al., in prep). A total of seven tie-points (Table 4; Fig. 32) were developed between U1418 and U1419 inclination features for the interval between 26,000 and 18,000 cal yr BP. The adjusted age model (Fig. 33) speaks to the efficiency of PSV as a regional chronostratigraphic tool, while presumably more accurately constraining the region's geomagnetic history. Due to the substantial change in sedimentation and sedimentation rates of almost two orders of magnitude between ~17,000 and 16,000 cal yr BP, the paleomagnetic record will be considered in two parts; from 0 to 16,000 cal yr BP, and from 16,000 to 28,000 cal yr BP.

Table 4: Tie-points to the U1419 age model (Walczak et al., in prep).

Tie-point	U1418 depth CCSF-A (m)	U1418 age (cal yr BP)	U1418 (cal yr BP) $-\sigma_1$	U1418 (cal yr BP) $+\sigma_1$	U1419 age (cal yr BP)	U1419 (cal yr BP) $-\sigma_1$	U1419 (cal yr BP) $+\sigma_1$
T1	30.33	18,564	18,449	18,668	18,763	18,705	18,842
T2	36.26	19,719	19,417	19,996	20,191	20,107	20,289
T3	40.35	20,855	20,678	21,020	20,601	20,526	20,678
T4	47.25	22,360	22,079	22,635	21,990	21,946	22,040
T5	49.38	22,753	22,501	22,950	22,220	22,144	22,144
T6	52.5	23,999	23,521	24,593	24,179	24,036	24,314
T7	55.43	25,225	24,753	25,422	24,952	24,831	25,076

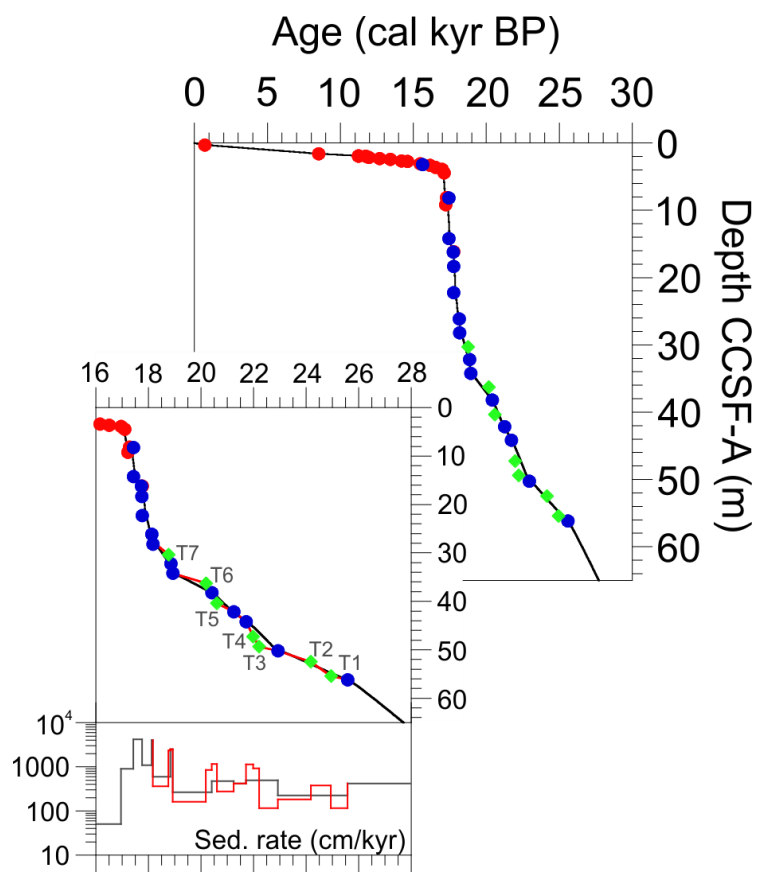


Figure 33: U1418 age model (in black) with tie-points to the U1419 age model (Walczak et al., in prep) via U1419 inclination (green diamonds). Adjusted age model and sedimentation rates are indicated in red.

Paleomagnetic secular variations (PSV)

When viewed on age (Fig. 34), it is evident that the shallow inclinations persisting over 10-15 meters (cf. Fig. 30) are, in fact, inclination features occurring over 1000-3000 years such as those typically observed in the Holocene (Thompson, 1973), but captured at extremely high temporal resolution. In Figure 34, the U1418 u-channel inclination is compared with the U1418 shipboard inclination as measured at 20 mT (in purple) and with other regional records of similar resolution, mostly from the Gulf of Alaska (Walczak et al., 2017; Velle et al., in prep), as well as northeastern Pacific and western North America

inclination stacks (Walczak et al., 2017; Reilly et al., 2018). Thirteen inclination features correlated across the different records are highlighted in Figure 34A and B, although more are observed. Similarities between the Gulf of Alaska records are especially pronounced, particularly in the higher resolution intervals >17,000 cal yr BP, where the sequence of features I1 through I10 are recognized in both U1418 and U1419 (Fig. 34B). This would be expected as these records are only ~80 km apart and should have recorded the same geomagnetic field. Additionally, some of these variations are similar to those observed in the recent WNAM North American PSV stack when relocated to the Gulf of Alaska using a dipole assumption (Reilly et al., 2018). The consistency between the three records in Figure 34B generally supports that these records have captured regional geomagnetic dynamics, although there are differences that will require further exploration. Especially pronounced in all these records is the steep inclination feature I8 around 19,500 cal yr BP (36-34 m CCSF-A in U1418) suggesting that this is a robust regional geomagnetic feature. In the deglacial-Holocene portion of the records (Fig. 34A), features I11, I12, and I13 are recognized in all of the Gulf of Alaska records, as well as in the NEPSIAS inclination stack (Walczak et al., 2017). This stack is based on records from Alaska to Hawaii and, thereby, further suggest that the U1418 record has captured regional-scale paleomagnetic inclination variations also in the Holocene.

Some discrepancies are observed between the U1418 shipboard and U1418 u-channel declination records (Fig. 34A and B). For example, is the shipboard declination generally less variable than the u-channel declination, especially evident in the deglacial and Holocene portion of the record (Fig. 34A). In the 16-28 ka interval (Fig 34B), large-scale variability is observed in the shipboard declination between 18,000 and 17,000 cal yr BP, whereas only minor variability is observed in the shipboard data. This is likely due to a number of factors, including deformation associated with half-core measurements compared with u-channels coming from the pristine central part of the core, the stacking and rotation approach used in the shipboard declination record, and differences in magnetometer response functions and, as a result, resolution. Comparing the U1418 declination with EW0408-85JC from the Gulf of Alaska (Walczak et al., 2017) and the WNAM western North America PSV stack (Reilly

et al., 2018) shows that five features can be correlated across the different records (Fig. 34A and B). Although less than that observed for the U1418 inclination, these tie-points indicate that the U1418 declination may also reflect a regional geomagnetic signal.

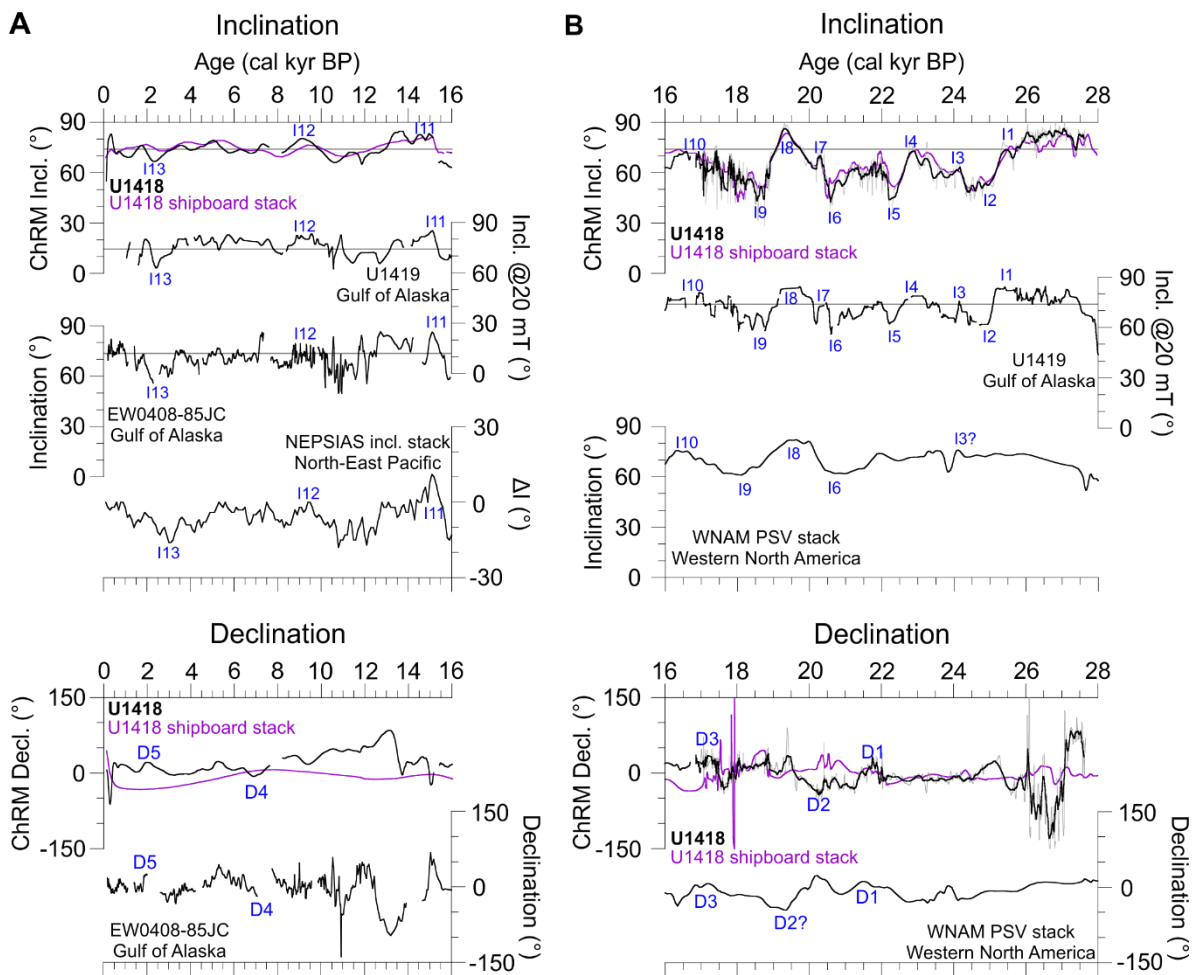


Figure 34: Comparison of Site U1418 ChRM (25-60 mT) inclination and declination with U1418 shipboard inclination as measured at 20 mT (Velle et al., in prep), U1418 shipboard declination stack, Site U1419 (Velle et al., in prep), EW0408-85JC (Walczak et al., 2017), the Western North America PSV stack rotated to the Gulf of Alaska using a GAD approximation (WNAM; Reilly et al., 2018), and the northeastern Pacific sedimentary inclination anomaly stack (NEPSIAS; Walczak et al., 2017) for the time periods 0-16 cal kyr BP (A) and 16-28 cal kyr BP (B). PSV features are numbered to facilitate discussion. A 40-point smoothing has been applied to parts of the U1418 record where sedimentation rates exceed 100 cm/kyr.

Paleointensity

As mentioned above, the final step in assessing the quality of a paleointensity proxy is to compare it with other regional, independently dated records of similar resolution. However, at this point in time there are no regionally comparable records. Figure 35B shows the U1418 normalized intensity compared to records from the western Pacific (MD98-2181; Stott et al., 2002), the southern Chile margin (ODP Site 1233; Lund et al., 2006), and an RPI stack (scaled to VADM) based on 15 globally distributed marine and lacustrine records (Channell et al., 2018). The resolution of the records included in the overall RPI stack (sedimentation rates between 19 and 66 cm/kyr) as well as likely smoothing during the stacking process (Channell et al., 2018), only allows a very general comparison with Site U1418. However, similarities are observed in the trend of the two records, especially the gradual increase in intensity from the base of the compared interval towards approx. 16,000 cal yr BP (Fig. 35B). Site U1418 may also contain the intensity high observed between 18 and 15 ka (17,000 to 15,000 cal yr BP in U1418), as well as the subsequent “notch” between 14 and 13 ka (15,000 and 14,000 cal yr BP in U1418), as detailed in Channell et al. (2018). The long-term similarities between these two records suggests that Site U1418 may have captured global geomagnetic field changes. However, on millennial timescales, no clear correlation is observed, suggesting that a global-scale signal may not be applicable at these time intervals. The deglacial-Holocene portion of the U1418 record was compared to records from the Arctic, namely the Chukchi and Beaufort Seas (Barletta et al., 2008; Deschamps et al., 2018; Fig. 35A), as well as the “overall” RPI record (Channell et al., 2018). Despite the lower resolution of this time interval, the U1418 paleointensity proxy displays some similarities to the RPI records from the Arctic, especially the Beaufort Sea record 02PC (Deschamps et al., 2018).

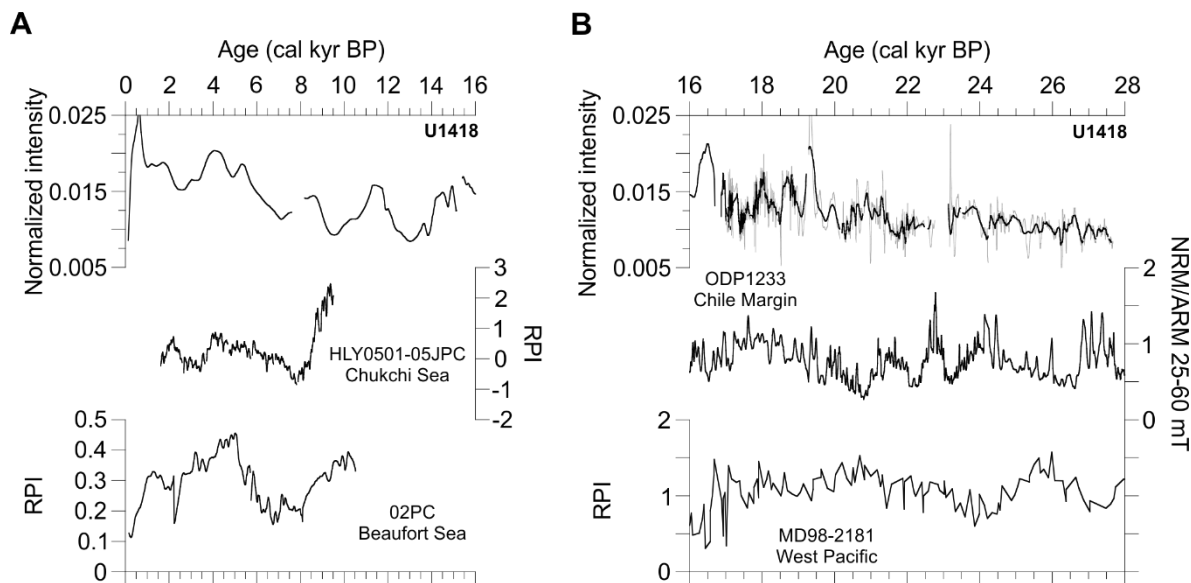


Figure 35: Comparison of Site U1418 normalized intensity (NRM/IRM slope) with other regional intensity records; HLY0501-05JPC (Barletta et al., 2008), 02PC (Deschamps et al., 2018), ODP Site 1233 (Lund et al., 2006), MD98-2181 (Stott et al., 2002), and the “overall” RPI record scaled to VADM (including the Iberian margin records and globally distributed marine and lakustrine records; cf. Channell et al., 2018) for the time periods 0-16 cal kyr BP (A) and 16-28 cal kyr BP (B). A 40-point smoothing has been applied to parts of the U1418 record where sedimentation rates exceed 100 cm/kyr.

Geomagnetic shielding has been suggested as the main control on the long-term (~2000 years; Beer et al., 2002) production rate of cosmogenic isotopes. Several studies have found inverse correlations between paleointensity and production rates (e.g., Stoner et al., 2000; St-Onge et al., 2003), whereas other records, such as the RPI record from the Black Sea (Nowaczyk et al., 2013), show less correlation in detail. Assuming that the flux of ^{10}Be measured in an ice core reflects the production rate of ^{10}Be , then the inverse record should reflect changes in the dipole intensity (e.g., Masarik & Beer, 1999). In Figure 36, the highest resolution portion of the U1418 paleointensity proxy record is compared to the ^{10}Be flux record from the Greenland Summit ice cores, plotted on the GICC05 time scale (Muscheler

et al., 2004). Similar to what was observed from the Black Sea, little inverse correlation is found.

The resolution of the U1418 RPI record provides an opportunity to study millennial-scale geomagnetic dynamics. However, the lack of regional and global records with similar resolution to compare with, makes it problematic to determine whether the U1418 paleointensity proxy represents regional or global variations in Earth's magnetic intensity. It is evident that more high-resolution records are needed in order to resolve millennial-scale geomagnetic variability, and Site U1418 represents a start.

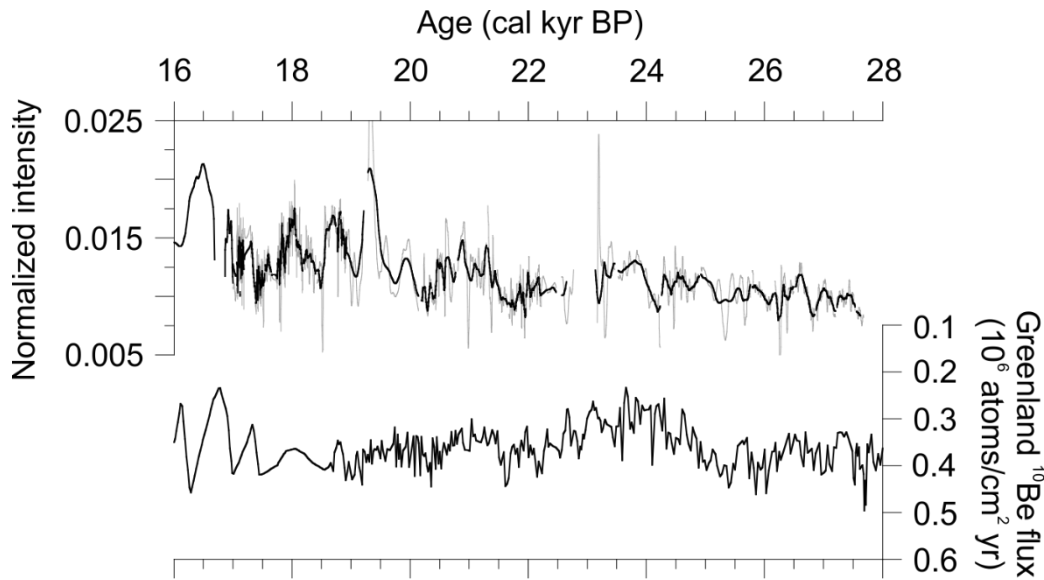


Figure 36: Comparison of the highest resolution interval (16-28 cal kyr BP) of the Site U1418 normalized intensity (NRM/IRM slope) and the Greenland ¹⁰Be flux record (Muscheler et al., 2004). A 40-point smoothing has been applied to parts of the U1418 record where sedimentation rates exceed 100 cm/kyr. Note the reversed Y axis for the Greenland ¹⁰Be flux record.

3.8 CONCLUSIONS

The high temporal resolution of Site U1418 presents a unique opportunity to study the full paleomagnetic vector in the northeast Pacific during the past ~27,000 cal yr BP. Comparisons between the U1418 PSV record and other Gulf of Alaska, western US and regional stacks show several apparent common features, indicating that Site U1418 has captured regional-scale PSV. Especially consistent are U1418 inclination features with those of Site U1419, supporting the interpretation of the U1419 inclination (Velle et al., in prep), which was derived only from the 20 mT AF demagnetization step, as a regional geomagnetic signal. Furthermore, the U1418 age model can be improved through inclination-based correlations to Site U1419. Site U1418 normalized intensity was based on the NRM/IRM slope of the 25-60 mT AF demagnetization steps but shows little correspondence to other RPI records or to the Greenland ^{10}Be flux record. More records of similar resolution are needed in order to determine the local, regional, or global characteristics of paleomagnetic variations in this region.

3.9 ACKNOWLEDGEMENTS

We thank R. Muscheler for sharing the Greenland ^{10}Be flux data. Expedition 341 was carried out by the Integrated Ocean Drilling Program (IODP). We thank the IODP-USIO and the captain and crew of the R/V JOIDES Resolution. Special thanks are due to the staff at the IODP Gulf Coast Repository, especially L. LeVey and P. Rumford, as well as B. Reilly and T. Hansen for their help during u-channel sampling. We are grateful to Q. Beauvais, M.-P. St-Onge and A.M. Ross for help in the lab. This study was possible thanks to a GEOTOP scholarship to the first author, as well a Natural Sciences and Engineering Council of Canada Discovery Grant to G. St-Onge.

3.10 REFERENCES

- Banerjee, S.K., King, J. & Marvin, J., 1981.** A rapid method for magnetic granulometry with applications to environmental studies. *Geophysical Research Letters*, **8(4)**, pp. 333-336, doi: 10.1029/GL008i004p00333
- Barletta, F., St-Onge, G., Channell, J.E.T., Rochon, A., Polyak, L. & Darby, D., 2008.** High-resolution paleomagnetic secular variation and relative paleointensity records from the western Canadian Arctic: implication for Holocene stratigraphy and geomagnetic field behavior. *Canadian Journal of Earth Sciences*, **45 (11)**, pp. 1265-1281, doi: 10.1139/E08-039
- Beer, J., Muscheler, R., Wagner, G., Laj, C., Kissel, C., Kubik, P.W. & Synal, H.-A., 2002.** Cosmogenic nuclides during Isotope Stages 2 and 3. *Quaternary Science Reviews*, **21**, pp. 1129-1139, doi: 10.1016/S0277-3791(01)00135-4
- Caron, M., St-One, G., Montero-Serrano, J.C., Rochon, A., Georgiadis, E., Giraudeau, J. & Masse, G., 2018.** Holocene chronostratigraphy of northeastern Baffin Bay based on radiocarbon and palaeomagnetic data. *Boreas*, **48**, pp. 147-165, doi: 10.1111/bor.12346
- Channell, J.E.T., Hodell, D.A., Crowhurst, S.J., Skinner, L.C. & Muscheler, R., 2018.** Relative paleointensity (RPI) in the latest Pleistocene (10-45 ka) and implications for deglacial atmospheric radiocarbon. *Quaternary Science Reviews*, **191**, pp. 57-72, doi: 10.1016/j.quascirev.2018.05.007
- Cowan, E.A., Brachfeld, S.A., Powell, R.D. & Schoolfield, S.C., 2006.** Terrane-specific rock magnetic characteristics preserved in glacial marine sediment from southern coastal Alaska. *Canadian Journal of Earth Sciences*, **43(9)**, pp. 1269-1282, doi: 10.1139/e06-042

- Davies, M.H., Mix, A.C., Stoner, J.S., Addison, J.A., Jaeger, J., Finney, B. & Wiest, J., 2011.** The deglacial transition on the southeastern Alaska Margin: Meltwater input, sea level rise, marine productivity, and sedimentary anoxia. *Paleoceanography*, **26**, PA2223, doi: 10.1029/2010PA002051
- Davies-Walczak, M., Mix, A.C., Stoner, J.S., Southon, J.R., Cheseby, M. & Xuan, C., 2014.** Late Glacial to Holocene radiocarbon constraints on North Pacific Intermediate Water ventilation and deglacial atmospheric CO₂ sources. *Earth and Planetary Science Letters*, **397**, pp. 57-66, doi: 10.1016/j.epsl.2014.04.004
- Day, R., Fuller, M. & Schmidt, V.A., 1977.** Hysteresis properties of titanomagnetites: Grain-size and compositional dependence. *Physics of the Earth and Planetary Interiors*, **13**, pp. 260-267, doi: 10.1016/0031-9201(77)90108-X
- Deschamps, C.E., St-Onge, G., Montero-Serrano, J.C. & Polyak, L., 2018.** Chronostratigraphy and spatial distribution of magnetic sediments in the Chukchi and Beaufort seas since the last deglaciation. *Boreas*, **47 (2)**, pp. 544-564, doi: 10.1111/bor.12296
- Dunlop, D. J., 2002a.** Theory and application of the Day plot (Mrs/Ms versus Hcr/Hc): 1. Theoretical curves and tests using titanomagnetite data, *Journal of Geophysical Research*, **107 B3**, 2056, doi:10.1029/2001JB000486.
- Dunlop, D. J., 2002b.** Theory and application of the Day plot (Mrs/Ms versus Hcr/Hc): 2. Application to data for rocks, sediments, and soils, *Journal of Geophysical Research*, **107 B3**, 2057, doi:10.1029/2001JB000487.
- Fortin, D., Francus, P., Gebhardt, A.C., Hahn, A., Kliem, P., Lisé-Pronovost, A., Roychowdhury, R., Labrie, J., St-Onge, G. & the PASADO Science Team, 2013.** Destructive and non-destructive density determination: method comparison and evaluation from the Laguna Potrok Aike sedimentary record. *Quaternary Science Reviews*, **71**, pp. 147-153, doi: 10.1016/j.quascirev.2012.08.024

- Geiss, C.E. & Banerjee, S.K., 2003.** A Holocene-Late Pleistocene geomagnetic inclination record from Grandfather Lake SW Alaska. *Geophysical Journal International*, **153**, pp. 497-507, doi: 10.1046/j.1365-246X.2003.01921.x
- Gulick, S.P.S., Jaeger, J.M., Mix, A.C., Asahi, H., Bahlburg, H., Belanger, C.L., Berbel, G.B.B., Childress, L., Cowan, E., Drab, L., Forwick, M., Fukumura, A., Ge, S., Gupta, S., Kioka, A., Konno, A., LeVay, L.J., März, C., Matsuzaki, K.M., McClymont, E.L., Moy, C., Müller, J., Nakamura, A., Ojima, T., Ribeiro, F.R., Ridgway, K.D., Romero, O.E., Slagle, A.L., Stoner, J.S., St-Onge, G., Suto, I., Walczak, M.D., Worthington, L.L., Bailey, I., Enkelmann, E., Reece, R. & Swartz, J.M., 2015.** Mid-Pleistocene climate transition drives net mass loss from rapidly uplifting St. Elias Mountains, Alaska. *PNAS*, **112(49)**, pp. 15042-15047, doi: 10.1073/pnas.1512549112
- Hagstrum, J.T. & Champion, D.E., 2002.** A Holocene paleosecular variation record from 14C dated volcanic rocks in western North America. *Journal of Geophysical Research*, **107 B1**, doi: 10.1029/2001JB000524, 2002
- Haslett, J. & Parnell, A., 2008.** A simple monotone process with application to radiocarbon-dated depth chronologies. *Journal of the Royal Statistical Society Series C Applied Statistics*, **57(4)**, pp. 399-418, doi: 10.1111/j.1467-9876.2008.00623.x
- Jaeger, J.M., Nittrouer, C.A., Scott, N.D & Milliman, J.D., 1998.** Sediment accumulation along glacially impacted mountainous coastline: north-east Gulf of Alaska. *Basin Research*, **10**, pp. 155-173, doi: 10.1046/j.1365-2117.1998.00059.x
- Jaeger, J.M., Gulick, S.P.S., LeVay, L.J., & the Expedition 341 Scientists, 2014.** Proc. IODP, 341, College Station, TX (Integrated Ocean Drilling Program).
- King, J., Banerjee, S.K., Marvin, J. & Özdemir, Ö., 1982.** A comparison of different magnetic methods for determining the relative grain size of magnetite in natural

materials: some results from lake sediments. *Earth and Planetary Science Letters*, **59**, pp. 404-419, doi: 10.1016/0012-821X(82)90142-X

King, J., Banerjee, S.K. & Marvin, J., 1983. A new rock-magnetic approach to selecting sediments for geomagnetic paleointensity studies: application to paleointensity for the last 4000 years. *Journal of Geophysical Research*, **88 B7**, pp. 5911-5921, doi: 10.1029/JB088iB07p05911

Kirschvink, J.L., 1980. The least-squares line and plane and the analysis of paleomagnetic data. *Geophysical Journal International*, **62(3)**, pp. 699-718, doi: 10.1111/j.1365-246X.1980.tb02601.x

Levi, S. & Banerjee, S.K., 1976. On the possibility of obtaining relative paleointensities from lake sediments. *Earth and Planetary Science Letters*, **29**, pp. 219-226, doi: 10.1016/0012-821X(76)90042-X

Lisé-Pronovost, A., St-Onge, G., Gogorza, C., Habertzettl, T., Preda, M., Kliem, P., Francus, P. & Zolitschka, B., 2013. High-resolution paleomagnetic secular variations and relative paleointensity since the Late Pleistocene in southern South America. *Quaternary Science Reviews*, **71**, pp. 91–108, doi: 10.1016/j.quascirev.2012.05.012

Lund, S.P., Stoner, J.S. & Lamy, F., 2006. Late Quaternary paleomagnetic secular variation and chronostratigraphy from ODP Sites 1233 and 1234. *In*: Tiedmann, R., Mix, A.C., Richter, C. & Ruddiman, W.F. (eds), Proceedings of the Ocean Drilling Program, Scientific Results, Volume 202.

Lund, S.P., Benson, L., Negrini, R., Liddicoat, J. & Mensing, S., 2017. A full-vector paleomagnetic secular variation record (PSV) from Pyramid Lake (Nevada) from 47-17 ka: Evidence for the successive Mono Lake and Laschamp Excursions. *Earth and Planetary Science Letters*, **458**, pp. 120-129, doi: 10.1016/j.epsl.2016.09.036

- Masarik, J. & Beer, J., 1999.** Simulation of particle fluxes and cosmogenic nuclide production in the Earth's atmosphere. *Journal of Geophysical Research*, **104 D10**, pp. 12,099-12,111, doi; 10.1029/1998JD200091
- Mazaud, A., 2005.** User-friendly software for vector analysis of the magnetization of long sediment cores. *Geochemistry Geophysics Geosystems*, **6(12)**, pp. 1525-2027, doi: 10.1029/2005GC001036
- McNeely, R., Dyke, A.S. & Southon, J.R., 2006.** Canadian marine reservoir ages, preliminary data assessment, Open File 5049, Geological Survey of Canada, Ottawa.
- Molnia, B.F. & Carlson, P.R., 1978.** Surface sedimentary units of northern Gulf of Alaska continental shelf. *The American Association of Petroleum Geologists Bulletin*, **62(4)**, pp. 633-643
- Muscheler, R., Beer, J., Wagner, G., Laj, C., Kissel, C., Raisbeck, G.M., You, F. & Kubik, P.W., 2004.** Changes in the carbon cycle during the last deglaciation as indicated by the comparison of ^{10}Be and ^{14}C records. *Earth and Planetary Science Letters*, **219**, pp. 325- 340, doi: 10.1016/S0012-821X(03)00722-2
- Nowaczyk, N.R., Frank, U., Kind, J. & Arz, H.W., 2013.** A high-resolution paleointensity stack of the past 14 to 68 ka from Black Sea sediments. *Earth and Planetary Science Letters*, **384**, pp. 1-16, doi: 10.1016/j.epsl.2013.09.028
- Oda, H. & Xuan, C., 2014.** Deconvolution of continuous paleomagnetic data from pass-through magnetometer: A new algorithm to restore geomagnetic and environmental information based on realistic optimization. *Geochemistry, Geophysics, Geosystems*, **15**, pp. 3907-3924, doi: 10.1002/2014GC005513.
- Ólafsdóttir, S., Geirsdóttir, Á., Miller, G.H., Stoner, J.S. & Channell, J.E.T., 2013.** Synchronizing Holocene lacustrine and marine sediment records using paleomagnetic secular variation. *Geology*, **41 (5)**, pp. 535–538, doi: 10.1130/G33946.1

- Panovska, S., Constable, C.G. & Brown, M.C., 2018.** Global and regional assessment of paleosecular variation activity over the past 100 ka. *Geochemistry, Geophysics, Geosystems*, **19**, pp. 1559-1580, doi: 10.1029/2017GC007271
- Peng, L. & King, J.W., 1992.** A Late Quaternary geomagnetic secular variation record from Lake Waiau, Hawaii, and the question of the Pacific nondipole low. *Journal of Geophysical Research*, **97 B4**, pp. 4407-4424, doi: 10.1029/91JB03074
- Praetorius, S.K., Mix, A.C., Walczak, M.H., Wolhowe, M.D., Addison, J.A. & Prahl, F.G., 2015.** North Pacific deglacial hypoxic events linked to abrupt ocean warming. *Nature*, **527**, pp. 362-366, doi: 10.1038/nature15753
- Reece, R.S., Gulick, S.P.S., Horton, B.K., Christeson, G.L. & Worthington, L.L., 2011.** Tectonic and climatic influence on the evolution of the Surveyor Fan and Channel system, Gulf of Alaska. *Geosphere*, **7**, pp. 830-844, doi: 10.1130/GES00654.1
- Reilly, B.T., Stoner, J.S., Hatfield, R.G., Abbott, M.B., Marchetti, D.W., Larsen, D.J., Finkenbinder, M.S., Hillman, A.L., Kuehn, S.C. & Heil, C.W., 2018.** Regionally consistent western North America paleomagnetic directions from 15 to 35 ka: Assessing chronology and uncertainty with paleosecular variation (PSV) stratigraphy, *Quaternary Science Reviews*, **201**, pp. 186-205, doi: 10.1016/j.quascirev.2018.10.016
- Reimer, P.J., Bard, E., Bayliss, A., Beck, J.W., Blackwell, P.G., Ramsey, C.B., Buck, C.E., Cheng, H., Edwards, R. L., Friedrich, M., Grootes, P.M., Guilderson, T. P., Hafliadason, H., Hajdas, I., Hatté, C., Heaton, T. J., Hoffmann, D.L., Hogg, A.G., Hughen, K.A., Kaiser, K.F., Kromer, B., Manning, S.W., Niu, M., Reimer, R.W., Richards, D.A., Scott, E.M., Southon, J.R., Staff, R.A., Turney, C.S. M. and van der Plicht, J., 2013.** IntCal13 and Marine13 Radiocarbon Age Calibration Curves 0–50,000 Years cal BP, *Radiocarbon*, **55(4)**, pp. 1869–1887

- Roberts, A.P., Lehman, B., Weeks, R.J., Verosub, K.L. & Laj, C., 1997.** Relative paleointensity of the geomagnetic field over the last 200,000 years from ODP Sites 883 and 884, North Pacific Ocean. *Earth and Planetary Science Letters*, **152**, pp. 11-23, doi: 10.1016/S0012-821X(97)00132-5
- Royer, T.C., 1982.** Coastal fresh water discharge in the Northeast Pacific. *Journal of Geophysical Research*, **87 C3**, pp. 2017-2021, doi: 10.1029/JC087iC03p02017
- Silberling, N.J., Jones, D.L., Monger, J.W.H., Coney, P.J., Berg, H.C., and Plafker, George, 1994.** Lithotectonic terrane map of Alaska and adjacent parts of Canada, *In*: Plafker, George, and Berg, H.C., eds., *The Geology of Alaska*: Geological Society of America, 1 sheet, scale 1:2,500,000
- Stabeno, P.J., Reed, R.K. & Schumacher, J.D., 1995.** The Alaska Coastal Current: Continuity of transport and forcing. *Journal of Geophysical Research*, **100 C2**, pp. 2477-2485, doi: 10.1029/94JC02842
- Stabeno, P.J., Bond, N.A., Hermann, A.J., Kachel, N.B., Mordy, C.W. & Overland, J.E., 2004.** Meteorology and oceanography of the northern Gulf of Alaska. *Continental Shelf Research*, **24**, pp. 859-897, doi: 10.1016/j.csr.2004.02.007
- Stoner, J.S., Channell, J.E.T. & Hillaire-Marcel, C., 1996.** The magnetic signature of rapidly deposited detrital layers from the deep Labrador Sea: Relationship to North Atlantic Heinrich layers. *Paleoceanography*, **11(3)**, pp. 309-325, doi: 10.1029/96PA00583
- Stoner, J.S., Channell, J.E.T., Hillaire-Marcel, C. & Kissel, C., 2000.** Geomagnetic paleointensity and environmental record from Labrador Sea core MD95-2024: Global marine sediment and ice core chronostratigraphy for the last 110 kyr. *Earth and Planetary Science Letters*, **183**, pp. 161-177, doi: 10.1016/S0012-821X(00)00272-7
- Stoner, J.S. & St-Onge, G., 2007.** Magnetic stratigraphy in paleoceanography: reversal, excursion, paleointensity and secular variation. *In*: Hillaire-Marcel, C. & De Vernal,

A. (eds) Proxies in Late Cenozoic Paleoceanography, Elsevier, pp. 99-138, doi: 10.1016/S1572-5480(07)01008-1

Stoner, J.S., Channell, J.E.T., Mazaud, A., Strano, S. & Xuan, C., 2013. The influence of high-latitude flux lobes in the Holocene paleomagnetic record of IODP Site U1305 and the northern North Atlantic. *Geochemistry Geophysics Geosystems*, **14(10)**, pp. 4623-4646, doi: 10.1002/ggge.20272

St-Onge, G., Stoner, J.S. & Hillaire-Marcel, C., 2003. Holocene paleomagnetic records from the St. Lawrence Estuary, eastern Canada: centennial- to millennial-scale geomagnetic modulation of cosmogenic isotopes. *Earth and Planetary Science Letters*, **209**, pp. 113-130, doi: 10.1016/S0012-821X(03)00079-7

Stott, L., Poulsen, C., Lund, S.P. & Thunell, R., 2002. Super ENSO and global climate oscillations at millennial time scales. *Science*, **297**, pp. 222-226, doi: 10.1126/science.1071627

Tauxe, L., 1993. Sedimentary records of relative paleointensity of the geomagnetic field: Theory and practice. *Reviews of Geophysics*, **31(3)**, pp. 319-354, doi: 10.1029/93RG01771

Tauxe, L., Pick, T. & Kok, Y.S., 1995. Relative paleointensity in sediments: a Pseudo-Thellier Approach. *Geophysical Research Letters*, **22**, pp. 2885–2888, doi: 10.1029/95GL03166

Tauxe, L., Mullender, T.A.T. & Pick, T., 1996. Potbellies, wasp-waists, and superparamagnetism in magnetic hysteresis. *Journal of Geophysical Research*, **101 B1**, pp. 571-583, doi: 10.1029/95JB03041

Thompson, R., 1973. Palaeolimnology and palaeomagnetism. *Nature*, **242**, pp. 182-184, doi: 10.1038/242182a0

- Thompson, R. & Oldfield, F., 1986.** Environmental magnetism. Allen and Unwin, Winchester, Mass.
- Velle, J.H., Walczak, M.H., Reilly, B., St-Onge, G., Stoner, J.S., Fallon, S. & Forwick, M., in prep.** A high-resolution late Quaternary inclination record from IODP Expedition 341 drill Site U1419 in the Gulf of Alaska
- Verosub, K.L., Mehringer Jr, P.J. & Waterstraat, P., 1986.** Holocene secular variation in western North America: Paleomagnetic record from Fish Lake, Harney County, Oregon. *Journal of Geophysical Research*, **91 B3**, pp. 3609-3623, doi: 10.1029/JB091iB03p03609
- Walczak, M.H., Stoner, J.S., Mix, A.C., Jaeger, J., Rosen, G.P., Channell, J.E.T., Heslop, D. & Xuan, C., 2017.** A 17,000 yr paleomagnetic secular variation record from the southeast Alaskan margin: Regional and global correlations, *Earth and Planetary Science Letters*, **473**, pp. 177-189, doi: 10.1016/j.epsl.2017.05.022
- Walczak, M.H., Mix, A.C., Fallon, S., Cowan, E., Praetorius, S., Du, J., Hobern, T., Padman, J., Fifield, K., Stoner, J.S., Haley, B., in prep,** Coupled changes in Northeast Pacific ventilation and Cordilleran Ice Sheet discharge may precede Heinrich Events. *Science*
- Weeks, R.J., Laj, C., Endignoux, L., Fuller, M., Roberts, A., Manganne, R., Blanchard, E. & Goree, W., 1993.** Improvements in long-core measurement techniques: applications in palaeomagnetism and palaeoceanography. *Geophysical Journal International*, **114**, pp. 651-662, doi: 10.1111/j.1365-246X.1993.tb06994.x
- Weeks, R.J., Roberts, A.P., Verosub, K.L., Okada, M. & Dubuisson, G.J., 1995.** 34 Magnetostratigraphy of upper Cenozoic sediments from Leg 145, North Pacific Ocean. *In: Rea D.K., Basov, I.A., Scholl, D.W. & Allan, J.F. (eds.), Proceedings of the Ocean Drilling Program, Scientific Results, Vol. 145*

- Yamamoto, Y., Yamazaki, T., Kanamatsu, T., Ioka, N. & Mishima, T., 2007.** Relative paleointensity stack during the last 250 kyr in the northwest Pacific. *Journal of Geophysical Research*, **112**, B01104, doi: 10.1029/2006JB004477
- Zijderveld, J.D.A., 1967.** Demagnetisation of rocks: Analysis of results, *In*: Collinson, D. et al., (eds) *Methods in Palaeomagnetism*, pp. 254–286, Elsevier, New York.

GENERAL CONCLUSION

Introduction

The study of IODP Exp. 341 drill Sites U1418 and U1419 as presented in the previous three chapters, permitted the overall objective of this thesis to be achieved; “*to construct a paleomagnetic record that will permit a detailed study of the Earth’s geomagnetic field dynamics, as well as the evolution of the northwestern Cordilleran Ice Sheet during the late Pleistocene and Holocene in the Gulf of Alaska*”. The latter part of the objective was achieved in chapter one, where the magnetic and physical properties of the U1419 sediment sequence were used to reconstruct the advance and retreat of the northwestern Cordilleran Ice Sheet. The paleomagnetic aspect of the objective was achieved in chapters two and three through studies of both Sites U1418 and U1419. Below, the main conclusions from each chapter will be summarized and discussed in terms of the objectives and the specific questions posed, their implications, and limitations. Following this, a section is dedicated to viewing all three chapters together, before the final paragraphs outline perspectives of future work.

Chapter 1

In chapter one, the study of physical and magnetic properties of the sediment at site U1419 was used to achieve the first objective and to answer the specific questions raised in connection with the Gulf of Alaska glacial history. The main question asked was; *How do the changes in magnetic properties (e.g., magnetic susceptibility, grain size and mineralogy) reflect changes such as advance and retreat phases of the NCIS?* The use of magnetic susceptibility in paleoenvironmental studies and reconstructions of glacial variability is well-

established (e.g., Andrews et al., 1995; Robinson et al., 1995; Stoner et al., 1996; Jessen et al., 2010). At Site U1419, magnetic susceptibility (k_{LF}) was used as a proxy for changes in input from land, i.e. glacial activity, where high (low) k_{LF} indicates high (low) glacial activity. It is likely that some of the variations in magnetic susceptibility observed at Site U1419 are related to the sediment source as well, as some southern Alaskan geological terranes are characterized by lower magnetic susceptibility (Yakutat and Chugach terranes; Cowan et al., 2006). Such changes in sediment provenance may be observed in the U1419 record as smaller variations in magnetic susceptibility (e.g., within Unit II). The large-scale changes in susceptibility, as those observed at Unit breaks, are, however, interpreted to relate to the amount of terrigenous material either through glacial advance or retreat. Although the main changes in glacial dynamics may have been interpreted from the magnetic susceptibility record, it is the combination of magnetic properties that informs on the details of the record. For example, facies 1 intervals are characterized by low magnetic susceptibility in combination with high coercivity (MDF_{ARM}), somewhat finer magnetic grain sizes (k_{ARM}/k_{LF} ; Banerjee/King plot), and generally lower magnetic concentration (magnetic remanences). Together with lithology and density, these characteristics have proven useful in identifying different depositional environments. Integral to the interpretation of the facies observed at Site U1419, was also the availability of lithological and rock magnetic analogues of more recent and well-constrained events, such as the Bølling-Allerød, via the studies of Davies et al. (2011), Davies-Walczak et al. (2014), Praetorius et al. (2015), and Walczak et al. (2017).

Another question related to the first objective was; *What were the dynamics of the NCIS prior to, and during the LGM?* The observation of sediment with physical, lithologic, and magnetic properties similar to that of the LGM at the base of the U1419 (facies 3) was tentatively interpreted to represent the final stages of a retreat of a pre-LGM glaciation occurring until 52,700 cal yr BP. In fact, the transition from this event (facies 3) to the following facies 1 interval is also similar to that observed for the final stages of the LGM and the deglacial transition observed between ~17,000 and 14,000 cal yr BP both in the U1419 record and in the site survey core EW0408-85JC (Davies et al., 2011). Early to mid- MIS 3

(52,700-42,700 cal yr BP) was characterized by environmental conditions similar to those previously observed for the deglacial transition (Bølling-Allerød and Younger Dryas) where high productivity intervals with very low magnetic concentration and high coercivity alternate with periods of stronger glacial influence characterized by high magnetic concentration and low coercivity. Following this period of alternating conditions, an increase in concentration parameters was interpreted to indicate a build-up of glacial conditions until 41,800 cal yr BP. With, what appears as, only minor variations in sedimentation and ice-front variability, this period lasted until approximately 25,000 cal yr BP, after which the ice front may have become more dynamic as suggested by larger amplitude variations in magnetic properties. The highest sedimentation rates observed (835 cm/kyr) and what may be a short-lived pulse of sediment from a different source region characterized the onset of deglaciation at 18,000 cal yr BP. Similar to observations made by Davies et al. (2011), IRD disappeared and laminations were deposited from 14,700 cal yr BP, indicating that glaciers had retreated onto land, or, at least, behind fjord sills. The glacial dynamics as interpreted from the environmental magnetic studies of Site U1419 are tentatively outlined in Figure 37 in order to summarize the conclusions from chapter one.

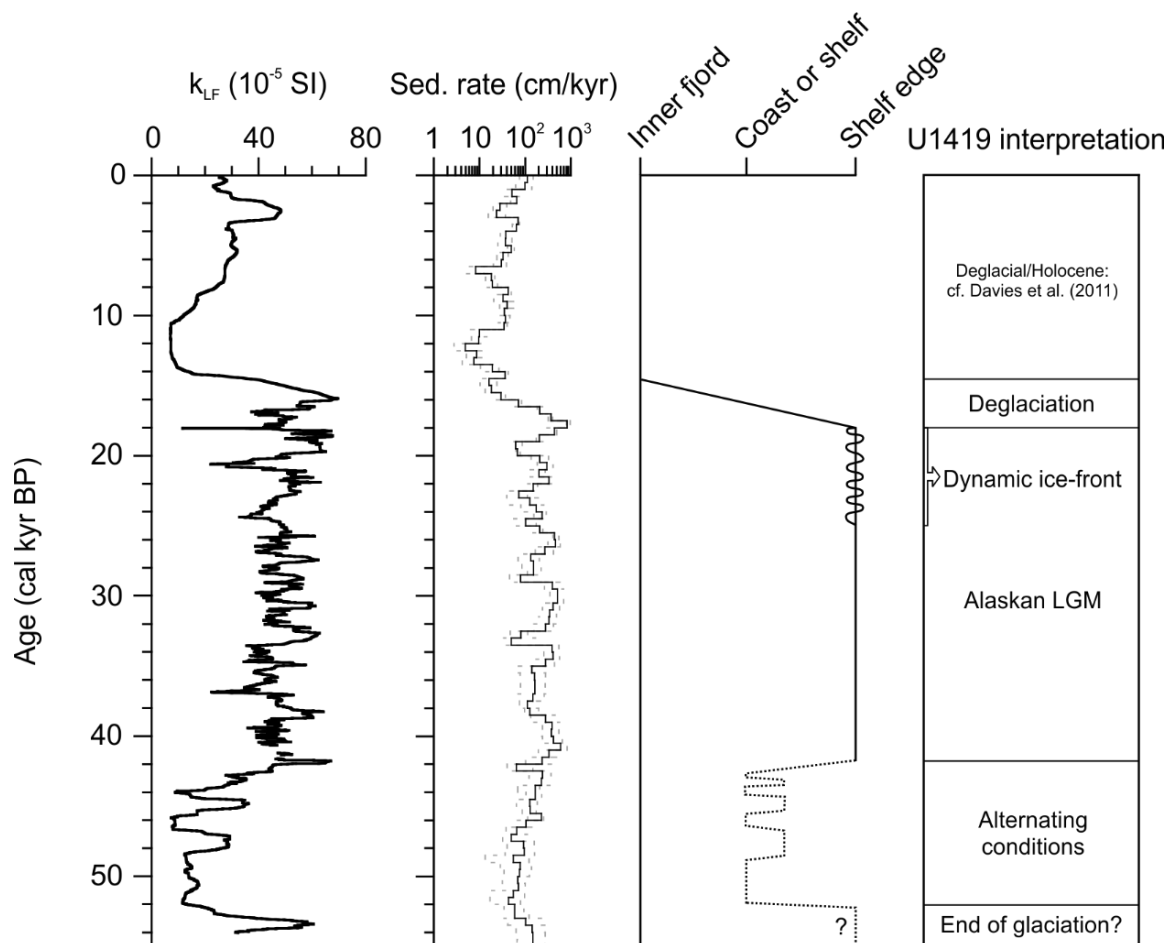


Figure 37: From the left: Site U1419 magnetic susceptibility and sedimentation rates (averaged over 500 years; Walczak et al., in prep), tentative interpretation of the ice front's position based on Site U1419, and a summary of the glacial history as interpreted from Site U1419.

The final question for the first objective was; *How does the U1419 record complement or add to our current understanding of the glacial history of this region?* As outlined in the introduction, the glacial history of the southern margin of the NCIS is incomplete both prior to and during the LGM. Although evidence exists for pre-LGM glacial advances to the shelf edge (e.g., Elmore et al., 2013; Montelli et al., 2017), the timing and extent of these are poorly constrained. The results from chapter one adds information on the

history of late Quaternary glacial dynamics in this region. If facies 3 truly does reflect the final stages of a pre-LGM shelf edge advance, this may correspond to some of the seismically inferred pre-LGM shelf-wide glaciations and possibly also to the regionally significant glaciation in Alaska with glacial retreat ages falling within MIS4/MIS3 (cf. Kaufman et al., 2011). Although Site U1419 alone is not enough to determine that facies 3 represent the final stages of an earlier glaciation, it is the first step towards constraining the pre-LGM glacial history in the Gulf of Alaska. Another new element to the glacial history is the period of alternating conditions between 52,700 and 42,700 cal yr BP. Although a parallel has been drawn between facies 1 and the Bølling-Allerød/early Holocene, and between facies 2 and the Younger Dryas, it is evident from the higher presence of clasts and the higher sedimentation rates that glaciers were a stronger influence at the core site during the early/mid MIS 3 than during the Bølling-Allerød, Younger Dryas, and early Holocene. Perhaps the ice sheet was at a “tipping point” during this time, fluctuating between more and less active stages, before the build-up to the full glacial conditions. The main contribution of chapter one is the observation of the prolonged glacial period, the *Alaskan LGM*, that may have commenced as early as 41,800 cal yr BP and lasted until the onset of laminated sediment at 14,700 cal yr BP. It is surprising that proximal glacial conditions prevailed for such an extended period of time. The LGM has previously been estimated between 23,000 and 14,700 cal yr BP (e.g., Mann & Peteet, 1994; Mann & Hamilton, 1995; Clapperton, 2000; Davies et al., 2011). With the results from chapter one, the onset of the Gulf of Alaska glacial maximum could be extended back to ~40,000 cal yr BP. However, the most dynamic period of the glacier front remains similar to the old estimates of the LGM, between ~25,000 and 18,000 cal yr BP.

An important limitation of chapter one is the lack of control samples from the different geological terranes of southern Alaska. With a set of such samples available, rock magnetic analyses may have allowed a sediment provenance study similar to that of Cowan et al. (2006) from the southern Alaska coast. This data could provide more detailed constraints on the dynamics and activity of different outlets of the NCIS. With the information available from chapter one, we have to assume that Site U1419 reflects the

general activity of the Bering Ice Stream only, as the drill Site is located adjacent to the Bering Trough. Although chapter one presents a general overview of glacial activity close to Site U1419, future provenance studies from IODP Exp. 341 working groups will shed more light on the glacial history of this region.

Chapter 2

In chapter two, the paleomagnetic record at Site U1419 was explored to achieve the second objective of the thesis, namely, to reconstruct late Pleistocene and Holocene geomagnetic variability from the Gulf of Alaska. Results from this chapter revealed that the Site is not suitable for paleointensity studies. This was inferred from the very weak remanent magnetization and complex magnetic mineralogy, likely resulting from a combination of the ice-proximal setting of the Site, and post-depositional processes such as reduction diagenesis related to periods of increased productivity (cf. chapter one). Nonetheless, Site U1419 seems to have preserved a reliable inclination record that, through careful evaluation and removal of disturbed and unreliable intervals, reflects regional-scale geomagnetic change. It was shown in this chapter that using the inclination as measured after the 20 mT AF demagnetization step alone provides the most reliable inclination estimate for Site U1419, as including higher demagnetization steps in a traditional characteristic remanent magnetization (ChRM) added noise rather than signal to the record. The high temporal resolution of the Site and the detailed age model (Walczak et al., in prep) provides a unique opportunity for regional stratigraphic correlation. Another result from the second chapter is the age model for Site U1418. Along with 23 radiocarbon dated intervals from the U1418 splice record, 18 tie-points based on magnetic susceptibility to the site survey core EW0408-87JC (Praetorius et al., 2015) allow the past ~40,000 cal yr BP to be fairly well constrained. This, in turn, permitted a detailed comparison between Site U1419 u-channel and Site U1418 shipboard inclination records, further supporting the recording of a regional geomagnetic signal at these Sites. An additional outcome from this chapter is the demonstration of the advantage of using

shipboard records; both to check for u-channel sampling disturbance in intervals that are difficult to sample (e.g., soupy mudline sediments, or clast-rich diamict), and for comparisons to other sites that have yet to be sampled for u-channels or analyzed. Furthermore, chapter two illustrates that “imperfect” records such as Site U1419 should not be immediately dismissed as they may still provide useful paleomagnetic records.

One of the specific questions related to the second objective was; *How do these records compare with other, independently dated, regional records? What are pronounced similarities or differences?* Site U1419 inclination was compared to other regional independently dated records from the Gulf of Alaska (EW0408-85JC and Site U1418), and the regional PSV stacks NEPSIAS (including records from Alaska, Oregon and Hawaii) and WNAM (British Columbia, Utah and Idaho). A total of 16 inclination features could be correlated across these records, with 10 of them being consistent across the broader northeastern Pacific/western North American region. Pronounced differences between these records relate to differences in temporal resolution. Although the high temporal resolution of Site U1419 provides a unique opportunity to study geomagnetic field changes in detail, it is also somewhat of an obstacle for comparison as few other regional records have similar resolutions. Especially pronounced similarities are the features *g* through *b* that are observed in all the Gulf of Alaska records, as well as in the WNAM17 inclination stack (Reilly et al., 2018). This sequence of features occurs between ~21,000 cal yr BP (*g*) and 15,000 cal yr BP (*b*) in portions of the age models constrained by both radiocarbon dates as well as tie-points to the site survey cores. The most prominent feature in this sequence is the steep feature *f* at 19,700 cal yr BP that is presumably observed in the WNAM17 stack as well. Feature *f* and/or the entire sequence of features from *g* to *b* provides a robust stratigraphic marker in regional correlation for other records that have less age control.

Another question investigated in the second chapter was; *What do the Gulf of Alaska paleomagnetic records indicate about the nature of the geomagnetic signal in the northeast Pacific, and what does that reveal about geomagnetic field dynamics?* One observation made from the second chapter is the apparent lack of recordings of the Laschamp (41 ka) and Mono

Lake (34-30 ka) excursions in the U1419 record. These events are often recognized in paleomagnetic records from around the world (e.g., Laj et al., 2000; Nowaczyk et al., 2012; Lisé-Pronovost et al., 2013; Lund et al., 2017a, 2017b). From the U1419 results alone, it is not clear whether the lack of the Laschamp and Mono Lake at Site U1419 is related to the quality of the record in these intervals, or if these events are recorded with a different signature in the northeast Pacific region, or a combination of the two. Another finding from this chapter relates to the several abrupt transitions observed in the inclination record either from steep to shallow, and from shallow to steep inclinations. These transitions of $\sim 20\text{-}40^\circ$ occur over periods of less than ~ 1000 years indicating that PSV rates of change are similar to late Pleistocene rates observed in the North Atlantic (Lund et al., 2005). As stated in chapter two, this implies that there is no more stability to the GAD field in the Pacific than elsewhere (e.g., Peng & King, 1992; McElhinny et al., 1996), at least on the timescales investigated at Site U1419. The timescales and persistence of these features may be constrained by further studies Pacific paleomagnetic records and other Exp. 341 drill Sites.

Chapter 3

Chapter three also concerns the second objective of reconstructing late Pleistocene and Holocene geomagnetic variability from the Gulf of Alaska. In order to achieve this objective, the paleomagnetic record of Surveyor Fan Site U1418 was explored. At this Site, a strong, single component magnetization is carried by a generally down-core stable magnetic mineralogy dominated by PSD magnetite. The characteristic remanent magnetization was defined between the AF demagnetization steps of 20 and 60 mT. The similarities between Site U1418 shipboard and U1419 u-channel inclinations were demonstrated already in chapter two, but in the third chapter the resemblance is further substantiated by the comparisons between U1418 u-channel data and Site U1419. The striking similarities between these two records provide an opportunity to increase the resolution of the U1418 age model through inclination tie-points to the U1419 age model (Walczak et al., in prep).

Seven tie-points were made between the ages of 26,000 and 18,000 cal yr BP, and the U1418 age model and sedimentation rates were adjusted accordingly. On this new age model, Site U1418 inclination and declination were compared to other regional directional records, suggesting a total of 13 and five similar features for inclination and declination, respectively. The relative paleointensity proxy from Site U1418 was developed using the slope method of NRM/IRM and was compared with previously published RPI records, as well as with the Greenland ^{10}Be flux record. However, the local, regional, global (and, likely, combination) intensity signal recorded at Site U1418 remains undetermined.

One of the specific questions asked in relation to the second objective was; *How do these records compare with other, independently dated, regional records? What are pronounced similarities or differences?* Both the U1418 inclination and declination records display similarities to other Gulf of Alaska and regional records, suggesting that this Site captured regional-scale inclination variability. As for Site U1419, the high resolution of Site U1418 provides a challenge when it comes to regional comparisons. Relative paleointensity records from the broader Pacific region were selected for comparison to U1418 based on their temporal resolution. In the Holocene and deglacial, two Arctic records were used, whereas equatorial and south Pacific records were selected for the late Pleistocene portion. For the late Pleistocene, millennial-scale paleointensity features were not definitively recognized across the compared records, whereas more similarities were observed for the Holocene. These ambiguities led to the postulation that a global or broader-regional geomagnetic intensity signal may not be applicable on millennial-scale variability. However, as Site U1418 is, per now, the only normalized intensity record available at this temporal resolution within this region, it is not possible to verify the validity of the record.

Another question posed in the context of the second objective was; *How do these records compare with North Atlantic records and global stacks?* The U1418 normalized intensity was also compared to an RPI stack composed of globally distributed marine and lacustrine records from, amongst others, the Iberian Margin, the Scotia Sea, Patagonia, the Bermuda Rise, South Atlantic Ocean, and France (Channell et al., 2018). Interestingly, this

comparison shows that the U1418 paleointensity record may have captured global-scale intensity trends over longer timescales, i.e. 5,000-10,000 years. There may be millennial-scale variations similar across these records that the lower resolution RPI stack does not reveal. This, again, highlights the use for more high-resolution records.

The Gulf of Alaska records

The study of rock magnetic properties of Site U1419 provides a deeper understanding of the paleomagnetic record from this Site. Having the overview that chapter one provides of the variations in sedimentary environments, offered a more complete understanding of factors that may have complicated the U1419 paleomagnetic record; e.g., the clast-rich diamict that may have made u-channel sampling difficult, the high sedimentation rates related to the ice proximal location of the site, and the periods of higher productivity and reductive diagenesis. All this information was obtained from the environmental magnetic analyses of the first chapter and was brought into consideration while working on the second chapter. This addresses the advantage and importance of rock and environmental magnetic analyses prior to the treatment and interpretation of paleomagnetic data.

The second and third chapters are both important constituents in achieving the second objective, and the two largely built upon and supported each other. In chapter two, using the U1418 shipboard inclination on its own age model was integral in supporting the interpretation of Site U1419 as a regional geomagnetic signal, as the noise and uncertainties related to this Site complicated interpretations. In chapter three, the roles were reversed when the detailed age model of Site U1419 was used to enhance the U1418 age model through correlations of inclination features, thereby improving the chronology of the U1418 age model. This, in turn, allowed for a more detailed comparison of the U1418 record to other regional records. The use of these two records through chapters two and three speak to the strength of using PSV as a regional correlative tool. Together, these two records, both with similar high temporal resolution and individual age constraints, make up a robust inclination

record from the Gulf of Alaska that is especially well-defined between 30,000 cal yr BP and the present. With the addition of declination and paleointensity from the third chapter, a record of the full paleomagnetic vector is available from the Gulf of Alaska, providing a first step towards defining the late Pleistocene and Holocene geomagnetic variability in the northeast Pacific.

Perspectives

As mentioned previously, the addition of rock-magnetic and geochemistry-based provenance studies to the U1419 record would provide a more detailed understanding of NCIS dynamics as well as sedimentary processes at this Site. Furthermore, an environmental magnetic study of Site U1418, similar to that of chapter one, could add a spatial perspective to the glacial history reconstruction. With the high temporal resolution of these Sites and the well-resolved age models available, there is potential for a detailed Gulf of Alaska glacial history record to be developed. With this, one of the main objectives of IODP Expedition 341 can be achieved; namely, to “*establish the timing of advance and retreat phases of the northwestern Cordilleran Ice Sheet to test its relation to dynamics of other global ice sheets*”. Such a comparison can provide new insights to the possible synchronicity between the large Pleistocene ice sheets and the understanding of the driving mechanisms behind global millennial-scale climatic cycles and the role of orbital and/or greenhouse gas forcing (cf. Jaeger et al., 2011).

With regards to the paleomagnetic records, continued u-channel analyses on Site U1418, below 64 m CCSF-A, would be of great interest as this could help verify or disprove the U1419 inclination record in this interval (i.e. the record older than ~30,000 cal yr BP). As U1419 is the only high-resolution inclination record from this region, there are no comparable records that can aid in defining the geomagnetic signal at this Site prior to 30,000 cal yr BP. Continued Site U1418 u-channel studies could resolve the remaining questions regarding the lack of observations of the Laschamp and Mono Lake geomagnetic excursions

at Site U1419 and whether this is related to the quality of the record, or if there are regional differences in the recording of such events. Furthermore, Site U1418 and U1419, along with other IODP Exp. 341 Sites, can define the geomagnetic signal for the northeast Pacific beyond the past ~30,000 cal yr BP, and form the potential for a robust regional paleomagnetic reference record.

REFERENCES

- Andrews, J.T., Maclean, B., Kerwin, M., Manley, W., Jennings, A.E. & Hall, F., 1995.** Final stages in the collapse of the Laurentide Ice Sheet, Hudson Strait, Canada, NWT: 14C AMS dates, seismic stratigraphy, and magnetic susceptibility logs, *Quaternary Science Reviews*, **14**, pp. 983-1004, doi: 10.1016/0277-3791(95)00059-3
- Channell, J.E.T., Hodell, D.A., Crowhurst, S.J., Skinner, L.C. & Muscheler, R., 2018.** Relative paleointensity (RPI) in the latest Pleistocene (10-45 ka) and implications for deglacial atmospheric radiocarbon. *Quaternary Science Reviews*, 191, pp. 57-72, doi: 10.1016/j.quascirev.2018.05.007
- Clapperton, C., 2000.** Interhemispheric synchronicity of Marine Oxygen Isotope Stage 2 glacier fluctuations along the American cordilleras transect. *Journal of Quaternary Science*, **15(4)**, pp. 435-468, doi: 10.1002/1099-1417(200005)15:4<435::AID-JQS552>3.0.CO;2-R
- Cowan, E.A., Brachfeld, S.A., Powell, R.D. & Schoolfield, S.C., 2006.** Terrane-specific rock magnetic characteristics preserved in glacial marine sediment from southern coastal Alaska. *Canadian Journal of Earth Sciences*, **43**, pp. 1269-1282, doi: 10.1139/E06-042
- Davies, M.H., Mix, A.C., Stoner, J.S., Addison, J.A., Jaeger, J., Finney, B. & Wiest, J., 2011.** The deglacial transition on the southeastern Alaska Margin: Meltwater input, sea level rise, marine productivity, and sedimentary anoxia. *Paleoceanography*, **26**, PA2223, doi: 10.1029/2010PA002051
- Davies-Walczak, M., Mix, A.C., Stoner, J.S., Southon, J.R., Cheseby, M. & Xuan, C., 2014.** Late Glacial to Holocene radiocarbon constraints on North Pacific Intermediate Water ventilation and deglacial atmospheric CO₂ sources. *Earth and Planetary Science Letters*, **397**, pp. 57-66, doi: 10.1016/j.epsl.2014.04.004
- Elmore, C.R., Gulick, S.P.S., Willems, B. & Powell, R., 2013.** Seismic stratigraphic evidence for glacial expanse during glacial maxima in the Yakutat Bay Region, Gulf of Alaska. *Geochemistry Geophysics Geosystems*, **14(4)**, pp. 1294-1311, doi: 10.1002/ggge.20097

- Jaeger, J., Gulick, S., Mix, A., and Petronotis, K., 2011.** Southern Alaska margin: interactions of tectonics, climate, and sedimentation. *IODP Scientific Prospectus*, **341**, doi:10.2204/iodp.sp.341.2011
- Jessen, S.P., Rasmussen, T.L., Nielsen, T. & Solheim, A., 2010.** A new late Weichselian and Holocene marine chronology for the western Svalbard slope 30,000-0 cal years BP, *Quaternary Science Reviews*, **9-10**, pp. 1301-1312, doi: 10.1016/j.quascirev.2010.02.020
- Kaufman, D.S., Young, N.E., Briner, J.P. & Manley, W.F., 2011.** Alaska palaeo-glacier atlas (version 2). *In*: Ehlers, J., Gibbard, P.L. & Hughes, P.D. (eds.) 2011. Quaternary Glaciations - Extent and Chronology - A Closer Look, Developments in Quaternary Science, vol. 15, pp. 427-445, doi: 10.1016/B978-0-444-53447-7.00033-7
- Laj, C., Kissel, C., Mazaud, A., Channell, J.E.T. & Beer, J., 2000.** North Atlantic palaeointensity stack since 75 ka (NAPIS-75) and the duration of the Laschamp event. *Philosophical Transactions of the Royal Society A*, **358(1768)**, pp. 1009-1025, doi: 10.1098/rsta.2000.0571
- Lisé-Pronovost, A., St-Onge, G., Gogorza, C., Haberzettl, T., Preda, M., Kliem, P., Francus, P., Zolitschka, B. & the PASADO Science Team, 2013.** High-resolution paleomagnetic secular variations and relative paleointensity since the Late Pleistocene in southern South America, *Quaternary Science Reviews*, **71**, pp. 91-108, doi: 10.1016/j.quascirev.2012.05.012
- Lund, S.P., Schwartz, M., Keigwin, L. & Johnson, T., 2005.** Deep-sea sediment records of the Laschamp geomagnetic field excursion (~41,000 calendar years before present). *Journal of Geophysical Research*, **110**, B04101, doi: 10.1029/2003JB002943
- Lund, S.P., Benson, L., Negrini, R., Liddicoat, J. & Mensing, S., 2017a.** A full-vector paleomagnetic secular variation record (PSV) from Pyramid Lake (Nevada) from 47-17 ka: Evidence for the successive Mono Lake and Laschamp Excursions. *Earth and Planetary Science Letters*, **458**, pp. 120-129, doi: doi.org/10.1016/j.epsl.2016.09.036
- Lund, S.P., Schwartz, M. & Stott, L., 2017b.** Long-term palaeomagnetic secular variation and excursions from the western Equatorial Pacific Ocean (MIS2-4). *Geophysical Journal International*, **209**, pp. 587-596, doi: 10.1093/gji/ggx029

- Mann, D.H. & Peteet, D.M., 1994.** Extent and timing of the Last Glacial Maximum in Southwestern Alaska. *Quaternary Research*, **42**, pp. 136-148, doi: 10.1006/qres.1994.1063
- Mann, D.H. & Hamilton, T.D., 1995.** Late Pleistocene and Holocene paleoenvironments of the North Pacific coast. *Quaternary Science Reviews*, **14**, pp. 449-471, doi: 10.1016/0277-3791(95)00016-I
- McElhinny, M.W., McFadden, P.L. & Merrill, R.T., 1996.** The myth of the Pacific dipole window. *Earth and Planetary Science Letters*, **143**, pp. 13-22, doi: 10.1016/0012-821X(96)00141-0
- Montelli, A., Gulick, S.P.S., Worthington, L.L., Mix, A., Davies-Walczak, M., Zellers, S.D. & Jaeger, J.M., 2017.** Late Quaternary glacial dynamics and sedimentation variability in the Bering Trough, Gulf of Alaska. *Geology*, **45(3)**, pp. 251-254, doi: 10.1130/G38836.1
- Nowaczyk, N.R., Arz, H.W., Frank, U., Kind, J. & Plessen, B., 2012.** Dynamics of the Laschamp geomagnetic excursion from Black Sea sediments. *Earth and Planetary Science Letters*, **351-352**, pp. 54-69, doi: 10.1016/j.epsl.2012.06.050
- Peng, L. & King, J.W., 1992.** A late Quaternary geomagnetic secular variation record from Lake Waiau, Hawaii, and the question of the Pacific nondipole low. *Journal of Geophysical Research*, **94 B4**, pp. 4407-4424, doi: 10.1029/91JB03074
- Praetorius, S.K., Mix, A.C., Walczak, M.H., Wolhowe, M.D., Addison, J.A. & Prahl, F.G., 2015.** North Pacific deglacial hypoxic events linked to abrupt ocean warming. *Nature*, **527**, pp. 362-366, doi: 10.1038/nature15753
- Reilly, B.T., Stoner, J.S., Hatfield, R.G., Abbott, M.B., Marchetti, D.W., Larsen, D.J., Finkenbinder, M.S., Hillman, A.L., Kuehn, S.C. & Heil, C.W., 2018.** Regionally consistent western North America paleomagnetic directions from 15 to 35 ka: Assessing chronology and uncertainty with paleosecular variation (PSV) stratigraphy, *Quaternary Science Reviews*, **201**, pp. 186-205, doi: 10.1016/j.quascirev.2018.10.016
- Robinson, S.G., Maslin, M.A. & McCave, I.N., 1995.** Magnetic Susceptibility variations in Upper Pleistocene deep-sea sediments of the NE Atlantic: Implications for ice rafting and paleocirculation at the last glacial maximum. *Paleoceanography*, **10(2)**, pp. 221-250, doi: 10.1029/94PA02683

- Stoner, J.S., Channell, J.E.T. & Hillaire-Marcel, C., 1996.** The magnetic signature of rapidly deposited detrital layers from the deep Labrador Sea: Relationship to North Atlantic Heinrich layers. *Paleoceanography*, **11(3)**, pp. 309-325, doi: 10.1029/96PA00583
- Walczak, M.H., Stoner, J.S., Mix, A.C., Jaeger, J., Rosen, G.P., Channell, J.E.T., Heslop, D. & Xuan, C., 2017.** A 17,000 yr paleomagnetic secular variation record from the southeast Alaskan margin: Regional and global correlations, *Earth and Planetary Science Letters*, **473**, pp. 177-189, doi: 10.1016/j.epsl.2017.05.022
- Walczak, M.H., Mix, A.C., Fallon, S., Cowan, E., Praetorius, S., Du, J., Hobern, T., Padman, J., Fifield, K., Stoner, J.S., Haley, B., in prep,** Coupled changes in Northeast Pacific ventilation and Cordilleran Ice Sheet discharge may precede Heinrich Events. *Science*

